Cable modelling for electromagnetic transients in power systems

Alberto Pagnetti

N° d'ordre : D. U : 2248
E D S P I C : 563

UNIVERSITE BLAISE PASCAL - CLERMONT II

ECOLE DOCTORALE
SCIENCES POUR L'INGENIEUR DE CLERMONT-FERRAND

T h è s e

Présentée par

Alberto Pagnetti

titre (ingénieur, DEA, Master [(1)]) [facultatif]

pour obtenir le grade de

DOCTEUR D'UNIVERSITÉ

SPECIALITE :
GENIE ELECTRIQUE ET ELECTRONIQUE

Titre de la thèse

Cable modelling for electromagnetic transients in power systems

Soutenue publiquement le 29/06/2012 devant le jury :

Prof. Akihiro Ametani	Rapporteur et Président
Prof. Farhad Rachidi-Haeri	Rapporteur
Dr. Alain Xémard	Examinateur
Prof. Alberto Borghetti	Examinateur
Prof. Françoise Paladian	Directrice de thèse
Prof. Carlo Alberto Nucci	Directeur de thèse

Mots-clés / Keywords : Cable, EMTP, submarine cable, modeling, electromagnetic, transients Câble, EMTP, câble sous-marin, modélisation, électromagnétisme, transitoires

Résumé :

Les câbles sont utilisés de plus en plus pour le transport et la distribution de l'électricité en courant alternatif sur des distances de plus en plus longues. La prolifération de fermes éoliennes offshore qui nécessitent d'interconnexions avec le continent a aussi propulsé leur utilisation sous-marine.

Modèles de câbles sont disponibles dans le bien connu logiciel Electro Magnetic Transient Program et sont destinés au domaine temporel. Ces modèles sont assemblés en utilisant différentes techniques, mais tous nécessitent une connaissance précise des paramètres des câbles dans le domaine fréquentiel.

Dans ce but, pour le calcul des impédances des câbles tripolaires cette thèse propose une méthode qui améliore la prise en compte de la proximité entre tous les conducteurs : il s'agit d'une méthode semi-analytique qui utilise le concept duale de fils minces et sous-conducteurs pour décrire la densité de courant à l'intérieur des conducteurs et le calcul des impédances.L'effet du retour par la mer est aussi analysé et une méthode quasi Monte Carlo est proposé, afin de résoudre les intégrales qui décrivent la formulation des impédances pour le sol à deux couches (la mer et son fond) sur lequel ces câbles sont posés. L'effet du à la présence des couches de semi-conducteur dans les câbles est aussi traitéLa méthode de collocation stochastique est aussi décrite et appliquée, afin de prendre en compte la variabilité des paramètres d'entrée.

Mots-clés / Keywords : Cable, EMTP, submarine cable, modeling, electromagnetic, transients Câble, EMTP, câble sous-marin, modélisation, électromagnétisme, transitoires

Abstract :

Cables are extensively used for underground alternating current electricity distribution and progressively over longer distances; the proliferation of offshore wind farms which require interconnections with the mainland has also increased their use underwater.

Models of cables are available in the well-known Electro Magnetic Transient Program software and are designed to the time-domain. These models are assembled using different techniques but all of them need a precise knowledge of the frequency domain parameters of the cables.

Accordingly, for the calculation of the impedances of three-core submarine power cables this thesis proposes an improved method to consider the proximity effect between all conductors. The method, which is a semi-analytical, uses the dual concept of thin-wires and sub-conductors to describe the current density inside the conductors and the calculation of the impedances.The effect of the sea return is also analyzed and a quasi Monte Carlo method is proposed, to solve the integrals describing the impedances formulations for the two layer soil (the sea and seabed) upon which the submarine cables are laid. The effect due to the presence of semi-conducting layers in the cables is also treated.

The stochastic collocation method is also described and applied, in order to account for the variability of the input parameters.

UNIVERSITE BLAISE PASCAL – CLERMONT II

Ecole Doctorale Sciences pour l'Ingénieur de Clermont-Ferrand

en co-tutelle avec

UNIVERSITÀ DI BOLOGNA - FACOLTÀ D'INGEGNERIA

Dottorato in Ingegneria Elettrotecnica

Cable modelling for electromagnetic transients in power systems

Thèse

présentée par :

Alberto Pagnetti

Directeurs :

Prof. Françoise Paladian

Prof. Carlo Alberto Nucci

Rapporteurs :

Prof. Akihiro Ametani, Président

Prof. Farhad Rachidi-Haeri

Examinateurs :

Prof. Alberto Borghetti

Dr. Alain Xémard

A.A. 2011/2012

SUMMARY 5

RÉSUMÉ DÉTAILLÉ 9

SOMMARIO 13

1. INTRODUCTION 17

2. A REVIEW OF EXISTING MODELS OF UNDERGROUND CABLES 21

2.1. PREFACE 21
2.1.1. Introductory definitions 21
2.1.2. Components and installation techniques of Medium and High Voltage Cables 22
2.2. TRANSMISSION LINE EQUATIONS AND RELEVANT MODELS 25
2.2.1. Multi-conductor transmission line equations 25
2.2.2. Generic modal approach to determine propagation modes 26
2.2.3. Solution for one mode or single phase line 29
2.2.4. Nodal equations 30
2.2.5. Popular models used in the software EMTP-RV 30
2.2.6. Phase domain models 32
2.3. SINGLE CORE CABLES PARAMETERS 34
2.3.1. Determination principle for the phase impedances and admittances 34
2.3.2. Impedance evaluation 36
2.3.3. Admittance evaluation 40
2.4. THREE-CORE CABLES PARAMETERS 41
2.4.2. Derivation of the inner surface impedance of the armour 44
2.4.3. Description of Tegopoulus and Kriezis approach 45
2.4.4. Study of the currents generated in a circular conductor of infinite length, by a parallel current filament. 47
2.4.5. Study of the currents generated in a hollow conductor of infinite length, by a parallel current filament inside it 49
2.4.6. Impedances' evaluation 51

3. IMPROVED METHOD FOR THE CALCULATION OF CABLE INTERNAL IMPEDANCES 55

3.1. SYNTHESIS OF THE METHOD PROPOSED 55
3.2. METHOD FOR THE CALCULATION OF INDUCED CURRENTS BASED ON THIN-WIRE APPROACH: TWO SOLID CONDUCTORS 58
3.2.1. Geometry description 58
3.2.2. Subdivision of the conductors in thin-wires and potentials expression 62
3.2.3. Resolution of the system: evaluation of currents and potentials coefficients 68
3.3. METHOD FOR THE CALCULATION OF INDUCED CURRENTS BASED ON THIN-WIRE APPROACH: ROUND CORE CONDUCTOR INSIDE A HOLLOW SCREEN CONDUCTOR 76
3.3.1. Methodology description 77
3.3.2. Case of core acting as a source (Case 1) 79
3.3.3. Case of screen acting as a source (Case 2) 82
3.4. NUMERICAL EVALUATION OF THE INTERNAL IMPEDANCES OF SOLID AND HOLLOW CONDUCTORS 86
3.4.1. Distribution of the filaments and validation of results 88
3.4.2. Validation of the results for the current density 89
3.4.3. Validation of the results for the internal resistance and inductance 94

4. ADDITIONAL EFFECTS TO BE INCLUDED IN CABLE MODELLING 97

4.1. GROUND AND SEA RETURN IMPEDANCE 97
4.1.1. Ground-return impedance 97
4.1.2. Quasi - Monte Carlo method for the solution of Pollaczek integral 100
4.1.3. Sea return impedance 102

4.1.4. Integral defining the ground return impedance 102
4.2. SEMI-CONDUCTING LAYER MODELLING 104
4.2.1. Core surface impedance 104
4.2.2. Screen surface impedances 105
4.2.3. Admittance 105
4.3. APPLICATION OF STOCHASTIC COLLOCATION TO SENSIBILITY ANALYSIS 106
4.3.1. Sensitivity analysis of the input parameters of sea return impedance 106
4.3.2. Sensibility analysis applied to the evaluation of the semi-conducting layer admittance 108

5. EMTP-RV SIMULATIONS OF THREE-CORE CABLES 111

5.1. ASSEMBLING THE THREE-CORE CABLE MODEL 111
5.1.1. Impedance calculation 111
5.1.2. Admittance calculation 113
5.1.3. Recommendations for input parameters 114
5.2. SIMULATIONS USING THE THREE-CORE CABLE MODEL 115
5.2.1. Description of the simulation design 116
5.2.2. Discussion of the results of the simulation 122
5.2.3. Simulations with soils of different resistivity 123

6. CONCLUSIONS 125

7. BIBLIOGRAPHY 127

ADDITIONAL REFERENCES 130

A. APPENDIX - HANDLING UNCERTAINTIES 135

B. APPENDIX - IMPEDANCES IN THE WIRES AND PT MODELS 138

SUMMARY

Chapter 1. The introduction describes the motivation behind this doctoral research whose general field is alternating current energy propagation in medium and high voltage cables with a focus on the simulation of the propagation in submarine cable systems.

It is introduced that these cable systems need improved modelling with transient simulation softwares, because though models have long been available, some of the effects intervening in the propagation of electromagnetic waves have been described in an approximate way or altogether neglected. Accordingly the thesis will concentrate in the description of the cable's parameters and in particular that of the impedances since their frequency dependence makes their representation crucial in the simulation of transient phenomena.

Chapter 2 is dedicated to the introduction of existing cable models.

In Section 2.1 introductory definitions are given which are to be used in the remainder of the manuscript, namely the concept of TEM lines and per unit length parameters. Also introduced is the software for which we develop cable models, namely the EMTP-RV. Follows a description of the cable technologies of interest and an explanation of the different cable metallic and insulating layers that have a bearing on the electromagnetic propagation and therefore impact on the description of the cable parameters. The features described are mostly common to all medium and high voltage cables but the interest of the thesis concentrates on the three-core submarine cables.

In Section 2.2 transmission line equations and relevant models derived from this description are introduced. The propagation constant and characteristic admittance, derived from the transverse parameters, are also introduced as their representation is the main objective of these models. Since in multi-conductor lines the relationship between currents and voltage is a matricial one, the parameters of interest are all in the form of vectors and matrices, and due to the presence of mutual parameters in the impedance and admittance matrices, the derived matrices are all full matrices so that the solution of the TL equations are not as simple as they are in the case of single conductor lines.

The modal domain is introduced for the scope of uncoupling these equations and transform the phase parameters into modal parameters, doing this allows each mode of propagation to be solved as a single phase line. The modes also express a decomposition of how the propagation can be represented through different current and voltage propagation modes, be they coaxial, homo-polar, or inter-sheath.

After this description, in Section 2.2.3 we introduce the nodal equations that allow adapting the model to the representation used in EMTP-RV: the line or cable system is represented with two nodes, the entrance and the exit of the line, and described by the currents and voltages present at these two nodes at a certain time. At each step of time, the currents and voltage at the previous step allow to represent the propagation on the line. From this representation one can define the Constant Parameters, CP and the Frequency Dependent (FD or FDQ) models. These models differ in the way they represent the frequency dependent parameters; the FD models need complex fitting procedures in order to represent the propagation constant, the characteristic admittance (and the transformation matrix Q in the FDQ model) using rational functions. This representation is needed to perform convolutions that allow taking into account for the previous values of currents and voltages at different nodes.

In Section 2.2.6 follows the description of phase domain models that operate directly in the phase domain.

In Section 2.3 is described in much detail the evaluation of the parameters of a single-core cable. The method used to evaluate the impedance, namely the loop theory, allows to take into account the different effects present in the cable, be they resistive or inductive, and represent as well the skin effect in surface impedances thus accounting for frequency dependence. The loop method splits the fore-mentioned effects into partial impedances and partial admittances and in Section 2.3.2 the derivation of these terms is obtained starting from Maxwell equations and illustrating the coaxial theory developed by Schelkunoff.

In Section 2.4 a similar procedure is followed for three-core cables, where the parameters that are

needed for this model are partly those obtained in Section 2.3, and the other parameters needed are related to the armour. It is explained how these parameters related to the inner surface of the armour partly include the proximity effect and in Section 2.4.3 the theory put forth by Tegopolous and Kriezis is described. This theory introduces the concept of a filament to represent the current flowing in the inner conductors and inducing a modification of the current density distribution inside the armour. The hypothesis used that shall also be the starting point of the theory we developed: displacement currents are neglected, the material is taken to be non ferro-magnetic, the filament described as source of induction is infinitely long and axially parallel to the conductor of interest thus neglecting edge effects and reducing the problem to a two dimensional one; the return of the current is through the conductor of interest.

In Section 2.4.6 it is shown how the theory by Tegopoulos has been used, first by Brown Rocamora and then by Kane, to obtain the impedances of solid and hollow conductors, with the inclusion of proximity effect.

Chapter 3 is devoted to the original method we propose for the evaluation of internal impedances.

In Section 3.2 is treated a configuration of two cylindrical parallel conductors which proximity causes induction to one another. The theoretical approach derived for this case is then extended to the case of hollow conductors (such as cable sheaths and armours) in Section 3.3. The conductor, source of the excitation, is represented by a number of sub-conductors considered as thin wires when they serve as source, but acting as sub-conductors when target of the induction. This procedure allows representing the mutual induction between conductors. The current from conductor 1 is taken to be returning in conductor 2, and furthermore the sum of the thin wires current intensities gives the total current circulating in the conductor.

In a first step the current density and vector potential will be represented with expressions containing the thin wires unknown current intensities. These current intensities will then be calculated in a successive step.

The procedure used to calculate vector potential and current density is based on the following steps:

- Derivation of generic expressions for vector potential A and current density J;

- The currents in the above mentioned thin wires, which cause induction, have intensities corresponding to the value of the current density calculated in the point occupied by the wire and multiplied by the surface of the sub-conductor. The sum of these currents gives the total current I, which is imposed as flowing in the conductors. This is also equivalent to the current density yet to be determined, integrated on the surface of the conductor.

- The magnetic vector potential is calculated inside and outside the conductor and is due to different contributions:

    - Outside the conductor, we consider:

        - The contribution of the thin wires in one of the conductors at a point in the dielectric (this is when the conductor is considered to be the source of the induction);

        - The contribution in the dielectric due to the expression of J that is established in the second conductor as a consequence of the excitation by the thin wires in the first conductor.

    - Inside the conductor, the Helmholtz equation is solved.

From the contribution in terms of vector potential inside and outside the conductor that we have derived, we can express the magnetic field radial and angular components and then write the continuity condition of both at the conductor's edge. This last step permits to obtain a system through which the unknown coefficients for the generic expression of J and A are calculated. From this point forth it is possible to explicitly express the current density inside the conductors.

The skin effect is accounted for in the 0th order terms; that remain the same as in the classical Schelkunoff theory.

In order to calculate the current intensity in the thin wires, we suppose that the thin wire carries a

current intensity equal to the value of the current density evaluated in the point where the wire is located and multiplied by a the surface of the sub-conductor. This enables us to write a system of 2N equations, where N is the number of wires in which the conductor has been split. The wire current intensity allows writing the current density in each conductor and the vector potential everywhere.

In Section 3.4 the explicit expression of the internal impedance is inferred, that is a function of current density and magnetic field inside the conductor.

In Section 3.5 some details are given for the filament distribution, and the method is validated using the Finite Element software Comsol. Both the current density value in the conductors and the internal impedance values are validated.

In **Chapter 4**, further effects to be included in cable modelling are represented.

In Section 4.1 the ground return impedance is handled and different formulations are compared. In Section 4.1.2 the method put forth by Legrand for the solution of Pollaczek integral using quasi Monte Carlo integration is explained.

In Section 4.1.3 this integration method is proposed as the solution of the integral of the sea return impedance which is of interest in the case of submarine cables. The integral to be solved in this second case is different, and so is the variable change utilised in order to adapt the integration bounds so that Monte Carlo method can be used.

In Section 4.2 the semi-conducting layer effect on impedance and admittance is analysed, using a modelling put forth by Ametani that adapt coaxial theory to this case.

Finally in Section 4.3 the terms of sea return impedance and admittance due to the semi-conducting layer are looked at with a sensibility analysis, as their input values (electrical and geometrical parameters) are to a certain extent uncertain. This is done using the stochastic collocation method, presented in an Appendix.

In **Chapter 5** the three-core cable global model is put together using the notions and the terms discussed through the rest of the manuscript, assembling existing terms with original contributions.

In Section 5.2 simulations are carried out in order to compare the model we put forth with the existing Pipe Type model, our point of departure for the development of our model.

In **Appendix A**, the stochastic collocation method is described. This method allows to analyze the variation of a function and define its statistical parameters (mean and variance) when one or more of the input variable are random but their distribution is known. This is similar to what can be obtained with Monte Carlo techniques, but only very few iterations (less than 10 compared to thousands for Monte Carlo methods are needed).

The derivation of this method, from Lagrange polynomial is discussed. It is shown how the method allows obtaining some values of the input random variable(s) depending on its distribution.

The formula is evaluated for these values (called collocation points) and some weights (given as well by the method depending on the distribution of the random variable) are used to evaluate mean and variance of the observed function. This method can be employed, in our case, for sensibility analysis of the impedance and admittance formulas to the variation of input parameters.

In **Appendix B** the impedances of the core and the armour, as evaluated using the proposed method and the Pipe Type method are compared.

RÉSUMÉ DÉTAILLÉ

Chapitre 1. L'introduction décrit les raisons qui ont motivé ces travaux de recherche centrés sur l'étude de la propagation électromagnétique dans les câbles en courant alternatif à haute et moyenne tension, avec un intérêt particulier pour la simulation de ces phénomènes dans les câbles sous-marins.

On introduit la nécessité d'intégrer les modèles de ces câbles aux logiciels de simulation transitoire : quand bien même certains sont disponibles depuis longtemps, certains effets intervenant dans la propagation électromagnétique sont négligés ou décrits de façon approchée.

Par conséquent, cette thèse se concentre sur l'évaluation des impédances linéiques des câbles, l'importance de leur variation en fonction la fréquence conduisant à la nécessité d'une précision accrue pour la simulation d'effets transitoires.

Le **Chapitre 2** est consacré à la description des modèles de câbles existants.

Dans la Section 2.1 , les concepts de ligne TEM et les définitions des paramètres linéiques, utilisés tout au long du manuscrit, sont introduites:. Le logiciel EMTP-RV donnant lieu au développement de modèles de câble, est également présenté.

On donne ensuite une description des technologies de câble et plus particulièrement les différentes couches conductrices et isolantes qui ont un effet sur la propagation, et ainsi, ont une influence sur les valeurs des paramètres linéiques. Les caractéristiques décrites sont communes à la plupart des câbles moyenne et haute tension, mais les travaux de thèse portent principalement sur les câbles tripolaires.

Dans la Section 2.2, on introduit la théorie des lignes de transmission puis les modèles principalement utilisés pour l'étude de la propagation par les câbles. Les constante de propagation et impédance caractéristique, qui se déduisent des paramètres transversaux et qui sont à la base des modèles de ligne, sont rappelés. Dans le cas de lignes multi-conductrices, la relation entre tensions et courants est matricielle, les configurations étudiées étant caractérisées par des matrices pleines dont les termes extra diagonaux correspondent aux paramètres linéiques traduisant les couplages inter-conducteurs. La résolution des équations est alors plus complexe. Leur principe de résolution dans une base modale est introduit, afin de découpler ces équations et d'en transformer les paramètres de phase en paramètres modaux, ce qui permet de déterminer chaque mode de propagation comme s'il s'agissait d'une ligne monophasée. Les modes peuvent aussi exprimer une décomposition physique de la propagation de courants et tensions en modes coaxiaux, homopolaires et inter-écran.

Après ceci, dans la Section 2.2.3 on introduit les équations nodales, permettant d'adapter les modèles à la représentation utilisée dans EMTP-RV : la ligne de transmission considérée est représentée par deux nœuds, à savoir l'entrée et la sortie du câble, décrits par les courants et tension au niveau de ces nœuds à chaque instant. A chaque pas de temps, les courants et les tensions à l'instant précédent permettent de représenter la propagation sur la ligne. De cette représentation on peut définir les modèles à paramètres constants (CP) et les modèles variables avec la fréquence (FD et FDQ).

Ces modèles diffèrent dans la manière de représenter les paramètres, les modèles FD nécessitant des procédures complexes de fitting pour représenter l'évolution de la constante de propagation et l'admittance caractéristique (et la matrice de transformation modale Q dans le modèle FDQ) en fonction de la fréquence, en utilisant des fonctions rationnelles. Cette représentation est nécessaire pour obtenir des convolutions qui permettent de prendre en compte les valeurs aux instants précédents des courants et des tensions sur les différents nœuds.

Dans la Section 2.2.6 suit une description des modèles qui sont directement utilisés dans le domaine des phases.

Dans la Section 2.3 on décrit dans le détail le calcul des paramètres d'un câble unipolaire.

La méthode utilisée pour calculer l'impédance, basée sur la théorie des boucles, permet de prendre en compte les différents effets présents dans les câbles, qu'ils soient résistifs ou inductifs en représentant en particulier l'effet de peau dans les impédances de surface, prenant ainsi en compte la dépendance en fonction de la fréquence. La méthode des boucles divise les effets mentionnés en impédances et

admittances partielles et dans la Section 2.3.2 on montre de quelle manière, en partant des équations de Maxwell et en employant la théorie coaxiale développé par Schelkunoff, ces grandeurs sont évaluées.

Dans la Section 2.4, par une procédure similaire, ces grandeurs sont évaluées pour les câbles tripolaires. Est notamment précisé comment les paramètres liés à la surface interne de l'armure incluent en partie l'effet de proximité et dans la Section 2.4.3, la théorie proposée par Tegopolous et Kriezis est décrite. Cette théorie introduit le concept de filament qui représente le courant qui circule dans les conducteurs internes et induit une variation de la distribution de la densité de courant à l'intérieur de l'armure. Les hypothèses, sur lesquelles s'appuie également la théorie proposée sont: les courants de déplacement sont négligés, les conducteurs sont non ferromagnétiques, le filament décrit est de longueur infinie et est parallèle au conducteur considéré, ce dernier assurant le retour du courant. Ces deux dernières hypothèses impliquent une invariance axiale de la structure et permettent, en négligeant les effets de bord, de ramener le problème à deux dimensions.

Dans la Section 2.4.6 on montre comment la théorie de Tegopoulos a été utilisé par Brown Rocamora et ensuite par Kane, pour obtenir les impédances des conducteurs solides et creux, en prenant en compte l'effet de proximité.

Le **Chapitre 3** est consacré à la méthode originale proposée pour l'évaluation des impédances internes.

Dans la Section 3.2 on traite une configuration de deux conducteurs cylindriques et parallèles, dont la proximité conduit à l'apparition de phénomènes d'induction mutuels. L'approche théorique dérivée pour ce type de câble est ensuite appliquée aussi au cas d'un conducteur creux (comme les écrans ou les armures) en Section 3.3. Le conducteur source est représenté par un ensemble de sous-conducteurs considérés comme des fils minces quand ils représentent la source, mais se comportent comme des sous-conducteurs quand ils sont « victimes » des phénomènes d'induction. Cette procédure permet de représenter l'induction mutuelle entre conducteurs, faisant agir chaque conducteur à la fois comme source et comme victime. C'est le second conducteur qui assure le retour du courant circulant dans l'un des conducteurs,

La procédure utilisée pour évaluer le potentiel vecteur et la densité de courant repose sur les étapes suivantes :

- Dans une première étape les solutions des équations d'Helmholtz pour la densité de courant et le potentiel vecteur sont représentées sous forme de séries dont les coefficients sont déterminés dans une étape ultérieure :

- Les courants dans les fils minces à l'origine des phénomènes d'induction, ont des intensités qui correspondent à la valeur de la densité du courant calculée au point correspondant au sous-conducteur, multiplié par la surface de celui-ci. La somme de ces courants donne le courant total I, imposé comme circulant dans les conducteurs, et équivalent à la densité de courant à déterminer, intégrée sur la surface du conducteur.

- Le potentiel magnétique vecteur est évalué à l'intérieur et à l'extérieur du conducteur et est dû à différentes contributions :

  - A l'extérieur du conducteur on a :

    - La contribution des fils minces dans l'un des conducteurs en un point du diélectrique;

    - La contribution dans le diélectrique due à la densité de courant J dans le deuxième conducteur dû à l'excitation par les fils minces dans le premier conducteur.

  - A l'intérieur de chacun des conducteurs, l'équation de Helmholtz est résolue.

A partir de l'expression du potentiel vecteur obtenue, on peut exprimer le champ magnétique radial et angulaire et écrire les équations de continuité à la frontière de chaque conducteur. On obtient alors un système à partir duquel il est possible d'écrire explicitement le courant à l'intérieur du conducteur.

L'effet de peau est pris en compte dans le terme d'ordre 0 qui est identique à celui de la théorie classique de Schelkunoff.

Afin d'évaluer l'intensité de courant dans les fils minces, on suppose que l'intensité de courant est constant sur le fil mince et équivaut à la densité de courant, au point correspondant au conducteur, multiplié par la surface du sous-conducteur. On obtient alors un système de 2N équations, N étant le nombre de fils minces constituant le conducteur, permettant d'évaluer le courant, puis de déterminer la densité de courant et le champ magnétique en tout point de chaque conducteur.

Dans la Section 3.4 une expression explicite de l'impédance interne, fonction de la densité de courant et du champ magnétique, est obtenue.

Dans la Section 3.5 certains détails sont donnés pour la distribution des fils minces, et la méthode est validée par le logiciel Comsol utilisant la méthode des Eléments Finis. La comparaison des résultats obtenus avec l'approche proposée pour la densité de courant et pour l'impédance interne des conducteurs est en effet satisfaisante.

Dans le **Chapitre 4**, d'autres effets à inclure dans les modèles de câble sont représentés. Dans la Section 4.1 l'impédance de retour par le sol est traitée et différentes formulations sont comparées.

Dans la Section 4.1.2 la méthode proposée par Legrand pour la résolution de l'intégrale de Pollaczek en utilisant l'intégration quasi Monte Carlo est présentée et appliquée à notre cas d'étude.

Dans la Section 4.1.3 cette méthode d'intégration est proposée, comme la solution de l'intégrale de l'impédance de retour par la mer, d'intérêt pour les câbles sous-marins. L'intégrale à résoudre dans ce deuxième cas est différente, comme l'est le changement de variable utilisé, afin d'adapter les bornes d'intégration afin que la méthode d'intégration quasi Monte Carlo puisse être utilisée.

Dans la Section 4.2 l'effet de la couche de semi-conducteur, existante entre l'isolant et les parties conductrices, sur l'impédance et l'admittance est analysé, en utilisant un modèle proposé par Ametani qui adapte la théorie coaxiale à ce cas.

Enfin dans la Section 4.3 une analyse de sensibilité est réalisée sur les termes décrits dans les deux sections précédentes. Ceci est réalisé en utilisant une analyse de sensibilité, prenant en compte l'incertitude des données d'entrée (électrique et géométrique) et son effet sur les valeurs des paramètres linéiques de câbles. Cette étude a donné lieu à l'application d'une méthode de collocation stochastique, présenté dans l'Annexe A.

Dans le **Chapitre 5** le modèle global de câble tripolaire est assemblé en utilisant les notions et les termes discutés le long du manuscrit, combinant des termes existants et des contributions originales.

Dans la Section 5.2 des simulations sont effectuées, afin de comparer le modèle proposé avec le modèle « Pipe Type » existant.

Dans l'**Appendice A**, la méthode de collocation stochastique est décrite. Cette méthode permet d'analyser la variation d'une fonction et de déterminer ses moments statistiques (moyenne et variance) quand une, ou davantage, des variables d'entrée sont aléatoires, leur loi de distribution étant connue.

Ceci est similaire à ce qui peut être réalisé avec des techniques de type Monte Carlo, mais avec très peu d'itérations (moins de 10, comparé à des milliers pour la méthode Monte Carlo). La dérivation de cette méthode consistant à développer la fonction d'une variable aléatoire sur une base de polynômes de Lagrange est discutée. On montre comment la méthode permet d'obtenir les moments statistiques de la fonction pour la (les) variable(s) d'entrée aléatoire selon sa(ses) loi(s) de distribution(s).

La formule est évaluée pour différentes valeurs (dits points de collocation) et poids (qui sont eux aussi donnés par la méthode selon la distribution de la variable aléatoire utilisés pour évaluer la moyenne et la variance de la fonction observée. Cette méthode peut être employée dans notre cas, pour des analyses de sensibilité de l'impédance et de l'admittance à la variation des données d'entrée.

Dans l'**Appendice B** on a comparé le calcul des impédances de l'âme et de l'armure entre la formulation qu'on propose et le modèle Pipe Type d'EMTP-RV.

SOMMARIO

Capitolo 1. L'introduzione descrive la motivazione di questa ricerca dottorale che si svolge nel campo generale della propagazione dell'energia a corrente alternata nei cavi a media ed alta tensione e si concentra sulla simulazione della propagazione nei sistemi di cavi sottomarini.

Si premette che per tali sistemi occorre migliorare la modellazione dei programmi di simulazione dei regimi transitori perché, sebbene modelli esistano già da lungo tempo, alcuni degli effetti che intervengono nella propagazione delle onde elettromagnetiche vi sono stati descritti in modo approssimato o del tutto trascurati. Pertanto questa tesi si concentra nella descrizione dei parametri dei cavi ed in particolare su quella delle impedenze in quanto la dipendenza dalla frequenza di esse necessita la loro corretta rappresentazione perché fondamentale nella simulazione dei fenomeni transitori.

Il **capitolo 2** è dedicato alla presentazione dei modelli di cavo esistenti.

Nella sezione 2.1 si danno definizioni introduttive, che saranno poi usate in tutto il lavoro, sul concetto di linee TEM e sui parametri per unità di lunghezza; si presenta inoltre il codice per quale svilupperemo i modelli di cavo che è l'EMTP-RV. Segue la descrizione della tecnologia impiegata nei cavi dei quali ci si occupa, dell'influenza dei vari strati di copertura metallica e dielettrica sulla propagazione elettromagnetica e pertanto dell'importanza di questi nella rappresentazione dei parametri dei cavi. Le caratteristiche descritte sono per lo più comuni a tutti i cavi a media ed a alta tensione ma l'interesse dello studio si concentra su quelli sottomarini tripolari.

Nella sezione 2.2 sono introdotte le equazioni dei telegrafisti e ed i modelli da esse derivati. Si introducono anche la costante di propagazione e l'ammettenza caratteristica derivate dai parametri trasversali la cui rappresentazione costituisce l'obiettivo principale di tali modelli. Siccome in linee a più conduttori la relazione tra correnti e tensione è di tipo matriciale, tutti i parametri che le riguardano hanno forma di vettori o matrici e, data la presenza di parametri mutui nelle matrici di impedenza ed ammettenza, tali matrici sono piene così che la soluzione delle equazioni TL sono meno semplici che nel caso di linee con un solo conduttore.

Viene introdotto il dominio modale con lo scopo di disaccoppiare tali equazioni e di trasformare i parametri di fase in parametri modali così che ogni modo di propagazione possa risolversi come in una linea monofase. I vari modi consentono una decomposizione così che la propagazione può essere rappresentata da modi diversi sia coassiali, omopolari o inter-schermo.

Dopo questa descrizione, nella sezione 2.2.3 si introducono le equazioni modali che consentono di adattare il modello alla rappresentazione usata nel codice EMTP-RV: la linea o il sistema di cavi sono rappresentati con due nodi: l'ingresso e l'uscita, e sono descritti dalle correnti e tensioni presenti a tali due nodi in un certo istante. Ad ogni istante successivo, le correnti e le tensioni all'istante precedente consentono di rappresentare la propagazione. Da questa rappresentazione possono ricavarsi i parametri costanti CP ed i modelli variabili con la frequenza FD o FDQ. Tali modelli differiscono per il modo con il quale essi rappresentano i parametri dipendenti dalla frequenza: i modelli FD richiedono complesse procedure d'adattamento per riprodurre la costante di propagazione, l'ammettenza caratteristica (e, nel modello FDQ, la matrice di trasformazione Q) mediante l'impiego di funzioni razionali. Questa rappresentazione è necessaria a consentire convoluzioni numeriche che permettono di prendere in conto i precedenti valori delle correnti e tensioni ai diversi nodi.

Nella sezione 2.2.6 segue la descrizione dei modelli nel dominio delle fasi.

Nella sezione 2.3 è descritta la valutazione dei parametri d'un cavo coassiale. Il metodo usato per valutare l'impedenza, e cioè quello della maglia, consente di prendere in conto i vari effetti presenti nel cavo, resistivi ed induttivi, compreso l'effetto pelle sulle impedenze superficiali così inglobando la dipendenza dalla frequenza, Il metodo della maglia separa i predetti effetti in impedenze parziali ed ammettenze parziali e, nella sezione 2.3.2 si derivano questi termini partendo dalle equazioni di Maxwell ed illustrando la teoria coassiale sviluppata da Schelkunoff.

Nella sezione 2.4 si segue un procedimento simile per i cavi tripolari per i quali i parametri necessari per il modello sono in parte quelli ottenuti nella sezione 2.3, mentre diversi sono i parametri che riguardano l'armatura. Si spiega come tali parametri, riferiti alla superficie interna dell'armatura, in parte comprendono l'effetto di prossimità e nella sezione 2.4.3 si descrive la teoria di Tegopulos e Kriezis. Tale teoria introduce il concetto di un filamento per rappresentare la corrente che cirola nei conduttori interni e che induce una variazione della distribuzione della densità di corrente nell'armatura. Le ipotesi introdotte, che sono anche alla base della teoria sviluppata da noi sono: le correnti di spostamento sono trascurate, il materiale è considerato non ferromagnetico, il filamento che costituisce la fonte dell'induzione è di lunghezza infinita ed è assialmente parallelo al conduttore interessato così che possono essere trascurati gli effetti di estremità riducendo il problema ad essere bidimensionale, infine la corrente di ritorno avviene attraverso il conduttore interessato.

Nella sezione 2.4.6 è mostrato come la teoria di Tegopulos è stata usata dapprima da Brown Rocamora e poi da Kane per ottenere le impedenze di conduttori sia solidi sia cavi includendo l'effetto di prossimità.

Il **capitolo 3** è dedicato al metodo originale che proponiamo per la valutazione delle impedenze interne.

Nella sezione 3.2 si tratta il caso di due conduttori cilindrici paralleli la cui prossimità dà luogo ad induzione reciproca. Nella sezione 3.3 l'approccio teorico derivato per questo caso è esteso a quello di conduttori cavi (come le guaine e le armature di cavi); il conduttore fonte dell'eccitazione è rappresentato da un numero di sub-conduttori che si considerano fili sottili quando si considerano fonte di induzione ma che acquistano sezione dimensionale quando se ne considerano bersaglio. Questo procedimento permette di rappresentare la mutua induzione tra i conduttori: la corrente nel conduttore 1 si considera ritornare nel conduttore 2 e, di più, la somma delle intensità di corrente nei conduttori sottili dà la corrente totale circolante nel conduttore.

In un primo tempo si rappresentano la densità di corrente ed il vettore potenziale con espressioni contenenti le intensità di corrente nei fili sottili ancora ignote. Tali intensità di corrente sono poi calcolate in un secondo tempo.

La procedura per calcolare intensità di corrente e vettore potenziale seguono i seguenti passi:

- Derivazione di una espressione generica per il vettore potenziale A e la densità di corrente J;
- le correnti nei fili sottili, sorgenti d'induzione, hanno intensità corrispondenti al valore della densità di corrente calcolata nel punto occupato dal filo moltiplicata per la sezione del sub-conduttore. La somma di tali correnti fornisce la corrente totale I che si impone come fluente nei conduttori; questa è equivalente alla densità di corrente ancora da determinare integrata sulla sezione del conduttore.
- Il vettore potenziale magnetico è calcolato interno ed esterno al conduttore ed è dovuto a due diversi contributi:
    - All'esterno del conduttore si considera:
        - il contributo dei fili sottili dei conduttori in un punto del dielettrico (ciò quando il conduttore è considerato come fonte dell'induzione);
        - il contributo entro il dielettrico dovuto alla J nel secondo conduttore come conseguenza della eccitazione da parte dei fili sottili nel primo conduttore.
    - All'interno del conduttore si risolve l'equazione di Helmholtz.

Conoscendo il contributo del potenziale vettore all'esterno e all'interno del conduttore, possiamo esprimere le componenti di campo magnetico radiale ed angolare ed scrivere la condizione di continuità di entrambi sul bordo del conduttore. Quest'ultimo passo consente di ottenere un sistema dal quale si calcolano i coefficienti ignoti per l'espressione di J ed A. A partire da questo punto è possibile esprimere esplicitamente la densità di corrente all'interno dei conduttori.

Dell'effetto pelle tengono conto i termini d'ordine 0 che sono gli stessi che nella teoria classica di

Schelkunoff.

Per calcolare l'intensità di corrente nei fili sottili noi supponiamo che essa sia uguale al valore della densità di corrente valutata nel punto nel quale si trova il filo moltiplicata per la sezione del sub-conduttore. Ciò consente di scrivere un sistema di 2N equazioni dove N è il numero dei fili nel quale il conduttore è stato suddiviso. L'intensità di corrente nel filo permette di scrivere la densità di corrente in ogni conduttore ed il vettore potenziale in ogni punto.

Nella sezione 3.4 si ricava il valore dell'impedenza interna in funzione della densità di corrente e del campo magnetico nel conduttore.

In 3.5 si danno particolari sulla distribuzione dei filamenti ed il metodo è comparato con i risultati dati dal programma Comsol. Vengono validati sia il valore della densità di corrente nei conduttori sia i valori dell'impedenza interna.

Nel **capitolo 4** si presentano ulteriori effetti da includere nei modelli di cavo.

In 4.1 si tratta dell'impedenza del ritorno di terra e si confrontano diverse formulazioni. In 4.1.2 si illustra il metodo proposto da Legrand per la soluzione dell'integrale di Pollaczek usando un'integrazione quasi Monte Carlo.

In 4.1.3 si propone tale metodo d'integrazione per risolvere l'integrale dell'impedenza del ritorno via mare che è d'interesse nel caso dei cavi sottomarini. In questo secondo caso l'integrale da risolvere è differente e così è il cambiamento di variabile utilizzato per adattare i limiti d'integrazione onde consentire l'applicazione del metodo quasi Monte Carlo.

In 4.2 si analizza l'effetto sull'impedenza ed ammettenza di uno strato semi-conduttore usando un modello dovuto ad Ametani che adatta a questo caso la teoria coassiale.

Nella sezione 4.3 si esaminano i termini dell'impedenza del ritorno via mare e dell'ammettenza dovuti allo strato semi-conduttore con un'analisi di sensibilità in quanto i dati (e cioè i parametri elettrici e geometrici) sono in qualche modo incerti. Ciò viene fatto impiegando il metodo di collocazione stocastica presentato in un'Appendice.

Nel **capitolo 5** si mette assieme un modello globale di cavo tripolare impiegando le nozioni ed i termini discussi nel resto del lavoro e ciò utilizzando i termini già esistenti ed i contributi originali.

Nella sezione 5.2 si svolgono simulazioni con lo scopo di confrontare il modello da noi proposto con l'esistente modello Pipe Type che è il punto di partenza per lo sviluppo del nostro modello.

Nell'**Appendice A** si descrive il metodo di collocazione stocastica. Questo metodo consente di analizzare la variazione di una funzione e definire i suoi parametri statistici (media e varianza) quando una o più delle variabili d'ingresso sono casuali ma è nota la loro distribuzione. Ciò è quanto può ottenersi anche con tecniche Monte Carlo ma con molte meno iterazioni (meno di 10 rispetto alle migliaia richieste dal Monte Carlo).

Si discute la derivazione di questo metodo dai polinomi di Lagrange e si mostra come esso

permette d'ottenere alcuni valori delle variabili d'ingresso causali a seconda della loro distribuzione statistica. Di questi valori (detti punti di collocazione) viene valutata la formula, ed alcuni pesi (forniti dal metodo e anch'essi funzione della distribuzione della variabile casuale) vengono usati per valutare la media e la varianza della funzione osservata.

Il metodo può essere impiegato nel nostro caso per l'analisi di sensibilità delle formule dell'impedenza e dell'ammettenza alla variazione dei dati iniziali.

Nell'**Appendice B** i risultati ottenuti per le impedenze dell'anima e dell'armatura tramite il modello proposto e il modello Pipe Type di EMTP-RV sono confrontati.

1. INTRODUCTION

Cables are extensively used for underground alternating current electricity distribution and progressively over longer distances. The proliferation of offshore wind farms which need interconnections with the mainland has also extended their use underwater. For the latter application, and for both low and high voltage, widespread use is made of three-core cables as their fabrication and installation costs are lower than of single-core ones.

Cable networks are affected, though in ways quantitative and qualitative different from the overhead ones, by many transient phenomena due to switching operations, lightning induced over-voltages, presence of harmonic frequencies and others, all with complex wave shapes. A proper analysis of their electromagnetic behaviour requires, therefore, the availability of models that can represent the cables in a large band of frequencies ranging from the industrial ones up to the hundreds of kilohertz.

Models of cables are available in the well-known Electro Magnetic Transient Program software (EMTP-RV) and are achieved in the time-domain. These models are assembled using different techniques but all of them need a precise knowledge of the frequency domain parameters of the cables. To obtain these parameters, namely the impedances and admittances, requires the analysis of the various electromagnetic phenomena which take place inside the cables' conductive and insulating parts.

Now, when compared to overhead lines which are only composed of conductors, cables have a much more complicated structure which also means a more complex geometrical and electromagnetic description. Their impedance is also more frequency dependent, by reason of the presence of different metallic layers.

Cables have been studied for a long time, first for the transmission of signals and then for that of energy at industrial frequencies, therefore many analytical formulations have existed for almost a century; though some effects like the proximity one have received secondary attention. Due to its frequency dependent nature the proximity effect is one of the main focuses of this dissertation.

New technological solutions have also been introduced in their fabrication, such as semi-conducting layers in the insulation and different types of armouring in submarine cables; the electromagnetic effect due to these added materials needs also to be accounted for. Other effects, like the presence of ground and water have been described using approximate formulations.

Much work on all these different subjects has been done in the last 30 years thanks also to the introduction of novel numerical techniques, like for instance the Finite Element Method, facilitated by ever more powerful computers.

The modelling of cable systems in the EMTP software follows two main steps, namely:

- the evaluation of the per unit length (p.u.l.) parameters in the frequency domain input for the second step;
- the representation of the cables systems in the time domain through the use of different models and fitting techniques.

This thesis focuses on the first step and our scope is dual: (a) to analyse the effect of some phenomena not accounted before, and (b) also try to improve the analysis of certain other phenomena already described, an issue that requires the implementation and use of our improved cable in the EMTP-RV environment.

Before dealing with these subjects we first mention the existing technology of cables; then we look at the state of the art of modelling describing in detail the existing models present in the EMTP-RV Cable Data module.

The EMTP-RV module Cable Data module calculates the cable parameters in the frequency domain; these parameters are then adapted to obtain different models that solve Transmission Line equations.

Every conductor (excepted the ground, that acts as zero volts reference) is described with phase currents and voltages. This means that a single-core cable with sheath has two "phases" and that those with three cores, each having a metallic sheath, plus a common armour have seven "phases". Some line models use the modal domain approach that uncouples the different propagating modes; some others operate directly on phase quantities.

Transmission line models. In Chapter 0 we show how the modal domain allows to uncouple and solve the Transmission Line equations, the modes for an underground cable system are defined. Finally transmission line models used in the EMTP-RV are discussed.

The loop method and single-core cables. In order to evaluate the impedances and admittances, the loop method is used. First introduced in [**1**] [**2**], this method consists in applying Kirchoff's laws to the individual different loops formed between each pair of conductors and use for this description loop voltages and currents; loop voltages are simply voltages between conductors, loop currents are surface currents defined ad-hoc in order to separate the electromagnetic effects of the different loops.

For a single-core cable, two loops are hence defined: one between core and sheath and a second between sheath and ground. In this way the effect of the surface impedance of conductors, the external inductance in the insulation and the admittance between conductors are correctly represented and accounted for. Transforming the quantities to the phase domain is straightforward and permits the evaluation of each term of the phase impedances and admittances matrices, as a sum of partial impedances and partial admittances. We show the electromagnetic derivation of these partial terms using electromagnetic notions and the coaxial theory introduced by Schelkunoff [**3**].

The Pipe Type cable model. The pipe type three-core cable model in the EMTP, first introduced in [**4**] [**2**], makes also use of the loop theory and since the inner cables contained into the pipe are similar in construction to single-core cables, the same formulas are used to build the matrices which in this case are restructured in one "internal matrix" where one additional loop represents the pipe (or armour) conductor.

The effect of the pipe is accounted for in two additional matrices:

- a matrix representing the inner surface of the pipe, that also partly includes the proximity effect due to the current circulating in the inner conductors;
- a matrix representing the shielding effect of the pipe and the skin effect present on its outer surface.

As mentioned, the pipe inner surface matrix partly includes the proximity effect. A theory for this effect was developed by Tegopoulos and Kriezis in [**5**] [**6**] and was further elaborated in [**7**] in order to apply it to cables. At the end of Chapter 0 we detail this theory and illustrate how it can be applied to the calculation of the matrix terms previously mentioned.

The proximity effect. This effect is of great interest to us, and we have developed a method, inspired by the works just cited, that corrects some of the approximations presently used in the literature on the subject, principally the use of one filament to represent a conductor. We also introduce a sort of mutual effect, which accounts for the proximity effect between all conductors. The method, which is semi-analytical, uses the dual concept of thin-wires and sub-conductors to describe the current density inside the conductors and the eddy currents due to magnetic induction. It is fully developed in Chapter 0 where we also explain how it is practically implemented.

Other effects. The effect due to the presence of semi-conducting layers and that of the ground return are treated in Chapter 4.

The effect of the ground return has been previously studied carefully in many publications, starting with those by Pollaczek [**8**] but other formulations have been given [**1**] [**9**] [**10**], as well for different soil configurations. We illustrate the work of Legrand et al. [**11**] in solving the Pollaczek integral using the Quasi Monte Carlo integration technique. This technique gives very accurate results, with fast computing time.

Since a good model is needed in submarine cables to describe the sea return impedance, we adapt what is described in [**12**] [**13**]. We show how quasi Monte Carlo method can also be used to solve the integrals describing impedances formulations for a two layer soil (i.e. the sea and seabed) upon which the submarine cables are laid.

We also introduce the formulations given by Ametani in [**14**] for the semi-conducting layer and deal with the effect they have on impedances and admittances; the effect on the latter is of greater importance and therefore needs to be included in a global model for both single-core and three-core cables.

The uncertainties. Inaccuracies in the models are introduced by uncertainties in the knowledge of certain of the parameters used in the description of cable systems. Geometrical parameters, like the thickness of insulation, and of metallic layers, are influenced by the manufacture and can be described using a uniform distribution. Many other parameters can vary in real situations and give rise to inaccuracies or uncertainties.

In order to understand how the different uncertainties affect the global model, and the simulations, a probabilistic approach must be taken. To do that we present in the Appendix the technique of stochastic collocation. This method is an alternative to the well known Monte Carlo method, and allows a complex numerical analysis, but with a reduced number of simulations.

The three-core cable model. Chapter 5 summarizes the implementation of a three-core cable model and gives recommendations for transient simulations: the model is then applied to real cable system and some transient simulations are carried out comparing them to other existing ones, in order to show its advantages.

2. A review of existing models of underground cables

2.1. Preface

2.1.1. Introductory definitions

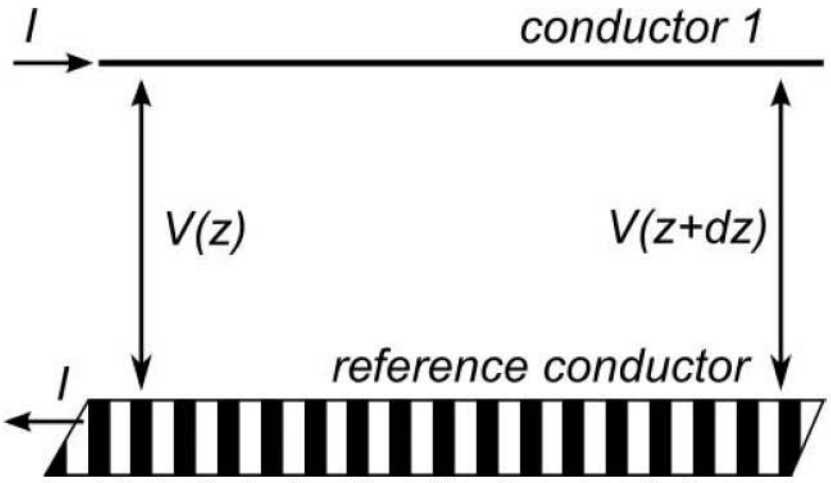

Fig.1 – Single phase line with reference conductor

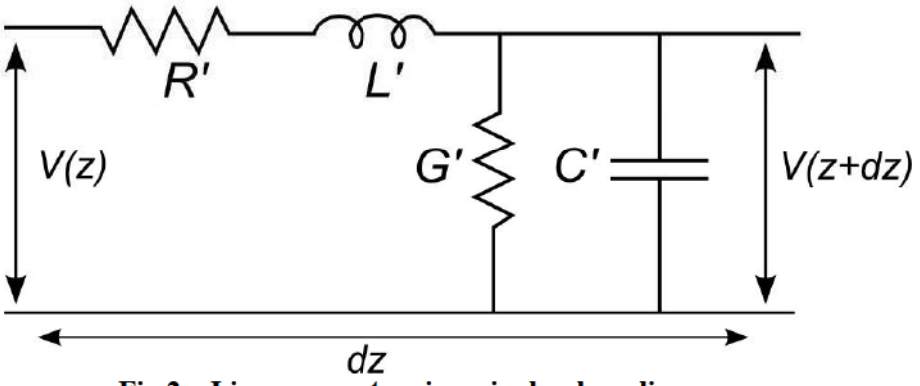

Fig.2 – Line parameters in a single-phase line

In Fig. 1 is shown a single conductor transmission line and the ground which acts as a reference conductor for the voltage and as a return conductor for the current. In our study we shall consider a Transverse Electromagnetic Mode of propagation (TEM). In Fig. 2 we present the equivalent circuit of a transmission line (of infinitesimally longitudinal length *dz*); this circuital representation requires the knowledge of the parameters represented in the figure, that describe the line, namely its per unit length (p.u.l) series impedance $Z = R' + j\omega L'$ and its per unit length shunt admittance $Y = G' + j\omega C'$.

This representation is called the Transmission Line (TL) approach and the system represented here is a single-phase one; a multi-phase system would generally consists of N line conductors plus the reference one, the latter, in real systems, is either the ground or a perfectly conducting plane.

When a multiphase system is considered, its electrical description is given by a matrix representation: currents and voltages are column vectors of dimension *[Nx1]* with N being the number of phases, the p.u.l. impedance and admittance are *[NxN]* matrices. The extra-diagonal terms of these matrices include mutual inductances and capacitances that lead to a coupled system to be solved in order to determine currents and voltages on the different phases. Accurate models based on the Transmission lines are introduced to solve this system and we analyse them in 2.2.

In the case of cable lines models exist of both the single core type that we examine in 0 and the three-core one that we shall analyse in 2.4. The improvement of these models is the main objective of our

thesis.

To evaluate currents and voltages on cables, we use EMTP-RV, namely the Electromagnetic Transient Program Restructured Version, which is a software for the simulation of transients in power systems. It allows representing complicated transmission and distribution networks, with different transmission lines of both the overhead and underground type. For cables various models exist and these shall be described in the next section.

We now give a brief overview of the different components of the cables that interest us, as they have an effect on the evaluation of cable parameters.

2.1.2. Components and installation techniques of Medium and High Voltage Cables

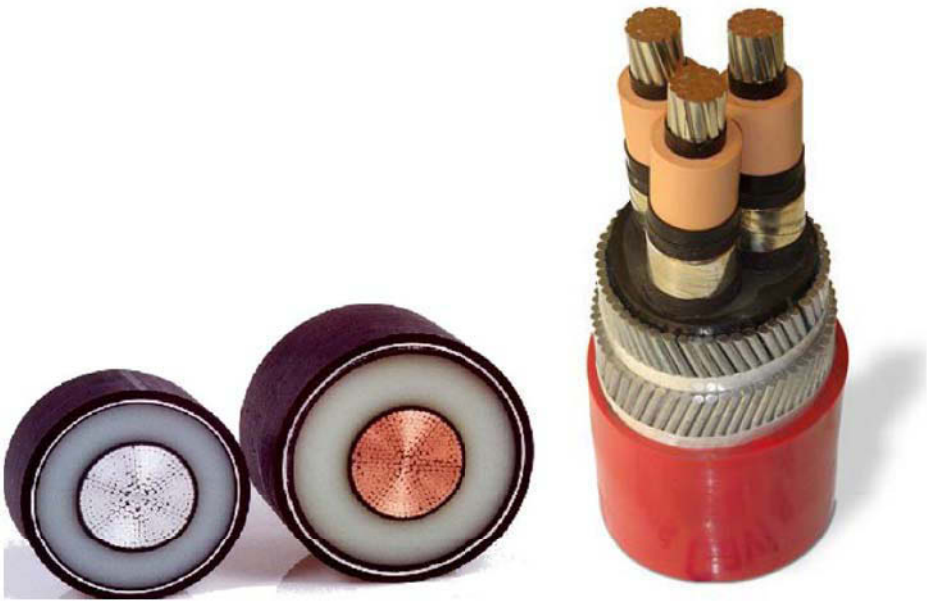

Fig.3 – Two single core cables with Milliken conductors and one submarine three-core cable with double armour

Medium and High Voltage Alternating Current (HVAC) underground and submarine cables generally consist of the following components (as shown in Fig.3 and Fig.4)

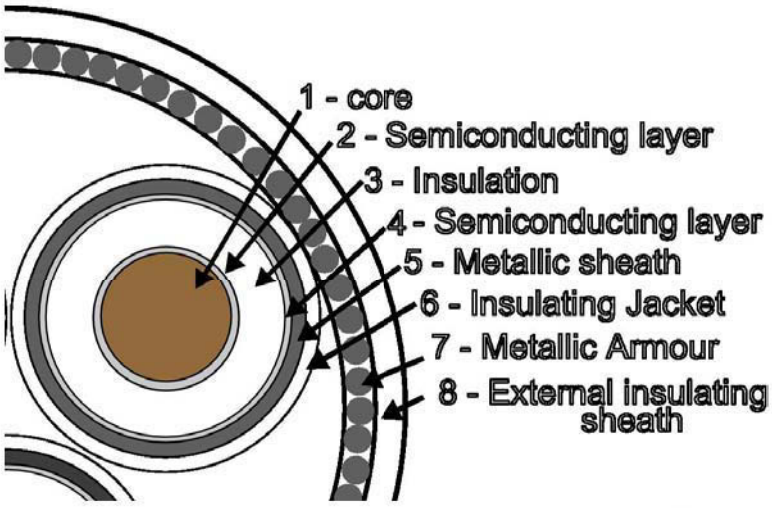

Fig.4 – Components of a submarine three-core cable

Core

Conductors of underground and submarine cables are made of either annealed copper or aluminium[1]; they are solid, round or even oval for the smaller cross-sections, most frequently they are stranded from round wires and submitted to compression in order to reduce the interstices between the strands; for the larger cross sections (greater than at least 1.000 mm^2 for copper and 1.200 mm^2 for aluminium), they are of a segmental-stranded (also known as Milliken) design. In the latter design the conductors are composed of some 5 to 7 segment-shaped sub-conductors spirally laid up into a round conductor and insulated from each other by means of semi-conductive or insulating tape; each sub-conductor is the result of rolling into segment shape a stranded assembly of round wires: each individual wire, as it proceeds along the sub-conductor changes its radial position from close to far of the centre and this considerably reduces the skin effect at industrial frequencies. And an almost complete elimination of the proximity effect at these frequencies is obtained by the spiral assembly of the segments as each conducting wire follows a path alternating between areas close and far away to the other phase conductors.

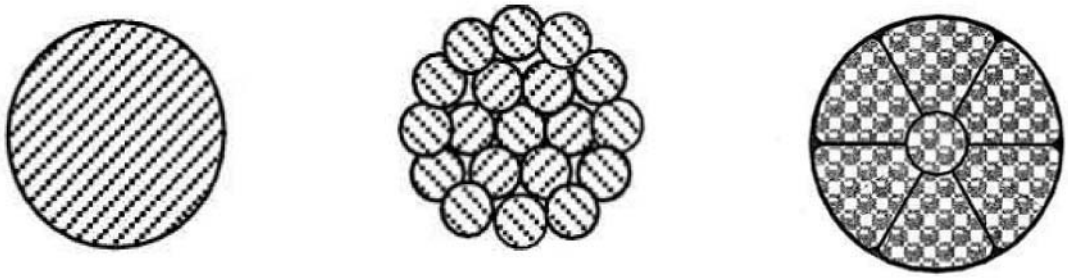

Solid conductor **Stranded conductor** **Milliken conductor**

Fig.5 – Different technologies for the core conductor

Insulation

The insulation must withstand the stress due to very high electric field present between core and metallic screen.

In the past impregnated-paper cable has been used extensively, but its use is now limited to some HVDC cables. Gaseous insulation is also possible, but not used in France.

Most cables for AC transmission used in France (both for medium and high-voltage, underground or submarine applications) use Ethylene Propylene Rubber (EPR), Polyethylene (PE) or Cross Linked Polyethylene (XLPE). Only slightly different in the chemical composition from PE, XLPE withstands a higher operating temperature of 90°C. Its use is now more and more widespread for all voltage levels.

Semi-conductive layer

Due to the high electric field, if small void are present between the insulating layer and the conductors partial discharges develop that can permanently damage the cable. The semi-conductive layer is used to avoid this problem, as well as to make the electric field perfectly radial. It is normally made of XLPE doped with carbon-black [**15**].

Screen

The screen conductor or metallic sheath can be made out of copper wires, aluminium or lead, the latter used in submarine cable for water-tightness. Its main function is to carry short-circuit current, and provide protection from water and electromagnetic interference.

Armour

Present only in submarine cables, it has mainly a mechanical function to sustain the weight of the cable during its laying, and to assure protection, from corrosion and from mechanical shocks. It is normally made out of helical ionised steel wires and can be double in low depth water near shores, to protect the cable from anchors.

[1] The choice depends on many technical and economic factors

Jacket

A further protection layer normally made out of plastic materials like PVC (Polyvinyl Chloride) or other plastics. In underground cables it is the layer in contact with the ground.

Further materials are used in the construction of submarine cables, like swelling tapes for water absorption, metal tapes to allow electric contact between metallic sheaths and the armour, and space fillers.

2.1.2.1. Installation techniques of MV and HV cables

Medium and High voltage cables can be installed in a conduit or laid in the ground.

When for three-phase systems three-single core cables are used two different installation techniques are possible: a triangular configuration and a flat configuration. The different configurations cause a difference in the electromagnetic and thermal coupling between the different cables.

Submarine cables are normally laid directly on the sea/seabed interface. In some cases robots are used to dig in the seabed and bury the cables to protect them from external mechanical aggressions.

2.2. Transmission line equations and relevant models

Models used for underground cables are generally based on transmission line theory and therefore the assumption of transverse electromagnetic (TEM) propagation. The propagation is represented by a propagation constant γ that describes how current/voltage waveforms are attenuated and phase shifted proportionally to the length of the line they cross.

A cable line section is represented by a block composed of two nodes that are the interfaces between the EMTP and the cable model that we shall now describe.

As we shall see in a multiphase line, the relationship between currents and voltages on the different "phases" is not straightforward. If the modal transformation is used, it is possible to mathematically decompose the propagation into a superposition of N modes (N being the number of phases in the system) each one having a characteristic delay and attenuation; each one of these modes is represented using a transfer function $H = e^{-\gamma l}$ (where γ is the propagation constant) and a characteristic admittance Y_c that links currents and voltages of each mode.

The more widespread models are the ones that use the modal transformation. A brief description of phase models[2] is given nonetheless at the end of this chapter, as their use is more and more common.

Transient models need to be valid for a vast range of frequencies and in EMTP-like software two models based on the modal transformation exist:

- A Constant Parameter (CP or Bergeron) model that is valid and correct at one frequency. In the CP the line is supposed to be lossless (the propagation constant only consists in the phase constant beta for each mode) and losses are reintroduced subsequently by lumped resistances.
- A Frequency Dependent (FD or FDQ) model that is valid for a wider range of frequencies. As the propagation constant and characteristic admittance are taken to be frequency-dependent, fitting techniques are employed to represent correctly H and Y_c in the time domain using rational functions.

Since EMTP works in the domain of phases and the Cable Auxiliary routine (the component that implements the cable models) operate in the modal domain, a transformation matrix, i.e. Q, is used to go back and forth between phase and modal domain. In the same way as for the H and Y_c matrices, Q is constant in the CP and FD model, whereas it is considered frequency dependent and fitted with rational functions in the FDQ model.

2.2.1. Multi-conductor transmission line equations

The propagation of current and voltage waves on transmission lines is described in the frequency domain by the two differential equations

$$-\frac{d[V]}{dz} = [Z'][I] \qquad (2.2.1)$$

$$-\frac{d[I]}{dz} = [Y'][V] \qquad (2.2.2)$$

where $[Z']$ and $[Y']$ are the per unit length (p.u.l.) impedances and admittances matrices and $[V]$ and $[I]$ are voltage and current vectors.

Deriving with respect to z and replacing they become

[2]Phase models represent the propagation always using the transmission line equations, and propagation constants, but without uncoupling these equations as done in the modal domain

$$\frac{d^2[V]}{dz^2} = [Z'][Y'][V] \tag{2.2.3}$$

$$\frac{d^2[I]}{dz^2} = [Y'][Z'][I] \tag{2.2.4}$$

In order to solve more easily the multi-conductor transmission line equations it is convenient to use the modal domain approach, because in that domain the p.u.l. parameters are represented by diagonal matrices and therefore the equations linking modal currents and modal voltages are uncoupled and can be solved separately as if each mode equations were describing a single-conductor line.

2.2.2. Generic modal approach to determine propagation modes

In multi-conductor systems the uncoupling of transmission equations (2.2.3) and (2.2.4) makes their solution easier. For this purpose we introduce a diagonalization matrix $[\Lambda]$, such as the equations become:

$$\frac{d^2[V_m]}{dz^2} = [\Lambda][V_m] \tag{2.2.5}$$

$$\frac{d^2[I_m]}{dz^2} = [\Lambda][I_m] \tag{2.2.6}$$

The elements of $[\Lambda]$ are the eigenvalues of the matrix product $[Z'][Y']$, whereas its eigenvectors constitute the voltage transformation matrix $[T_v]$ which in turn allows the definition of the modal voltages V_m and currents I_m:

$$[V] = [T_v][V_m] \qquad [V_m] = [T_v]^{-1}[V] \tag{2.2.7}$$

$$[I] = [T_i][I_m] \qquad [I_m] = [T_i]^{-1}[I] \tag{2.2.8}$$

where $[T_i]^t = [T_v]^{-1}$

Similarly, modal impedances and admittances can be defined:

$$[Z_m] = [T_v][Z][T_i]^{-1} \quad [Y_m] = [T_i][Y][T_v]^{-1} \tag{2.2.9}$$

The equations are now uncoupled, since matrix $[\Lambda]$ is diagonal and its diagonal terms are the square of the propagation constants γ_{mi} of the different modes.

$$\frac{d^2V_{mi}}{dx^2} = \lambda_i V_{mi} \text{ with } \lambda_i = \gamma_{mi}^2$$

The modal characteristic impedance can be obtained as

$Z_{cm} = \sqrt{Z_{mi} / Y_{mi}}$ and back in the phase domain the characteristic impedance matrix is $[Z_c] = [T_v][Z_{cm}][T_i]^{-1}$

2.2.2.1. Fortesque transform

The Fortesque transformation introduces symmetrical components. It can be applied only if the matrices of the line parameters are symmetrical, i.e. that all self-impedances are the same and all mutual impedances are the same; in this case the line is said to be balanced, and equations can be transformed using a constant (frequency independent) transformation matrix.

The transformation matrix is complex and in three phase systems is:

$$S = \frac{1}{\sqrt{3}}\begin{bmatrix} 1 & 1 & 1 \\ 1 & a^2 & a \\ 1 & a & a^2 \end{bmatrix} \tag{2.2.10}$$

where $a = e^{j\frac{2}{3}\pi}$. The components can be obtained as:

$$V = SV_{sym}$$
$$V_{sym} = S^{-1}V \tag{2.2.11}$$

and the transmission equations expressed using the symmetrical components are uncoupled:

$$-\frac{dV_0}{dx} = Z_0 I_0$$
$$-\frac{dV_p}{dx} = Z_p I_p \tag{2.2.12}$$
$$-\frac{dV_n}{dx} = Z_n I_n$$

where the 0, p and n stand for zero, positive and negative sequence.

Only overhead lines can be generally considered balanced, if their conductors are transposed regularly, whereas due to the geometrical arrangement of their conductors, underground and submarine cable lines cannot. For unbalanced overhead and cable lines, the modes have to be determined using a more general approach.

2.2.2.2. Clarke tranforms

Another transformation method is the α , β , 0 method (or Clarke Method). This is the method used in EMTP; its advantage compared to the symmetrical components is that the transformation matrix is real:

$$S = \frac{1}{\sqrt{3}}\begin{bmatrix} 1 & \sqrt{2} & 0 \\ 1 & \frac{-1}{\sqrt{2}} & \frac{\sqrt{3}}{\sqrt{2}} \\ 1 & \frac{-1}{\sqrt{2}} & \frac{-\sqrt{3}}{\sqrt{2}} \end{bmatrix} \tag{2.2.13}$$

The voltages can be transformed as

$$V = TV_{\alpha\beta 0} \quad V_{\alpha\beta 0} = T^{-1}V$$

And the uncoupled equations are:

$$-\frac{dV_0}{dx} = Z_0 I_0$$
$$-\frac{dV_\alpha}{dx} = Z_\alpha I_\alpha \tag{2.2.14}$$
$$-\frac{dV_\beta}{dx} = Z_\beta I_\beta$$

2.2.2.3. Propagation modes in underground cables

As a result of the decomposition mentioned before the total waves propagating on a multi-conductor transmission line can be represented as the superposition of separate propagating modes, being current and voltage waves with different propagation constants.

These modes can be individuated by observing the transformation matrices T_i and T_v described in section 2.2.2.

We add that these modes are only a mathematical representation and are precisely defined only in ideal cases and, as we shall see, the voltage/current modal transformation matrices from which these modes are defined are complex and frequency dependent. The frequency dependency is particularly strong for underground cables (due to the frequency dependence of internal resistances and inductances and to ground return impedance). The propagation also varies depending upon the installation techniques of the cables (see 2.1.2) since the ground return mutual impedances are a function of the mutual position of the individual cables.

We shall show that, in analogy with what is done with three-phase overhead lines, the current modes of a set of three underground cables laid in a flat configuration can be divided in three types of modes, each one representing the path followed by the currents flowing in the three phases of the transmission system [**16**] [**17**]. Since each sheathed cable consists of 2 conductors, there are 6 possible modes which give 6 possible configurations that could be used in practical measurements.

Table 1 – Characteristics of each single-core cable

	Material	Radius
Core	Aluminium	19.6 mm
Insulation	Cross-linked Polyethylene	36 mm
Sheath	Aluminium	37.6 mm
Jacket	Polyethylene	43.6 mm

For three single-core cables with characteristics given in Table 1 laid in both flat and trefoil formation, the cables being 25 cm apart, the evaluation of the transformation matrix T_i and T_v at 1MHz clearly show the different modes in each column.

$$T_{i-flat} = \begin{pmatrix} 1 & 0 & 0 & 0 & 0 & 0 \\ -1 & 0 & 0 & -0.60 & 0.796 & -1 \\ 0 & 1 & 0 & 0 & 0 & 0 \\ 0 & -1 & 0 & 1.12 & 0.854 & 0 \\ 0 & 0 & 1 & 0 & 0 & 0 \\ 0 & 0 & -1 & -0.60 & 0.796 & 1 \end{pmatrix} \quad T_{v-flat} = \begin{pmatrix} 1 & 0 & 0 & -0.302 & 0.398 & -0.5 \\ 0 & 0 & 0 & -0.302 & 0.398 & -0.5 \\ 0 & 1 & 0 & 0.563 & 0.427 & 0 \\ 0 & 0 & 0 & 0.563 & 0.427 & 0 \\ 0 & 0 & 1 & -0.302 & 0.398 & 0.5 \\ 0 & 0 & 0 & -0.302 & 0.398 & 0.5 \end{pmatrix}$$

$$T_{i-trefoil} = \begin{pmatrix} 1 & 0 & 0 & 0 & 0 & 0 \\ -1 & 0 & 0 & -0.578 & 0.816 & -1 \\ 0 & 1 & 0 & 0 & 0 & 0 \\ 0 & -1 & 0 & 1.15 & 0.816 & 0 \\ 0 & 0 & 1 & 0 & 0 & 0 \\ 0 & 0 & -1 & -0.578 & 0.816 & 1 \end{pmatrix} \quad T_{v-trefoil} = \begin{pmatrix} 1 & 0 & 0 & -0.289 & 0.40 & -0.5 \\ 0 & 0 & 0 & -0.289 & 0.40 & -0.5 \\ 0 & 1 & 0 & 0.577 & 0.40 & 0 \\ 0 & 0 & 0 & 0.577 & 0.40 & 0 \\ 0 & 0 & 1 & -0.289 & 0.40 & 0.5 \\ 0 & 0 & 0 & -0.289 & 0.40 & 0.5 \end{pmatrix}$$

The current transformation matrices are the easier to interpret. We can see that we always find 3

coaxial modes (one for each cable), one inter-sheath mode, one 0-sequence (or common) mode with injection on the sheaths and one bifilar mode. A graphical representation of the different modes is given in Fig.6.

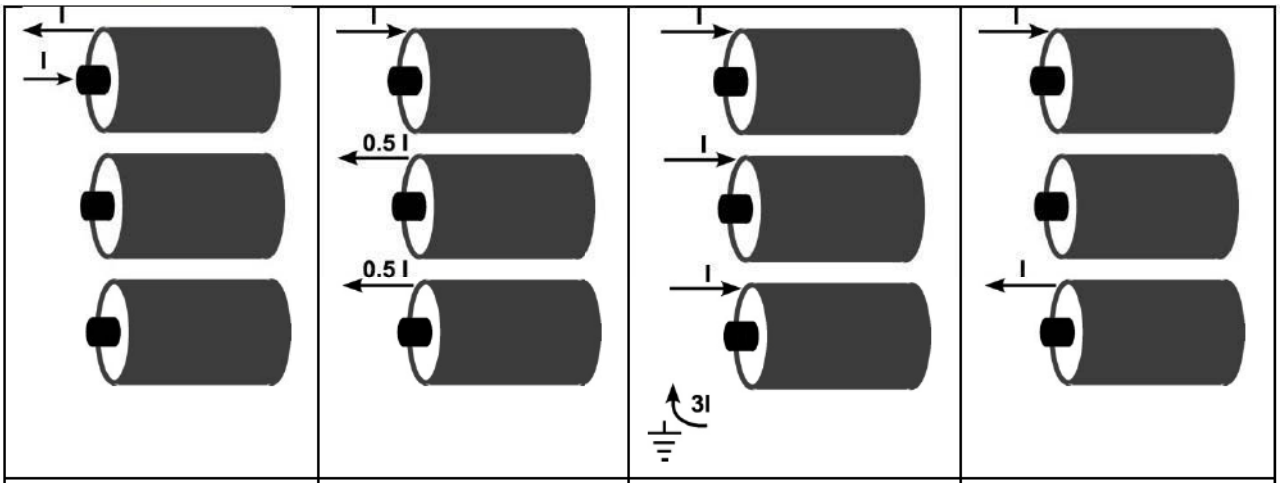

Coaxial mode	Inter-sheath mode	0-sequence mode	Bifilar mode

Fig.6 – Current modes in three single-core cables laid together in flat or trefoil formation

2.2.3. Solution for one mode or single phase line

If we consider a single phase line, or one of the modal equations obtained before, phase voltages and currents (or modal voltages and currents) are scalars and a solution to the TL equations can be found as a combination of a forward and a backward travelling wave:

$$V = V_+ e^{-\gamma z} + V_- e^{\gamma z} \tag{2.2.15}$$

$$I = I_+ e^{-\gamma z} + I_- e^{\gamma z} \tag{2.2.16}$$

here $\gamma = \sqrt{Z'Y'}$ is the propagation constant, that can also be written as $\gamma = \alpha + j\beta$, α and β being termed the attenuation and the phase constants respectively; V_+ V_- I_+ I_- are the forward and backward voltages and currents constants. Defining the characteristic admittance as $Y_c = \sqrt{(Y'Z')^{-1}}Y'$ (2.2.15) can be rewritten as:

$$V = Y_c^{-1}\left(I_+ e^{-\gamma z} - I_- e^{\gamma z}\right) \tag{2.2.17}$$

These expressions can be manipulated in order to obtain $Y_c V + I = 2e^{-\gamma z} I_+$

2.2.4. Nodal equations

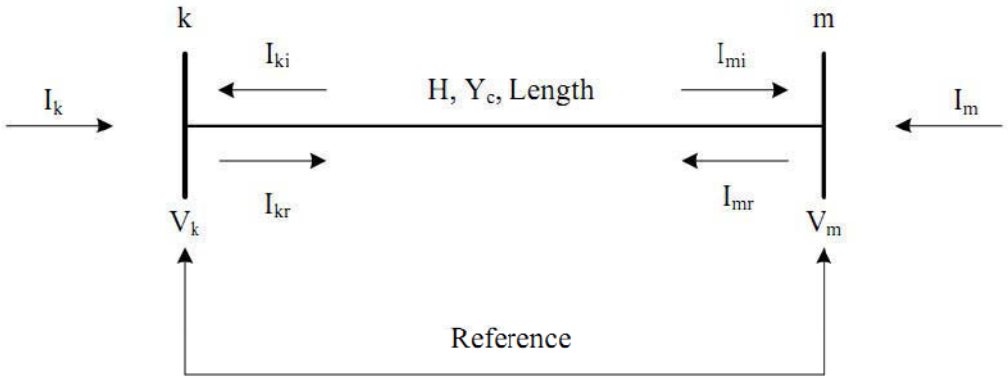

Fig.7 – Single phase line of length L between two nodes (k and m) with impinging current waves, adapted from [18]

We can see in the scheme of Fig.7 two nodes that allow us to set boundary conditions for a transmission line of length l.

I_k, I_m, V_k, V_m are currents and voltages at the two nodes; I_{ki}, I_{kr}, I_{mi}, I_{mr} are the incident and reflected currents at nodes k and m; using this representation it is possible to obtain the two nodal equations.

$$I_m = Y_c V_m - H(Y_c V_k + I_k) \tag{2.2.18}$$

$$I_k = Y_c V_k - H(Y_c V_m + I_m) \tag{2.2.19}$$

with $H = e^{-\gamma l}$.

Analogue equations can also be written for nodal voltages, and their expression is:

$$V_m = Z_c I_m + H^t(Z_c I_k + V_k) \tag{2.2.20}$$

$$I_k = Z_c I_k + H^t(Z_c I_m + V_m) \tag{2.2.21}$$

These are the two equations at the basis of the EMTP-RV distributed transmission line models.

2.2.5. Popular models used in the software EMTP-RV

We shall shortly describe the different time models used in the EMTP-RV (but as well in other Electromagnetic transient simulation softwares) for underground cable description.

Of the two representations of a transmission line - that using distributed parameters and that using lumped parameters - only the former is based upon the travelling wave theory **[19]** **[20]** and includes therefore the notion of propagation. It is the one to be used for better accuracy. As a matter of fact the use of a lumped model, shown in Fig. 8 would not permit the consideration of the frequency dependence of the parameters.

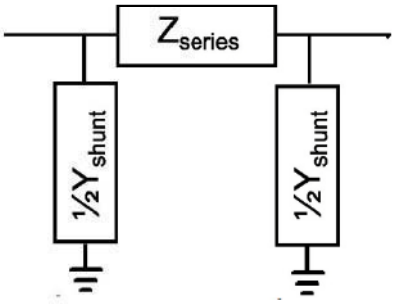

Fig.8 – PI model for a single phase transmission line

The different distributed parameters models used in the EMTP, namely CP (Constant Parameters), FD (Frequency Dependent) and FDQ differ in the way they treat the parameters.

All these model start though from the same assumptions and they work in the time domain.

Consequently, equations (2.2.18)(2.2.19) must be transformed in that domain, where they become convolutions

$$i_k = y_c * v_k - h * u_m \tag{2.2.22}$$

$$i_m = y_c * v_m - h * u_k \tag{2.2.23}$$

with $u_m = (y_c * v_m + i_m)$ and $u_k = (y_c * v_k + i_k)$, and the small letter designating the time domain equivalent of the quantities denoted with capital letters in(2.2.18)(2.2.19).

Since the recursive convolution would need to keep in memory all the values of voltages and currents at previous time steps of the time simulation other models have been devised, based on approximations of y_c and h.

2.2.5.1. CP MODEL

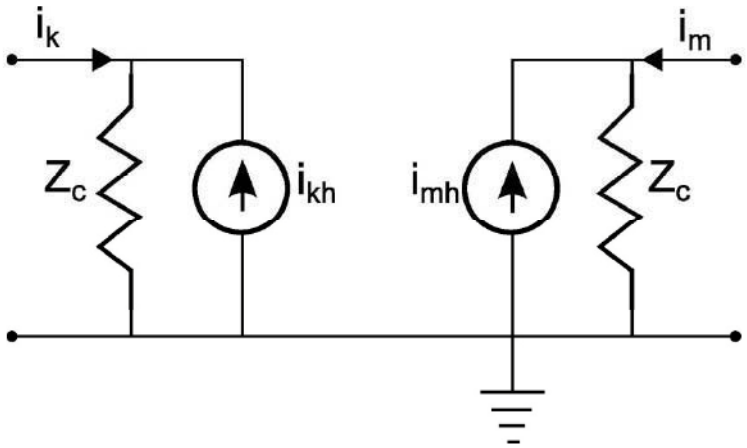

Fig.9 – Bergeron, or "Travelling wave" model

To develop this model nodal voltage equations are used; it is first assumed that the line be perfect, thus having no losses R'= G'=0. If that is the case the surge impedance becomes purely real $Z_c = \sqrt{\frac{L'}{C'}}$ and the function $H = e^{-j\omega\sqrt{L'C'}l}$ only introduces a phase shift, which in the time domain results in a delay. Nodal equations (2.2.20)(2.2.21) can be now written as:

$$v_m(t) = Z_c i_m(t) + \left(Z_c i_k(t-\tau) + v_k(t-\tau)\right) \tag{2.2.24}$$

$$v_k(t) = Z_c i_k(t) + \left(Z_c i_m(t-\tau) + v_m(t-\tau)\right) \tag{2.2.25}$$

Where the delay is $\tau = \sqrt{L'C'}\,l$, that is the time for the wave to travel along the line of length l at a speed $v = 1/\sqrt{L'C'}$.

This model is equivalent to what is shown in Fig.9 , namely the Bergeron model [**21**] where two Norton equivalent generators represent the voltage and current values at the preceding time-step, i.e. the "history" needed to calculate the actual values at the other end of the line. The values of the current generators are

$$i_{mh} = \left(i_k(t-\tau) + \frac{v_k(t-\tau)}{Z_c} \right) \quad (2.2.26)$$

$$i_{kh} = \left(i_m(t-\tau) + \frac{v_m(t-\tau)}{Z_c} \right) \quad (2.2.27)$$

In the CP model the parameters are not supposed to be frequency dependent; they are in fact calculated at a single frequency. Whereas the inductance and capacitance are distributed, as in the lossless Bergeron model that we just described, the resistance is reintroduced after the model is generated. To do that the line is split in two halves and the resistance is lumped in three points, namely entrance, middle and end of the cable section; this resistance is calculated at a given frequency.

Since the model needs not to have some fitting procedures, but only modal transformations, it is faster compared to the frequency dependent models, but only precise if the phenomena to be analysed do not cover a too large bandwidth.

2.2.5.2. FDQ-Time domain

Firstly developed by Semlyen [**22**] and Ametani [**23**] and then by JR Marti [**24**]and L Marti [**25**] [**26**] frequency dependent models allow to represent the variations of the cables parameters in the frequency domain.

The basis of these models is always the Bergeron model, shown in section 2.2.5.1 but:

- The line is not supposed to be lossless.
- The Tv , Y_c and H matrices are not constant with the frequency.

The convolutions present in equations (2.2.22)(2.2.23) that appear in the time domain cannot be avoided, nor can the simplification due to the lossless line present in the CP model; it is therefore necessary to use recursive techniques in order to calculate them.

In the FD model, see [**24**], the transformation matrix T_v which allows to transform the quantities in the modal domain (this matrix can also be called Q, thus the FDQ) is considered to be non-frequency-dependent, but instead constant and real.

In the FDQ, the Transformation matrix T_v (or Q) is also fitted and so are the propagation functions H and Y_c. All these functions are approximated using rational functions obtained through Bode asymptotic fitting techniques.

The fact of having approximated the propagation function and the admittance matrices using rational functions permits to obtain the convolutions needed when integrating using the trapezoidal method.

The fitting has to be done in the modal domain, so that the matrices are diagonalized and have a smooth form, since modes have different speeds, which combine themselves in the time domain.

The fitting introduces approximations errors, which, in the case of the FDQ, also affects the modal transformation matrix. Details are given in [**27**].

2.2.6. Phase domain models

The fitting procedures used in modal domain models may introduce approximations. Models have been developed that fit the parameters directly in the phase domain [**28**].

A phase domain method was implemented by Noda Nagoya and Ametani in [**29**]. In this method an Auto-regressive moving average is used, which minimizes computation; here the elements of H and Z are fitted in the z-domain (or delay domain) and time delays are obtained from the modes. The model is dependent on the time step used in the simulation because the z domain is used.

A different model which is implemented in EMTP-RV together with the FDQ is the so called Universal line model by Morched et al. [**30**] (named Wideband in the EMTP-RV implementation).

This model uses vector fitting [**31**] in order to obtain a least square approximation, i.e. a function can be approximated using the following form:

$$f(s) = \sum_{n=1}^{N} \frac{c_n}{s - a_n}$$

The quantities c_n and a_n being the residues and the poles and s the Laplace variable.

The model works in the phase domain. One of its peculiarities is the use of the same poles for each mode and also to associate the mode introducing a similar propagation delay.

Some improvements to this model have been introduced by [**27**].

The accuracy of these models depends significantly on the precision of the estimation of the impedance and admittance matrix in the phase domain. This is one of the reason which justifies describing in detail the derivation of these matrices in the next sections.

2.3. Single core cables parameters

In this section we present the calculation of the per unit length parameters of a single-core cable, and this is already somewhat a complex task.

If the propagation in the cable only consists of a TEM mode, the Telegrapher's equations (2.2.1) (2.2.2) can be applied taking into account all conductors: the core, the screen if present and the reference conductor, generally the ground.

The parameters of these equations, namely the series impedances Z and shunt admittances Y are represented by matrices, which have a dimension [NxN] (N being the number of conductors excluding the reference), [$2x2$] in the case of a single core cable. The phase voltages, vectors of dimension [$Nx1$], are referenced to the ground conductor.

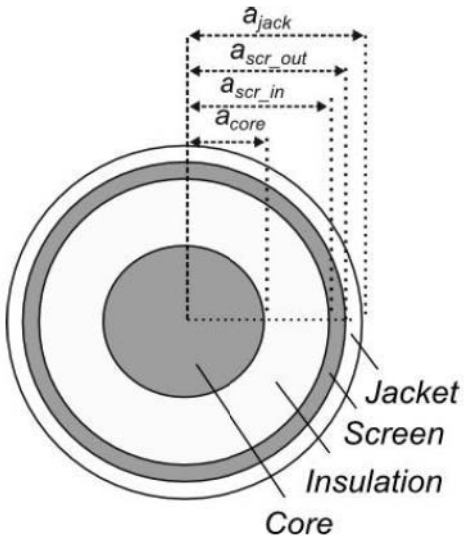

Fig.10: Transversal section of a single-core cable

For the case of a two conductor system (core + sheath) equations (2.2.1)(2.2.2) read:

$$\frac{d}{dz}\begin{bmatrix} V_C \\ V_S \end{bmatrix} = \begin{bmatrix} Z_{CC} & Z_{CS} \\ Z_{SC} & Z_{SS} \end{bmatrix}\begin{bmatrix} I_C \\ I_S \end{bmatrix} \tag{2.3.1}$$

$$\frac{d}{dz}\begin{bmatrix} I_C \\ I_S \end{bmatrix} = \begin{bmatrix} Y_{CC} & Y_{CS} \\ Y_{SC} & Y_{SS} \end{bmatrix}\begin{bmatrix} V_C \\ V_S \end{bmatrix} \tag{2.3.2}$$

2.3.1. Determination principle for the phase impedances and admittances

Let us consider the cable of Fig.10. It has a core with radius a_{core}, an insulating layer, a sheath having internal radius a_{scr_in} and external radius a_{scr_out}, then another insulating layer with external radius a_{jack}.

In order to calculate its distributed parameters one possible approach is the one given by Wedepohl [**1**]. This is partly derived from the coaxial line theory of Schelkunoff [**3**].

The parameters are not evaluated directly, but through the use of loops, that is the cable is split into its layers, in order to account for the different electromagnetic phenomena present.

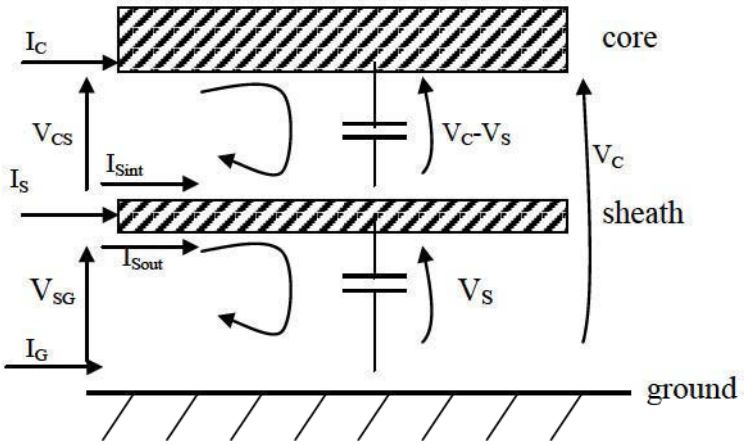

Fig.11: Equivalent circuit for the longitudinal section of a single-core cable [adapted from [2]].

In this case, we consider two loops; these are seen in Fig.11; in one loop the current is injected in the core and returns by the sheath, whereas in the other the current is injected on the sheath and returns by the ground. We define loop currents and voltages, that is I_{Sint} and I_{Sout} , currents on the internal and external surfaces of the sheath, as well as loop voltages V_{CS} and V_{SG} , which are the core-sheath and sheath-ground voltages. The sheaths currents have a physical substance only at high frequency, when the currents effectively flow on the conductors' surfaces, but the loop quantities must always be defined as means to evaluate phase quantities.

On each loop, applying Kirchoff voltage law, we consider the various terms, which take into account different effects:

- $z_{\text{int}-c}$ the core internal impedance accounting for the resistive and inductive nature of the core conductor and also for skin effect [**3**]. Calculations of this term will be shown later;

- z_{iso-cs} and z_{iso-sg} the impedances (purely inductive) due to the varying magnetic flux in the two insulating layers (the one between core and sheath and the one between sheath and ground) ;

- $z_{\text{int}-s}$ the sheath internal surface impedance which accounts for the voltage drop on the internal surface caused by the current circulating on it;

- z_{t-s} the mutual impedance of the sheath, or transfer impedance, representing the voltage drop on the outer sheath surface due to the current circulating on the inner surface or vice versa, this term is due to the imperfection of the sheath shielding;

- z_{out-s} the sheath external surface impedance which accounts for the voltage drop on the external surface caused by the current circulating on it;

- z_g the ground return impedance. This term will be described in Section 4.1 in detail.

To construct the admittance matrix the Kirchoff current law is applied and only two terms are defined, these are:

- y_{cs} core-sheath admittance;

- y_{sg} sheath-ground admittance.

The relation between currents and voltages, obtained with the application of Kirchoff's law in the two loops is:

$$\begin{cases} \dfrac{dVcs}{dz} = I_C z_{\text{int}-c} + I_C z_{iso-cs} - I_{Sin} z_{\text{int}-s} - I_{Sout} z_{t-s} \\ \dfrac{dV_{SE}}{dz} = I_{Sout} z_{out-s} + I_{Sout} z_{iso-sg} - I_E z_g + I_{Sin} z_{t-s} \end{cases} \tag{2.3.3}$$

Knowing that

$$\begin{cases} I_C = -I_{Sin} \\ I_E = -I_{Sout} \\ I_S = -(I_C + I_E) \end{cases} \tag{2.3.4}$$

$$\begin{cases} V_C = V_{CS} + V_{SE} \\ V_S = V_{SE} \end{cases} \tag{2.3.5}$$

The terms of the impedance matrix (2.3.1) can be found as:

$$Z_{CC} = z_{\text{int}-c} + z_{iso-cs} + z_{in-s} - 2z_{t-s} + z_{out-s} + z_{iso-sg} + z_g \tag{2.3.6}$$

$$Z_{CS} = z_{out-s} + z_{iso-sg} + z_g - z_{t-s} \tag{2.3.7}$$

$$Z_{SS} = z_{out-s} + z_{iso-sg} + z_g \tag{2.3.8}$$

In a similar way, writing the currents as a function of the voltages(with currents Kirchoff's law) one finds:

$$\begin{cases} \dfrac{dI_C}{dz} = y_{cs}(V_C - V_S) \\ \dfrac{dI_S}{dz} = y_{cs}(V_S - V_C) + y_{sg} V_S \end{cases} \tag{2.3.9}$$

The terms of the admittance matrix (2.3.2) can be found as:

$$Y_{CC} = y_{cs} \tag{2.3.10}$$

$$Y_{CS} = -y_{cs} \tag{2.3.11}$$

$$Y_{SS} = y_{cs} + y_{sg} \tag{2.3.12}$$

2.3.2. Impedance evaluation

We consider a single-core cable and show, as earlier mentioned, how we can obtain the expressions of

the various terms which form the impedance using the Schelkunoff approach [Shelk].

The evaluation starts with the consideration that the field present in the dielectric and on the surface of the conductors of a coaxial cable can be expressed as a function of the currents circulating in the conductors.

2.3.2.1. Evaluation of the impedances in the dielectric

The inductance can be decomposed in an internal and an external term. The external term derives from the magnetic field flux, which is generated by the currents flowing in the conductors; this flux exists in all the dielectric parts and can be expressed as a function of the magnetic field.

The external inductance can be written as:

$$L_e = \frac{\mu \int_{r_{int}}^{r_{ext}} H_\phi d\rho}{I} = \frac{\mu}{2\pi} \log\left(\frac{r_{ext}}{r_{int}}\right) \qquad (2.3.13)$$

This term allows to find directly $z_{iso\text{-}cs}$ and $z_{iso\text{-}sg}$ that can be expressed as $j\omega L_e$, where in (2.3.13) r_{ext} and r_{int} are replaced respectively with a_{scr_in}, a_{core} to evaluate $z_{iso\text{-}cs}$ and with a_{jack} , a_{scr_out} for $z_{iso\text{-}sg}$.

2.3.2.2. Evaluation of the surface impedances in the conductors

The surface impedance is defined as the ratio between the axial electric field on the conductor's surface and the current flowing on it[3].The losses in the conductors cause a voltage drop (and therefore an electric field) in the axial direction of the conductor, which also implies an axial current density.

If we define $E_{z\text{-}int}$ and $E_{z\text{-}out}$ as the axial electric field on the inner and outer surface of the screen, it is then possible to define:

$$z_{int-s} = \frac{E_{z-int}}{I_{s-int}} \qquad z_{out-s} = \frac{E_{z-out}}{I_{s-out}} \qquad (2.3.14)$$

These are the surface impedances that link the current on the inner/outer surface of the screen conductor with the electric field on the related surface.

$$z_{t-s} = \frac{E_{z-out}}{I_{s-int}} = \frac{E_{z-int}}{I_{s-out}} \qquad (2.3.15)$$

The transfer impedance instead links the current present on the conductor inner surface and the field on the outer surface (or viceversa).This transfer impedance accounts, as earlier mentioned, for the imperfection of the screen or its shielding properties.

Since the cable itself is invariant in the axial direction, the field on the transversal plane does not depend on the z coordinate.

For purpose of clarity we resume the passages presented in [**3**]in order to obtain the expressions needed for the surface impedances.

Maxwell equations in the conductive medium characterised by μ, ε, σ (namely its permeability, permittivity and conductivity) can be written in cylindrical coordinates, in order to correctly represent the cylindrical geometry of the conductor.

It must also be considered that:

[3]It must be stressed that the concept of surface current only has a physical meaning at higher frequencies where the skin depth is very low, whereas at lower frequencies it is only a mathematical construct which allows the calculation of the impedances.

- the coaxial structure assures that the fields do not depend on the angular coordinate;
- the electric field does not have a component in the angular direction.

These considerations allow some simplifications and it is therefore only necessary to write the following equations, as the angular electric field and the axial and radial magnetic field components are null:

$$\frac{\partial H_\phi}{\partial z} = -(\sigma + j\omega\varepsilon)E_\rho \tag{2.3.16}$$

which is the projection of the Maxwell-Ampère law on the ρ axis, whereas

$$\frac{\partial E_z}{\partial \rho} - \frac{\partial E_\rho}{\partial z} = j\omega\mu H_\phi \tag{2.3.17}$$

is the Maxwell-Faraday equation projected on the ϕ axis.

$$\frac{1}{\rho}\left(\frac{\partial(\rho H_\phi)}{\partial \rho}\right) = (\sigma + j\omega\varepsilon)E_z \tag{2.3.18}$$

which is the projection of the Maxwell-Ampère law on the z axis.

In order to obtain a differential equation for the magnetic field, substituting (2.3.16) and(2.3.18) into (2.3.17) we obtain

$$\frac{\partial}{\partial \rho}\left(\frac{1}{\rho}\frac{\partial(\rho H_\phi)}{\partial \rho}\right) + \frac{\partial^2 H_\phi}{\partial z^2} = k^2 H_\phi \tag{2.3.19}$$

with $k^2 = j\omega\mu(\sigma + j\omega\varepsilon)$

The solution of (2.3.19) can be written, by means of variable separation as a purely radial and a purely axial component as:

$$H_\phi = R(\rho)Z(z) \tag{2.3.20}$$

$$\frac{1}{Z}\frac{\partial^2 Z}{\partial z^2} = \gamma^2 \tag{2.3.21}$$

Imposing as a solution for the axial part equation (2.3.21) the constant gamma(that we shall see to be the longitudinal propagation constant) is defined and replacing this in (2.3.19) we obtain

$$\frac{1}{R}\frac{d}{d\rho}\left(\frac{1}{\rho}\frac{d(\rho R)}{\partial \rho}\right) = k^2 - \gamma^2 \tag{2.3.22}$$

that is solution of (2.3.21) gives the exponential dependence of the axial components.

Now, as shown in [3], if every component of the field is written making the exponential dependence explicit (for instance $E_\rho e^{-\gamma z}$ and so on), we obtain the equations

$$E_\rho = \frac{\gamma}{\sigma + j\omega\varepsilon}H_\phi \;,\; j\omega\mu H_\phi = \frac{dE_z}{\rho} + \gamma E_\rho \;,\; \frac{d(\rho H_\phi)}{d\rho} = (\sigma + j\omega\varepsilon)\rho E_z \tag{2.3.23}$$

to analyze what is happening in the conductors we let the permittivity ε be zero and define the intrinsic propagation constant of the medium, namely $\xi = \sqrt{j\omega\mu\sigma}$. Since we are interested in the magnetic field only, we substitute the first and the third equation in the central one, thus obtaining

$$\frac{d}{d\rho}\left(\frac{1}{\rho}\frac{d(\rho H_\phi)}{d\rho}\right)=(\xi^2-\gamma^2)H_\phi \tag{2.3.24}$$

this can be developed into

$$\frac{d^2H_\phi}{d\rho^2}+\frac{1}{\rho}\frac{dH_\phi}{d\rho}-\frac{H_\phi}{\rho^2}=(\xi^2-\gamma^2)H_\phi \tag{2.3.25}$$

The solution of this differential equation in a circular/hollow conductor is given as

$$H_\phi = AI_1(\xi\rho)+BK_1(\xi\rho) \tag{2.3.26}$$

where I_1 and K_1 are the modified Bessel functions of first and second kind and first order. The coefficients A and B will be determined later.

The axial electric field is related to the magnetic field through equation (2.3.23) and can be expressed using Bessel functions properties and the intrinsic impedance of the conductor $\eta=\frac{\xi}{\sigma}$

$$E_z=\eta\left(AI_0(\xi\rho)-BK_0(\xi\rho)\right) \tag{2.3.27}$$

Previously, the surface impedance has been defined as the ratio between electric field on the surface of the conductor and the current circulating on that surface.

We take Fig.10 as the reference, pertaining to the geometry of the system.

2.3.2.3. Core surface impedance

Concerning the solid core (the term $z_{int\text{-}c}$), it must be noted that the modified Bessel function K diverges as its argument goes to 0, therefore when adapting (2.3.26) to this case the coefficient B must be zero.The magnetic field on the core surface can be expressed as:

$$H_\phi(a_{core})=\frac{\boldsymbol{I}}{2\pi a_{core}}=AI_1(\xi a_{core}) \tag{2.3.28}$$

with $\boldsymbol{I}$ the current circulating in the core, $A=\frac{\boldsymbol{I}}{2\pi I_1(\xi a_{core})a_{core}}$ and, from (2.3.27), the electric field as:

$$E_z(r_1)=\eta\frac{\boldsymbol{I}}{2\pi r_1}\frac{I_0(\xi a_{core})}{I_1(\xi a_{core})} \tag{2.3.29}$$

which gives us the expression of $z_{int\text{-}c}$:

$$z_{int-c}=\frac{\eta}{2\pi r_1}\frac{I_0(\xi a_{core})}{I_1(\xi a_{core})} \tag{2.3.30}$$

This term accounts for the losses in the conductor as well as for the skin effect.

2.3.2.4. Screen surface impedances

The screen of the cable is a hollow conductor with internal and external radiuses $a_{scr\text{-}in}$ and $a_{scr\text{-}out}$.

As shown in Fig.11 $I_{S\text{-}int}$ and $I_{S\text{-}out}$ are the screen inner/outer surface currents. We write the electric field on these surfaces as:

$$\begin{aligned}E_z(a_{scr\_in})&=z_{int-s}I_{s-int}+z_{t-s}I_{s-out}\\E_z(a_{scr\_out})&=z_{out-s}I_{s-out}+z_{t-s}I_{s-int}\end{aligned} \tag{2.3.31}$$

If the magnetic field is written on the surface using Bessel functions and also Ampère's Law we have:

$$H_\phi(a_{scr\_in}) = AI_1(\xi a_{scr\_in}) + BK_1(\xi a_{scr\_in}) = -\frac{I_{s-int}}{2\pi a_{scr\_in}} \tag{2.3.32}$$

$$H_\phi(a_{scr\_out}) = AI_1(\xi a_{scr\_out}) + BK_1(\xi a_{scr\_out}) = \frac{I_{S-out}}{2\pi a_{scr\_out}} \tag{2.3.33}$$

(the minus in (2.3.32) is for the current circulation direction)

As before, the coefficients in (2.3.32)(2.3.33) can be found, and replacing them in the electric field expression gives the surface impedances and the transfer impedances defined before:

$$z_{int-s} = \frac{\eta}{2\pi r_2 D}\left[I_0(\xi a_{scr\_in})K_1(\xi a_{scr\_out}) + I_1(\xi a_{scr\_out})K_0(\xi a_{scr\_in})\right] \tag{2.3.34}$$

$$z_{out-s} = \frac{\eta}{2\pi r_3 D}\left[I_0(\xi a_{scr\_out})K_1(\xi a_{scr\_in}) + I_1(\xi a_{scr\_in})K_0(\xi a_{scr\_out})\right] \tag{2.3.35}$$

$$z_{t-s} = \frac{1}{2\pi\sigma a_{scr\_in} a_{scr\_out} D} \tag{2.3.36}$$

Where $D = I_1(\xi a_{scr\_out})K_1(\xi a_{scr\_in}) - I_1(\xi a_{scr\_in})K_1(\xi a_{scr\_out})$

2.3.3. Admittance evaluation

The electric potential between two coaxial cylinders (core and screen) is obtained by integrating the radial electric field:

$$V = \int_{r_{int}}^{r^{ext}} E_\rho d\rho = \gamma I \frac{\log\left(\frac{r_{ext}}{r_{int}}\right)}{2\pi(\sigma + j\omega\varepsilon)} \tag{2.3.37}$$

This potential produces a transverse electric current, due to conduction and displacement phenomena.

$$I_\rho = 2\pi\rho(\sigma + j\omega\varepsilon) = \gamma \boldsymbol{I} \tag{2.3.38}$$

Therefore

$$V = I_\rho \frac{\log\left(\frac{r_{ext}}{r_{int}}\right)}{2\pi(\sigma + j\omega\varepsilon)} \tag{2.3.39}$$

And the admittance can be then written as

$$y = \frac{2\pi(\sigma + j\omega\varepsilon)}{\log\frac{r_{ext}}{r_{int}}} \tag{2.3.40}$$

Where r_{ext} and r_{int} are respectively a_{scr_in}, a_{core} and a_{jack} , a_{scr_out} if we want to evaluate either y_{cs} or y_{sg} and σ and ε are the conductivity and the permittivity of the dielectric. We can rewrite this formula using the loss factor *tan* δ (which is normally more used in the praxis).

$$y = g + j\omega c = (\omega \tan\delta + j\omega)c \tag{2.3.41}$$

2.4. Three-core cables parameters

The scope of this section is to describe the existing models for three-core cables, and introduce part of the theory on which our model is based.

The loop method we have described for the case of single-core cables is used as well in the case of three-core cables. Three-core cables consist mainly in:

- pipe-type cables (oil and gas filled cables);
- some types of submarine cables;
- some types of low voltage cables.

Since a three-core cable is made out of coaxial cables inside a common armour (or pipe) the same formulations developed by Schelkunoff can be used for the core-screen loop.

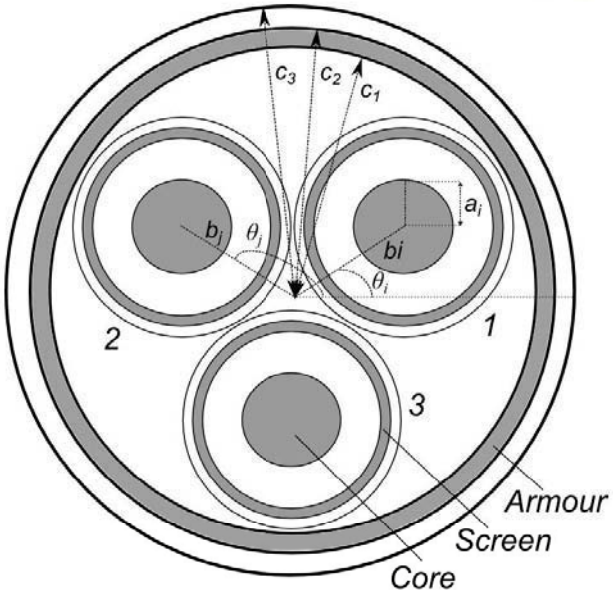

Fig.12 – Geometry of a three-core cable

The armour adds a conductor and this implies globally a 7x7 or 4x4 matrix (depending if the inner cables have or not a metallic screen). Voltages and currents referred to the different conductors follow this relationship

$$\begin{bmatrix} V_{core1} \\ V_{screen1} \\ V_{core2} \\ V_{screen2} \\ V_{core3} \\ V_{screen3} \\ V_{armour} \end{bmatrix} = Z_{tot[7X7]} \begin{bmatrix} I_{core1} \\ I_{screen1} \\ I_{core2} \\ I_{screen2} \\ I_{core3} \\ I_{screen3} \\ I_{armour} \end{bmatrix} \qquad (2.4.1)$$

The global matrix Z_{tot} for the cable of Fig.12 can be constructed, as is detailed in **[2]**, summing the following four matrices, $Z_{tot} = Z_{\text{int}} + Z_{arm-in} + Z_{arm-out} + Z_{ground}$

All the terms contained in the following matrices are detailed in the next section.

$$Z_{\text{int}} = \begin{bmatrix} [Z_{\text{int}1}] & [0] & [0] & 0 \\ [0] & [Z_{\text{int}2}] & [0] & 0 \\ [0] & [0] & [Z_{\text{int}2}] & 0 \\ 0 & 0 & 0 & 0 \end{bmatrix} \tag{2.4.2}$$

with the sub-matrix being equal to (2.3.1), but without the ground-return term that is reintroduced after.

$$Z_{arm-in} = \begin{bmatrix} [Z_{a11}] & [Z_{a12}] & [Z_{a13}] & 0 \\ [Z_{a12}] & [Z_{a22}] & [Z_{a23}] & 0 \\ [Z_{a13}] & [Z_{a23}] & [Z_{a33}] & 0 \\ 0 & 0 & 0 & 0 \end{bmatrix} \tag{2.4.3}$$

with the sub-matrix $[Z_{aij}] = \begin{bmatrix} z_{aij} & z_{aij} \\ z_{aij} & z_{aij} \end{bmatrix}$

$$Z_{arm-out} = \begin{bmatrix} [Z_{c1}] & [Z_{c1}] & [Z_{c1}] & z_{c2} \\ [Z_{c1}] & [Z_{c1}] & [Z_{c1}] & z_{c2} \\ [Z_{c1}] & [Z_{c1}] & [Z_{c1}] & z_{c2} \\ z_{c2} & z_{c2} & z_{c2} & z_{c3} \end{bmatrix} \tag{2.4.4}$$

With the sub-matrix $[Z_{c1}] = \begin{bmatrix} z_{c1} & z_{c1} \\ z_{c1} & z_{c1} \end{bmatrix}$

these are

$$\begin{aligned} z_{c1} &= z_{arm-out} + z_{arm-iso} - 2 \cdot z_{t-arm} \\ z_{c2} &= z_{arm-out} + z_{arm-iso} - z_{t-arm} \\ z_{c3} &= z_{arm-out} + z_{arm-iso} \end{aligned} \tag{2.4.5}$$

$z_{arm\text{-}out}$ and $z_{t\text{-}arm}$ are obtained as in section 2.3.2.4 using instead the radiuses of the pipe

$$z_{arm-out} = \frac{\xi_a}{2\pi c_2 \sigma_a D}\left[I_0(\xi_a c_2)K_1(\xi_a c_1) + I_1(\xi_a c_1)K_0(\xi_a c_2)\right] \tag{2.4.6}$$

$$z_{t-arm} = \frac{1}{2\pi c_1 c_2 \sigma_a D} \tag{2.4.7}$$

with $D = I_1(\xi_a c_2)K_1(\xi_a c_1) - I_1(\xi_a c_1)K_1(\xi_a c_2)$

whereas $z_{arm\text{-}iso}$ is obtained as in section 2.3.2.1 and is

$$z_{arm-iso} = \frac{j\omega\mu}{2\pi}\log\left(\frac{c_3}{c_2}\right) \tag{2.4.8}$$

$$Z_{ground} = \begin{bmatrix} z_g & \cdots & \cdots & z_g \\ \vdots & \ddots & & \vdots \\ \vdots & & \ddots & \vdots \\ z_g & \cdots & \cdots & z_g \end{bmatrix} \tag{2.4.9}$$

The mutual terms (that is, the terms relating core and screen which are not part of the same cable) are not purely inductive as one would expect; this is due to the fact that the phase voltages are referred to the ground, passing through the armour reference, and when the loop method is applied to the global armoured cable both the screen impedance, and the ground return impedance intervene.

We feel now important to stress that whereas the terms of the matrix $Z_{arm\text{-}out}$ are derived as in the Schelkunoff theory, the same does not hold true in the $Z_{arm\text{-}in}$ matrix. The eccentric position of the inner cables inside the armour implies an eddy current distribution which is not uniform along the armour; this distribution depends upon the position of the cables and upon their distance from the screen. This effect is one the main interest of our thesis, and is defined as proximity effect. This effect has to be accounted, together with skin effect, in order to calculate correctly the terms of the $Z_{arm\text{-}in}$ matrix.

We shall explain why the proximity effect is only relevant for the terms z_{aij} and not for the terms in the $Z_{arm\text{-}out}$. When the loop between the conductors and inside the screen is considered, this is equivalent to consider the potential reference, as being on the outer surface of the armour; if this is the case, the current induced in the screen can only flow in the inner surface[4]. This current's distribution on the screen is the reason for the modified impedance of the screen.

As we shall describe later, also the term $z_{int\text{-}c}$ part of the matrix Z_{int} is modified due to the proximity effect induced by other conductors, but this modification is not included in existing EMTP modelling (based on Ametani's model). We will show how Kane handled this problem with the concept of filament, and in the next chapter we will present the theory that we developed to deal with eddy currents and their effect on internal impedances.

We will show how the terms related to the screen are derived, in the following section, and therefore also present the genesis of Ametani's model and Kane's improvement to it.

2.4.1.1. Armour inner surface parameters

We shall first detail the terms present in the matrix $Z_{arm\text{-}in}$.

$$z_{aii} = z^{self}_{a-diel} + z_{arm-in-ij} \tag{2.4.10}$$

$$z_{aij} = z^{mut}_{a-diel} + z_{arm-in-ij} \tag{2.4.11}$$

As we see there are two terms for the matrix which represent the armour impedance terms, these are:

- A purely inductive term $z_{a\text{-}diel}$, whose derivation is detailed in [**32**]and represents the self and mutual inductance between inner cables using the pipe as the reference conductor;
- A term $z_{arm\text{-}in\text{-}ij}$ which represents the cable's armour inner surface impedance.

The second term is the one which interest us, as it includes the proximity effect due to the inner cores. The derivation of this term will be analyzed in the following paragraphs.

$$z^{self}_{a-diel} = \frac{j\omega\mu_0}{2\pi}\ln\left(\frac{c_1^2 - b_i^2}{c_1 a_i}\right) \tag{2.4.12}$$

$$z^{mut}_{a-diel} = \frac{j\omega\mu_0}{2\pi}\ln\left(\frac{b_j}{c_1}\sqrt{\frac{(b_i b_j)^2 + c_1^4 - 2b_i b_j c_1^2\cos\theta_{ij}}{(b_i b_j)^2 + b_i^4 - 2b_i b_j^3\cos\theta_{ij}}}\right) \tag{2.4.13}$$

$$z_{arm-in-ij} = \frac{j\omega\mu_0}{2\pi}\left[\frac{\mu_{r-arm}}{x_1}\frac{K_0(x_1)}{K_1(x_1)} + \sum_{n=1}^{\infty}\left(\frac{b_i b_j}{c_1^2}\right)^n \frac{1}{n(1+\mu_{r-arm}) + x_1\dfrac{K_{n-1}(x_1)}{K_n(x_1)}}\right] \tag{2.4.14}$$

with $x_1 = c_1\xi_a$, $\xi_a = \sqrt{j\omega\mu_a\sigma_a}$ and μ_a , σ_a the permeability and conductivity of the armour conductor

[4] It must again be stressed that the hypothesis of currents circulating purely on the surface are physically only valid at higher frequency, but conceptually these assumptions are used at all frequency to define surface impedances.

2.4.2. Derivation of the inner surface impedance of the armour

A current distribution circulating in the inner conductors induces some eddy currents in the armour, and this in turn modifies the surface impedance of this conductor.

We will show how the current density is obtained in the armour, as well as the magnetic vector potential both in the armour and in the dielectric inside it. This has been discussed starting with the works of Tegopoulos and Kriezis [**5**] [**6**] who have derived the current densities and vector potential expressions for different configurations; the expressions they have obtained have been used both by Brown-Rocamora [**4**], Ametani [**2**] and Kane [**33**] [**34**] [**7**] to obtain impedance analytical formulas.

We shall now analyse into detail the theory of Tegopoulos and Kriezis, as a significant part of it will be the basis of our study.

2.4.3. Description of Tegopoulus and Kriezis approach

2.4.3.1. Summary of the article [5] [6]

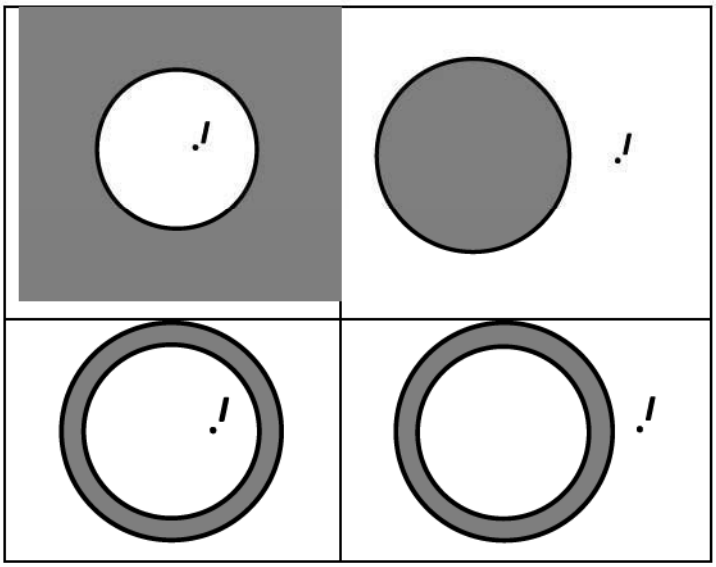

Fig.13 – Different cases treated in [5] [6] - First line: cases with one boundary; second line: cases with two boundaries.

The article is divided into two parts (each subdivided into two sub-cases) that are explained in Fig.13.

- In the first part there is only one boundary between conductor and dielectric:
  - In the second case of the first part a solid circular conductor with a current filament parallel to it is described. This configuration is the basis for the first case treated by Kane which we shall explain in the next paragraph.
  - In the first case of the first part the situation is reversed, i.e. the conductor is taken as infinite and with a hole in which the filamentary current is located. This configuration is the starting point for Ametani's Pipe Type model [**2**].
- In the second part a hollow conductor is described, therefore two boundaries are present; a current filament is always the source of the induction; and more in detail:
  - In the first case of the second part the filamentary current is located inside the hollow conductor. This is the starting point for the second case treated by Kane, also detailed later.
  - In the second case of the second part the filamentary current is located outside the conductor.

The starting hypotheses for the theory are:

- Displacement currents are neglected (low frequency and conductive domain) $\omega\epsilon \ll \sigma$;
- The material is considered as non-ferromagnetic (μ_r is constant and not a function of the magnetic field intensity) ;
- The exciting currents are supposed filamentary, with the current I concentrated in an infinitesimal point;

- Conductor and filament are parallel, of infinite length (edge effects which would be present for a finite length are neglected), the problem is therefore simplified and can be treated in two dimensions, on the transversal section of the conductor;
- Current returns through the conductor, this is equivalent to treat the propagation mode of a coaxial cable.

These hypotheses simplify the way in which the problem is handled.

In order to evaluate the eddy current distribution, the problem is approached using a formulation in terms of vector potential, as with a quasi-TEM line the potential (as well as the current density and the electric field in the conductive regions) has only one component that is oriented along the z direction. The magnetic field angular and radial components are used only for writing continuity conditions.

The potential is evaluated in the different regions (conductive and dielectric medium) and some boundary conditions are imposed on the separation surfaces between the regions; these conditions allow to explicitly write the formulation of the current density in the conductors and to obtain the surface impedance expression.

For our purposes we think it worth to detail two of the cases introduced by Tegopoulus and Kriezis and used by Kane, namely case 2 of part 1 and case 1 of part 2.

Generic expression for the current density

The vector magnetic potential A and current density J inside the conductor are solution of the following differential equation, which is written in the frequency domain, as sinusoidal conditions have been assumed

$$\frac{\partial^2 \vec{J}}{\partial \rho^2} + \frac{1}{\rho}\frac{\partial \vec{J}}{\rho} + \frac{1}{\rho^2}\frac{\partial^2 \vec{J}}{\partial \phi^2} = j\omega\mu\sigma\vec{J} \tag{2.4.15}$$

Its solution can be obtained by use of variable separation as

$$J(r,\phi) = J_1(r)J_2(\phi)e^{j\omega t}\hat{z} \tag{2.4.16}$$

the two differential equations are decomposed as

$$\frac{d^2 J_1}{dr^2} + \frac{1}{r}\frac{dJ_1}{dr} - (j\omega\mu\sigma + \frac{n^2}{r^2})J_1 = 0 \tag{2.4.17}$$

$$\frac{d^2 J_2}{d\phi^2} + n^2 J_2 = 0 \tag{2.4.18}$$

and their respective general solutions are

$$J_1(r) = F_{1n} I_n(r\sqrt{j\omega\mu\sigma}) + C_{1n} K_n(r\sqrt{j\omega\mu\sigma}) \tag{2.4.19}$$

$$J_2(\phi) = F_{2n} sin(n\phi) + C_{2n} cos(n\phi) \tag{2.4.20}$$

These equations can be recombined, in order to have a general solution which is adapted to the case treated, as we shall see in the next paragraphs.

The generic point inside the conductive medium is described by coordinates (r,ϕ) whereas the points in the dielectric are described using coordinates (ρ,θ).

2.4.4. Study of the currents generated in a circular conductor of infinite length, by a parallel current filament.

This paragraph considers the principal elements of the article by Tegopoulos et Kriezis[11] and explains in detail the case of a solid conductor of infinite length having a current flowing parallel to it outside the conductive medium.

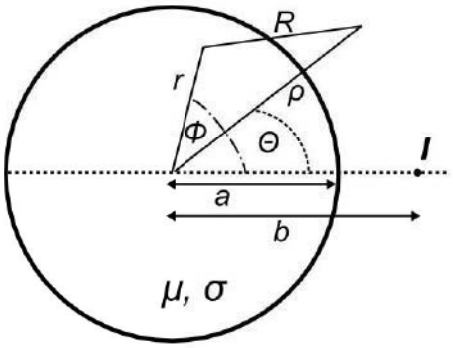

Fig.14 – Transversal section of a circular conductor with a current filament parallel to it

As we see in Fig.14 a solid cylindrical conductor with radius a is taken; the current filament is located at a distance b from the conductor's centre in a dielectric medium having vacuum electrical properties. The conductor has permeability μ and conductivity σ.

Expression of the potential in the different regions.

Inside the conductive medium, the generic solution for the current density can be written as:

$$J(r,\phi)=\sum_{n=0}^{\infty}F_nI_n(r\xi)cos(n\phi) \tag{2.4.21}$$

F_{1n} being an unknown coefficient to be determined and $\xi=\sqrt{j\omega\mu\sigma}$

In the dielectric there are two contributions to the magnetic field (and therefore to the potential), namely.

- one due to the current filament, which writes itself:

$$\vec{A}_I=\frac{\mu_0 \boldsymbol{I}}{2\pi}ln(r)\hat{z}+const \tag{2.4.22}$$

- one due to the current density distribution of the conductor, which is obtained by integrating the contribution of an infinitesimal element of surface of the conductor, namely

$$d^2\vec{A}_\sigma(\rho,\theta)=\frac{\mu_0}{2\pi}J(r,\phi)lnRrdrd\phi \tag{2.4.23}$$

Expression (2.4.23)needs integrating on the surface of the conductor to have the global contribution of the current density to the potential:

$$A_\sigma(\rho,\theta)=\frac{\mu_0}{2\pi}\sum_{n=0}^{\infty}\int_0^a\int_0^{2\pi}F_nI_n(r\xi)ln(\rho)cos(n\phi)rdrd\phi+$$

$$-\frac{\mu_0}{2\pi}\sum_{n=1}^{\infty}\sum_{m=1}^{\infty}\int_0^a\int_0^{2\pi}\frac{1}{m}\left(\frac{r}{\rho}\right)^m F_nI_n(r\xi)(cos(m\phi)cos(m\theta)+sin(m\phi)sin(m\theta))cos(n\phi)rdrd\phi= \tag{2.4.24}$$

$$\mu_0L_0\frac{a}{\xi}ln(\rho)I_1(a\xi)-\frac{\mu_0}{2}\sum_{n=1}^{\infty}L_n\frac{a^n}{n\rho^n}\frac{I_n(a\xi)}{j\omega\mu\sigma}cos(n\theta)$$

and unknown coefficients F_n have been changed to L_n to account for the different medium.

The total potential in the dielectric is

$$A_{diel}(\rho,\theta) = A_I + A_\sigma = \frac{\mu_0 \boldsymbol{I}}{2\pi}\left[lnb - \sum_{n=1}\frac{1}{n}\left(\frac{\rho}{b}\right)^n cos(n\theta)\right] + \\ +\mu_0 L_0 \frac{a}{\xi} ln(\rho) I_1(a\xi) - \frac{\mu_0}{2}\sum_{n=1}^{\infty} L_n \frac{a^n}{n\rho^n}\frac{I_n(a\xi)}{\xi^2} cos(n\theta) \tag{2.4.25}$$

Whereas in the conductive medium we have:

$$A_{cond}(r,\phi) = -\frac{1}{j\omega\sigma}\sum_{n=0} F_n I_n(r\xi) cos(n\phi) \tag{2.4.26}$$

Solution of system and determination of current density coefficients

The following continuity conditions are applied

$$B_{r-cond} = B_{\rho-diel}\,|_{\theta=\phi}^{r=\rho=a} \tag{2.4.27}$$

$$\frac{1}{\mu} B_{\phi-cond} = \frac{1}{\mu_0} B_{\theta-diel}\,|_{\theta=\phi}^{r=\rho=a} \tag{2.4.28}$$

Which are defined as:

$$B_{r-cond} = \frac{1}{r}\frac{\partial A_{cond}}{\partial \phi} \quad B_{\rho-diel} = \frac{1}{\rho}\frac{\partial A_{diel}}{\partial \theta} \tag{2.4.29}$$

$$B_{\phi-cond} = -\frac{\partial A_{cond}}{\partial r} \quad B_{\theta-diel} = -\frac{\partial A_{diel}}{\partial \rho} \tag{2.4.30}$$

Solving these gives the unknown coefficients as:

$$F_n = \frac{\xi \boldsymbol{I}}{2\pi}\frac{\left(\frac{a}{b}\right)^n \frac{1}{a}}{[(1+\mu_r) I_n'(a\xi) - \mu_r I_{n+1}(a\xi)]} \tag{2.4.31}$$

And the current density can be written as:

$$J(r,\phi) = \frac{\boldsymbol{I}\xi}{2\pi}\frac{I_0(r\xi)}{I_1(a\xi)} + \sum_{n=1}^{\infty}\frac{\boldsymbol{I}\xi}{2\pi}\frac{\left(\frac{a}{b}\right)^n \frac{1}{a}}{[(1+\mu_r) I_n'(a\xi) - \mu_r I_{n+1}(a\xi)]} I_n(r\xi) cos(n\phi) \tag{2.4.32}$$

The first term accounts for skin effect and the second one for proximity effect.

The coefficient of the potential is:

$$L_n = \frac{\boldsymbol{I}\xi}{\pi I_{n+1}(a\xi)}\left(\frac{a}{b}\right)^n \frac{1}{a}\frac{\left[\frac{n}{a} I_n(a\xi) - \frac{\xi}{\mu_r} I_n'(a\xi)\right]}{\left[\frac{n}{a} I_n(a\xi) + \frac{\xi}{\mu_r} I_n'(a\xi)\right]} \tag{2.4.33}$$

2.4.5. Study of the currents generated in a hollow conductor of infinite length, by a parallel current filament inside it

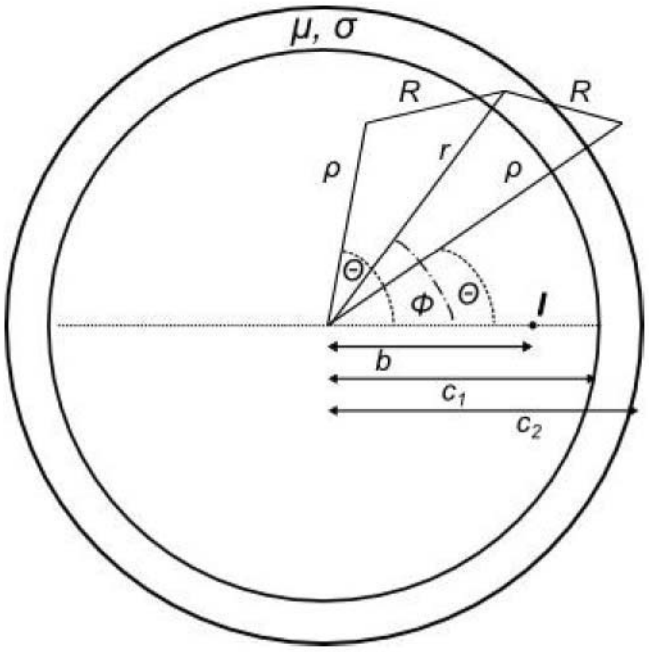

Fig.15 – Hollow conductor with filamentary current inside it

In this second case we consider a hollow conductor, having radiuses c_1 and c_2 as shown in Fig.15 and a current filament inside of it and distant b from the centre of the conductor.

In this case the generic solution for the current density is

$$J(r,\phi)=\sum_{n=0}^{\infty}\left[F_n I_n(r\xi)+C_n K_n(r\xi)\right]cos(n\phi) \tag{2.4.34}$$

The potential in the dielectric is different in the regions inside and outside the hollow conductor.

Inside the hollow conductor it is, as before, made up of two contributions:

- the one due to the current filament A_I

$$A_I(\rho,\theta)=\frac{\mu_0 \boldsymbol{I}}{2\pi}ln(d)=\frac{\mu_0 \boldsymbol{I}}{4\pi}ln(\rho^2+b^2\text{-}2b\rho cos(\theta)) \tag{2.4.35}$$

- the one obtained by integrating the contribution of the current density due to the infinitesimal surface element $d^2A_{\sigma-\text{int}}=\frac{\mu_0}{2\pi}J(r,\phi)lnRrdrd\phi$ between 0 and π and between c_1 and c_2 which we write this as $A_{\sigma-\text{int}}$

  or resumed as $A_{diel-\text{int}}=A_I+A_{\sigma-\text{int}}$

Outside the hollow conductor there is only the contribution of the current density, but the logarithm present in the potential expression has a different form; we write this as $A_{diel-ext}=A_{\sigma-ext}$

$$A_{\sigma-\text{int}}=L_0\bar{L}_0+V_0\bar{V}_0-\sum_{n=1}^{\infty}L_n\frac{\rho^n}{n}S_{1n}\cos(n\theta)-\sum_{n=1}^{\infty}V_n\frac{\rho^n}{n}S_{2n}\cos(n\theta) \tag{2.4.36}$$

with

$$\bar{L}_0 = \frac{\mu_0}{\xi}\left[c_1 ln(c_1) K_1(c_1\xi) - c_2 ln(c_2) K_1(c_2\xi) - \frac{1}{\xi} K_0(c_1\xi) + \frac{1}{\xi} K_0(c_2\xi) \right]$$

$$\bar{V}_0 = \frac{\mu_0}{\xi}\left[c_2 ln(c_2) I_1(c_2\xi) - c_1 ln(c_1) I_1(c_1\xi) - \frac{1}{\xi} I_0(c_2\xi) + \frac{1}{\xi} I_0(c_2\xi) \right]$$

and

$$S_{1n} = \frac{\mu_0}{2\xi}\left[\frac{K_{n-1}(c_1\xi)}{c_1^{n-1}} - \frac{K_{n-1}(c_2\xi)}{c_2^{n-1}} \right] \qquad S_{2n} = \frac{\mu_0}{2\xi}\left[\frac{I_{n-1}(c_2\xi)}{c_2^{n-1}} - \frac{I_{n-1}(c_1\xi)}{c_1^{n-1}} \right]$$

$$A_{\sigma-ext} = L_0\bar{L}_0 + V_0\bar{V}_0 - \sum_{n=1}^{\infty} L_n \frac{1}{n\rho^n} Y_{1n}\cos(n\theta) - \sum_{n=1}^{\infty} V_n \frac{1}{n\rho^n} Y_{2n}\cos(n\theta) \tag{2.4.37}$$

$$Y_{1n} = \frac{\mu_0}{2\xi}\left[c_1^{n+1} K_{n+1}(c_1\xi) - c_2^{n+1} K_{n+1}(c_2\xi) - \right] \qquad Y_{2n} = \frac{\mu_0}{2\xi}\left[c_2^{n+1} I_{n+1}(c_2\xi) - c_1^{n+1} I_{n+1}(c_1\xi) \right]$$

Inside the conductor the potential is obtained from the current density as:

$$A_{cond} = -\frac{1}{j\omega\sigma}\sum_{n=0}^{\infty}\left[F_n I_n(r\xi) + C_n K_n(r\xi) \right] cos(n\phi) \tag{2.4.38}$$

As shown in the paragraph before, continuity conditions must be written, that leads to a system of equations, which allows finding the expression for the unknown coefficients. In this case there are twice the conditions as before, as the hollow conductor has an inner and an outer radius.

The conditions on the internal boundary are:

- $B_{\rho-diel-int} = B_{r-cond}$ (2.4.39)
- $\frac{1}{\mu_0} B_{\theta-diel-\text{int}} = \frac{1}{\mu} B_{\phi-cond}$ (2.4.40)

The conditions on the external boundary are:

- $B_{r-cond} = B_{\rho-diel-ext}$ (2.4.41)
- $\frac{1}{\mu} B_{\phi-cond} = \frac{1}{\mu_0} B_{\theta-diel-ext}$ (2.4.42)

And these components are obtained as:

$$B_{r-cond} = \frac{1}{r}\frac{\partial A_{cond}}{\partial \phi} \qquad B_{\rho-diel} = \frac{1}{\rho}\frac{\partial A_{diel}}{\partial \theta} \tag{2.4.43}$$

$$B_{\phi-cond} = -\frac{\partial A_{cond}}{\partial r} \qquad B_{\theta-diel} = -\frac{\partial A_{diel}}{\partial \rho} \tag{2.4.44}$$

The coefficients obtained for the current density of (2.4.34) are:

$$F_n = \frac{1}{D_n}\frac{\boldsymbol{I}\xi}{2\pi}(P_n + Q_n)\left[\frac{\mu_r n K_n(c_2\xi)}{c_2\xi} + K_n^{'}(c_2\xi) \right] \tag{2.4.45}$$

$$C_n = -\frac{1}{D_n}\frac{\boldsymbol{I}\xi}{2\pi}(P_n + Q_n)\left[\frac{\mu_r n I_n(c_2\xi)}{c_2\xi} + I_n^{'}(c_2\xi) \right] \tag{2.4.46}$$

with $P_n = Q_n = \frac{1}{c_1}\left(\frac{b}{c_1}\right)^n \quad P_0 = \frac{1}{c}\, Q_0 = 0$

$$D_n = \left[\frac{n}{c_1\xi}(\mu_r - 1)I_n(c_1\xi) - I_{n+1}(c_1\xi)\right]\left[\frac{n}{c_2\xi}(\mu_r + 1)K_n(c_2\xi) - K_{n+1}(c_2\xi)\right] + \\ -\left[\frac{n}{c_2\xi}(\mu_r + 1)I_n(c_2\xi) - I_{n+1}(c_2\xi)\right]\left[\frac{n}{c_1\xi}(\mu_r - 1)K_n(c_1\xi) + K_{n+1}(c_1\xi)\right] \tag{2.4.47}$$

which allows to write the expression of the current density, replacing (2.4.45) and (2.4.46) into (2.4.34).

Also the potentials in the dielectric must be written, in order to be able, as we will show, to evaluate impedances, using Faraday Law. The coefficients of the potential are:

$$L_n = \mu_0 \frac{1}{\xi}\frac{Y_{2n}}{c_1^{n-1}[S_{1n}Y_{2n} - Y_{1n}S_{2n}]}\left[\frac{\mu_r n}{c_1\xi}\left(F_n I_n(c_1\xi) + C_n K_n(c_1\xi)\right) - \frac{\boldsymbol{I}\xi}{2\pi}Q_n\right] + \\ -\mu_0 \frac{1}{\xi}\frac{c_2^{n+1}S_{2n}}{[S_{1n}Y_{2n} - Y_{1n}S_{2n}]}\left[\frac{\mu_r n}{c_2\xi}\left(F_n I_n(c_2\xi) + C_n K_n(c_2\xi)\right)\right] \tag{2.4.48}$$

$$V_n = \mu_0 \frac{1}{\xi}\frac{c_2^{n+1}S_{1n}}{[S_{1n}Y_{2n} - Y_{1n}S_{2n}]}\left[\frac{\mu_r n}{c_2\xi}\left(F_n I_n(c_2\xi) + C_n K_n(c_2\xi)\right)\right] + \\ -\mu_0 \frac{1}{\xi}\frac{Y_{1n}}{c_1^{n-1}[S_{1n}Y_{2n} - Y_{1n}S_{2n}]}\left[\frac{\mu_r n}{c_1\xi}\left(F_n I_n(c_1\xi) + C_n K_n(c_1\xi)\right) - \frac{\boldsymbol{I}\xi}{2\pi}Q_n\right] \tag{2.4.49}$$

2.4.6. Impedances' evaluation

The method put forth by Tegopoulos and Kriezis in their publication has been used by Brown Rocamora and successively Ametani to obtain impedance formulations, for the configuration of a cable with an eccentric inner conductor.

In this case the authors considered the hollow conductor, which represents the pipe of a pipe-type cable, as having an infinite outer layer (this is Case 1 of [**5**]) which we did not detail.

2.4.6.1. Two parallel circular conductors

We analyze here how the impedance is evaluated for the case of two parallel conductors, namely what we detailed in paragraph 2.4.4 which has been developed by Kane [**7**].

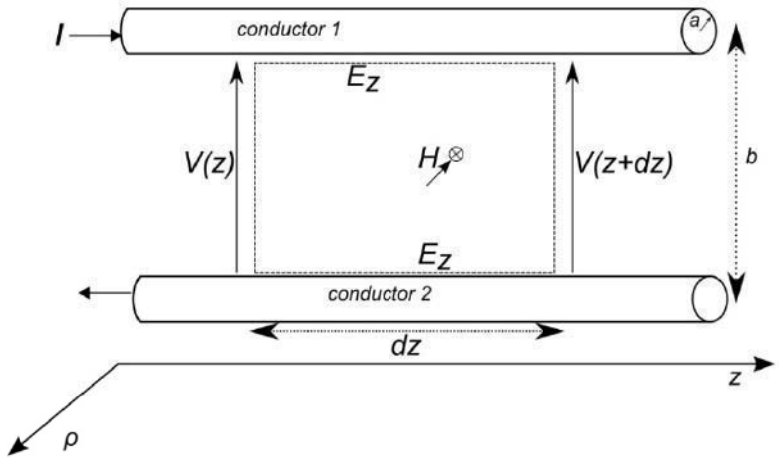

Fig.16 – Description of the loop formed by the conductor of which we want to represent the impedance, and conductor 2 which is represented by a filament

The loop described in Fig.16 allows writing the following expression

$$-\frac{dV(z)}{dz} = Z_{loop} I$$
$$Z_{loop} I = \frac{d\phi_{loop}}{dt} + \vec{E}_{z1}(a,\theta) \qquad (2.4.50)$$

that is Faraday law with the inclusion of the axial electric field which represents the losses in the conductor and the voltage drop that it introduces. θ is the generic angle.

This expression is developed in the frequency domain as

$$-\frac{dV(z)}{dz} = j\omega\left[\vec{A}_{diel}(a,\theta) - \vec{A}_{diel}(b,0\ )\right] + \vec{E}_{z1}(a,\theta) \qquad (2.4.51)$$

where the potential A_{diel} is the total potential present in the dielectric from equation (2.4.25)

It must be noted that in the figure, conductor 2 corresponds to the one that is represented by a filament in the situations described before; for this reason no losses are present on the second conductor in equation (2.4.50). The axial electric field is obtained by the current density with the following relation

$$E_z(\rho,\theta) = \frac{1}{\sigma} J\ (\rho,\theta) \qquad (2.4.52)$$

Developing these expressions with the terms given before allows obtaining the expression

$$Z_{loop} = \frac{\xi}{\sigma}\frac{\boldsymbol{I}}{2\pi a}\frac{I_0(\xi a)}{I_1(\xi a)} + \frac{j\omega\mu}{\pi}\boldsymbol{I}\sum_{n=1}^{\infty}\frac{I_n(\xi a)}{\left[n(1+\mu_r)I_n(\xi a) + \xi a I_{n+1}(\xi a)\right]}\left(\frac{a}{b}\right)^{2n}$$
$$+\frac{j\omega\mu_0}{2\pi}\ln\left(\frac{b^2-a^2}{ba}\right) \qquad (2.4.53)$$

In this expression the first term is the classic Schelkunoff term, which expresses the skin effect, the second term is the proximity effect, which is dependent on frequency, the electrical parameters and the ratio of radius to distance; the last term is the external inductance.

In a similar manner it is possible to express the impedance in the other cases that have been described.

2.4.6.2. Eccentric solid conductor inside a hollow conductor

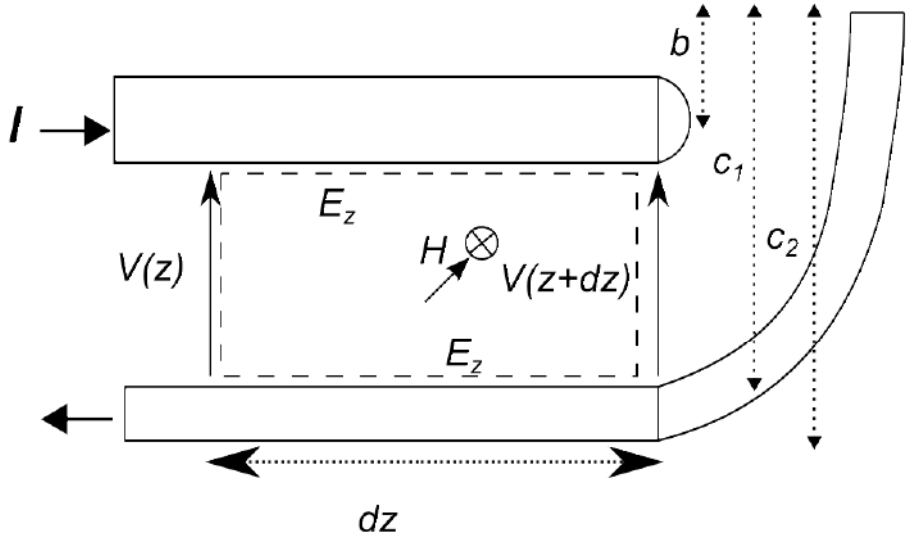

Fig.17 – Loop for the evaluation of the impedance in a cable with eccentric inner conductor represented by a filament

If equation (2.4.50) is applied to this case (described by Fig.17) in order to obtain the impedance of the loop, again considering the inner conductor to be filamentary so that its impedance is null, one obtains:

$$Z_{loop} = \frac{1}{\sigma}\left[F_0 I_0(c_1\xi) + C_0 K_0(c_1\xi)\right] + \\ + \frac{1}{\sigma}\sum_{n=1}^{\infty}\left(\frac{b_i}{c_1}\right)^n \left[F_n I_n(c_1\xi) + C_n K_n(c_1\xi)\right] + \\ + \frac{j\omega\mu_0}{2\pi}\ln\left(\frac{c_1^2 - b_i^2}{c_1 a_i}\right) \qquad (2.4.54)$$

The first term is the skin effect part of the surface impedance of the armour/pipe; the second term the proximity term part and the third the external inductance. The terms F_n and C_n have been detailed in equations(2.4.45)(2.4.46).

3. Improved method for the calculation of cable internal impedances

3.1. Synthesis of the method proposed

As mentioned in the introduction the principal aim of this thesis is to present a method for the calculation of cables impedances, which takes into account the eddy currents induction, and consequently skin and proximity effect. The purpose is to improve the present method of calculating these quantities, [1] where the proximity effect is taken into account[5] only partially.

As a matter of fact, the proximity effect may have a significant consequence on the value of the self-impedances of the cables and particularly of submarine cables, since in these the various conductors are very close to each other.

We shall proceed by first considering a configuration of two cylindrical parallel conductors which proximity causes induction to one another. The theoretical approach which we derive for this case will be then extended to the case of hollow conductors (such as cable sheaths and armours).

The proximity effect depends upon the same induction mechanism that causes skin effect and therefore is dependent upon the conductive media electrical characteristics, the geometry of the system and the frequency. It will be represented as additional terms which intervene in the calculation of the self-impedance of a cylindrical conductor.

Maxwell's equations, adapted to our case, will include the magnetic flux variation and the axial electric field, both written in terms of magnetic vector potential and current density: for this reason we calculate the two latter quantities. This we do using an electromagnetic approach and the quasi-TEM propagation assumption (two conductors are initially considered, and one is the return for the current flowing in the other one).

Since Maxwell equations cannot be solved in the heterogeneous medium formed by the conductive and dielectric ones, we need to express the magnetic field inside and outside the conductors and write some continuity conditions on the boundary between each conductor and the dielectric.

In previous publications **[2]** **[5]** **[6]** **[4]** **[7]**, that we have described in some detail in the previous chapters, the conductor, source of the excitation, is represented by a current filament, or thin wire, that is a flow of current having no transversal dimensions and parallel to the conductor considered. This allows the authors to obtain the current distribution density in the considered conductor as a function of the current filament intensity: the current filament is purely the source of the induction.

In our approach, since we want to represent the mutual induction, we split the conductors in a number of sub-conductors; these are small enough to be represented as thin wires when they serve as source, but they act as sub-conductors with a surface and can be target of the induction.

[5] The proximity effect is considered by Ametani in the calculation of the impedance of the pipe with respect to the inner conductor's proximity. This is done with two approximations, namely the use of the current filament approximation, and the assumption that the pipe is thick enough (with respect to skin penetration depth) and can be therefore be treated as having an infinite outside radius.

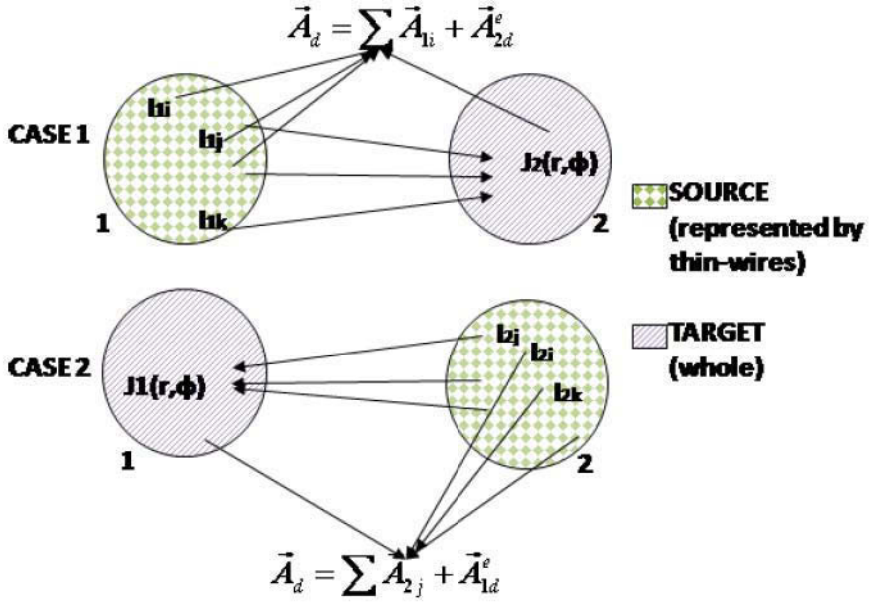

Fig.18 – Dual nature of the conductors, being source and target of the induction

The approach is therefore dual as represented by Fig.18. When conductor *1* is considered to be the target we represent it as whole, and the conductor 2, cause of the induction, is represented by a multitude of thin wires, each filament *"j"* having an unknown current intensity I_{2j}. Vice versa when conductor *2* is considered the target, conductor 1 is represented by currents on a number of filaments *"i"* having unknown current intensity I_{1i}.

We shall impose the current from conductor 1 to be returning in conductor 2, furthermore the sum of the thin wires current intensities gives the total current circulating in the conductor.

To proceed, in a first step the current density and vector potential will be represented with expressions containing thin wires unknown current intensities. These intensities will then be calculated in a successive step.

The procedure used to calculate vector potential and current density is based on the following steps:

- Generic expressions for vector potential *A* and current density *J* are derived.

- The currents in the above mentioned thin wires, which cause induction, have intensities corresponding to the value of the current density, calculated in the point occupied by the wire, and multiplied by the surface of the sub-conductor. The sum of these currents gives the total current I, which is imposed as flowing in the conductors. This is also equivalent to the current density, yet to be determined, integrated on the surface of the conductor.

- The magnetic vector potential is calculated inside and outside the conductor and is due to different contributions:

Outside the conductor, we consider:

- The contribution of the thin wires in one of the conductors, at a point in the dielectric (this is when the conductor is considered to be the source of the induction);

- The contribution in the dielectric, due to the expression of *J* that is established in the second conductor as a consequence of the excitation by the thin wires in the first conductor.

Inside the conductor, the Helmholtz equation is solved.

From the contribution in terms of vector potential inside and outside the conductor that we have derived, we can express the magnetic field radial and angular components and then write the continuity condition of both at the conductor's edge.

This last step permits to obtain a system through which the unknown coefficients for the generic expression of J and A are calculated.

From this point forth it is possible to write an explicit expression of the current density inside the conductors, expressions which include the proximity effect, but these will be a function of the thin wires current intensity.

The skin effect is accounted for in the 0^{th} order terms; these terms, that contain the total current circulating in the conductors, remain the same as in the classical Schelkunoff theory. We shall see how the thin wires intensities (and therefore the coefficient representing proximity effect) depend upon this 0^{th} term. This is equivalent to considering the conductor as isolated and therefore only subject to skin effect. The current distribution found this way is then employed as the source of induction on the other conductor.

In order to calculate the current intensity in the thin wires, one assumption is made: we suppose that the thin wire has a current intensity equal to the value of the current density evaluated in the point where the wire is located and multiplied by the surface of the sub-conductor.

This assumption enables us to write a system of $2N$ equations, where N is the number of wires in which the conductor has been split. The wire current intensity found from the system of equations, which is a fraction of the total current, allows writing the current density in each conductor and the vector potential everywhere.

Having obtained the intensity value of the current flowing in the thin wires as a fraction of the total current flowing in the conductors, it is possible to infer the explicit expression of the impedance, as a function of current density and vector potential on the edges of the conductor.

3.2. Method for the calculation of induced currents based on thin-wire approach: two solid conductors

In the following table we show the notation used in this following section.

Table 2 - Notations used in Section 3.2

A	Magnetic vector potential	ϕ /θ	Angular coordinate inside/outside the conductor
A_d^e / A_d^s	Magnetic vector potential in the dielectric due to current density inside the conductor / thin wires	$\boldsymbol{I}$, $\boldsymbol{I}_{ij}$	Total current / current of jth thin wire of ith conductor
A_{ij}	Magnetic vector potential due to jth thin wire of ith conductor	I_n	Bessel modified function of first kind and n-th order
a_i	Radius of ith conductor	j	Imaginary unity
B / H	Magnetic flux density / magnetic field	J_i / J_i^e	Total current density / eddy current in ith conductor
b	Distances between conductors/sub-conductors	μ $\mu_0\mu_r$	Magnetic permeability , magnetic permeability in vacuum, relative magnetic permeability
d	Distance between a point of the dielectric and a generic thin wire	r / ρ	Radial coordinate inside / outside the conductor
E	Electric field	σ	Conductivity
e_n, f_n / g_n, h_n	Unknown coefficients of the current density / magnetic vector potential	V	Scalar potential

3.2.1. Geometry description

We shall consider two circular conductors with radiuses a_1 and a_2 (Fig.19).

Two polar coordinate systems are used to define the internal points in the conductors: for the first conductor the coordinate system is (r_1, ϕ_1) with its origin in the centre of the conductor, for the second conductor the coordinates are (r_2, ϕ_2).

There are two more polar coordinate systems (ρ_1, θ_1) and (ρ_2, θ_2) used to identify point in the dielectric medium surrounding the conductors.

An additional coordinate system (ρ_0, θ_0) can be defined that allows to identify the absolute position of the conductors and to indicate the origins of the before-mentioned coordinate systems, in the points (ρ_{01}, θ_{01}) and (ρ_{02}, θ_{02}).

The two conductors have a radius of a_1 and a_2 and the distance between their centres is b.

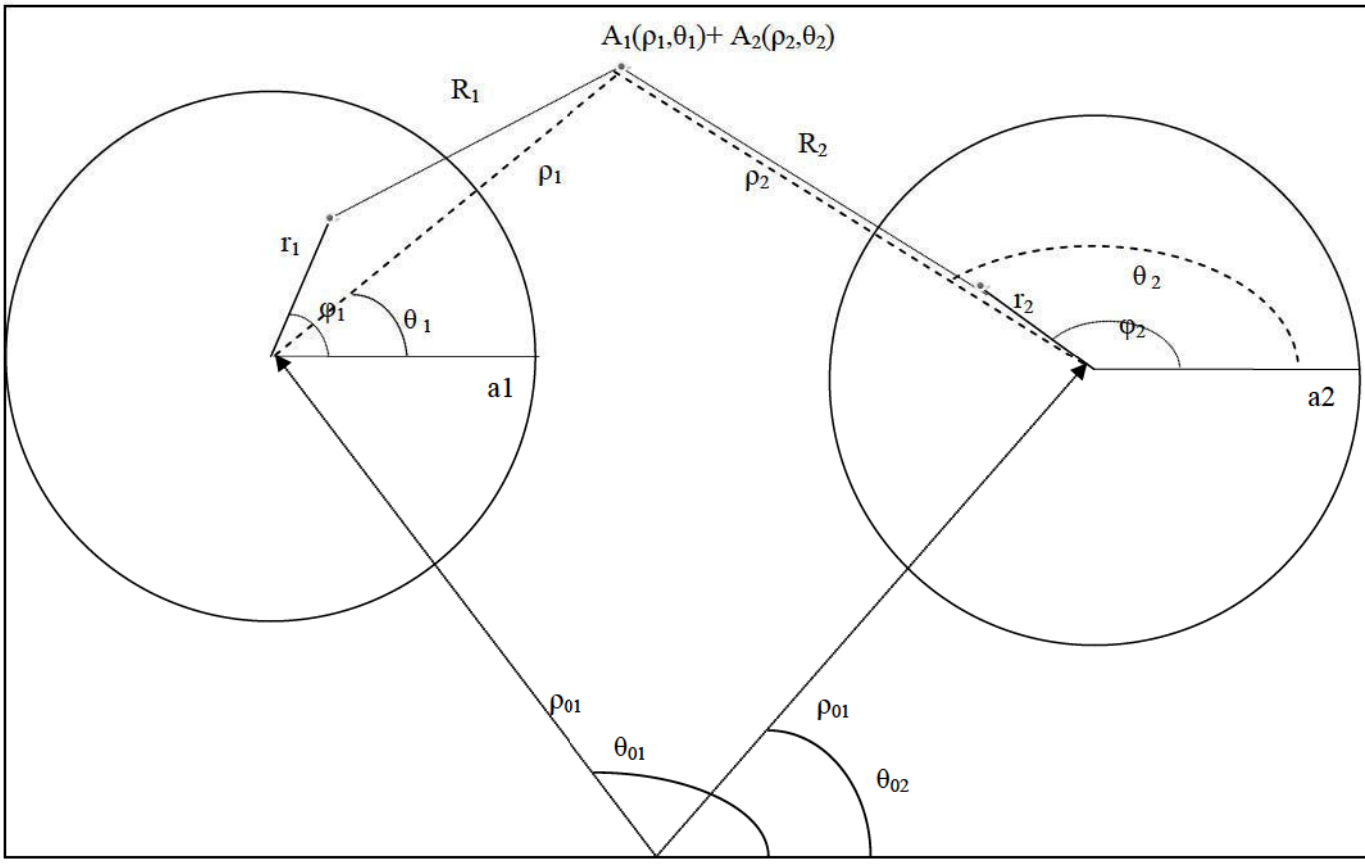

Fig.19 – Geometry description for the section of two cylindrical conductors on the (ρ,θ) transversal plane.

Derivation of general equations for magnetic potential and current density

We want to obtain an expression for the magnetic vector potential A in all the regions and one for the current density J in the conductive media.

Both expressions can be derived from Maxwell equations.

Derivation of A

Starting from Maxwell's equations, and considering a generic conductor, in the conductive medium we have:

$$\vec{\nabla} \times \vec{H} = j\omega\varepsilon_c \vec{E} = \vec{J}_d + \vec{J}_c \qquad (3.2.1)$$

where $\epsilon_c = \epsilon + \frac{\sigma}{j\omega}$ is the complex permittivity, used to account for displacement and conduction currents, J_d and J_c are respectively displacement and conduction currents.

Since $\nabla \cdot \vec{H} = 0$ the magnetic field can be expressed as:

$$\vec{H} = \frac{1}{\mu}\vec{\nabla} \times \vec{A} \qquad (3.2.2)$$

Replacing in (3.2.1)we have:

$$\vec{\nabla}\times(\frac{1}{\mu}\nabla\times\vec{A})=\vec{J} \tag{3.2.3}$$

Where J is the sum of displacement and conduction currents.

The propagation is quasi-TEM. The magnetic vector potential only consists of the z-component (the other components being equal to zero), but for simplicity is here called A instead of A_z; the same is true for J which represents J_z.

If we consider the medium to be isotropic and apply the vector identity

$$\vec{\nabla}\times\vec{\nabla}\times\vec{A}=\vec{\nabla}(\vec{\nabla}\cdot\vec{A})-\nabla^2\vec{A} \tag{3.2.4}$$

Using the Lorentz gauge

$$\vec{\nabla}\cdot\vec{A}=-j\omega\mu\epsilon_c V \tag{3.2.5}$$

and the expression

$$\vec{E}=-\vec{\nabla}V-j\omega\vec{A} \tag{3.2.6}$$

Some terms simplify on both sides.

We then neglect displacement currents in the complex permittivity, since we are interested in the current distribution in a conductive medium; and so we obtain an homogeneous Helmholtz equation for the magnetic vector potential:

$$\nabla^2\vec{A}-j\omega\mu\sigma\vec{A}=\vec{0} \tag{3.2.7}$$

Derivation of J

We can obtain a similar expression for the current density, if we apply the curl operator to the Maxwell equation

$$\vec{\nabla}\times\vec{E}=-j\omega\mu\vec{H} \tag{3.2.8}$$

We have:

$$\vec{\nabla}\times(\vec{\nabla}\times\vec{E})=-j\omega\mu\vec{\nabla}\times\vec{H} \tag{3.2.9}$$

Applying again (3.2.4) to E on the left side, and applying (3.2.1) on the right side, we have:

$$\vec{\nabla}(\vec{\nabla}\cdot\vec{E})-\vec{\nabla}^2\vec{E}=-j\omega\mu(j\omega\varepsilon_c\vec{E}) \tag{3.2.10}$$

Since we want the equations to be valid in a conductor we shall again neglect the displacement currents and knowing that:

$$\vec{J}=\sigma\vec{E} \tag{3.2.11}$$

$$\vec{\nabla}(\vec{\nabla}\cdot\vec{J})-\vec{\nabla}^2\vec{J}=-j\omega\mu\sigma(\vec{J}) \tag{3.2.12}$$

If we take the divergence of equation(3.2.1), neglecting displacement currents gives:

$$\nabla\cdot\vec{J}=0 \tag{3.2.13}$$

Rearranging equation (3.2.12) gives:

$$\nabla^2\vec{J}-j\omega\mu\sigma\vec{J}=\vec{0} \tag{3.2.14}$$

which is a Helmholtz equation for the current density.

This expression can be seen to be equivalent to the one found for the vector potential in equation(3.2.7); this relation will be shown in the next section.

Expressions (3.2.7) and (3.2.14) can also be written in cylindrical coordinates, giving:

$$\frac{\partial^2 \vec{A}}{\partial \rho^2}+\frac{1}{\rho}\frac{\partial \vec{A}}{\partial \rho}+\frac{1}{\rho^2}\frac{\partial^2 \vec{A}}{\partial \phi^2}=j\omega\mu\sigma\vec{A} \tag{3.2.15}$$

$$\frac{\partial^2 \vec{J}}{\partial \rho^2}+\frac{1}{\rho}\frac{\partial \vec{J}}{\partial \rho}+\frac{1}{\rho^2}\frac{\partial^2 \vec{J}}{\partial \phi^2}=j\omega\mu\sigma\vec{J} \tag{3.2.16}$$

It must be noted that the Laplace operator has been rewritten without the derivative along the z direction: this is one of the hypotheses of the theory used to calculate distributed line parameters (and generically valid for cylindrical structures). Since the structure is invariant along the z direction, it is only necessary to see what happens on the transversal planes disregarding the variations along z (which are represented by a factor of the kind $e^{-\gamma z}$), these variations can thus be provisionally neglected and added again when we calculate the parameters and the transmission line (TL) equations are written.

We shall show that there is a relationship between the current density and vector potential.

Using Maxwell equations and definition of vector potential :

$$\vec{\nabla}\times\vec{E}=-j\omega\vec{B}\ \ \vec{\nabla}\times\vec{A}=\vec{B} \tag{3.2.17}$$

$$\vec{\nabla}\times\vec{E}=-j\omega\vec{\nabla}\times\vec{A} \tag{3.2.18}$$

This can be rewritten as:

$$\vec{\nabla}\times\left(\vec{E}+j\omega\vec{A}\right)=\vec{0} \tag{3.2.19}$$

We know $\vec{E}=\frac{\vec{J}}{\sigma}$ and we must remember that A, E and J in the problem we considered, only have the z component. If we write the curl in cylindrical coordinates we obtain

$$\frac{1}{\rho\sigma}\frac{\partial J_z}{\partial \phi}\hat{\rho}+j\omega\frac{1}{\rho\sigma}\frac{\partial A_z}{\partial \phi}\hat{\rho}-\frac{1}{\sigma}\frac{\partial J_z}{\partial \rho}\hat{\phi}-j\omega\frac{\partial A_z}{\partial \rho}\hat{\phi} \tag{3.2.20}$$

Now equating components

$$\begin{cases}\dfrac{1}{\rho}\dfrac{\partial J_z}{\partial \phi}=j\omega\sigma\dfrac{1}{\rho}\dfrac{\partial A_z}{\partial \phi}\\ \dfrac{\partial J_z}{\partial \rho}=j\omega\sigma\dfrac{\partial A_z}{\partial \rho}\hat{\phi}\end{cases} \tag{3.2.21}$$

And therefore

$$\vec{J}=-j\omega\sigma\vec{A} \tag{3.2.22}$$

For the geometry of interest, the solution for the current density inside the circular conductors, namely $J_i\,(i=1,2)$can be written as a function of some unknown coefficients g_n, h_n, etc.[6].

$$\vec{J}_i(r_i,\phi_i)=\sum_{n=0}^{\infty} g_{in}I_n(\xi r_i)cos(n\phi_i)+h_{in}I_n(\xi r_i)sin(n\phi_i)\,\hat{z} \tag{3.2.23}$$

The magnetic vector potential inside the conductor has a solution of the same kind, and using relation (3.2.22) it can be written using the same coefficients used for the current:

[6] The solution is obtained by firstly using variable separation and then combining the two solutions obtained for the radial and angular part; the modified Bessel function Kn is not a part of the radial solution. It is omitted because it diverges when its argument goes to zero and is therefore not a physical solution.

$$\vec{A}_i(r_i,\phi_i) = -\frac{1}{j\omega\sigma}\sum_{n=0}^{\infty} g_{in} I_n(\xi r_i) co\ (n\phi_i) + h_{in} I_n(\xi r_i) sin(n\phi_i)\,\hat{z} \tag{3.2.24}$$

with $\xi = \sqrt{j\omega\mu\sigma}$ and I_n the Bessel modified function of first kind and n-th order.

In order to find the unknown coefficients g_{in}, h_{in} we need to express the potential (and from it the magnetic field) in all the regions, following the same reasoning already detailed in[2]).

We proceed this way because Maxwell's equations cannot be solved directly in an inhomogeneous medium (that is a medium where the parameters μ, ε, σ are not constant); instead a "perturbative" approach must be used, which consists in writing the potential in the different regions, inferring from that the magnetic field and writing continuity conditions at the boundary between the two homogeneous media.

Evaluation of the different contributions to the potential

In the conductive mediums the potential is written as in the equation(3.2.24).

In the dielectric medium the potential is a function of the current density in the two conductors and writes itself $\vec{A}_d = \vec{A}_d^s + \vec{A}_d^e$, namely the sum of a source and induced (eddy) component.

If we have a current source, represented as a filament, with intensity ***I***, the potential, evaluated in a point which is located at a distance *r* from the current source is[7]:

$$\vec{A}_d^s = \vec{A}_I = \frac{\mu_0 \boldsymbol{I}}{2\pi} ln(r)\,\hat{z} \tag{3.2.25}$$

Where $\hat{z}$ is a unitary vector which identifies the direction *z*.

The approach used in [2], and that we also use, is to define the potential in the same way than the one due to an infinitesimal current element[8] and then integrate it over the whole conductive surface in order to obtain the $\vec{A}_d^e$ term:

$$d^2\vec{A}_d^e(\rho,\theta) = \frac{\mu_0}{2\pi}\vec{J}(r,\phi) lnR\, r\, dr\, d\phi \tag{3.2.26}$$

The current density here is still unknown. This approach will be employed for the contribution of both conductors using a slightly different notation (for the different regions and contributions) specified in the following paragraph.

The distance *R* between the infinitesimal element and the point where the potential is calculated, which appears in equation (3.2.26), must be expressed using the coordinates (ρ_i,θ_i) and (r_i,ϕ_i) when identifying points in the dielectric medium or inside the conductors respectively (using the sub-index identifying the conductor).

3.2.2. Subdivision of the conductors in thin-wires and potentials expression

We intend to write the expression of the potential in the dielectric as the sum of the potential due to the independent current sources, namely $\vec{A}_d^s = \sum_{i=1}^{N} \vec{A}_{1i}$ called thin wires, and the potential due to the current density integrated upon the whole conductors, namely $\vec{A}_d^e$.

Every conductor is subdivided in N thin wires that will be identified by coordinates (r_{ij},ϕ_{ij}); the

[7] This potential due to a filamentary current source can be derived from Biot-Savart Law

[8] It is a current because the current density is multiplied by the infinitesimal area of the element

sub-index *i* *(i=1,2)*indicates the conductor in question, whereas the sub-index *j* indicates the *j*-th sub-conductor (of conductor *i*).

We treat at the same time two conductors, and use two cases, each conductor acts either as a source (then represented by thin-wires and being the source of $\vec{A}_d^s$) or a target (then represented as solid and being the source of $\vec{A}_d^e$.

In Fig.20 we show the notation used in both cases, to describe points inside the conductors, and the position of the thin-wires, both from a conductor and from the other.

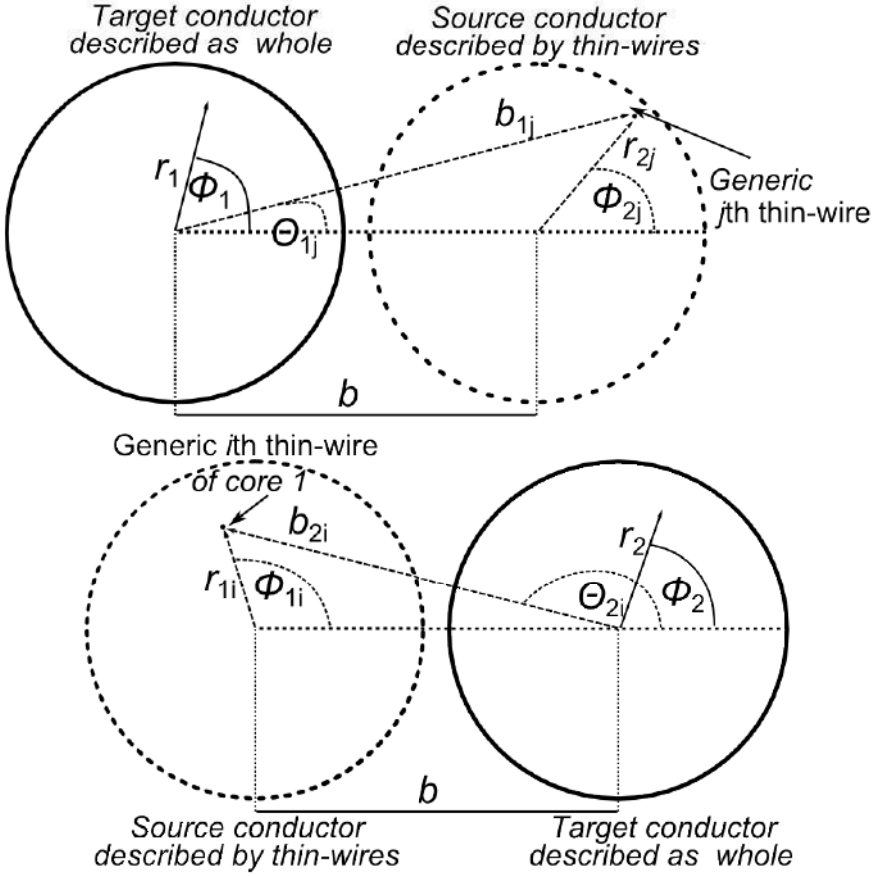

Fig.20 – The geometric notation used in case 1 and case 2 to describe the conductors

In order to write a system of equations, we have to write continuity conditions on the edge of the conductors. In order to do this, we will consider (see Fig.20 for the dual situation):

- Two equations for the edge of conductor *2* (in this case conductor *1* is replaced by a number of thin wires that represent the source of the excitation on conductor *2*, which is the target and has a continuous current density);
- Two equations for the opposite situation (edge of conductor *1*, itself being whole while conductor *2* is replaced by wires).

Definition of the potentials in the different regions and due to different contributions

The contribution to the external potential for each source thin wire is indicated with $\vec{A}_{1i}$ and $\vec{A}_{2j}$ for the first and for the second conductor, whereas the potential due to current density is indicated with $\vec{A}_{1d}^e$ and $\vec{A}_{2d}^e$. Inside the conductors the potential will be indicated as $\vec{A}_1$ and $\vec{A}_2$.

We know that in each conductor circulates a current ***I***. This current corresponds to current density

integrated upon the whole conductor, but is also the sum of the current on each thin wire:

$$\boldsymbol{I} = \sum_i \boldsymbol{I}_{1i} = \int_{cond1} \vec{J}_1(r_1, \phi_1)\, dS \tag{3.2.27}$$

$$\boldsymbol{I} = \sum_j \boldsymbol{I}_{2j} = \int_{cond2} \vec{J}_2(r_2, \phi_2)\, dS \tag{3.2.28}$$

Contribution of the thin wire current sources

The contribution of the *i*-th (or *j*-th) thin wire of the first (or second) conductor can be written as:

$$\vec{A}_{1i}(\rho_1, \theta_1) = \frac{\mu_0}{2\pi} \boldsymbol{I}_{1i} \ln d_{1i}\, \hat{z} \tag{3.2.29}$$

$$\vec{A}_{2j}(\rho_2, \theta_2) = \frac{\mu_0}{2\pi} \boldsymbol{I}_{2j} \ln d_{2j}\, \hat{z} \tag{3.2.30}$$

with d_{1i}, d_{2j} the distances between the *i*-th (or *j*-th) wire and the generic point of the dielectric.

The logarithmic terms of equations (3.2.29) and (3.2.30) can be then written (as is demonstrated in section 3.2.3.1 though using different coordinates) as:

$$\ln d_{1i} = \ln(b_{2i}) - \sum_{m=1}^{\infty} \frac{1}{m} \left(\frac{\rho_2}{b_{2i}} \right)^m \cos\left(m(\theta_2 - \theta_{2i}) \right) \tag{3.2.31}$$

$$\ln d_{2j} = \ln(b_{1j}) - \sum_{m=1}^{\infty} \frac{1}{m} \left(\frac{\rho_1}{b_{1j}} \right)^m \cos\left(m(\theta_1 - \theta_{1j}) \right) \tag{3.2.32}$$

with the condition that $\rho_1 / b_{1j} < 1$ and $\rho_2 / b_{2i} < 1$ which is necessary for the series to converge.

We then have:

$$\vec{A}_{1i}(\rho_2, \theta_2) = \frac{\mu_0}{2\pi} \boldsymbol{I}_{1i} \left[\ln(b_{2i}) - \sum_{n=1}^{\infty} \frac{1}{n} \left(\frac{\rho_2}{b_{2i}} \right)^n \cos\left(n(\theta_2 - \theta_{2i}) \right) \right] \hat{z} \tag{3.2.33}$$

$$\vec{A}_{2j}(\rho_1, \theta_1) = \frac{\mu_0}{2\pi} \boldsymbol{I}_{2j} \left[\ln(b_{1j}) - \sum_{n=1}^{\infty} \frac{1}{n} \left(\frac{\rho_1}{b_{1j}} \right)^n \cos\left(n(\theta_1 - \theta_{1j}) \right) \right] \hat{z} \tag{3.2.34}$$

Here b_{2i} is the distance between the centre of conductor *2* and the *i*-th wire of conductor *1* and θ_{2i} the angle which identifies it in the coordinate system of conductor *2*, whereas b_{1j} is the distance between the centre of conductor *1* and the *j*-th wire of conductor *2* and θ_{1j} is the angle which identifies it. All these quantities are defined in Fig.20.

To calculate the distances b_{1j} and b_{2i} and the angles θ_{1j} ,θ_{2i} as a function of the coordinates of the relative wires we can write the relations:

$$b = b_{1j} cos(\theta_{1j}) + r_{2j} cos(\phi_{2j})$$
$$b_{1j} sin(\theta_{1j}) = r_{2j} sin(\phi_{2j})$$

$$b = b_{2i} cos(\theta_{2i}) + r_{1i} cos(\phi_{1i})$$
$$b_{2i} sin(\theta_{2i}) = r_{1i} sin(\phi_{1i})$$

We obtain expressions allowing the calculation of these parameters as:

$$b_{1j} = \sqrt{b^2 + r_{2j}^2 - 2br_{2j}cos(\phi_{2j})} \tag{3.2.35}$$

$$\theta_{1j} = \arctan\left(\frac{r_{2j}\sin\phi_{2j}}{b - r_{2j}\cos\phi_{2j}}\right) \tag{3.2.36}$$

$$b_{2i} = \sqrt{b^2 + r_{1i}^2 - 2br_{1i}cos(\phi_{1i})} \tag{3.2.37}$$

$$\theta_{2i} = \arctan\left(\frac{r_{1i}\sin\phi_{1i}}{b - r_{1i}\cos\phi_{1i}}\right) \tag{3.2.38}$$

Contribution of the current density in the "target conductors"

We know that the potential in the dielectric due to an infinitesimal surface element with a current distribution $\vec{J}_1(r_1,\phi_1)$ is:

$$d^2\vec{A}_{ext}(\rho,\theta) = \frac{\mu_0}{2\pi}\vec{J}(r,\phi)lnRrdrd\phi \tag{3.2.39}$$

In order to find the potential due to a whole circular conductor this expression must be integrated upon the whole section of the conductor

$$\vec{A}_{1d}^{e} = (\rho_1,\theta_1) = \int_0^{a_1}\int_0^{2\pi}\frac{\mu_0}{2\pi}\vec{J}_1(r,\phi)lnR_1\, r_1\, dr_1\, d\phi_1\,\hat{z} \tag{3.2.40}$$

$$\vec{A}_{2d}^{e}(\rho_2,\theta_2) = \int_0^{a_2}\int_0^{2\pi}\frac{\mu_0}{2\pi}\vec{J}_2(r,\phi)lnR_2\, r_2\, dr_2\, d\phi_2\,\hat{z} \tag{3.2.41}$$

We shall develop only the calculation of one of the two expressions, namely the one on the first conductor; to do this we integrate the following part of the current density (3.2.23), namely

$$\vec{J}_1(r_1,\phi_1) = \sum_{n=0}^{\infty} g_{1n}I_n(\xi r_1)cos(n\phi_1) + h_{1n}I_n(\xi r_1)sin(n\phi_1)\,\hat{z} \tag{3.2.42}$$

and use the development present in 3.2.3.1 obtaining[9]:

$$\vec{A}_{1d}^{e}(\rho_1,\theta_1) = \frac{\mu_0}{2\pi}\sum_{n=0}^{\infty}\int_0^{a_1}\int_0^{2\pi}\left[e_{1n}I_n(\xi r_1)cos(n\phi_1) + f_{1n}I_n(\xi r_1)sin(n\phi_1)\right]ln(\rho_1)r_1dr_1d\phi_1\,\hat{z} +$$

$$-\frac{\mu_0}{2\pi}\sum_{n=0}^{\infty}\sum_{m=1}^{\infty}\int_0^{a_1}\int_0^{2\pi}\frac{1}{m}\left(\frac{r_1}{\rho_1}\right)^m\left[e_{1n}I_n(\xi r_1)cos(n\phi_1) + f_{1n}I_n(\xi r_1)sin(n\phi_1)\right]cos(m(\phi_1-\theta_1))r_1dr_1d\phi_1\,\hat{z} \tag{3.2.43}$$

Concerning the first term of this equation, knowing that

$$\int_0^{2\pi} cos(n\phi) = \begin{cases} 2\pi \ if\ n=0 \\ 0\ othwerwise \end{cases} \tag{3.2.44}$$

$$\int_0^{2\pi} sin(n\phi) = 0\ \forall n \tag{3.2.45}$$

only the term with the coefficient e_{10} will remain.

[9]Here we have changed the coefficients, using e_n, f_n instead of g_n, h_n because the medium has changed, therefore the potential will follow the form of the current density in the conductive medium, but the coefficients are dependent upon the medium properties.

For the second term we know that

$$\cos(m(\phi-\theta)) = \cos(m\phi)\cos(m\theta) + \sin(m\phi)\sin(m\theta) \tag{3.2.46}$$

and

$$\int_0^{2\pi} sin(m\phi)cos(n\phi) = 0 \ \forall n,m \tag{3.2.47}$$

$$\int_0^{2\pi} cos(m\phi)cos(n\phi) = \begin{cases} 0 \ for\, m \neq n \\ \pi \ for\, m = n \neq 0 \\ 2\pi \ for\, m = n = 0 \end{cases} \tag{3.2.48}$$

$$\int_0^{2\pi} \sin(m\phi)\sin(n\phi) = \begin{cases} 0 \ for\, m \neq n \\ \pi \ for\, m = n \neq 0 \\ 0 \ for\, m = n = 0 \end{cases} \tag{3.2.49}$$

We can therefore eliminate the terms of 0^{th} order and (since the terms with m≠n are zero) we can consider only one sum with index n starting from 1.

The angular variable has been integrated (and therefore eliminated):

$$\begin{aligned} &\vec{A}_{1d}^{e}(\rho_1,\theta_1) = \mu_0 e_{10} ln(\rho_1)\int_0^{a_1} I_0(\xi r_1) r_1 dr_1 \,\hat{z} + \\ &-\frac{\mu_0}{2}\sum_{n=1}^{\infty}\frac{1}{n\rho_1^n}\left[e_{1n}cos(n\theta_1) + f_{1n}sin(n\theta_1)\right]\int_0^{a_1} I_n(\xi r_1) r_1^{n+1} dr_1 \,\hat{z} \end{aligned} \tag{3.2.50}$$

In order to integrate the radial variable in both terms, a property of the modified Bessel functions must be used, that is:

$$\int x^n I_{n-1}(\xi x)dx = \frac{x^n}{\xi} I_n(\xi x) \tag{3.2.51}$$

This gives:

$$\vec{A}_{1d}^{e}(\rho_1,\theta_1) = \frac{\mu_0 e_{10} a_1}{\xi} ln(\rho_1) I_1(\xi a_1) - \frac{\mu_0}{2}\sum_{n=1}^{\infty}\frac{a_1^{n+1}}{n\xi\rho_1^n}\left[e_{1n}cos(n\theta_1) + f_{1n}sin(n\theta_1)\right] I_{n+1}(\xi a_1)\,\hat{z} \tag{3.2.52}$$

$$\vec{A}_{2d}^{e}(\rho_2,\theta_2) = \frac{\mu_0 e_{20} a_2}{\xi} ln(\rho_2) I_1(\xi a_2) - \frac{\mu_0}{2}\sum_{n=1}^{\infty}\frac{a_2^{n+1}}{n\xi\rho_2^n}\left[e_{2n}cos(n\theta_2) + f_{2n}\sin(n\theta_2)\right] I_{n+1}(\xi a_2)\,\hat{z} \tag{3.2.53}$$

Continuity conditions on the interfaces between regions

We shall now write the continuity conditions on the interface conductor - dielectric, that is on the conductors' circumferences; these are the same as in [2], namely:

- the continuity of the radial component of the magnetic flux density B

$$B_{r-int} = B_{\rho-ext}\Big|_{\theta=\phi}^{r=\rho=a} \tag{3.2.54}$$

- the continuity of the angular component of the magnetic field H[10]

[10] Differently from the magnetic flux density, the magnetic field H is dependent upon the medium; that said the relation expressed in equation(3.2.55), namely H=B/μ , is only valid if the conductor is not ferromagnetic.

$$\frac{1}{\mu}B_{\phi-\text{int}} = \frac{1}{\mu_0}B_{\theta-ext}\Big|_{\theta=\phi}^{r=\rho=a} \tag{3.2.55}$$

These components can be obtained in all the regions from the magnetic vector potential by derivation:

$$B_{r-\text{int}} = \frac{1}{r}\frac{\partial \vec{A}_i}{\partial \phi} \qquad B_{\rho-ext} = \frac{1}{\rho}\frac{\partial \vec{A}_d}{\partial \theta} \tag{3.2.56}$$

$$B_{\phi-\text{int}} = -\frac{\partial \vec{A}_i}{\partial r} \qquad B_{\theta-ext} = -\frac{\partial \vec{A}_d}{\partial \rho} \tag{3.2.57}$$

We now have in the dielectric the total potential $\vec{A}_{2d}^{e} + \sum_{i=1}^{N}\vec{A}_{1i}$ and, inside the material of the conductor we have $\vec{A}_2$ and vice versa $\vec{A}_{1d}^{e} + \sum_{i=1}^{N}\vec{A}_{2i}$ outside and $\vec{A}_1$ inside when we consider the second conductor to be the source (represented by thin-wires).

We can now write continuity conditions(3.2.54)(3.2.55) for both cases.

When we consider the first conductor as source and the second as target, the continuity conditions, written on the edge of conductor 1 are:

$$B_{r-\text{int}-2} = B_{\rho-ext-2}\begin{cases}\sum_{i=1}^{N}\frac{\mu_0}{2\pi}\boldsymbol{I}_{1i}\left[\sum_{n=1}^{\infty}\frac{1}{a_2}\left(\frac{a_2}{b_{2i}}\right)^n \sin\left(n(\theta_2-\theta_{2i})\right)\right] \\ +\frac{\mu_0}{2}\left[\sum_{n=1}^{\infty}e_{2n}\frac{I_{n+1}(\xi a_2)}{\xi}\sin(n\theta_2) - f_{2n}\frac{I_{n+1}(a_2\xi)}{\xi}\cos(n\theta_2)\right] = \\ = \frac{1}{j\omega\sigma a_2}\sum_{n=0}\left[g_{2n}I_n(\xi a_2)\sin(n\theta_2)n - h_{2n}I_n(\xi a_2)\cos(n\theta_2)n\right]\end{cases} \tag{3.2.58}$$

$$H_{\phi-\text{int}-2} = H_{\theta-ext-2}\begin{cases}\sum_{i=1}^{N}\frac{1}{2\pi}\boldsymbol{I}_{1i}\left[\sum_{n=1}^{\infty}\frac{1}{a_2}\left(\frac{a_2}{b_{2i}}\right)^n \cos\left(n(\theta_2-\theta_{2i})\right)\right] - e_{20}\frac{1}{\xi}I_1(\xi a_2) + \\ -\frac{1}{2}\sum_{n=1}^{\infty}\left[e_{2n}\frac{I_{n+1}(\xi a_2)}{\xi}\cos(n\theta_2) + f_{2n}\frac{I_{n+1}(\xi a_2)}{\xi}\sin(n\theta_2)\right] = \\ = \frac{\xi}{j\omega\sigma\mu}\sum_{n=0}\left[g_{2n}I_n'(\xi a_2)\cos(n\theta_2) + h_{2n}I_n'(\xi a_2)\sin(n\theta_2)\right]\end{cases} \tag{3.2.59}$$

where I_n' is the derivative of the Bessel modified function of the first kind.

When we consider the second conductor as source and the first as target, the continuity conditions, written on the edge of conductor 2 are:

$$B_{r-\text{int}-1} = B_{\rho-ext-1}\begin{cases}\sum_{j=1}^{N}\frac{\mu_0}{2\pi}\boldsymbol{I}_{2j}\left[\sum_{n=1}^{\infty}\frac{1}{a_1}\left(\frac{a_1}{b_{1j}}\right)^n \sin\left(n(\theta_1-\theta_{1j})\right)\right]+ \\ +\frac{\mu_0}{2}\left[\sum_{n=1}^{\infty}e_{1n}\frac{I_{n+1}(\xi a_1)}{\xi}\sin(n\theta_1)-f_{1n}\frac{I_{n+1}(\xi a_1)}{\xi}\cos(n\theta_1)\right]= \\ =\frac{1}{j\omega\sigma a_1}\sum_{n=0}\left[g_{1n}I_n(\xi a_1)\sin(n\theta_1)n-h_{1n}I_n(\xi a_1)\sin(n\theta_1)n\right]\end{cases} \tag{3.2.60}$$

$$H_{\phi-\text{int}-1} = H_{\theta-ext-1}\begin{cases}\sum_{j=1}^{N}\frac{1}{2\pi}\boldsymbol{I}_{2j}\left[\sum_{n=1}^{\infty}\frac{1}{a_1}\left(\frac{a_1}{b_{1j}}\right)^n \cos\left(n(\theta_1-\theta_{1j})\right)\right]-e_{10}\frac{1}{\xi}I_1(\xi a_1)+ \\ -\frac{1}{2}\sum_{n=1}^{\infty}\left[e_{1n}\frac{I_{n+1}(\xi a_1)}{\xi}\cos(n\theta_1)+f_{1n}\frac{I_{n+1}(\xi a_1)}{\xi}\sin(n\theta_1)\right]= \\ =\frac{\xi}{j\omega\sigma\mu}\sum_{n=0}\left[g_{1n}I_n'(\xi a_1)\cos(n\theta_1)+h_{1n}I_n'(\xi a_1)\sin(n\theta_1)\right]\end{cases} \tag{3.2.61}$$

3.2.3. Resolution of the system: evaluation of currents and potentials coefficients

In order to solve the equations and find the expression for the generic coefficient we intend to find a system of equations in which every equation resembles a Fourier series, that is:

$$f(\theta) = \alpha_0 + \sum_{n=1}^{\infty}\alpha_n\cos n\theta + \beta_n \sin n\theta = 0 \tag{3.2.62}$$

this will allow us to find an expression for the generic coefficient e_{1n} , f_{1n}, g_{1n}, etc.

This can be done because α_n ,β_n have to be zero for every n in order to satisfy equation (3.2.62), which can be proved, by multiplying equation (3.2.62) respectively by *cos(nθ)* and *sin(nθ)* and integrate each, between *0* and *2π*. This allows showing the double implication that if the Fourier coefficients are zero, so is the function, and vice-versa.

To obtain expressions of the kind of (3.2.62) we shall apply the following trigonometric properties to equations (3.2.58)(3.2.59)(3.2.60)(3.2.61)

$$\cos(a+b) = \cos a\cos b - \sin a\sin b$$

$$\sin(a+b) = \sin a\cos b + \sin b\cos a$$

which become

$$\sin(n(\theta_2-\theta_{2i})) = \sin(n\theta_2)\cos(n\theta_{2i}) - cos(n\theta_2)sin(n\theta_{2i})$$

$$\cos(n(\theta_2-\theta_{2i})) = \cos(n\theta_2)\cos(n\theta_{2i}) + \sin(n\theta_2)\sin(n\theta_{2i})$$

The terms must be rearranged, inverting the sums and grouping together terms which multiply the same Fourier base function. This gives:

$$\sum_{n=1}^{\infty}\left[\frac{\mu_0}{2\pi}\sum_{i=1}^{N}\frac{\boldsymbol{I}_{1i}}{a_2}\left(\frac{a_2}{b_{2i}}\right)^n\cos n\theta_{2i}+\frac{\mu_0}{2}e_{2n}\frac{I_{n+1}(\xi a_2)}{\xi}-\frac{n}{j\omega\sigma a_2}g_{2n}I_n(\xi a_2)\right]\sin(n\theta_2)+$$
$$-\sum_{n=1}^{\infty}\left[\frac{\mu_0}{2\pi}\sum_{i=1}^{N}\frac{\boldsymbol{I}_{1i}}{a_2}\left(\frac{a_2}{b_{2i}}\right)^n\sin n\theta_{2i}+\frac{\mu_0}{2}f_{2n}\frac{I_{n+1}(\xi a_2)}{\xi}-\frac{n}{j\omega\sigma a_2}h_{2n}I_n(\xi a_2)\right]\cos(n\theta_2)=0 \tag{3.2.63}$$

$$-e_{20}\frac{1}{\xi}I_1(\xi a_2)-\frac{\xi}{j\omega\sigma\mu}g_{20}I_1(\xi a_2)+$$
$$+\sum_{n=1}^{\infty}\left[\frac{1}{2\pi}\sum_{i=1}^{N}\frac{\boldsymbol{I}_{1i}}{a_2}\left(\frac{a_2}{b_{2i}}\right)^n\cos n\theta_{2i}-\frac{1}{2}e_{2n}\frac{I_{n+1}(\xi a_2)}{\xi}-\frac{\xi}{j\omega\sigma\mu}g_{2n}I_n'(\xi a_2)\right]\cos(n\theta_2)+ \tag{3.2.64}$$
$$+\sum_{n=1}^{\infty}\left[\frac{1}{2\pi}\sum_{i=1}^{N}\frac{\boldsymbol{I}_{1i}}{a_2}\left(\frac{a_2}{b_{2i}}\right)^n\sin n\theta_{2i}-\frac{1}{2}f_{2n}\frac{I_{n+1}(\xi a_2)}{\xi}-\frac{\xi}{j\omega\sigma\mu}h_{2n}I_n'(\xi a_2)\right]\sin(n\theta_2)=0$$

$$\sum_{n=1}^{\infty}\left[\frac{\mu_0}{2\pi}\sum_{j=1}^{N}\frac{\boldsymbol{I}_{2j}}{a_1}\left(\frac{a_1}{b_{1j}}\right)^n\cos n\theta_{1j}+\frac{\mu_0}{2}e_{1n}\frac{I_{n+1}(\xi a_1)}{\xi}-\frac{n}{j\omega\sigma a_1}g_{1n}I_n(\xi a_1)\right]\sin(n\theta_1)+$$
$$-\sum_{n=1}^{\infty}\left[\frac{\mu_0}{2\pi}\sum_{j=1}^{N}\frac{\boldsymbol{I}_{2j}}{a_1}\left(\frac{a_1}{b_{1j}}\right)^n\sin n\theta_{1j}+\frac{\mu_0}{2}f_{1n}\frac{I_{n+1}(\xi a_1)}{\xi}-\frac{n}{j\omega\sigma a_1}h_{1n}I_n(\xi a_1)\right]\cos(n\theta_1)=0 \tag{3.2.65}$$

$$-e_{10}\frac{1}{\xi}I_1(\xi a_1)-\frac{\xi}{j\omega\sigma\mu}g_{10}I_1(\xi a_1)+$$
$$+\sum_{n=1}^{\infty}\left[\frac{1}{2\pi}\sum_{j=1}^{N}\frac{\boldsymbol{I}_{2j}}{a_1}\left(\frac{a_1}{b_{1j}}\right)^n\cos n\theta_{1j}-\frac{1}{2}e_{1n}\frac{I_{n+1}(\xi a_1)}{\xi}-\frac{\xi}{j\omega\sigma\mu}g_{1n}I_n'(\xi a_1)\right]\cos(n\theta_1)+ \tag{3.2.66}$$
$$+\sum_{n=1}^{\infty}\left[\frac{1}{2\pi}\sum_{j=1}^{N}\frac{\boldsymbol{I}_{2j}}{a_1}\left(\frac{a_1}{b_{1j}}\right)^n\sin n\theta_{1j}-\frac{1}{2}f_{1n}\frac{I_{n+1}(\xi a_1)}{\xi}-\frac{\xi}{j\omega\sigma\mu}h_{1n}I_n'(\xi a_1)\right]\sin(n\theta_1)=0$$

We can now consider the generic term, as we explained before in this section, that multiplies the base functions *cos(nθ), sin(nθ)*, eliminating the infinite sum. This gives two equation systems:

$$\begin{cases}\dfrac{\mu_0}{2\pi}\displaystyle\sum_{i=1}^{N}\frac{\boldsymbol{I}_{1i}}{a_2}\left(\frac{a_2}{b_{2i}}\right)^n\cos n\theta_{2i}+\frac{\mu_0}{2}e_{2n}\frac{I_{n+1}(\xi a_2)}{\xi}-\frac{n}{j\omega\sigma a_2}g_{2n}I_n(\xi a_2)=0\\ \dfrac{\mu_0}{2\pi}\displaystyle\sum_{i=1}^{N}\frac{\boldsymbol{I}_{1i}}{a_2}\left(\frac{a_2}{b_{2i}}\right)^n\sin n\theta_{2i}+\frac{\mu_0}{2}f_{2n}\frac{I_{n+1}(\xi a_2)}{\xi}-\frac{n}{j\omega\sigma a_2}h_{2n}I_n(\xi a_2)=0\\ -e_{20}\dfrac{1}{\xi}I_1(\xi a_2)-\dfrac{\xi}{j\omega\sigma\mu}g_{20}I_1(\xi a_2)=0\\ \dfrac{1}{2\pi}\displaystyle\sum_{i-1}^{N}\frac{\boldsymbol{I}_{1i}}{a_2}\left(\frac{a_2}{b_{2i}}\right)^n\cos n\theta_{2i}-\frac{1}{2}e_{2n}\frac{I_{n+1}(\xi a_2)}{\xi}-\frac{\xi}{j\omega\sigma\mu}g_{2n}I_n'(\xi a_2)=0\\ \dfrac{1}{2\pi}\displaystyle\sum_{i=1}^{N}\frac{\boldsymbol{I}_{1i}}{a_2}\left(\frac{a_2}{b_{2i}}\right)^n\sin n\theta_{2i}-\frac{1}{2}f_{2n}\frac{I_{n+1}(\xi a_2)}{\xi}-\frac{\xi}{j\omega\sigma\mu}h_{2n}I_n'(\xi a_2)=0\end{cases} \tag{3.2.67}$$

$$\begin{cases} \frac{\mu_0}{2\pi}\sum_{j=1}^{N}\frac{\boldsymbol{I}_{2j}}{a_1}(\frac{a_1}{b_{1j}})^n\cos n\theta_{1j}+\frac{\mu_0}{2}e_{1n}\frac{I_{n+1}(\xi a_1)}{\xi}-\frac{n}{j\omega\sigma a_1}g_{1n}I_n(\xi a_1)=0 \\ \frac{\mu_0}{2\pi}\sum_{j=1}^{N}\frac{\boldsymbol{I}_{2j}}{a_1}(\frac{a_1}{b_{1j}})^n\sin n\theta_{1j}+\frac{\mu_0}{2}f_{1n}\frac{I_{n+1}(\xi a_1)}{\xi}-\frac{n}{j\omega\sigma a_1}h_{1n}I_n(\xi a_1)=0 \\ -e_{10}\frac{1}{\xi}I_1(\xi a_1)-\frac{\xi}{j\omega\sigma\mu}g_1\ I_1(\xi a_1)=0 \\ \frac{1}{2\pi}\sum_{j=1}^{N}\frac{\boldsymbol{I}_{2j}}{a_1}(\frac{a_1}{b_{1j}})^n\cos n\theta_{1j}-\frac{1}{2}e_{1n}\frac{I_{n+1}(\xi a_1)}{\xi}-\frac{\xi}{j\omega\sigma\mu}g_{1n}I_n'(\xi a_1)=0 \\ \frac{1}{2\pi}\sum_{j=1}^{N}\frac{\boldsymbol{I}_{2j}}{a_1}(\frac{a_1}{b_{1j}})^n\sin n\theta_{1j}-\frac{1}{2}f_{1n}\frac{I_{n+1}(\xi a_1)}{\xi}-\frac{\xi}{j\omega\sigma\mu}h_{1n}I_n'(\xi a_1)=0 \end{cases} \tag{3.2.68}$$

We shall now solve the system for n>0 and calculate the generic coefficient of n-th order, subsequently we shall calculate the coefficient of zero-order

Evaluation of nth order coefficients

We can rewrite the first equation system (neglecting the third equation) as:

$$\begin{cases} R+Se_{2n}-Tg_{2n}=0 \\ U+Sf_{2n}-Th_{2n}=0 \\ X-We_{2n}-Yg_{2n}=0 \\ L-Wf_{2n}-Yh_{2n}=0 \end{cases} \tag{3.2.69}$$

with

$$R=\frac{\mu_0}{2\pi}\sum_{i=1}^{N}\frac{\boldsymbol{I}_{1i}}{a_2}(\frac{a_2}{b_{2i}})^n\cos n\theta_{2i}\quad U=\frac{\mu_0}{2\pi}\sum_{i=1}^{N}\frac{\boldsymbol{I}_{1i}}{a_2}(\frac{a_2}{b_{2i}})^n\sin n\theta_{2i}$$

$$X=\frac{1}{2\pi}\sum_{i=1}^{N}\frac{\boldsymbol{I}_{1i}}{a_2}(\frac{a_2}{b_{2i}})^n\cos n\theta_{2i}\quad L=\frac{1}{2\pi}\sum_{i=1}^{N}\frac{\boldsymbol{I}_{1i}}{a_2}(\frac{a_2}{b_{2i}})^n\sin n\theta_{2i}$$

$$S=\frac{\mu_0}{2}\frac{I_{n+1}(\xi a_2)}{\xi}\quad T=\frac{n}{j\omega\sigma a_2}I_n(\xi a_2)\quad W=\frac{1}{2}\frac{I_{n+1}(\xi a_2)}{\xi}\quad Y=\frac{\xi}{j\omega\sigma\mu}I_n'(\xi a_2)$$

We can solve it[11] obtaining the expressions of the generic coefficients symbolically as:

$$e_{2n}=\frac{-RY+XT}{SY+WT}\quad f_{2n}=\frac{-UY+LT}{SY+WT}$$

$$g_{2n}=\frac{XS+RW}{SY+WT}\quad h_{2n}=\frac{LS+UW}{SY+WT}$$

The expressions can be then written as:

$$e_{2n}=\frac{\frac{1}{2\pi}\sum_{i=1}^{N}\frac{\boldsymbol{I}_{1i}}{a_2}(\frac{a_2}{b_{2i}})^n\cos n\theta_{2i}\ \frac{1}{a_2}\left[nI_n(\xi a_2)-\frac{\xi a_2}{\mu_r}I_n'(\xi a_2)\right]}{\frac{1}{2}\frac{I_{n+1}(\xi a_2)}{\xi}\qquad\qquad\frac{1}{a_2}\left[nI_n(\xi a_2)+\frac{\xi a_2}{\mu_r}I_n'(\xi a_2)\right]} \tag{3.2.70}$$

[11] The same system is equally valid for the second set of equations, just changing the sub-indexes 2 with 1; this will hold true also for the solution.

$$f_{2n} = \frac{\frac{1}{2\pi}\sum_{i=1}^{N}\frac{\boldsymbol{I}_{1i}}{a_2}\left(\frac{a_2}{b_{2i}}\right)^n \sin n\theta_{2i}}{\frac{1}{2}\frac{I_{n+1}(\xi a_2)}{\xi}} \frac{\frac{1}{a_2}\left[nI_n(\xi a_2) - \frac{\xi a_2}{\mu_r} I_n{}'(\xi a_2)\right]}{\frac{1}{a_2}\left[nI_n(\xi a_2) + \frac{\xi a_2}{\mu_r} I_n{}'(\xi a_2)\right]} \tag{3.2.71}$$

$$g_{2n} = \frac{\frac{\mu_0}{2\pi}\sum_{i=1}^{N}\frac{\boldsymbol{I}_{1i}}{a_2}\left(\frac{a_2}{b_{2i}}\right)^n \cos n\theta_{2i}}{\frac{1}{j\omega\sigma}\frac{1}{2}\frac{I_{n+1}(\xi a_2)}{\xi}} \frac{\frac{I_{n+1}(\xi a_2)}{\xi}}{\frac{1}{a_2}\left[nI_n(\xi a_2) + \frac{\xi a_2}{\mu_r} I_n{}'(\xi a_2)\right]} \tag{3.2.72}$$

$$h_{2n} = \frac{\frac{\mu_0}{2\pi}\sum_{i=1}^{N}\frac{\boldsymbol{I}_{1i}}{a_2}\left(\frac{a_2}{b_{2i}}\right)^n \sin n\theta_{2i}}{\frac{1}{j\omega\sigma}\frac{1}{2}\frac{I_{n+1}(\xi a_2)}{\xi}} \frac{-\frac{I_{n+1}(\xi a_2)}{\xi}}{\frac{1}{a_2}\left[nI_n(\xi a_2) + \frac{\xi a_2}{\mu_r} I_n{}'(\xi a_2)\right]} \tag{3.2.73}$$

We can now apply the Bessel function property $xI_n{}'(x) = nI_n(x) + xI_{n+1}(x)$ and simplify, obtaining:

$$e_{2n} = \frac{\frac{1}{\pi}\sum_{i=1}^{N}\frac{\boldsymbol{I}_{1i}}{a_2}\left(\frac{a_2}{b_{2i}}\right)^n \cos n\theta_{2i}}{\frac{I_{n+1}(\xi a_2)}{\xi}} \frac{\left[n\left(1-\frac{1}{\mu_r}\right)I_n(\xi a_2) - \frac{\xi a_1}{\mu_r} I_{n+1}(\xi a_2)\right]}{\left[n\left(1+\frac{1}{\mu_r}\right)I_n(\xi a_2) + \frac{\xi a_1}{\mu_r} I_{n+1}(\xi a_2)\right]} \tag{3.2.74}$$

$$f_{2n} = \frac{\frac{1}{\pi}\sum_{i=1}^{N}\frac{\boldsymbol{I}_{1i}}{a_2}\left(\frac{a_2}{b_{2i}}\right)^n \sin n\theta_{2i}}{\frac{I_{n+1}(\xi a_2)}{\xi}} \frac{\left[n\left(1-\frac{1}{\mu_r}\right)I_n(\xi a_2) - \frac{\xi a_1}{\mu_r} I_{n+1}(\xi a_2)\right]}{\left[n\left(1+\frac{1}{\mu_r}\right)I_n(\xi a_2) + \frac{\xi a_1}{\mu_r} I_{n+1}(\xi a_2)\right]} \tag{3.2.75}$$

$$g_{2n} = \frac{\frac{j\omega\sigma\mu_0}{\pi}\sum_{i=1}^{N}\boldsymbol{I}_{1i}\left(\frac{a_2}{b_{2i}}\right)^n \cos n\theta_{2i}}{\left[n\left(1+\frac{1}{\mu_r}\right)I_n(\xi a_2) + \frac{\xi a_1}{\mu_r} I_{n+1}(\xi a_2)\right]} \tag{3.2.76}$$

$$h_{2n} = \frac{\frac{j\omega\sigma\mu_0}{\pi}\sum_{i=1}^{N}\boldsymbol{I}_{1i}\left(\frac{a_2}{b_{2i}}\right)^n \sin n\theta_{2i}}{\left[n\left(1+\frac{1}{\mu_r}\right)I_n(\xi a_2) + \frac{\xi a_1}{\mu_r} I_{n+1}(\xi a_2)\right]} \tag{3.2.77}$$

The coefficients for the other conductor are equally obtained and are:

$$e_{1n} = \frac{\frac{1}{\pi}\sum_{j=1}^{N}\frac{\boldsymbol{I}_{2j}}{a_1}\left(\frac{a_1}{b_{1j}}\right)^n \cos n\theta_{1j}}{\frac{I_{n+1}(\xi a_1)}{\xi}} \frac{\left[n\left(1-\frac{1}{\mu_r}\right)I_n(\xi a_1) - \frac{\xi a_1}{\mu_r} I_{n+1}(\xi a_1)\right]}{\left[n\left(1+\frac{1}{\mu_r}\right)I_n(\xi a_1) + \frac{\xi a_1}{\mu_r} I_{n+1}(\xi a_1)\right]} \tag{3.2.78}$$

$$f_{1n}=\frac{\frac{1}{\pi}\sum_{j=1}^{N}\frac{\boldsymbol{I}_{2j}}{a_1}(\frac{a_1}{b_{1j}})^n\sin n\theta_{1j}}{\frac{I_{n+1}(\xi a_1)}{\xi}}\frac{\left[n\left(1-\frac{1}{\mu_r}\right)I_n(\xi a_1)-\frac{\xi a_1}{\mu_r}I_{n+1}(\xi a_1)\right]}{\left[n\left(1+\frac{1}{\mu_r}\right)I_n(\xi a_1)+\frac{\xi a_1}{\mu_r}I_{n+1}(\xi a_1)\right]} \tag{3.2.79}$$

$$g_{1n}=\frac{\frac{j\omega\sigma\mu_0}{\pi}\sum_{j=1}^{N}\boldsymbol{I}_{2j}(\frac{a_1}{b_{1j}})^n\cos n\theta_{1j}}{\left[n\left(1+\frac{1}{\mu_r}\right)I_n(\xi a_1)+\frac{\xi a_1}{\mu_r}I_{n+1}(\xi a_1)\right]} \tag{3.2.80}$$

$$h_{1n}=\frac{\frac{j\omega\sigma\mu_0}{\pi}\sum_{j=1}^{N}\boldsymbol{I}_{2j}(\frac{a_1}{b_{1j}})^n\sin n\theta_{1j}}{\left[n\left(1+\frac{1}{\mu_r}\right)I_n(\xi a_1)+\frac{\xi a_1}{\mu_r}I_{n+1}(\xi a_1)\right]} \tag{3.2.81}$$

Evaluation of zero-order coefficients

The zero order term, that we cannot infer from the generic expression, represents the classical skin effect term, as derived by Schelkunoff [**3**], namely:

$$g_{10}=\frac{\xi}{2\pi a_1 I_1(\xi a_1)} \tag{3.2.82}$$

$$g_{20}=\frac{\xi}{2\pi a_2 I_1(\xi a_2)} \tag{3.2.83}$$

The potential coefficients in the dielectric are related to the current density coefficient in the conductor by the relation

$$-e_{10}\frac{1}{\xi}I_1(\xi a_2)-\frac{\xi}{j\omega\sigma\mu}g_{10}I_1(\xi a_2)=0 \tag{3.2.84}$$

$$-e_{20}\frac{1}{\xi}I_1(\xi a_2)-\frac{\xi}{j\omega\sigma\mu}g_{20}I_1(\xi a_2)=0 \tag{3.2.85}$$

$$e_{10}=-\frac{\xi}{2\pi a_1 I_1(\xi a_1)} \tag{3.2.86}$$

$$e_{20}=-\frac{\xi}{2\pi a_2 I_1(\xi a_2)} \tag{3.2.87}$$

Expression for the current density and calculation of thin wires current intensities

Using the coefficients that we have just calculated (actually for writing J we just need g_n and h_n) we are able to write the current density in both conductors, as a function of the total current circulating on the conductor, and the thin wire current intensity.

$$\vec{J}_1(r_1,\phi_1)=\frac{\xi\boldsymbol{I}}{2\pi a_1}\frac{I_0(\xi r_1)}{I_1(\xi a_1)}\hat{z}+\frac{\xi}{\pi}\sum_{n=1}^{\infty}L_{1n}I_n(\xi r_1)\sum_{j=1}^{N}\boldsymbol{I}_{2j}(\frac{a_1}{b_{1j}})^n\left(\cos n\theta_{1j}\cos n\phi_1+\sin n\theta_{1j}\sin n\phi_1\right)\hat{z} \tag{3.2.88}$$

$$\vec{J}_2(r_2,\phi_2)=\frac{\xi\boldsymbol{I}}{2\pi a_2}\frac{I_0(\xi r_2)}{I_1(\xi a_2)}\hat{z}+\frac{\xi}{\pi}\sum_{n=1}^{\infty}L_{2n}I_n(\xi r_2)\sum_{i=1}^{N}\boldsymbol{I}_{1i}(\frac{a_2}{b_{2i}})^n\left(\cos n\theta_{2j}\cos n\phi_2+\sin n\theta_{2j}\sin n\phi_2\right)\hat{z} \tag{3.2.89}$$

Here we regrouped all the terms which are not functions of i or j but only of n in the coefficients L_{1n}, L_{2n}, this in order to obtain a more compact expression.

$$L_{1n} = \frac{1}{\left[n\left(1+\frac{1}{\mu_r}\right) I_n(\xi a_1) + \frac{\xi a_1}{\mu_r} I_{n+1}(\xi a_1) \right]}$$

$$L_{2n} = \frac{1}{\left[n\left(1+\frac{1}{\mu_r}\right) I_n(\xi a_2) + \frac{\xi a_2}{\mu_r} I_{n+1}(\xi a_2) \right]}$$

These expressions for the current densities are a function of the geometrical mutual positions of the wires (expressed through distances and relative angles) and their amplitude.

The mutual positions being already known, we now need to find the current intensity on the thin wires.

Having solved the continuity equations for the magnetic vector potential, we have calculated the coefficients that allow writing the current density inside the conductors. These densities depend on the intensity value of the thin wires, which are still unknown quantities.

In order to find these quantities, we express the thin wire sources as a function of the current density in the sub-conductor which is identified by the thin wire.

To do that we can say that the thin wire current intensity corresponds to the value of the current density at the point where the wire is, multiplied by the surface of the sub-conductor in which we assume the current density to be constant, namely:

$$\boldsymbol{I}_{1i} = \vec{J}_1(r_{1i}, \phi_{1i}) dS_{1i} \tag{3.2.90}$$

$$\boldsymbol{I}_{2j} = \vec{J}_2(r_{2j}, \phi_{2j}) dS_{2j} \tag{3.2.91}$$

dS_{1i} and dS_{2j} are the surfaces of the sub-conductors in whose midpoint is located the ith or jth thin wire.

We now write the current density in one specific point where the wire is located as:

$$\vec{J}_1(r_{1i}, \phi_{1i}) = \frac{\boldsymbol{I}\xi}{2\pi a_1} \frac{I_0(\xi r_{1i})}{I_1(\xi a_1)} + \frac{\xi}{\pi} \sum_{n=1}^{\infty} L_{1n} I_n(\xi r_{1i}) \sum_{j=1}^{N} I_{2j} \left(\frac{a_1}{b_{1j}}\right)^n \left(\cos n\left(\theta_{1j} - \phi_{1i}\right)\right) \hat{z} \tag{3.2.92}$$

$$\vec{J}_2(r_{2j}, \phi_{2j}) = \frac{-\boldsymbol{I}\xi}{2\pi a_2} \frac{I_0(\xi r_{2j})}{I_1(\xi a_2)} + \frac{\xi}{\pi} \sum_{n=1}^{\infty} L_{2n} I_n(\xi r_{2j}) \sum_{i=1}^{N} I_{1i} \left(\frac{a_2}{b_{2i}}\right)^n \left(\cos n\left(\theta_{2i} - \phi_{2j}\right)\right) \hat{z} \tag{3.2.93}$$

And from the definitions given before:

$$I_{1i} = \left[\frac{\boldsymbol{I}\xi}{2\pi a_1} \frac{I_0(\xi r_{1i})}{I_1(\xi a_1)} + \frac{\xi}{\pi} \sum_{n=1}^{\infty} L_{1n} I_n(\xi r_{1i}) \sum_{j=1}^{N} I_{2j} \left(\frac{a_1}{b_{1j}}\right)^n \left(\cos n\left(\theta_{1j} - \phi_{1i}\right)\right) \right] dS_{1i} \tag{3.2.94}$$

$$I_{2j} = \left[\frac{\boldsymbol{I}\xi}{2\pi a_2} \frac{I_0(\xi r_{2j})}{I_1(\xi a_2)} + \frac{\xi}{\pi} \sum_{n=1}^{\infty} L_{2n} I_n(\xi r_{2j}) \sum_{i=1}^{N} I_{1i} \left(\frac{a_2}{b_{2i}}\right)^n \left(\cos n\left(\theta_{2i} - \phi_{2j}\right)\right) \right] dS_{2j} \tag{3.2.95}$$

Rewritten as

$$\frac{\boldsymbol{I}\xi}{2\pi a_1} \frac{I_0(\xi r_{1i})}{I_1(\xi a_1)} dS_{1i} + \sum_{j=1}^{N} \boldsymbol{I}_{2j} \frac{\xi}{\pi} dS_{1i} \sum_{n=1}^{\infty} L_{1n} I_n(\xi r_{1i}) \left(\frac{a_1}{b_{1j}}\right)^n \left(\cos n\left(\theta_{1j} - \phi_{1i}\right)\right) - I_{1i} = 0 \tag{3.2.96}$$

$$\frac{\boldsymbol{I}\xi}{2\pi a_2}\frac{I_0(\xi r_{2j})}{I_1(\xi a_2)}dS_{2j}+\sum_{i=1}^{N}\boldsymbol{I}_{1i}\frac{\xi}{\pi}dS_{2j}\sum_{n=1}^{\infty}L_{2n}I_n(\xi r_{2j})(\frac{a_2}{b_{2i}})^n\left(\cos n\left(\theta_{2i}-\phi_{2j}\right)\right)-I_{2j}=0 \qquad (3.2.97)$$

This last set of equations can be rewritten as a matrix *[2Nx2N]* of the sort:

$$\begin{array}{c} \\ i \\ \\ \\ \\ \\ \\ \\ j \\ \\ \\ \end{array}\begin{array}{c} \begin{array}{cccccc} & & & i & & \end{array} \\ \left[\begin{array}{cccccc|cccccc} -1 & 0 & 0 & & & & & & & & & \\ 0 & -1 & 0 & 0 & & & & & & & & \\ & 0 & . & & & & & Q_{ij} & & & & \\ & & & . & 0 & & & & & & & \\ & & & 0 & -1 & & & & & & & \\ - & - & - & - & - & - & - & - & - & - & - & - \\ & & & & & & -1 & 0 & 0 & 0 & 0 & \\ & & & & & & 0 & -1 & & & & \\ & R_{ij} & & & & & & & & & & \\ & & & & & & & & & & 0 & \\ & & & & & & 0 & & 0 & 0 & -1 & \end{array}\right] \end{array}\begin{array}{c} \\ \\ \\ \\ \\ \\ \\ \\ j \\ \\ \\ \end{array}\begin{array}{c} \begin{array}{c} \end{array} \\ \left[\begin{array}{c} I_{11} \\ . \\ I_{1i} \\ . \\ I_{1N}\cdot \\ --- \\ I_{21} \\ . \\ I_{2j} \\ . \\ I_{2N} \end{array}\right] \end{array}=\begin{array}{c} \\ \\ \\ \\ \\ \\ \\ \\ \\ \\ \\ \end{array}\begin{array}{c} \begin{array}{c} \end{array} \\ \left[\begin{array}{c} \frac{\boldsymbol{I}\xi}{2\pi a_1 I_1(\xi a_1)} \\ \\ \\ \\ \\ --------- \\ \\ \\ \frac{-\boldsymbol{I}\xi}{2\pi a_2 I_1(\xi a_2)} \\ \\ \\ \end{array}\right] \end{array}\begin{array}{c} \\ \\ \\ \\ \\ \\ \\ \\ \\ \\ \\ \end{array}\begin{array}{c} \begin{array}{c} \end{array} \\ \left[\begin{array}{c} I_0(\xi r_{11})dS_{11} \\ . \\ I_0(\xi r_{1i})dS_{1i} \\ . \\ I_0(\xi r_{1N})dS_{1N} \\ ----- \\ I_0(\xi r_{21})dS_{21} \\ . \\ I_0(\xi r_{2j})dS_{2j} \\ . \\ I_0(\xi r_{2N})dS_{2N} \end{array}\right]_{2N} \end{array} \qquad (3.2.98)$$

where

$$Q_{ij}=\frac{j\omega\sigma\mu}{\pi}dS_1\sum_{n=1}^{\infty}L_{1n}I_n(\xi r_{1i})\left(\frac{a_1}{b_{1j}}\right)^n\left(\cos n\left(\theta_{1j}-\phi_{1i}\right)\right) \qquad (3.2.99)$$

$$R_{ij}=\frac{j\omega\sigma\mu}{\pi}dS_2\sum_{n=1}^{\infty}L_{2n}I_n(\xi r_{2j})\left(\frac{a_2}{b_{2i}}\right)^n\left(\cos n\left(\theta_{2i}-\phi_{2j}\right)\right) \qquad (3.2.100)$$

Note that the sum with the index n must be limited to a finite value in order to be calculated.

It is possible to solve this system because the matrix is non singular and therefore invertible.

Once the thin wire current intensities have been calculated (they will all be a function of the total current ***I***) these can be used to calculate the impedances, as shown in the next paragraphs.

3.2.3.1. Development of logarithm as a series

We show here how we evaluate the logarithm that is used in the previous chapter in obtaining equation(3.2.43).

The first step is to express the distance R_1 as a function of the coordinates (ρ_1,θ_1) and to do that we will use the equivalence

$$log_e(R_1)=log_e(\rho_1)-\sum_{n=1}^{+\infty}\frac{1}{n}\left(\frac{r_1}{\rho_1}\right)^n\cos(n(\phi_1-\theta_1)) \qquad (3.2.101)$$

We now turn to the demonstration of this equivalence.

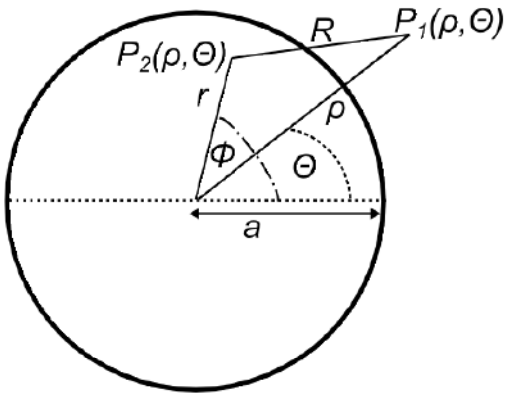

Fig.21 – Description of the coordinate systems for the generic conductor section

If we consider Fig.21 and take into consideration the points $P_1(\rho,\theta)$, $P_2(r,\phi)$ we can rotate the reference of –θ so that the points now have coordinates $P_1(\rho,0)$, $P_2(r,\phi-\theta)$.

Using a complex notation it is easy to demonstrate that, z being a complex number[12],

$Re\{ln(z)\} = ln|z|$ since we can write

$ln(z) = ln|z| + j\,Arg(z)$

Now we can write

$$\ln(R) = \ln\left(\rho - re^{j(\phi-\theta)}\right) = \ln\left(\rho\left(1-\frac{r}{\rho}e^{j(\phi-\theta)}\right)\right) = \ln(\rho) + \ln\left(1-\frac{r}{\rho}e^{j(\phi-\theta)}\right) \tag{3.2.102}$$

We can rewrite the second right term applying a series development for the logarithm:

$$\ln(1-x) = -\sum_{n=1}^{\infty}\frac{x^n}{n} \quad for\ |x|<1 \tag{3.2.103}$$

We have $\ln(R) = \ln(\rho) - \sum_{n=1}^{\infty}\frac{1}{n}\left(\frac{r}{\rho}\right)^n e^{jn(\phi-\theta)}$ (3.2.104)

And since we are interested only in the logarithm of the modulus of R we will take the real part and obtain (3.2.101)

[12] From now on we will indicate the neperian logarithm with ln instead of the notation $\log_e$

3.3. Method for the calculation of induced currents based on thin-wire approach: round core conductor inside a hollow screen conductor

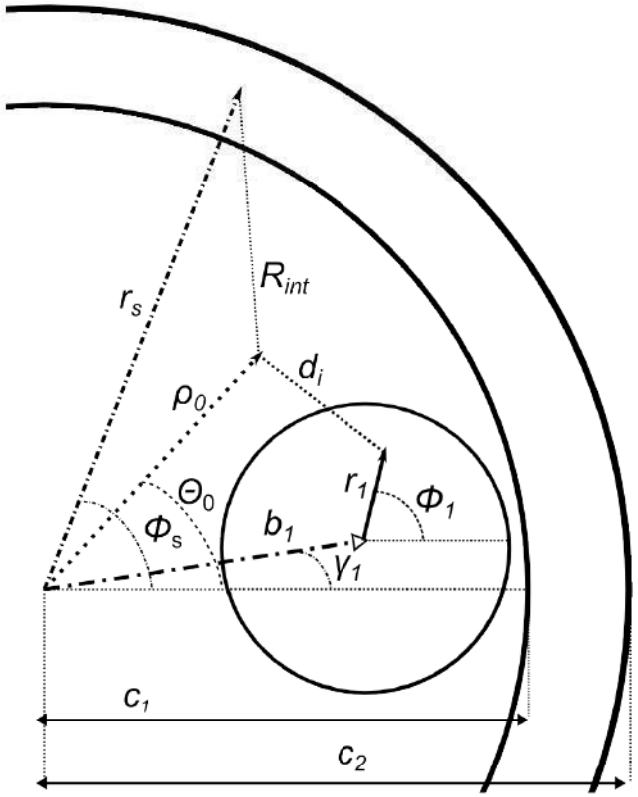

Fig.22 – Description of the geometry of cable considered, with relevant notations

In the following table we show the notation used in this section.

Table 3 - Notations used in Section3.3

A^e_{sd} / A^s_{sd}	Magnetic vector potential in the dielectric due to current density inside the screen conductor / thin wires	ϕ / θ	Angular coordinate inside/outside the conductor
A^e_{id} / A^s_{id}	Magnetic vector potential in the dielectric due to current density inside the *i*th conductor / thin wires	$\boldsymbol{I}$, $\boldsymbol{I_{ij}}$	Total current / current of *j*th thin wire of *i*th conductor
A_{ij} / A_{sj}	Magnetic vector potential due to *j*th thin wire of *i*th conductor	K_n	Bessel modified function of second kind and n-th order
a_i	Radius of *i*th conductor	j	Imaginary unity
b_i	Distance of *i*th conductor from the pipe's centre	J_i / J^e_i	Total current density / eddy current in *i*th conductor
c1 / *c2*	Inner / outer radius of the pipe	μ / μ_o/μ_r	Magnetic permeability / permeability in vacuum, relative permeability
d	Distance between a point of the dielectric and a generic thin wire	r / ρ	Radial coordinate inside / outside the conductor

3.3.1. Methodology description

We shall use two different cases, as shown in Fig.23, in order to be able to calculate the mutual effect of the conductors on each other's expression of the current density (and therefore impedance). As in the earlier chapter the terms we find are only the corrections which account for proximity effects, whereas the skin effect is evaluated using Schelkunoff precise formulas.

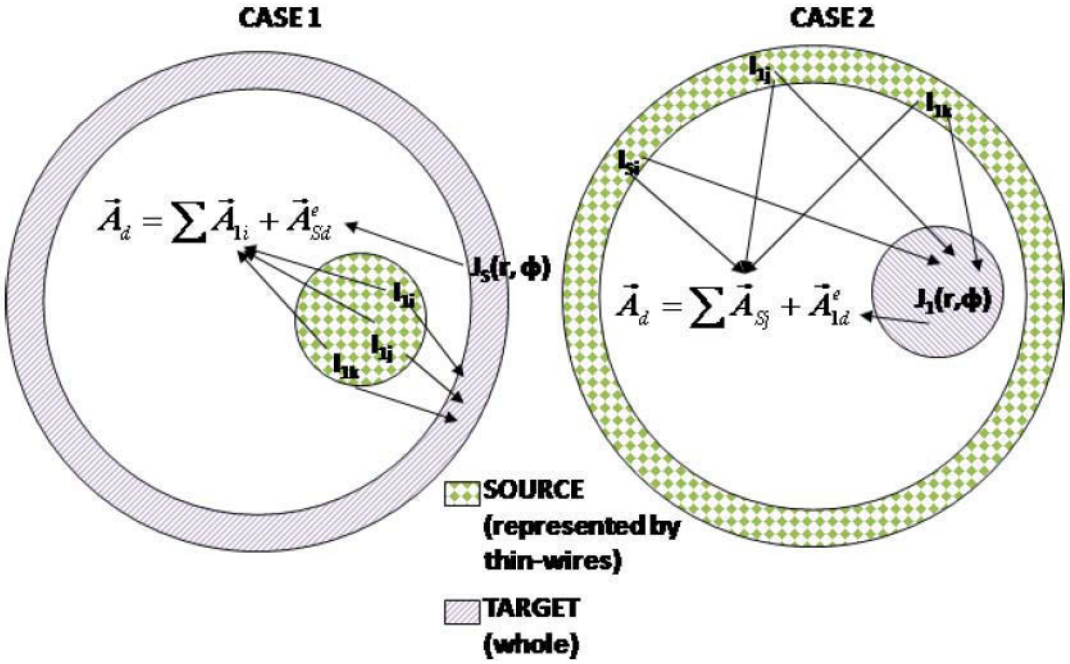

Fig.23 – Two cases (step) used for the calculation of current density distribution in the conductors

The situations we analyse (see Fig.23) and solve in parallel, in order to evaluate the unknown coefficients that are present in the expression of current density and vector potential, are the following:

- In CASE 1
  - The inner core conductor is represented as the source of the induction, that is as a multitude of thin wires, each of which induces a current density in the hollow conductor and also a vector potential in the dielectric
  - The "screen" hollow conductor is represented as solid, but it is considered as having an infinite outer radius. This approximation, which allows us to obtain simpler expressions, introduces an error, but this error should be compensated by the thin wires distribution of case 2.
- In CASE 2
  - The outer screen conductor is represented by a multitude of thin wires. The position of the wires follows the actual surface of the conductor; this should act as a counterweight to compensate the approximation used before. This consideration follows from the fact that the actual current density distribution depends upon the intensity value of each thin wire, and this is determined by "uniting" case 1 and case 2 with one another.
  - The inner core conductor is represented as solid, and its current density / potential is represented as in the prior chapter.

As before, we proceed by finding the vector potential in each region, but contrary to the two conductor's case, here the situation is not symmetrical; therefore we will treat the two cases

separately.

Once the potential has been found, in each case the coefficients are calculated through the resolution of a system of equation, deduced from the boundary conditions (on the screen's inner surface in case 1 and on the core's outer surface in case 2).

The last step is exactly analogue to what has been done before for the case of the two wires.

The matrix equation system, which relates the thin wires of the two cases, allows solving their intensities.

As for the case of two conductors, the current which is "injected" in the core conductor returns entirely through the screen.

Finally the resistance and inductance are defined, using the "energetic method".

Description of the notation

The core conductor has a radius a_1, the screen conductor has inner and outer radiuses c_1 and c_2.

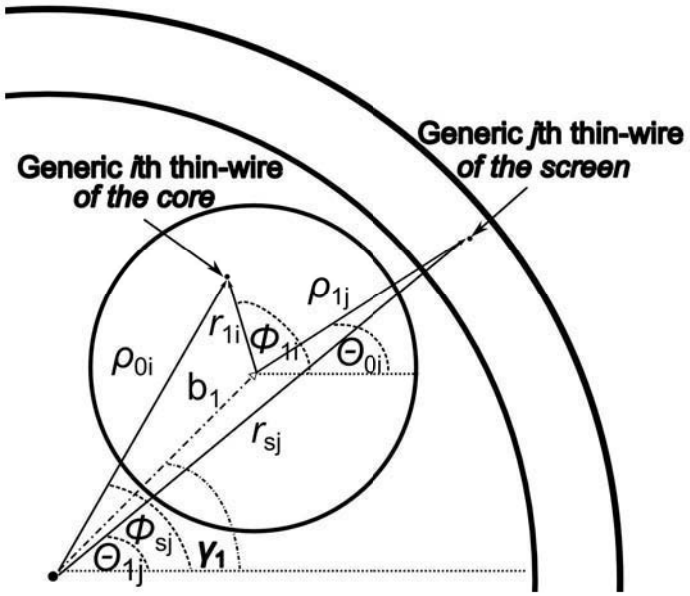

Fig.24 – Coordinates of filaments in the screen and core conductors

- In CASE 1

-(b_1,γ_1) are the coordinates of the centre of the core conductor; (r_s,ϕ_s) are the generic coordinates of the screen, (ρ_0,θ_0) are the coordinates of a generic point in the dielectric and R_{int} is the distance between a point in the screen and the generic point in the dielectric;

- (r_{1i},ϕ_{1i}) are the coordinates of the *i*th thin-wire inside the core (identified in the core's coordinate system), whereas the same wire is identified as (ρ_{0i},θ_{0i}) in the screen coordinate system (the transformation is detailed in the following).

- In CASE 2

(r_1,ϕ_1) are the coordinates of the core conductor (centred in its centre). (ρ_0,θ_0) are the coordinates of the dielectric medium, coordinates which are centred in the core conductor.

(r_{si},ϕ_{si}) are the coordinates of the *j*th thin wire representing the screen conductor, whereas the thin wire is represented as (ρ_{1j},θ_{1j}) when viewed from the coordinate system of the core

conductor.

3.3.2. Case of core acting as a source (Case 1)

Generic expression for current and potential inside the conductor

We shall now write the generic expression for the current density and the vector potential inside the screen, approximated as having an infinite outer layer.

$$\vec{J}_S(r_S,\phi_S)=\sum_{n=0}^{\infty}\left[o_n cos(n\phi_S)+p_n sin(n\phi_S)\right]K_n(\xi_S r_S)\,\hat{z} \tag{3.3.1}$$

$$\vec{A}_S(r_S,\phi_S)=\frac{-1}{j\omega\sigma_S}\sum_{n=0}^{\infty}\left[o_n cos(n\phi_S)+p_n sin(n\phi_S)\right]K_n(\xi_S r_S)\,\hat{z} \tag{3.3.2}$$

where o_n, p_n are coefficients functions of n later to be determined, $\xi_S=\sqrt{j\omega\mu_S\sigma_S}$ and K_n the modified Bessel function of second kind and *n-th* order.

Potential in the dielectric, due to current density in the screen

We consider that an infinitesimal element of the screen's surface contributes, in terms of current density, to the potential in the dielectric (inside the screen) as:

$$d^2{}_{Sd}^{\,e}\vec{A}(\rho,\theta)=\frac{\mu_0}{2\pi}\vec{J}_S(r,\phi)\ln R_{\text{int}}\,r\,dr\,d\phi \tag{3.3.3}$$

The logarithmic development, used in the previous chapter, is here again employed for the calculation of the logarithm of the generic distances, which are:

$$\ln(R_{\text{int}})=\ln(r_S)-\sum_{n=1}^{+\infty}\frac{1}{n}\left(\frac{\rho_0}{r_S}\right)^n\cos(n(\phi_S-\theta_0)) \tag{3.3.4}$$

The integrals are[13]:

$$\vec{A}_{Sd}^{\,e}(\rho_0,\theta_0)=\frac{\mu_0}{2\pi}\int_{c_1}^{\infty}\int_0^{2\pi}\ln r_s)\sum_{n=0}^{\infty}\left[s_n cos(n\phi_S)+t_n sin(n\phi_S)\right]K_n(\xi_S r_S)\,r_S\,dr_s d\phi_s\,+$$

$$-\frac{\mu_0}{2\pi}\int_{c_1}^{\infty}\int_0^{2\pi}\sum_{m=1}^{\infty}\frac{1}{m}\left(\frac{\rho_0}{r_S}\right)^m\sum_{n=0}^{\infty}\left[s_n cos(n\phi_S)+t_n sin(n\phi_S)\right]K_n(\xi_S r_S)\cdot \tag{3.3.5}$$

$$\cdot\left[\cos(m\phi_S)\cos(m\theta_0)+\sin(m\phi_S)\sin(m\theta_0)\right]r_S\,dr_s d\phi_s$$

For simplicity we shall rewrite the potential as the sum of two parts:

$$\vec{A}_{Sd}^{\,e}(\rho,\theta)=I_1+I_2$$

The trigonometric properties applied, the angular part is integrated, giving

$$I_1=\mu_0\int_{c_1}^{\infty}\ln(r_s)s_0K_0(\xi_S r_S)r_s\,dr \tag{3.3.6}$$

[13]Note that the coefficients are not the same as in the expression of *Js* but are changed in order to account for the medium discontinuity; we introduce s_n and t_n .

Using integration by parts, namely $\int u dv = uv - \int v du$ with or $dv = K_0(\xi_S r_S) r_S$ and $u = \ln(r_s)$, whilst applying Bessel function property $\int x^n K_{n-1}(\xi x) dx = -\frac{x^n}{\xi} K_n(\xi x)$

We have

$$I_1 = \frac{\mu_0 s_0}{\xi_S}\left[c_1 \ln(c_1) K_1(\xi_S c_1) - \frac{K_0(\xi_S c_1)}{\xi_S}\right] = \frac{\mu_0}{\xi} s_0 S_0 \tag{3.3.7}$$

with $S_0 = \left[c_1 \ln(c_1) K_1(\xi_S c_1) + \frac{K_0(\xi_S c_1)}{\xi_S}\right]$

For the other integral, applying trigonometric properties, only the terms with n=m result different from zero, and this gives:

$$I_2 = -\frac{\mu_0}{2}\int_{c_1}^{\infty}\sum_{n=1}^{\infty}\frac{1}{n}\left(\frac{\rho_0}{r_S}\right)^n \left[s_n cos(n\theta_0) + t_n sin(n\theta_0)\right] K_n(\xi_S r_S)\cdot r_S \, dr_S \tag{3.3.8}$$

Now in order to solve this integral we apply again Bessel's function properties and we obtain

$$I_2 = -\frac{\mu_0}{2\xi_S}\sum_{n=1}^{\infty}\frac{\rho_0^n}{n}\frac{K_{n-1}(\xi_S c_1)}{c_1^{n-1}}\left\{\left[s_n cos(n\theta_0) + t_n sin(n\theta_0)\right]\right\} \tag{3.3.9}$$

and the final expression of the potential is

$$\vec{A}^e_{Sd}(\rho,\theta) = s_0 S_0 + \\ -\frac{\mu_0}{2\xi_S}\sum_{n=1}^{\infty}\frac{\rho_0^n}{n}\frac{K_{n-1}(\xi_S c_1)}{c_1^{n-1}}\left[s_n cos(n\theta_0) + t_n sin(n\theta_0)\right] \tag{3.3.10}$$

Contribution of the thin wires representing the inner conductor.

The potential due to the thin wires is written in the same way as in the last chapter, namely for the *i-th* wire:

$$\vec{A}_{1i}(\rho_0,\theta_0) = \frac{\mu_0}{2\pi}\boldsymbol{I}_{1i}\left[\ln(\rho_0) - \sum_{n=1}^{\infty}\frac{1}{n}\left(\frac{\rho_{0i}}{\rho_0}\right)^n \cos\left(n(\theta_{0i} - \theta_0)\right)\right] \tag{3.3.11}$$

The quantity (ρ_{0i}, θ_{0i}) is evaluated as:

$$\rho_{0i} = \sqrt{b_1^2 + r_{1i}^2 + 2b_1 r_{1i} cos(\phi_{1i} - \gamma_1)} \tag{3.3.12}$$

$$\theta_{0i} = \arctan\left(\frac{b_1 \sin\gamma_1 + r_{1i}\sin(\phi_{1i})}{b_1\cos\gamma_1 + r_{1i}cos(\phi_{1i})}\right) \tag{3.3.13}$$

Solution of Case 1

Continuity conditions (analogue to(3.2.54)(3.2.55)) are written on the screen inner boundary using all the potentials contributions found for the two mediums.

$$B_{\rho-\text{int}} = B_{r-screen}\begin{cases}\dfrac{\mu_0}{2\xi}\displaystyle\sum_{n=1}^{\infty}K_{n-1}(\xi_S c_1)\{[s_n\sin(n\theta_0)-t_n\cos(n\theta_0)]\}+\\ \displaystyle\sum_{i=1}^{N}\frac{\mu_0}{2\pi}\boldsymbol{I}_{1i}\left[\sum_{n=1}^{\infty}\frac{1}{c_1}\left(\frac{\rho_{0i}}{c_1}\right)^n\sin\left(n(\theta_{0i}-\theta_0)\right)\right]=\\ =\dfrac{n}{j\omega\sigma_S c_1}\displaystyle\sum_{n=0}^{\infty}[o_n\sin(n\phi_S)-p_n\cos(n\phi_S)]K_n(\xi_S c_1)\end{cases} \tag{3.3.14}$$

$$H_{\theta-\text{int}} = H_{\phi-screen}\begin{cases}\dfrac{1}{2\xi}\displaystyle\sum_{n=1}^{\infty}K_{n-1}(\xi_S c_1)\{[s_n\cos(n\theta_0)+t_n\sin(n\theta_0)]\}+\\ -\displaystyle\sum_{i=1}^{N}\frac{1}{2\pi}\boldsymbol{I}_{1i}\left[\sum_{n=1}^{\infty}\frac{1}{c_1}\left(\frac{\rho_{0i}}{c_1}\right)^n\cos\left(n(\theta_{0i}-\theta_0)\right)\right]=\\ =\dfrac{\xi}{j\omega\sigma_S\mu_S}\displaystyle\sum_{n=0}^{\infty}[o_n\cos(n\phi_S)+p_n\sin(n\phi_S)]K_n'(\xi_S c_1)\end{cases} \tag{3.3.15}$$

$$\begin{cases}-\dfrac{\mu_0}{2\xi_S}K_{n-1}(\xi_S c_1)s_n-\dfrac{\mu_0}{2\pi}\displaystyle\sum_{i=1}^{\infty}\boldsymbol{I}_{1i}\frac{1}{c_1}\left(\frac{\rho_{0i}}{c_1}\right)^n\text{co}\ (n\theta_{0i})-\dfrac{n}{j\omega\sigma_S c_1}o_n K_n(\xi_S c_1)=0\\ +\dfrac{\mu_0}{2\xi_S}K_{n-1}(\xi_S c_1)t_n+\dfrac{\mu_0}{2\pi}\displaystyle\sum_{i=1}^{N}\boldsymbol{I}_{1i}\frac{1}{c_1}\left(\frac{\rho_{0i}}{c_1}\right)^n\sin(n\theta_{0i})+\dfrac{n}{j\omega\sigma_S c_1}p_n K_n(\xi_S c_1)=0\\ \dfrac{1}{2\xi_S}K_{n-1}(\xi_S c_1)s_n-\dfrac{1}{2\pi}\displaystyle\sum_{i=1}^{N}\boldsymbol{I}_{1i}\frac{1}{c_1}\left(\frac{\rho_{0i}}{c_1}\right)^n\cos(n\theta_{0i})-\dfrac{\xi_S}{j\omega\sigma_S\mu_S}o_n K_n'(\xi_S c_1)=0\\ \dfrac{1}{2\xi_S}K_{n-1}(\xi_S c_1)t_n-\dfrac{1}{2\pi}\displaystyle\sum_{i=1}^{N}\boldsymbol{I}_{1i}\frac{1}{c_1}\left(\frac{\rho_{0i}}{c_1}\right)^n\sin(n\theta_{0i})-\dfrac{\xi_S}{j\omega\sigma_S\mu_S}p_n K_n'(\xi_S c_1)=0\end{cases} \tag{3.3.16}$$

The coefficients of the current density are found to be[14]:

$$o_n=-\frac{\xi_S}{\pi}\frac{\displaystyle\sum_{i=1}^{N}\boldsymbol{I}_{1i}\frac{1}{c_1}\left(\frac{\rho_{0i}}{c_1}\right)^n\cos(n\theta_{0i})}{(1+\mu_r)K_n'(\xi_S c_1)+\mu_r K_{n-1}(\xi_S c_1)}=\frac{j\omega\mu_S\sigma_S}{\pi}\frac{\displaystyle\sum_{i=1}^{N}\boldsymbol{I}_{1i}\left(\frac{\rho_{0i}}{c_1}\right)^n\cos(n\theta_{0i})}{n(1+\mu_r)K_n(\xi_S c_1)+\xi_S c_1 K_{n-1}(\xi_S c_1)} \tag{3.3.17}$$

$$p_n=-\frac{\xi_S}{\pi}\frac{\displaystyle\sum_{i=1}^{N}\boldsymbol{I}_{1i}\frac{1}{c_1}\left(\frac{\rho_{0i}}{c_1}\right)^n\sin(n\theta_{0i})}{(1+\mu_{rs})K_n'(\xi_S c_1)+\mu_r K_{n-1}(\xi_S c_1)}=\frac{j\omega\mu_S\sigma_S}{\pi}\frac{\displaystyle\sum_{i=1}^{N}\boldsymbol{I}_{1i}\left(\frac{\rho_{0i}}{c_1}\right)^n\sin(n\theta_{0i})}{n(1+\mu_{rs})K_n(\xi_S c_1)+\xi_S c_1 K_{n-1}(\xi_S c_1)} \tag{3.3.18}$$

whereas the coefficients for the vector potential are:

$$s_n=\frac{1}{\pi}\frac{\displaystyle\sum_{i=1}^{N}\boldsymbol{I}_{1i}\left(\frac{\rho_{0i}}{c_1}\right)^n\cos(n\theta_{0i})}{K_{n-1}(\xi_S c_1)}\frac{\left[\dfrac{n}{\xi_s c_1}(\mu_{rs}-1)K_n(\xi_S c_1)+K_{n-1}(\xi_S c_1)\right]}{\left[\dfrac{n}{\xi_s c_1}(\mu_{rs}-1)K_n(\xi_S c_1)-K_{n-1}(\xi_S c_1)\right]} \tag{3.3.19}$$

[14] The passage is found using Bessel functions properties, namely formula 116 at page 165 of [**73**]

$$t_n = \frac{1}{\pi}\frac{\sum_{i=1}^{N} \boldsymbol{I}_{1i}\left(\frac{\rho_{0i}}{c_1}\right)^n \sin(n\theta_{0i})\left[\frac{n}{\xi_S c_1}(\mu_{rs}-1)K_n(\xi_S c_1)+K_{n-1}(\xi_S c_1)\right]}{K_{n-1}(\xi_S c_1)\left[\frac{n}{\xi_S c_1}(\mu_{rs}-1)K_n(\xi_S c_1)-K_{n-1}(\xi_S c_1)\right]} \tag{3.3.20}$$

Term of zero-order for the current density in the screen

The term which accounts for the skin effect in the screen is found, from Schelkunoff as

$$J_{skin}(r,\phi) = \frac{\xi_S}{2\pi c_1}\frac{\left[I_0(\xi_S r)K_1(\xi_S c_2)+I_1(\xi_S c_2)K_0(\xi_S r)\right]}{\left[I_1(\xi_S c_2)K_1(\xi_S c_1)-I_1(\xi_S c_1)K_1(\xi_S c_2)\right]} \tag{3.3.21}$$

In evaluating this term, the finite thickness of the screen is taken into account.

3.3.3. Case of screen acting as a source (Case 2)

The expressions for the current density and potentials (obtained in the previous section) are:

$$\vec{J}_1(r_1,\phi_1) = \sum_{n=0}^{\infty} g_{1n}I_n(\xi_c r_1)cos(n\phi_1) + h_{1n}I_n(\xi_c r_1)sin(n\phi_1)\,\hat{z} \tag{3.3.22}$$

$$\vec{A}_1(r_1,\phi_1) = -\frac{1}{j\omega\sigma_c}\sum_{n=0}^{\infty} g_{1n}I_n(\xi_c r_1)cos(n\phi_1) + h_{1n}I_n(\xi_c r_1)sin(n\phi_1)\,\hat{z} \tag{3.3.23}$$

Integration of the potential due to J_1 as is found in the previous chapter is:

$$\vec{A}^e_{1d}(\rho_1,\theta_1) = \mu_0 e_1\, ln(\rho_{01})\frac{a_1}{\xi_c}I_1(\xi_c a_1) - \frac{\mu_0}{2}\sum_{n=1}^{\infty}\frac{1}{n\rho_1^n}\frac{a_1^{n+1}}{\xi_c}\left[e_{1n}cos(n\theta_1)+f_{1n}sin(n\theta_1)\right]I_{n+1}(\xi_c a_1) \tag{3.3.24}$$

Contribution of the thin wires representing the screen conductor.

We now need to account for the contribution of the thin wires inside the screen. Each wire gives a contribution[15]:

$$\vec{A}_{Sj}(\rho_0,\theta_0) = \frac{\mu_0}{2\pi}\boldsymbol{I}_{Sj}\ln d_{Sj} \tag{3.3.25}$$

We need to express the distance d_{Sj} between each filament, and the generic point in the dielectric as a function of the coordinate (ρ_0,θ_0) this because continuity equations shall be written on the screen/dielectric interface. The logarithm becomes:

$$\ln d_{Sj} = \ln(\rho_{1j}) - \sum_{m=1}^{\infty}\frac{1}{m}\left(\frac{\rho_1}{\rho_{1j}}\right)^m \cos\left(m(\theta_1-\theta_{1j})\right) \tag{3.3.26}$$

[15] All these contributions will be summed to give a total potential, due to the superposition of the field given by the single wires, namely $\sum_{j=1}^{N\,wires}\vec{A}_{Sj}$

$$\vec{A}_{Sj}(\rho_0,\theta_0)=\frac{\mu_0}{2\pi}\boldsymbol{I}_{Sj}\left[\ln(\rho_{1j})-\sum_{m=1}^{\infty}\frac{1}{m}\left(\frac{\rho_1}{\rho_{1j}}\right)^m\cos\left(m(\theta_1-\theta_{1j})\right)\right] \tag{3.3.27}$$

The distance vectors of the thin wires representing the screen, seen in the coordinate system of the inner conductor are found using cosine law, namely:

$$\rho_{1j}=\sqrt{b_1^2+r_{Sj}^2-2b_1r_{Sj}cos(\gamma_1-\phi_{Sj})} \tag{3.3.28}$$

Whereas the angle is found as:

$$\theta_{1j}=\arctan\left(\frac{b_1\sin\gamma_1-r_{Sj}\sin(\phi_{Sj})}{b_1\cos\gamma_1-r_{Sj}cos(\phi_{Sj})}\right) \tag{3.3.29}$$

Solution of CASE 2

The coefficients, in this case, will have the same expression as in the last case, therefore we do not state again the whole procedure (continuity conditions – solution of the derived system of equations), but just rewrite the coefficients. The only difference here is that the thin wires currents are from the screen conductor (when it is represented as a source and split in thin wires).

$$g_{1n}=\frac{j\omega\sigma_c\mu_c}{\pi}\frac{\sum_{i=1}^{N}\boldsymbol{I}_{sj}\left(\frac{a_1}{\rho_{1j}}\right)^n\cos n\theta_{1j}}{\left[n\left(1+\frac{1}{\mu_{rc}}\right)I_n(\xi_c a_1)+\frac{\xi_c a_1}{\mu_{rc}}I_{n+1}(\xi_c a_1)\right]} \tag{3.3.30}$$

$$h_{1n}=\frac{j\omega\sigma_c\mu_c}{\pi}\frac{\sum_{i=1}^{N}\boldsymbol{I}_{sj}\left(\frac{a_1}{\rho_{1j}}\right)^n\sin n\theta_{1j}}{\left[n\left(1+\frac{1}{\mu_{rc}}\right)I_n(\xi_c a_1)+\frac{\xi_c a_1}{\mu_{rc}}I_{n+1}(\xi a_1)\right]} \tag{3.3.31}$$

Expressions for the current density in the conductors

The current density in the infinite screen is written as:

$$J_S(r_s,\phi_s)=\frac{-\mathbf{I}\xi}{2\pi c_1}\frac{\left[I_0(\xi_s r_s)K_1(\xi_s c_2)+I_1(\xi_s c_2)K_0(\xi r_s)\right]}{\left[I_1(\xi_s c_2)K_1(\xi_s c_1)-I_1(\xi_s c_1)K_1(\xi_s c_2)\right]}\hat{z}+$$
$$+\frac{j\omega\mu_s\sigma_s}{\pi}\sum_{n=1}^{\infty}L_{sn}K_n(\xi_s r_s)\sum_{i=1}^{N}\boldsymbol{I}_{1i}\left(\frac{\rho_{0i}}{c_1}\right)^n\left[\cos(n\theta_{0i})\cos(n\phi_s)+\sin(n\theta_{0i})\sin(n\phi_s)\right]\hat{z} \quad (3.3.32)$$

$$L_{sn}=\frac{1}{n(1+\mu_{rs})K_n(\xi_s c_1)+\xi_s c_1 K_{n-1}(\xi_s c_1)}$$

Whereas the current density in the core is:

$$\vec{J}_1(r_1,\phi_1)=\frac{\xi_c\boldsymbol{I}}{2\pi a_1}\frac{I_0(\xi_c r_1)}{I_1(\xi_c a_1)}\hat{z}+$$
$$+\frac{j\omega\mu_c\sigma_c}{\pi}\sum_{n=1}^{\infty}L_{1n}I_n(\xi_c r_1)\sum_{j=1}^{N}\boldsymbol{I}_{sj}\left(\frac{a_1}{\rho_{1j}}\right)^n\left(\cos n\theta_{1j}\cos n\phi_1+\sin n\theta_{1j}\sin n\phi_1\right)\hat{z} \quad (3.3.33)$$

$$L_{1n}=\frac{1}{\left[n\left(1+\frac{1}{\mu_{rc}}\right)I_n(\xi_c a_1)+\frac{\xi a_1}{\mu_{rc}}I_{n+1}(\xi_c a_1)\right]}$$

Calculation of thin wires intensity

We follow the same procedure used for the case of two conductors, which allows to write:

$$\boldsymbol{I}_{Sj}=\vec{J}_S(r_{sj},\phi_{sj})dS_{sj} \quad (3.3.34)$$

$$\boldsymbol{I}_{1i}=\vec{J}_1(r_{1i},\phi_{1i})dS_{1i} \quad (3.3.35)$$

with dS_{sj} and dS_{1i} the surfaces of the *i-th* and *j-th* sub-conductor (centred in the corresponding thin wire) of the screen and the core conductors respectively.

$$J_S(r_{sj},\phi_{sj})=\frac{-\boldsymbol{I}\xi_s}{2\pi c_1}B_{sj}+$$
$$+\frac{j\omega\mu_s\sigma_s}{\pi}\sum_{n=1}^{\infty}L_{Sn}K_n(\xi_s r_{sj})\sum_{i=1}^{N}\boldsymbol{I}_{1i}\left(\frac{\rho_{0i}}{c_1}\right)^n\left[\cos(n\theta_{0i})\cos(n\phi_{sj})+\sin(n\theta_{0i})\sin(n\phi_{sj})\right] \quad (3.3.36)$$

with

$$B_{Sj}=\frac{\left[I_0(\xi_s r_{sj})K_1(\xi_s c_2)+I_1(\xi_s c_2)K_0(\xi_s r_{sj})\right]}{\left[I_1(\xi_s c_2)K_1(\xi_s c_1)-I_1(\xi_s c_1)K_1(\xi_s c_2)\right]} \quad (3.3.37)$$

$$J_1(r_{1i},\phi_{1i})=\frac{\boldsymbol{I}\xi_c}{2\pi a_1}\frac{I_0(\xi_c r_{1i})}{I_1(\xi_c a_1)}+\frac{j\omega\mu_c\sigma_c}{\pi}\sum_{n=1}^{\infty}L_{1n}I_n(\xi_c r_{1i})\sum_{j=1}^{N}\boldsymbol{I}_{sj}\left(\frac{a_1}{\rho_{1j}}\right)^n\left(\cos n\left(\theta_{1j}-\phi_{1i}\right)\right) \quad (3.3.38)$$

Those are rearranged as:

$$I_{1i}=\left[\frac{\boldsymbol{I}\xi_c}{2\pi a_1}\frac{I_0(\xi_c r_{1i})}{I_1(\xi_c a_1)}+\frac{j\omega\mu_c\sigma_c}{\pi}\sum_{n=1}^{\infty}L_{1n}I_n(\xi_c r_{1i})\sum_{j=1}^{N}\boldsymbol{I}_{sj}\left(\frac{a_1}{\rho_{1j}}\right)^n\left(\cos n\left(\theta_{1j}-\phi_{1i}\right)\right)\right]dS_{1i} \quad (3.3.39)$$

$$I_{Sj} = \left[\frac{-\boldsymbol{I}\xi_s}{2\pi c_1} B_{Sj} + \frac{j\omega\mu_s\sigma_s}{\pi} \sum_{n=1}^{\infty} L_{Sn} K_n(\xi_s r_{sj}) \sum_{i=1}^{N} \boldsymbol{I}_{1i} \left(\frac{\rho_{0i}}{c_1} \right)^n \left(\cos n(\theta_{0i} - \phi_{sj}) \right) \right] dS_{sj} \tag{3.3.40}$$

$$\frac{\boldsymbol{I}\xi_c}{2\pi a_1} \frac{I_0(\xi_c r_{1i})}{I_1(\xi_c a_1)} dS_{1i} + \frac{j\omega\mu_c\sigma_c}{\pi} \sum_{n=1}^{\infty} L_{1n} I_n(\xi_c r_{1i}) \sum_{j=1}^{N} \boldsymbol{I}_{sj} \left(\frac{a_1}{\rho_{1j}} \right)^n \left(\cos n\left(\theta_{1j} - \phi_{1i}\right) \right) dS_{1i} - I_{1i} = 0 \tag{3.3.41}$$

$$\frac{-\boldsymbol{I}\xi_s}{2\pi c_1} B_{Sj} dS_{si} + \frac{j\omega\mu_s\sigma_s}{\pi} \sum_{n=1}^{\infty} L_{Sn} K_n(\xi_s r_{sj}) \sum_{i=1}^{N} \boldsymbol{I}_{1i} \left(\frac{\rho_{0i}}{c_1} \right)^n \left(\cos n(\theta_{0i} - \phi_{sj}) \right) dS_{sj} - I_{Sj} = 0 \tag{3.3.42}$$

And that, considering each sub-conductor can be written in matrix form, as:

$$\begin{array}{c} \\ i \\ \\ \\ \\ \\ \\ \\ \\ j \\ \\ \\ \\ \\ \end{array} \begin{array}{c} \begin{array}{ccccccccccc} & & i & & & & & & j & & \end{array} \\ \left[\begin{array}{ccccc|ccccc} -1 & 0 & 0 & & & & & & & \\ 0 & -1 & 0 & 0 & & & & & & \\ & 0 & . & & & & & S_{ij} & & \\ & & & . & 0 & & & & & \\ & & & 0 & -1 & & & & & \\ \hline & & & & & -1 & 0 & 0 & 0 & 0 \\ & & & & & 0 & -1 & & & \\ & T_{ij} & & & & & & & & \\ & & & & & & & & & 0 \\ & & & & & 0 & & 0 & 0 & -1 \end{array} \right] \end{array} \left[\begin{array}{c} I_{11} \\ . \\ I_{1i} \\ . \\ I_{1N} \\ \hline I_{S1} \\ . \\ I_{Sj} \\ . \\ I_{SN} \end{array} \right] = \begin{array}{c} \\ \\ \dfrac{-\mathbf{I}\xi_c}{2\pi a_1 I_1(\xi_c a_1)} \\ \\ \\ \\ \\ \dfrac{\mathbf{I}\xi_s}{2\pi c_1} \\ \\ \\ \end{array} \left[\begin{array}{c} I_0(\xi_c r_{11}) dS_{11} \\ . \\ I_0(\xi_c r_{1i}) dS_{1i} \\ . \\ I_0(\xi_c r_{1N}) dS_{1N} \\ \hline B_{S1} dS_{S1} \\ . \\ B_{Sj} dS_{Sj} \\ . \\ B_{SN} dS_{SN} \end{array} \right]_{2N} \tag{3.3.43}$$

where

$$S_{ij} = \frac{j\omega\mu_c\sigma_c}{\pi} dS_{1i} \sum_{n=1}^{\infty} L_{1n} I_n(\xi_c r_{1i}) \left(\frac{a_1}{\rho_{1j}} \right)^n \left(\cos n\left(\theta_{1j} - \phi_{1i}\right) \right) \tag{3.3.44}$$

$$T_{ij} = \frac{j\omega\mu_s\sigma_s}{\pi} dS_{sj} \sum_{n=1}^{\infty} L_{Sn} K_n(\xi_s r_{sj}) \left(\frac{\rho_{0i}}{c_1} \right)^n \left(\cos n(\theta_{0i} - \phi_{sj}) \right) \tag{3.3.45}$$

The solution of this system of equations gives the current density of both conductors, with the inclusion of proximity effect.

3.4. Numerical evaluation of the internal impedances of solid and hollow conductors

The internal impedance of each sub-conductor is then calculated using the energetic definitions of resistance and inductance.

$$R_{1\text{int}} = \frac{1}{\sigma |\boldsymbol{I}_1|^2} \int_{cond1} \left|\vec{J}_1\right|^2 dS \tag{3.4.1}$$

$$L_{1\text{int}} = \frac{1}{|\boldsymbol{I}_1|^2} \int_{cond1} \mu \left|\vec{H}\right|^2 dS \tag{3.4.2}$$

$$\boldsymbol{I}_1 = \int_{cond1} \vec{J}_1 dS \tag{3.4.3}$$

These definitions have to be applied to the current density and magnetic fields expression of core or screen conductors, which are found to be:

$$\vec{J}_1(r_1,\phi_1) = \frac{\boldsymbol{I}\xi_c}{2\pi a_1} \frac{I_0(\xi_c r_{1i})}{I_1(\xi_c a_1)} + \sum_{n=1}^{\infty} \left[g_{1n} cos(n\phi_1) + h_{1n} sin(n\phi_1)\right] I_n(\xi r_1)\,\hat{z} \tag{3.4.4}$$

$$H_{r1}(r_1,\phi_1) = \frac{n}{j\omega\mu_c\sigma_c r_1} \sum_{n=1}^{\infty} \left[g_{1n} \sin(n\phi_1) - h_{1n} \cos(n\phi_1)\right] I_n(\xi r_1) \tag{3.4.5}$$

$$H_{\phi 1}(r_1,\phi_1) = \frac{\boldsymbol{I}}{2\pi a_1} \frac{I_1(\xi_c r_{1i})}{I_1(\xi_c a_1)} + \frac{1}{\xi_c} \sum_{n=1}^{\infty} \left[g_{1n} cos(n\phi_1) + h_{1n} sin(n\phi_1)\right] I_n{}'(\xi r_1) \tag{3.4.6}$$

$$\vec{J}_s(r_1,\phi_1) = \frac{-\boldsymbol{I}\xi}{2\pi c_1} \frac{\left[I_0(\xi_s r_s)K_1(\xi_s c_2) + I_1(\xi_s c_2)K_0(\xi r_s)\right]}{\left[I_1(\xi_s c_2)K_1(\xi_s c_1) - I_1(\xi_s c_1)K_1(\xi_s c_2)\right]}\,\hat{z} + \\ + \sum_{n=1}^{\infty} \left[o_n cos(n\phi_s) + p_n sin(n\phi_s)\right] K_n(\xi r_s)\,\hat{z} \tag{3.4.7}$$

$$H_{rs}(r_s,\phi_s) = \frac{n}{j\omega\mu_c\sigma_c r_s} \sum_{n=0}^{\infty} \left[o_n \sin(n\phi_s) - p_n \cos(n\phi_s)\right] K_n(\xi r_s) \tag{3.4.8}$$

$$H_{\phi s}(r_s,\phi_s) = \frac{-\boldsymbol{I}}{2\pi c_1} \frac{\left[I_1(\xi_s r_s)K_1(\xi_s c_2) - I_1(\xi_s c_2)K_1(\xi r_s)\right]}{\left[I_1(\xi_s c_2)K_1(\xi_s c_1) - I_1(\xi_s c_1)K_1(\xi_s c_2)\right]} + \\ + \frac{1}{\xi_c} \sum_{n=0}^{\infty} \left[o_n cos(n\phi_s) + p_n sin(n\phi_s)\right] K_n{}'(\xi r_s) \tag{3.4.9}$$

It must be noted that the radial magnetic field has a null 0-th order term; the radial part of the magnetic field in the case of a coaxial cable is zero, whereas here there exists a nonzero part which intervenes as proximity effect terms.

In order to evaluate the integrals, they are approximated by finite sums, which are calculated for each point in which the EM quantity has been calculated (that is, the position of each thin wire).

The expressions become therefore

$$R_{1\text{int}} = \sum_{i=1}^{N\,cond\,core} \frac{\left|J_{1i}\right|^2 dS_{1i}}{\sigma_c |\boldsymbol{I}|^2} \tag{3.4.10}$$

$$L_{1\text{int}} = \sum_{i=1}^{N\,cond\,core} \frac{\mu \left| H_{ri} \right| dS_{1i}{}^{2} + \left| H_{\phi i} \right| dS_{1i}{}^{2}}{|\boldsymbol{I}|^{2}} \tag{3.4.11}$$

$$R_{screen\,\text{int}} = \sum_{i=1}^{N\,cond\,screen} \frac{\left| J_{si} \right|^{2} dS_{si}}{\sigma_{s} |\boldsymbol{I}|^{2}} \tag{3.4.12}$$

$$L_{screen\,\text{int}} = \sum_{i=1}^{N\,cond\,screen} \frac{\mu \left| H_{ri} \right| dS_{si}{}^{2} + \left| H_{\phi i} \right| dS_{si}{}^{2}}{|\boldsymbol{I}|^{2}} \tag{3.4.13}$$

3.4.1. Distribution of the filaments and validation of results

The filaments are distributed following a uniform law as in the examples given in the following figures, Fig.25 and Fig.26:

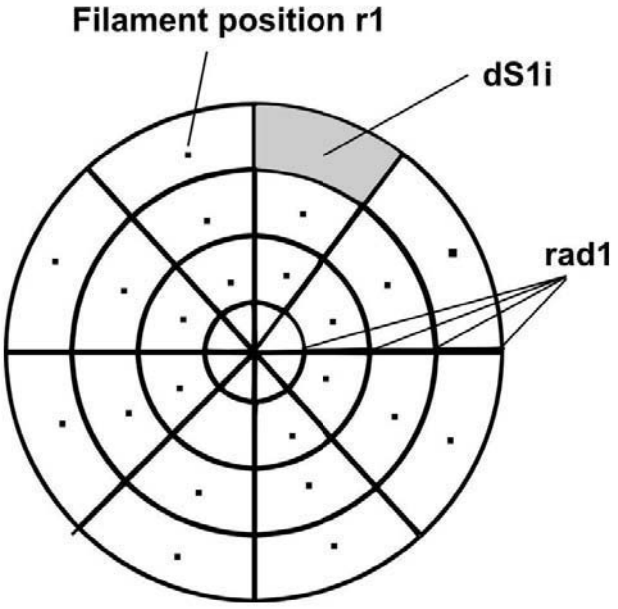

Fig.25 – Distribution of the filaments inside the solid conductor

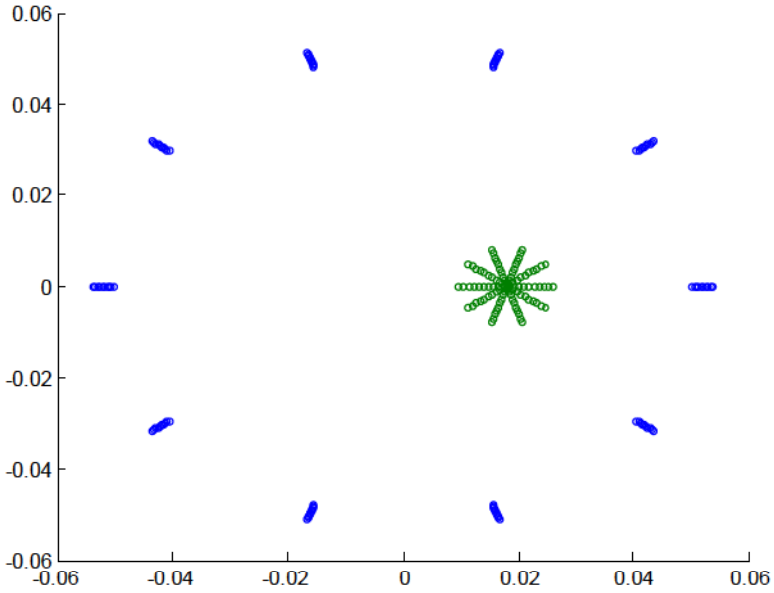

Fig.26 – Distribution of the filaments for the conductor and for the screen using Matlab – abscissa and ordinate are the distance from the centre of the screen

In our simulations we have seen that the number in the angular direction does not significantly modify the convergence if a number between 6 and 10 is taken.

The radial direction instead is very important in the convergence; in order to have a convergence in our code the number varies iteratively, at each frequency step, according to a convergence

criterion, which is represented by

$$\left| \boldsymbol{I}_1 - \sum_{i=1}^{N} \boldsymbol{I}_{1i} \right| < \varepsilon$$

The quantity ε is chosen between $1 \cdot 10^{-4}$ and $0.5 \cdot 10^{-4}$ in order to have a good degree of accuracy.

3.4.2. Validation of the results for the current density

The scope of this section is to validate the results obtained for the current density, comparing them with those obtained using Comsol Multiphysics, a Finite Element Method program. We do this for both configurations we studied.

3.4.2.1. Configuration of the two conductors

Here we considered the configuration of two conductors, having each a radius of 5mm, the distance between the centers of the conductors is 15mm, and the conductivity is $3.8 \cdot 10^7$ S/m. We show on the following graphs, the norm of the current density of the first conductor (as modified due to proximity/skin effects) at the frequency of 10 kHz.

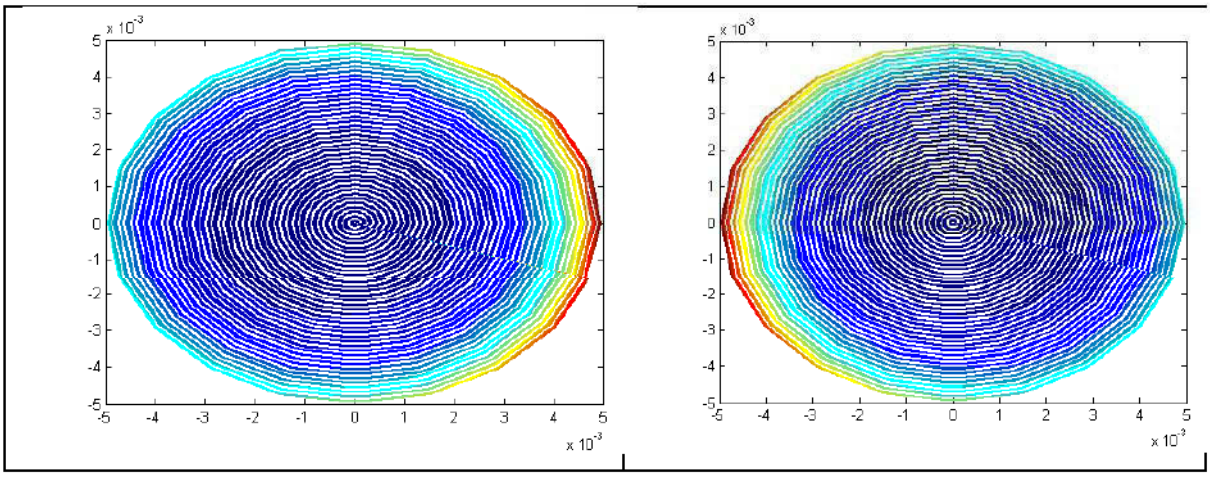

Fig.27 – Norm of the current density at 10 kHz in the two conductors, plotted in Matlab using the method we propose (|J| from higher to lower, from red to blue)

In Fig.27 we see how the two opposite current flowing in the two conductors attract themselves due to the proximity effect; the skin effect is also evident, as in the middle of the conductor the current density is very low as compared to that at the conductor's surface.

In the following figures we compare current density as evaluated in our method and using Comsol AC/DC magnetic module; the comparison is done:

- looking at the radial direction and having fixed the angular position at 0, 90 and 180 degrees;
- looking at the angular direction and having fixed the radial position at the core surface (r=5 mm), in the middle of the core (r= 2.5 mm) and in the centre of the core (r=0 mm).

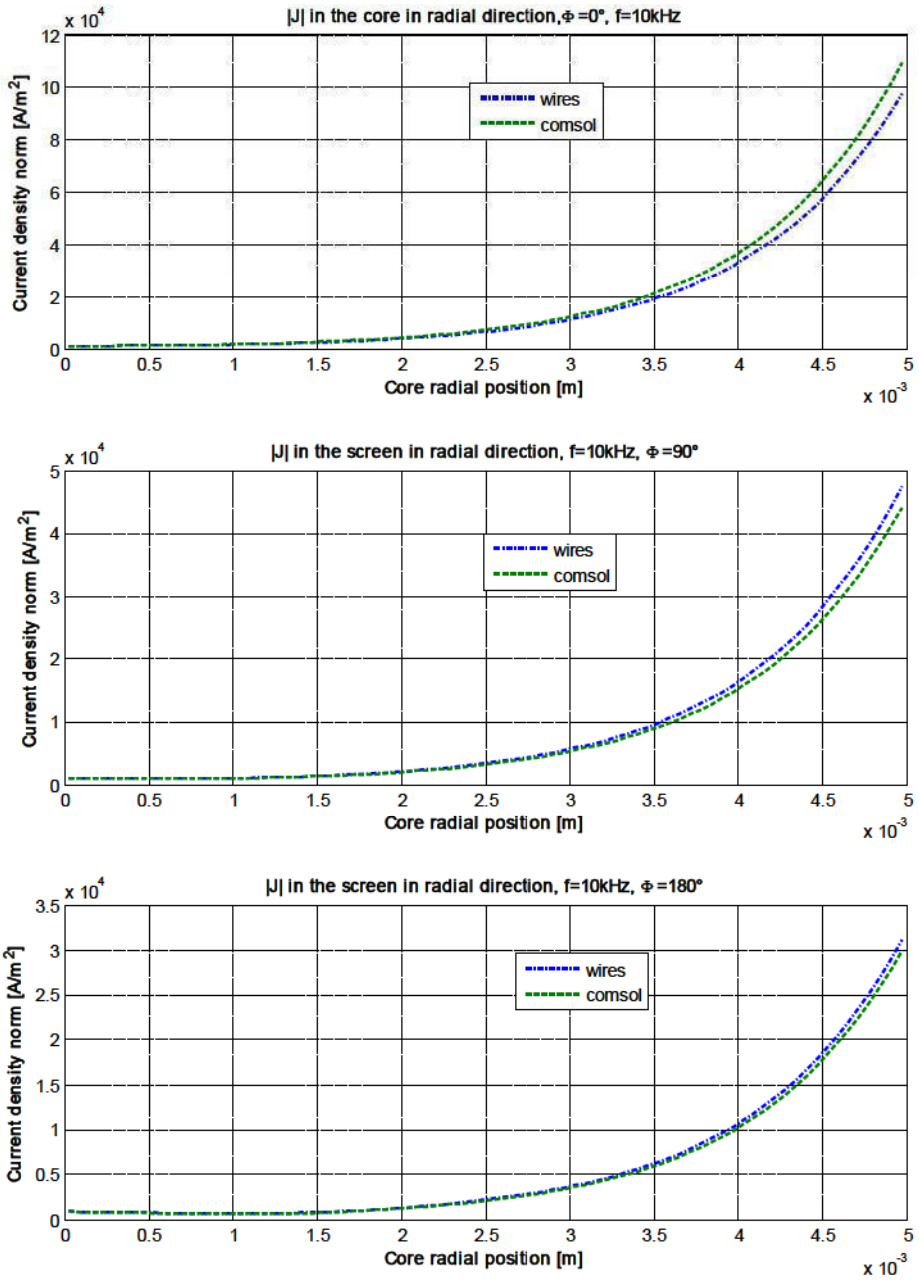

Fig.28 - Norm of the current density in the core, in radial direction, at different angles, comparing "wires" formulation and Comsol

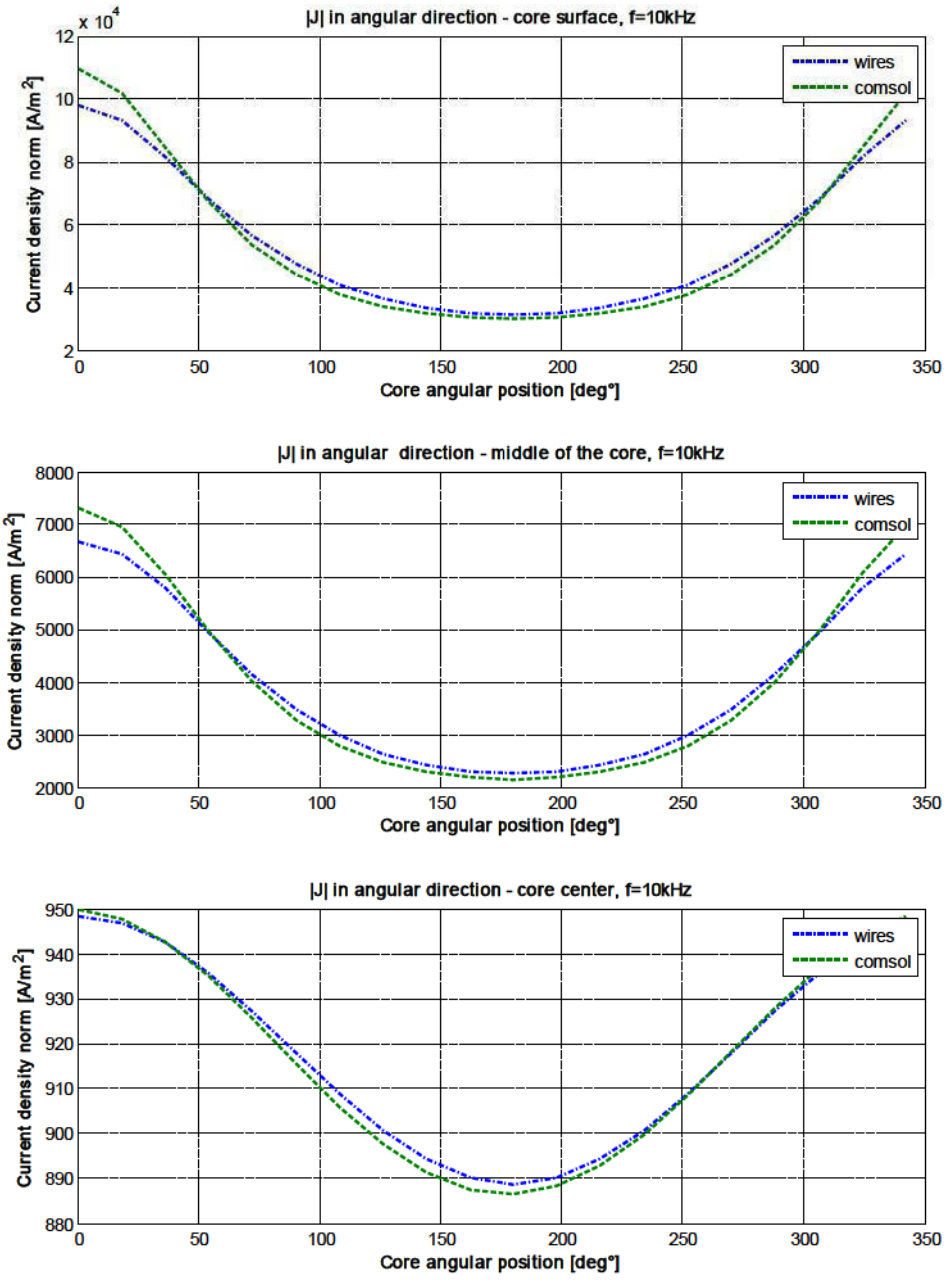

Fig.29 - Norm of the current density in the core, in angular direction, at different depth of the conductor, comparing "wires" formulation and Comsol

We can see from Fig.28 and Fig.29 that there is very good agreement between the formulation we propose for the case of two conductors and the Finite Element program Comsol. Whereas Fig.28, which details the norm of the current density following the radial direction, shows principally the skin effect, Fig.29 makes the proximity effect well evident.

We chose the frequency of 10 kHz for this validation, because at this frequency proximity effect becomes relevant, but the skin effect is not too intense and the current is not uniquely concentrated on the conductors' surface.

3.4.2.2. Configuration of the conductor inside a screen

The inner conductor here has always a radius of 5 mm, the screen has inner/outer radiuses of 15/16 mm; the conductor is placed 5 mm from the centre of the screen. The conductor we consider in the following two figures has a conductivity of $3.8 \cdot 10^7$ S/m and relative permeability μ_r=1.

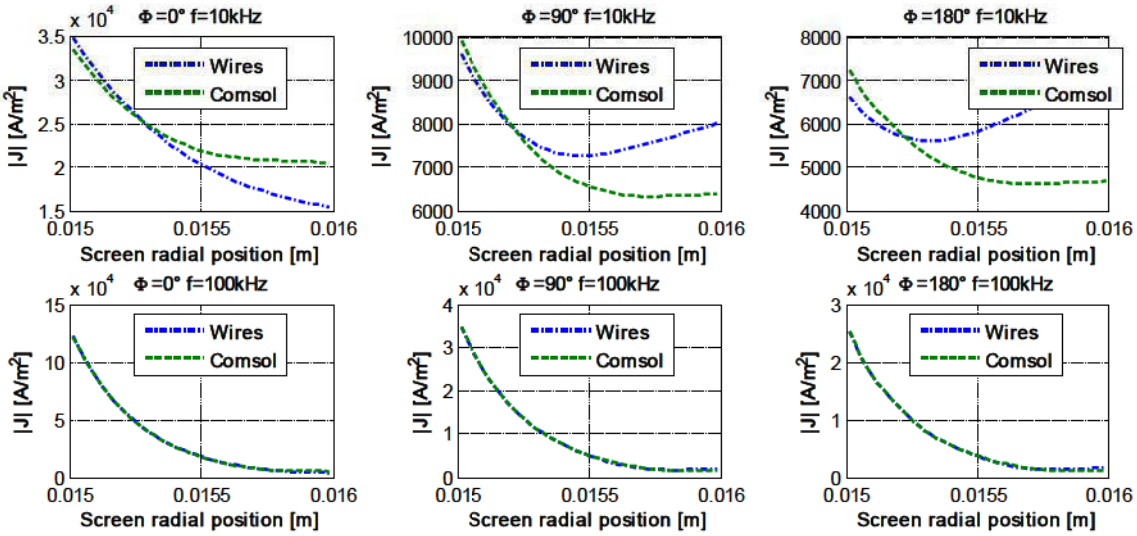

Fig.30 - Norm of the current density in the screen, in radial direction, at different angles, comparing "wires" formulation and Comsol.

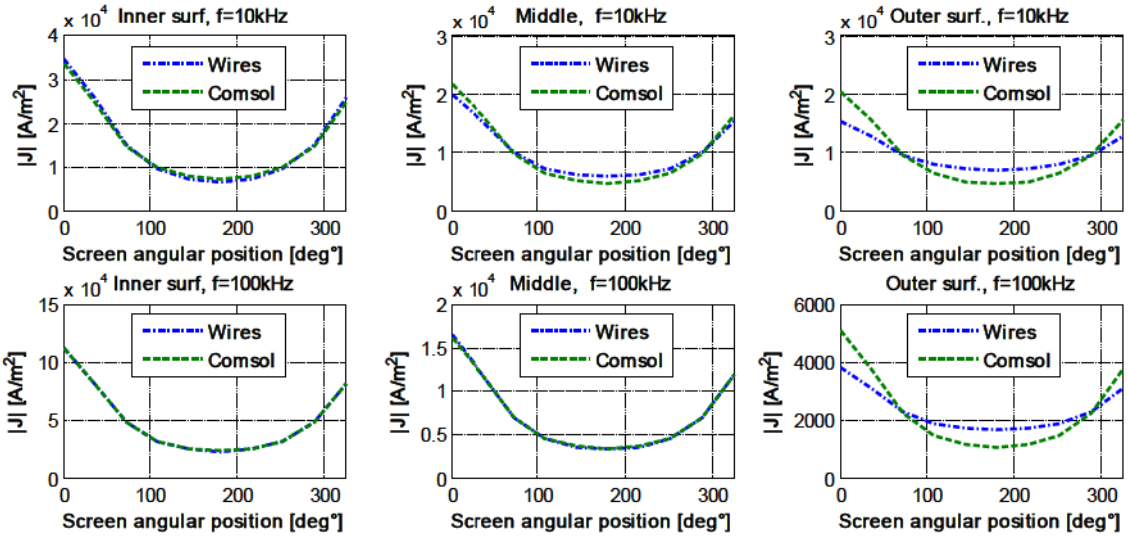

Fig.31 - Norm of the current density in the screen, in angular direction, at different depth of the conductor, comparing "wires" formulation and Comsol

We can see that the formulations we propose well agree with the Finite Element method also in this second case, although some problems arise in the evaluation of current density in the screen at 10kHz. These problems are due to the approximation we used of semi-infinite screen, and this is evident from the current density at 10 kHz in Fig.31. We consider this not being a very big problem for two reasons:

- The current density gives bad results toward the outer surface of the conductor, where the current absolute value is much lower than on the inner surface; since the resistance is evaluated globally on the whole conductor's surface this causes only a small error

- The types of screen which interest us are generally the armour of submarine cables that are much thicker than the one we have shown here, and made out of steel, that has a much lower penetration depth than the other conductors, due to its ferromagnetic behaviour.

We now show the validation for the current density in the same geometrical configuration, but with the screen made out of steel (conductivity $3.3 \cdot 10^6$ S/m and relative permeability μ_r=300).

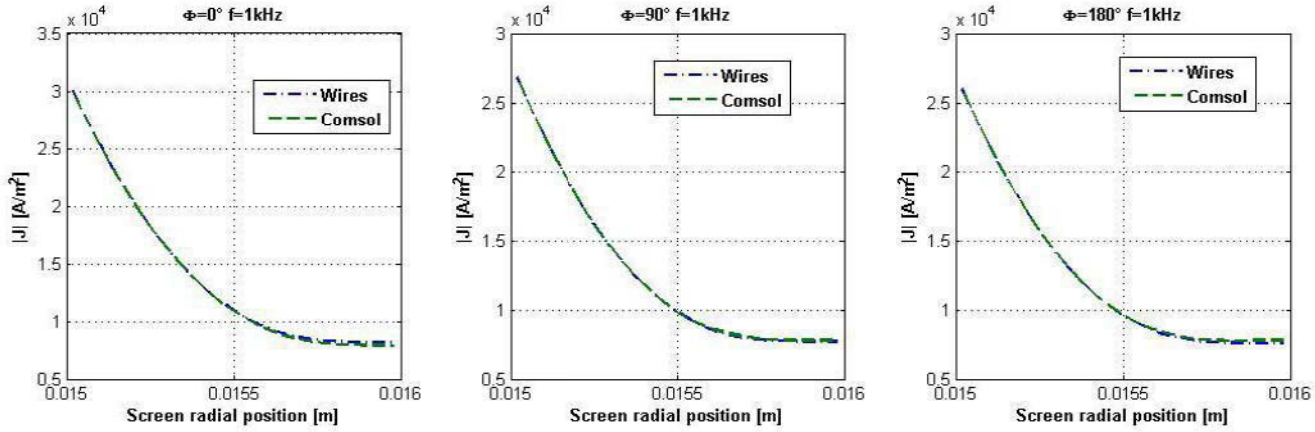

Fig.32 - Norm of the current density in the screen, in radial direction, at different angles, comparing "wires" formulation and Comsol.

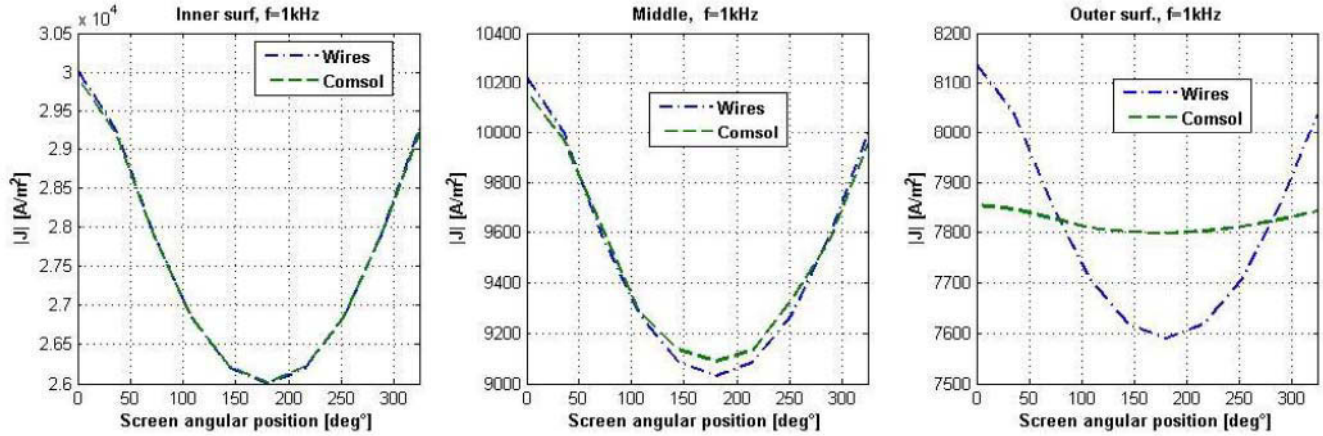

Fig.33 - Norm of the current density in the screen, in angular direction, at different depth of the conductor, comparing "wires" formulation and Comsol

We can see from Fig.32 and Fig.33 that, since the skin depth is here much reduced, due to the high permeability of steel, the formulation gives better results in this case.

To have a reference, we give here the different values of the skin depth for aluminium and steel.

Table 4 – Skin depth of aluminium and steel

Frequency	Skin depth aluminium	Skin depth steel (μ_r=300)
50 Hz	11.5 mm	2.25 mm
1 kHz	2.58 mm	0.5 mm
10 kHz	0.81 mm	0.15 mm
100 kHz	0.258 mm	0.05 mm
1 MHz	0.081 mm	0.015 mm

As a rule of thumb if the thickness of the screen is 4 times smaller than the skin depth then the error given by the approximation of semi-infinite outer screen is very small.

3.4.3. Validation of the results for the internal resistance and inductance

We consider here the core conductors and the screen (armour) of a submarine 90kV cable (that is a realistic configuration) and we deal with the two configurations described in the previous sections. In the following table are the characteristics and geometry of the cable used in the calculation of the internal impedances.

Table 5 – Geometrical and electrical parameters of the cable

	Diameter / Thickness	μ_r	ε_r	σ
Copper core	23.5 mm	1	1	$5.8 \cdot 10^7$ S/m
XLPE insulation	14 mm	1	2.4	-
Lead sheath	2.5 mm	1	1	$3.89 \cdot 10^6$ S/m
PE jacket	2 mm	1	2.3	-
Steel armour	5 mm	300	1	$3.271 \cdot 10^6$ S/m

We show the graphs of the internal per unit length (p.u.l.) resistances and inductances and we compare them to those obtained with existing methods, and a FEM model implemented in the Comsol Multiphysics simulation environment.

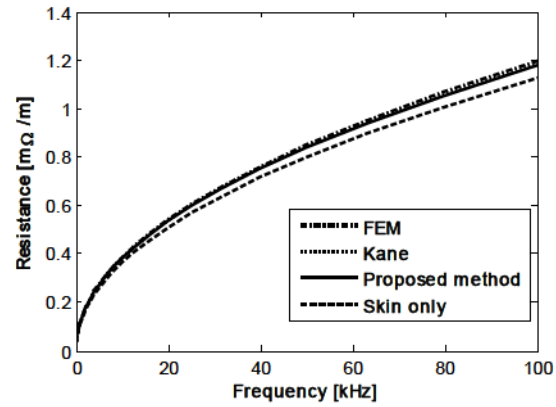

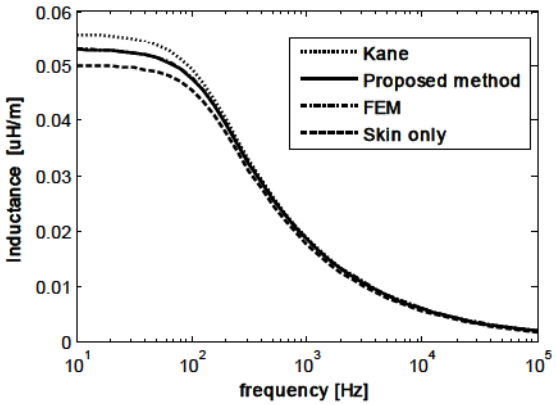

Fig.34 – Internal p.u.l. resistance and inductance for the case of two solid conductors

Table 6 – Internal p.u.l. resistance for two solid conductors [Ω/m]

Method\ Frequency	50 Hz	1 kHz	10 kHz	100 kHz
Skin only	$4.17 \cdot 10^{-5}$	$1.22 \cdot 10^{-4}$	$3.63 \cdot 10^{-4}$	$1.12 \cdot 10^{-4}$
Kane	$4.23 \cdot 10^{-5}$	$1.28 \cdot 10^{-4}$	$3.84 \cdot 10^{-4}$	$1.19 \cdot 10^{-4}$
Proposed	$4.23 \cdot 10^{-5}$	$1.28 \cdot 10^{-4}$	$3.82 \cdot 10^{-4}$	$1.18 \cdot 10^{-4}$
FEM	$4.23 \cdot 10^{-5}$	$1.28 \cdot 10^{-4}$	$3.85 \cdot 10^{-4}$	$1.19 \cdot 10^{-4}$

Table 7 – Internal p.u.l. inductance for two solid conductors [H/m]

Method\ Frequency	50 Hz	1 kHz	10 kHz	100 kHz
Skin only	$4.87 \cdot 10^{-8}$	$1.76 \cdot 10^{-8}$	$5.62 \cdot 10^{-9}$	$1.77 \cdot 10^{-9}$
Kane	$5.37 \cdot 10^{-8}$	$1.87 \cdot 10^{-8}$	$5.96 \cdot 10^{-9}$	$1.88 \cdot 10^{-9}$
Proposed	$5.12 \cdot 10^{-8}$	$1.85 \cdot 10^{-8}$	$5.90 \cdot 10^{-9}$	$1.86 \cdot 10^{-9}$
FEM	$5.13 \cdot 10^{-8}$	$1.86 \cdot 10^{-8}$	$5.96 \cdot 10^{-9}$	$1.89 \cdot 10^{-9}$

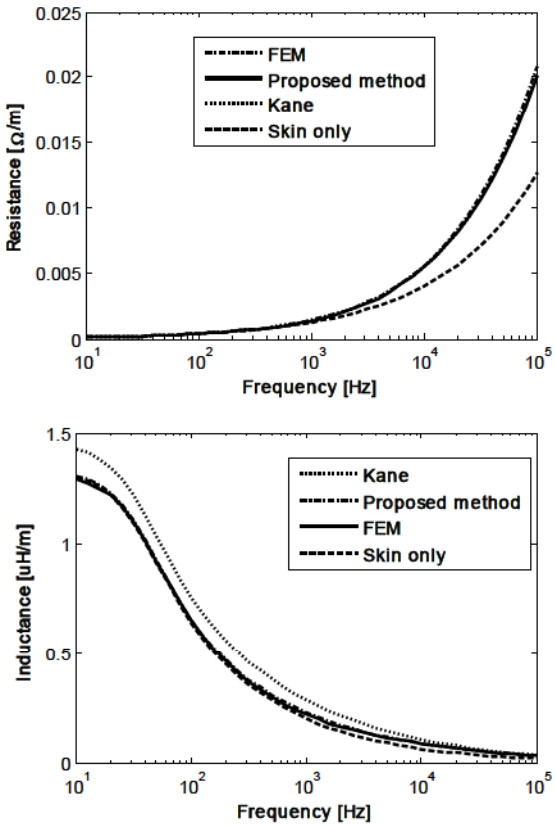

Fig.35 – Internal resistance and inductance for the screen, under the influence of an eccentric core conductor

Table 8 – Internal resistance for the screen [Ω/m]

Method\ Frequency	50 Hz	1 kHz	10 kHz	100 kHz
Skin only	$2.70 \cdot 10^{-4}$	$1.26 \cdot 10^{-3}$	$4.00 \cdot 10^{-3}$	$2.01 \cdot 10^{-2}$
Kane	$2.74 \cdot 10^{-4}$	$1.42 \cdot 10^{-3}$	$5.49 \cdot 10^{-3}$	$3.56 \cdot 10^{-2}$
Proposed	$2.74 \cdot 10^{-4}$	$1.36 \cdot 10^{-3}$	$5.49 \cdot 10^{-3}$	$3.20 \cdot 10^{-2}$
FEM	$2.74 \cdot 10^{-4}$	$1.41 \cdot 10^{-3}$	$5.52 \cdot 10^{-3}$	$3.32 \cdot 10^{-2}$

Table 9 – Internal inductance for the screen[H/m]

Method\ Frequency	50 Hz	1 kHz	10 kHz	100 kHz
Skin only	$9.13 \cdot 10^{-7}$	$2.01 \cdot 10^{-8}$	$6.36 \cdot 10^{-8}$	$2.01 \cdot 10^{-8}$
Kane	$1.03 \cdot 10^{-6}$	$2.85 \cdot 10^{-8}$	$1.05 \cdot 10^{-7}$	$3.56 \cdot 10^{-8}$
Proposed	$9.22 \cdot 10^{-7}$	$2.18 \cdot 10^{-8}$	$8.75 \cdot 10^{-8}$	$3.20 \cdot 10^{-8}$
FEM	$9.24 \cdot 10^{-7}$	$2.26 \cdot 10^{-8}$	$8.80 \cdot 10^{-8}$	$3.32 \cdot 10^{-8}$

These results altogether show the validity of our model. As we can see in Fig.34 and Table 8 the fact of having a ferromagnetic armour and therefore very low penetration depth implies that the results obtained even using the approximation of semi-infinite screen are acceptable, and this is also due to the fact that this approximation is only used for the proximity effect term which is very small at low frequencies where the approximation could be questionable.

It must be noted that the internal inductance, as evaluated by Kane gives results that are slightly overestimations. This is probably due to the way the inductance is evaluated (that we have shown in 2.4.6) and the fact that a single filament is used to represent a conductor, which may lead to inaccuracies when the conductors are close.

The proximity is not the only effect to be accounted for in transient simulations, in fact additional terms exist that are frequency dependent and impact the impedance matrix, as for instance the ground return impedance, or the semi-conducting layer. We describe these two effects in the next chapter.

4. Additional effects to be included in cable modelling

4.1. Ground and Sea return impedance

When analyzing transient phenomena the presence of the ground implies some modes of propagation (namely 0-sequence or homo-polar mode as we have seen in 2.2.2.3) for the current flow in this conductor. It is therefore necessary to have an accurate description of the effects of the ground upon the phase parameters of cables.

The same modes of propagation can be described for submarine cables, where the medium instead of the ground is the sea, or the seabed.

These effects are described by the so called ground-return term (namely z_g) that is:

- a self-impedance term for each cable (or a single three-core cable) ($z_{ground\text{-}self}$);
- a mutual impedance term, to express the mutual induction between two cables laid near one to the other ($z_{ground\text{-}mut}$).

We shall detail in this section the existing formulation for the ground-return term, as well as for the sea-return term.

4.1.1. Ground-return impedance

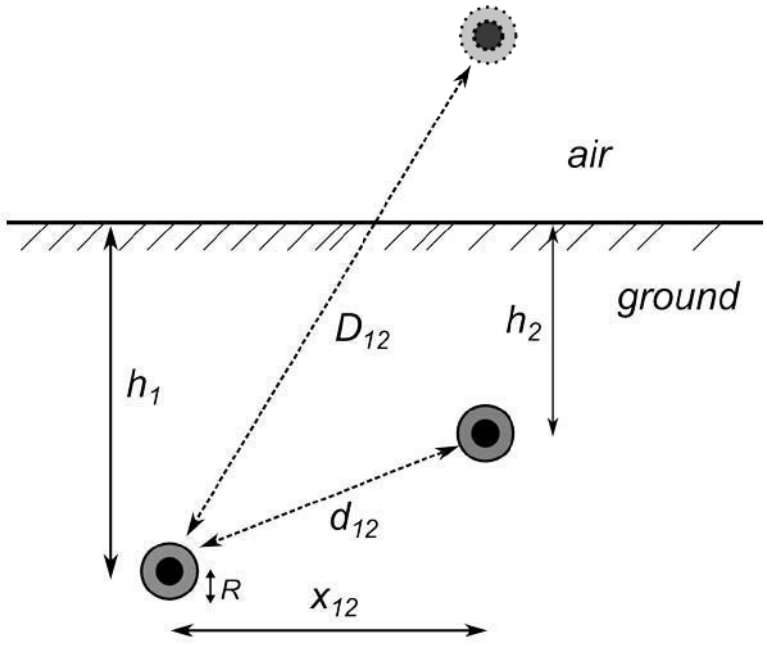

Fig.36 – Configuration used by Pollaczek for the evaluation of ground return term

The ground-return impedance term has been derived, for the configuration we show in Fig.36 using different formulas, derived from the rigorous approach described by Pollaczek [**8**] :

$$Z'_{ground-mut} = \frac{j\omega\mu_0}{2\pi}[K_0(\xi_g\sqrt{x_{12}^2+(h_1-h_2)^2}) - K_0(2\xi_g\sqrt{x_{12}^2+(h_1+h_2)^2}) + \\ + \int_{-\infty}^{+\infty}\frac{exp[-2(h_1+h_2)\sqrt{\alpha^2+\xi_g}]}{|\alpha|+\sqrt{\alpha^2+\xi_g}}exp(j\omega\alpha)d\alpha] \quad (4.1.1)$$

$$Z'_{ground-self} = \frac{j\omega\mu_0}{2\pi}[K_0(\xi R) - K_0(2\sqrt{R^2 + 4h_1^2}\,\xi) + \int_{-\infty}^{+\infty} \frac{exp[-2h_1\sqrt{\alpha^2 + \xi_g}\,]}{|\alpha| + \sqrt{\alpha^2 + \xi_g}} exp(j\omega\alpha)d\alpha] \quad (4.1.2)$$

where K_0 is the modified Bessel function of second kind, R is the external radius of the cable; in the second integral the self-return impedance of cable 1 is calculated considering only cable 1 and therefore its laying depth h_1 is used in the formulas, as well as its external radius R (which is the radius of the layer of the cable in contact with the ground).

All the other geometrical quantities are shown in Fig.36; $\xi_g = \sqrt{j\omega\mu_g\sigma_g}$ with μ_g and σ_g permittivity and conductivity of the ground, respectively.

Sunde has proposed [**9**] an expression similar to the one given by Pollaczek, but where displacement currents are not neglected, instead the complete intrinsic constant $\gamma_g = \sqrt{j\omega\mu_0(\sigma_g + j\omega\varepsilon_g)}$ is used; this constant contains ε_g the permeability of the soil. The integral proposed by Sunde is the same as (4.1.1), where γ_g replaces ξ_g.

The Pollaczek integral has been approximated, as well, using different analytical formulas.

We can mention:

- Wedepohl in [**1**] has proposed an approximation obtained from an infinite series:

$$Z_{ground-self} = \frac{j\omega\mu_0}{2\pi}\left[-ln\left(\frac{\gamma\xi R}{2}\right) + 0.5 - \frac{4\xi h_1}{3}\right] \quad (4.1.3)$$

$$Z_{ground-mut} = \frac{j\omega\mu_0}{2\pi}\left[-ln\left(\frac{\gamma\xi d_{12}}{2}\right) + 0.5 - \frac{2\xi(h_1 + h_2)}{3}\right] \quad (4.1.4)$$

γ is Euler's constant;

- Vance [**35**] has also given an approximation, that utilizes Hankel functions

$$Z_{ground-self} = \frac{j\omega\mu_0}{2\pi}\frac{H_0^1(j\gamma_g R)}{H_1^1(j\gamma_g R)} \quad (4.1.5)$$

- Petrache et al. [**36**] have given a formula easier to evaluate numerically:

$$Z_{ground-self} = \frac{j\omega\mu_0}{2\pi} ln\left(\frac{1 + \gamma_g R}{\gamma_g R}\right) \quad (4.1.6)$$

- Saad et al. [**10**] have given an expression that is a very good approximation even at higher frequencies:

$$Z_{ground-self} = \frac{j\omega\mu_0}{2\pi}\left[K_0(\gamma_g R) + \frac{2e^{-2d\gamma_g}}{4 + R^2\gamma_g^2}\right] \quad (4.1.7)$$

- In the EMTP an approximation is used, see page 5-16 of the EMTP Theory Book [**21**] that allows the use Carson series development [**37**] (normally employed for ground return impedance of overhead lines) for the calculation of ground return impedance of underground cables as well, as Carson and Pollaczek integrals are similar.
- Finally Legrand et al. [**11**] have shown an implementation of the quasi-Monte Carlo method that allows solving the Pollaczek integral in a precise way. We shall deal with this

method in more detail in the next section, as it will be the basis for the sea-impedance term that we propose.

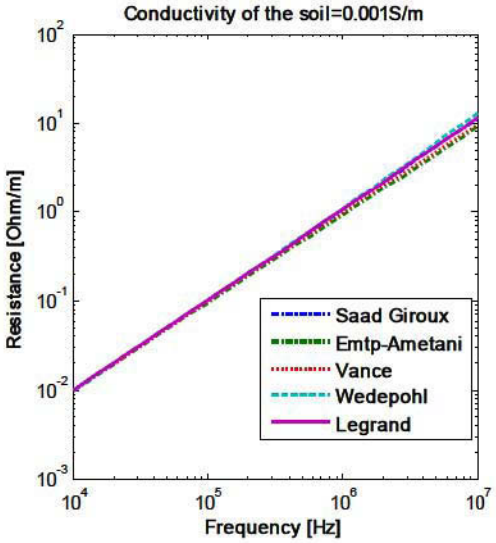

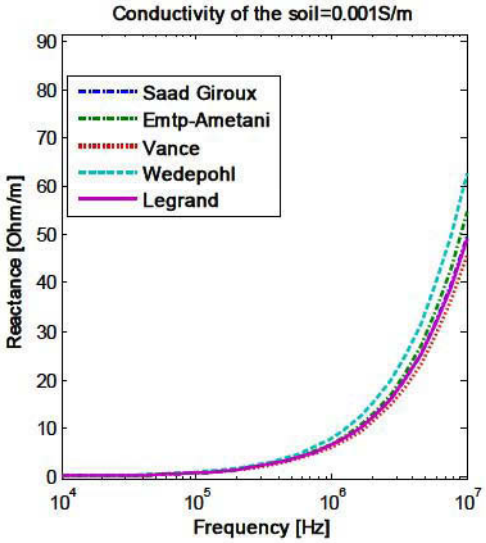

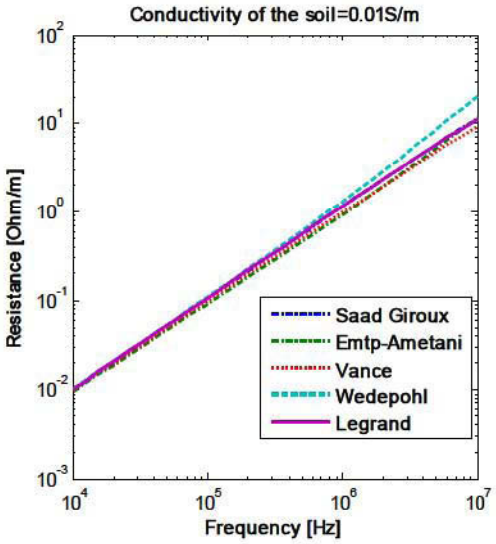

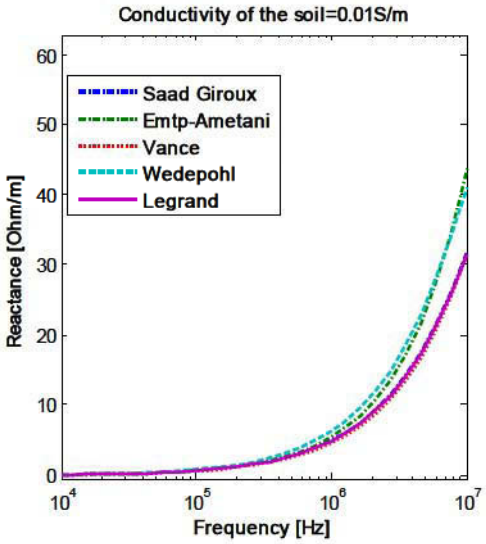

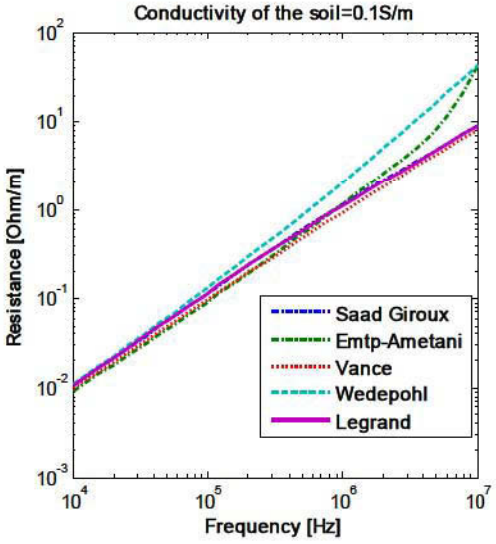

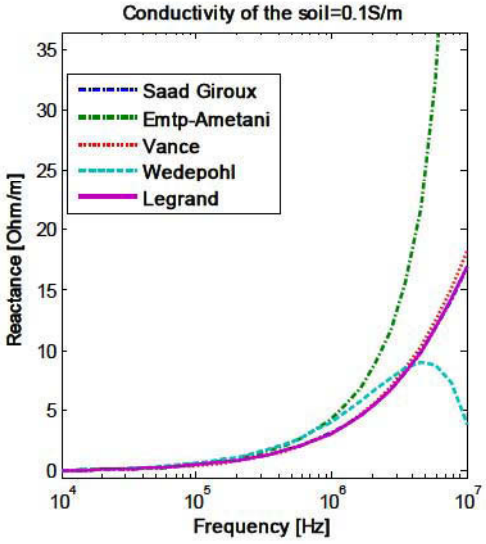

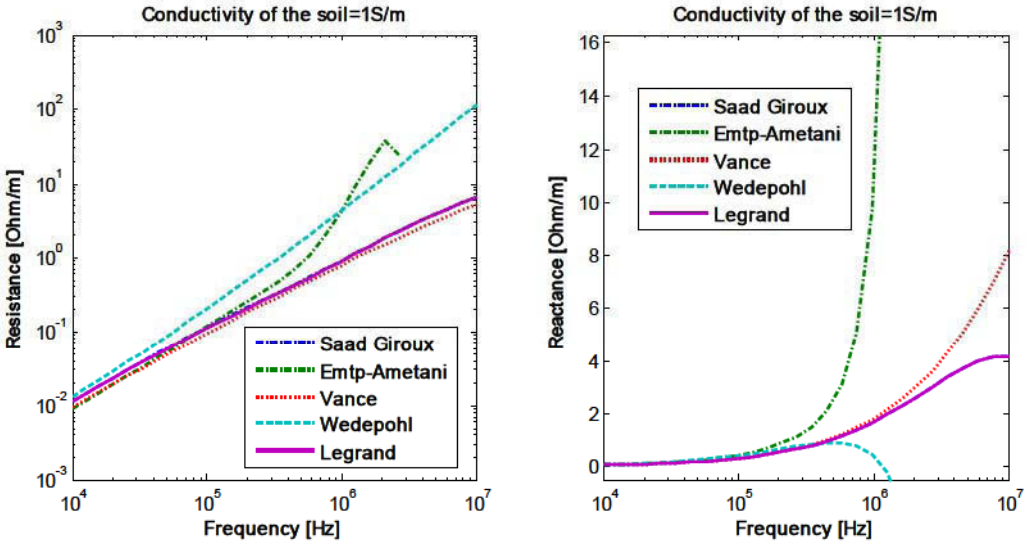

Fig.37 – Resistance and reactance of the ground return impedance comparing different formulations

We have shown in Fig.37 the results obtained with different formulations of ground return impedance. Only the high frequency part of the curve has been shown, as it is only at higher frequencies that the different formulations diverge. We have plotted the formulations for different values of conductivity of the soil, namely from low conductive soils (0.001 S/m) up to sea conductivity (1 S/m).

We can see that Wedepohl's approximation is not valid for higher conductivities, and that the formulation used in the EMTP is also not valid for very high frequency and higher conductivities. We can see that Saad-Giroux's formulation is in good agreement with the one proposed by Legrand, the one we use in our modeling. This last method we describe in the next section in some detail.

4.1.2. Quasi - Monte Carlo method for the solution of Pollaczek integral

4.1.2.1. Quasi Monte Carlo method

We can write the mean value of a function f(x) on the interval [0,1] as:

$$f_m = \int_0^1 f(x)dx \tag{4.1.8}$$

The evaluation of integrals using numerical approximations is a complicated task. In order to overcome the difficulty, the properties of the Monte Carlo method [**38**] can be exploited.

The method consists in:

- Define a domain of possible variable inputs for the function or process we are interested to;
- generate randomly a set of values in the input domain that follow a probability distribution;
- evaluate the simulation or the function at these inputs;
- combine together the results, for example calculating their mean value.

Through the use of the law of large numbers, one can say that, if the simulation is performed a great number of times, and if the variables $[x_1,x_2...,x_n]$ are independent and uniformly distributed on

the domain of variation then the combination of the results will converge to the desired solution, if N is a large number, we can then write:

$$\int_0^1 f(x)d \approx \frac{1}{N}\sum_{n=1}^{N} f(x_n) \tag{4.1.9}$$

It is therefore possible, to evaluate the integral which defines a mean value, using a numerical approximation. A confidence interval can also be defined, by defining the variance of the random variables x_n; but since this interval is probabilistic, it does not constitute an upper bound for the error.

In order to evaluate the integral with Monte Carlo method, variables should be independent uniform random variables. It is possible to use only certain variables, chosen because they have good properties altogether in the interval of variation of interest, namely the interval [0,1]. When that is the case, the Quasi Monte Carlo [**39**] method is defined.

The sequences of variables, which are then called quasi-random, are characterized using the concept of discrepancy; this concept reflects the properties of the sub-sequences of being uniformly distributed, a smaller value of the discrepancy $D_n(x)$ indicating quasi-random sequences.

One possible sequence to be used is the Van der Corput sequence, see [**40**].

In [**11**] the Pollaczek integral is solved, using the quasi-Monte Carlo method and the method is also itself described.

4.1.2.2. Solution of the integral

We shall look here only at the self-ground-return impedance calculation. The same mathematical considerations can be applied to the mutual term as well.

The Pollaczek integral for the calculation of the self-ground-return impedance as in (4.1.2) writes itself as:

$$J = -j\int_0^{\infty} \frac{e^{-2h\sqrt{\alpha^2+\xi^2}}}{|\alpha|+\sqrt{\alpha^2+\xi^2}} e^{j\beta R} d\alpha \tag{4.1.10}$$

This integral needs must be transformed into an integral having as integration bounds [0,1] in order that we be able to use the Quasi Monte Carlo method.

This can be done, as shown in [**11**] using some transformations, splitting the integral in two, and finally using a variable change for the second integral.

One obtains

$$J = J_1 + J_2 \tag{4.1.11}$$

$$J_1 = \int_0^1 \left[\sqrt{u^2+j} - u\right] e^{-2h|\xi|\sqrt{u^2+j}} du \tag{4.1.12}$$

$$J_2 = \int_0^1 \left[\sqrt{v^2+j} - v\right] e^{-2h|\xi|\sqrt{v^2+j}} dv \text{ where } v = \frac{1}{u}\ dv = \frac{1}{u^2} du \tag{4.1.13}$$

Then we can rewrite the integral, defining a function $f(u)$

$$f(u) = \left[\sqrt{u^2+j} - u\right] e^{-2h|\xi|\sqrt{u^2+j}} \tag{4.1.14}$$

Using the previously defined Van der Corput suite terms x_i, one can evaluate the integral, as a

mean, namely

$$J_1 \approx \frac{1}{n}\sum_{i=1}^{n}[f(x_i)] \qquad J_2 \approx \frac{1}{n}\sum_{i=1}^{n}\left[f\left(\frac{1}{x_i}\right)\cdot\left(\frac{1}{x_i}\right)^2\right] \tag{4.1.15}$$

This allows a fast and simple calculation of the integral, with a good precision.

4.1.3. Sea return impedance

In the same way as Legrand et al. evaluated the Pollaczek integral, we shall show how this method of solution can be applied to the integral described in [**13**] which allows calculating the sea-return impedance.

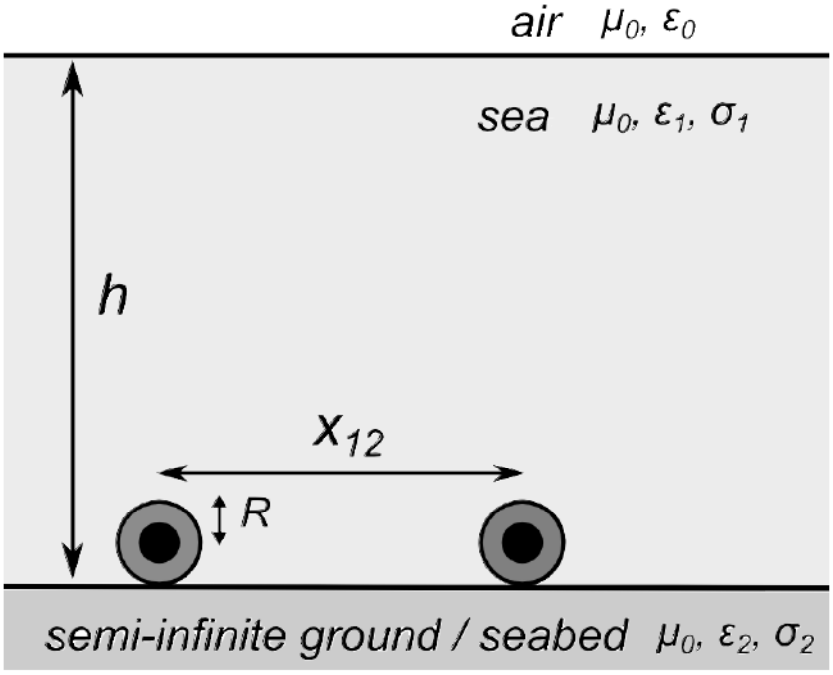

Fig.38 – Description of the two-layered soil formed by sea water and the seabed

4.1.4. Integral defining the ground return impedance

The authors in [**12**] describe a two-layer soil. An integral is derived, which describe the cables as being in the first layer, with one semi-infinite second layer below it.

Lucca et Al. [**13**] applied the integral to the case of the sea and the seabed, with the cable at the interface between them, as described in Fig.38.

When applied, the resulting integrals for self and mutual impedance are:

$$Z'_{ground-self} = \frac{j\omega\mu_0}{\pi}\int_0^{+\infty}\frac{\alpha_1+\alpha_0+(\alpha_1-\alpha_0)e^{-2\alpha_1 h}}{(\alpha_1+\alpha_0)(\alpha_1+\alpha_2)-(\alpha_1-\alpha_0)(\alpha_1-\alpha_2)e^{-2\alpha_1 h}}\cos(uR)du \tag{4.1.16}$$

$$Z'_{ground-mut} = \frac{j\omega\mu_0}{\pi}\int_0^{+\infty}\frac{\alpha_1+\alpha_0+(\alpha_1-\alpha_0)e^{-2\alpha_1 h}}{(\alpha_1+\alpha_0)(\alpha_1+\alpha_2)-(\alpha_1-\alpha_0)(\alpha_1-\alpha_2)e^{-2\alpha_1 h}}\cos(ux_{12})du \tag{4.1.17}$$

With $\alpha_i = \sqrt{u^2+\gamma_i^2}$ $\qquad \gamma_i^2 = j\omega\mu_0(\sigma_i + j\omega\varepsilon_i)$

In order to solve these integrals, we want to apply the same methodology resumed in the previous section, namely the Quasi Monte Carlo integration method.

To do that, first we need to have an integral that is bounded in the interval [0,1].

To accomplish that, we use a different change of variable than that used in the last chapter.

The change of variable is

$$\begin{aligned} v &= \exp(-u) \\ u &= -\log(v) \\ du &= -\frac{1}{v}dv \end{aligned} \tag{4.1.18}$$

Applying this to(4.1.16), the integral of the self-impedance, we obtain:

$$Z'_{ground-self} = \frac{j\omega\mu_0}{\pi}\int_0^1 \frac{\alpha'_1+\alpha'_0+(\alpha'_1-\alpha'_0)e^{-2\alpha_1 h}}{(\alpha'_1+\alpha'_0)(\alpha'_1+\alpha'_2)-(\alpha'_1-\alpha'_0)(\alpha'_1-\alpha'_2)e^{-2\alpha'_1 h}}\cos(-\log(v)R)\frac{dv}{v} \tag{4.1.19}$$

$$\alpha'_i = \sqrt{(-\log(v))^2+\gamma_i^2}$$

We can define a function

$$f_{self}(u) = \frac{\alpha_1+\alpha_0+(\alpha_1-\alpha_0)e^{-2\alpha_1 h}}{(\alpha_1+\alpha_0)(\alpha_1+\alpha_2)-(\alpha_1-\alpha_0)(\alpha_1-\alpha_2)e^{-2\alpha_1 h}}\cos(uR) \tag{4.1.20}$$

then

$$Z'_{ground-self} = \frac{j\omega\mu_0}{\pi}\frac{1}{n}\sum_{i=1}^{n} f_{self}(u=-\log(x_i))\frac{1}{x_i} \tag{4.1.21}$$

In the same way, if we define

$$f_{mut}(u) = \frac{\alpha_1+\alpha_0+(\alpha_1-\alpha_0)e^{-2\alpha_1 h}}{(\alpha_1+\alpha_0)(\alpha_1+\alpha_2)-(\alpha_1-\alpha_0)(\alpha_1-\alpha_2)e^{-2\alpha_1 h}}\cos(yR) \tag{4.1.22}$$

We obtain the mutual return impedance as:

$$Z'_{ground-self} = \frac{j\omega\mu_0}{\pi}\frac{1}{n}\sum_{i=1}^{n} f_{mut}(u=-\log(x_i))\frac{1}{x_i} \tag{4.1.23}$$

4.2. Semi-conducting layer modelling

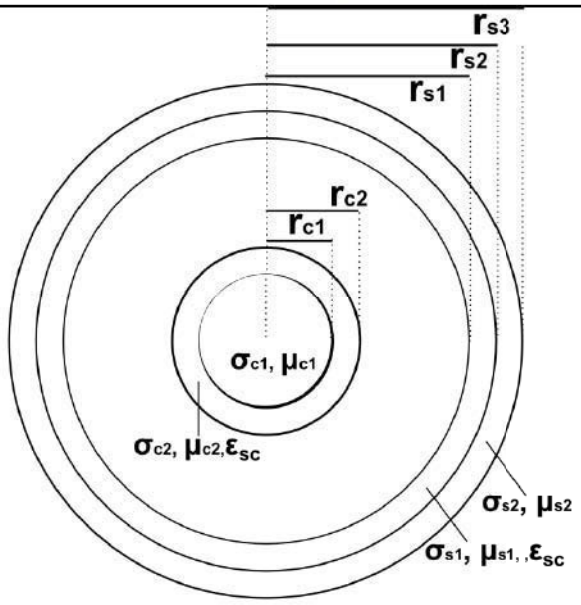

Fig. 39 – Description of a coaxial cable with semi-conducting layers, from inside to outside:

a) core with radius rc1

b) semi-conducting layer radius rc2

c) dielectric

d) semi-conducting layer radius rs1-rs2

e)screen with radius rs2-rs3

4.2.1. Core surface impedance

When the impedance calculation is considered, we can ignore the semi-conducting layer permittivity and suppose it to be a good conductor; the calculation of these terms is carried out using coaxial theory as shown in **[3]**.

The electric and magnetic field are written on the different edges shown in the Figure, and continuity conditions allow to obtain the expression of the impedance, as a function of the electric field and currents.

Taking the formulation from **[14]** we have the surface impedance of a core in parallel with a semi-conducting layer as

$$Z_{c//sc}\frac{\xi_{c2}}{2\pi\sigma_{c2}r_{c2}}\frac{\left[\xi_{c1}\rho_{c1}R_cI_0\left(\xi_{c1}r_{c1}\right)+\xi_{c2}\rho_{c2}S_cI_1\left(\xi_{c1}r_{c1}\right)\right]}{\left[\xi_{c1}\rho_{c1}F_cI_0\left(\xi_{c1}r_{c1}\right)+\xi_{c2}\rho_{c2}E_cI_1\left(\xi_{c1}r_{c1}\right)\right]} \tag{4.2.1}$$

where

$$E_c = I_0(\xi_{c2}r_{c1})K_1(\xi_{c2}r_{c2}) + K_0(\xi_{c2}r_{c1})I_1(\xi_{c2}r_{c2})$$
$$F_c = K_1(\xi_{c2}r_{c1})I_1(\xi_{c2}r_{c2}) - I_1(\xi_{c2}r_{c1})K_1(\xi_{c2}r_{c2})$$
$$R_c = K_1(\xi_{c2}r_{c1})I_0(\xi_{c2}r_{c2}) + I_1(\xi_{c2}r_{c1})K_0(\xi_{c2}r_{c2})$$
$$S_c = K_0(\xi_{c2}r_{c1})I_0(\xi_{c2}r_{c2}) - I_0(\xi_{c2}r_{c1})K_0(\xi_{c2}r_{c2})$$

and $\xi = \sqrt{j\omega\mu\sigma}$ with σ and μ the conductivities and permeability of the different media, and $\rho = \frac{1}{\sigma}$ with the different subscript as indicated in the Figure.

4.2.2. Screen surface impedances

$$Z_{in\_sc//s}\frac{\xi_{s1}\rho_{s1}}{2\pi r_{s1}D_s}\left[\xi_{s1}\rho_{s1}F_sQ_s+\xi_{s2}\rho_{s2}E_sP_s\right] \tag{4.2.2}$$

$$Z_{tran\_sc//s}\frac{\rho_{s1}\rho_{s2}}{2\pi r_{s1}r_{s2}r_{s3}D_s} \tag{4.2.3}$$

$$Z_{out\_sc//s}\frac{\xi_{s1}\rho_{s1}}{2\pi r_{s1}D_s}\left[\xi_{s1}\rho_{s1}F_sQ_s+\xi_{s2}\rho_{s2}E_sP_s\right] \tag{4.2.4}$$

$$D_s=\xi_{s1}\rho_{s1}F_sG_s+\xi_{s2}\rho_{s2}E_sH_s$$
$$E_s=I_0(\xi_{s2}r_{s2})K_1(\xi_{s2}r_{s3})+K_0(\xi_{s2}r_{s2})I_1(\xi_{s2}r_{s3})$$
$$F_s=K_1(\xi_{s2}r_{s2})I_1(\xi_{s2}r_{s3})-I_1(\xi_{s2}r_{s2})K_1(\xi_{s2}r_{s3})$$
$$G_s=I_0(\xi_{s1}r_{s2})K_1(\xi_{s1}r_{s1})+K_0(\xi_{s1}r_{s2})I_1(\xi_{s1}r_{s1})$$
$$H_s=K_1(\xi_{s1}r_{s1})I_1(\xi_{s1}r_{s2})-I_1(\xi_{s1}r_{s1})K_1(\xi_{s1}r_{s2})$$
$$P_s=I_0(\xi_{s1}r_{s1})K_1(\xi_{s1}r_{s2})+K_0(\xi_{s1}r_{s1})I_1(\xi_{s1}r_{s2})$$
$$Q_s=I_0(\xi_{s1}r_{s2})K_0(\xi_{s1}r_{s1})-K_0(\xi_{s1}r_{s2})I_0(\xi_{s1}r_{s1})$$
$$R_s=I_0(\xi_{s2}r_{s3})K_1(\xi_{s2}r_{s2})+K_0(\xi_{s2}r_{s3})I_1(\xi_{s2}r_{s2})$$
$$S_s=I_0(\xi_{s2}r_{s3})K_0(\xi_{s2}r_{s2})-K_0(\xi_{s2}r_{s3})I_0(\xi_{s2}r_{s2})$$

4.2.3. Admittance

When the admittance is considered, one can see the semi-conducting layer as dielectric (having some losses). It can be easily seen that the two semi-conducting layers admittances intervene in the coaxial loop, and are in series with the admittance of the dielectric.

We can easily write the three admittances in the same way as done in section 2.3 and obtain:

$$Y_{c1}=\frac{j\omega 2\pi\varepsilon_{c1}'}{\ln\left(\frac{r_{c2}}{r_{c1}}\right)} \tag{4.2.5}$$

$$Y_{diel}=\frac{j\omega 2\pi\varepsilon_{diel}}{\ln\left(\frac{r_{s1}}{r_{c2}}\right)} \tag{4.2.6}$$

$$Y_{s1}=\frac{j\omega 2\pi\varepsilon_{s1}'}{\ln\left(\frac{r_{s2}}{r_{s1}}\right)} \tag{4.2.7}$$

$$\varepsilon_{c1}'=\varepsilon_{sc}+\frac{1}{j\omega\rho_{c2}}\qquad \varepsilon_{s1}'=\varepsilon_{sc}+\frac{1}{j\omega\rho_{s1}}$$

The resulting total admittance is the series of the three terms.

$$Y_{coax}=\left(1/Y_{c1}+1/Y_{diel}+1/Y_{s1}\right)^{-1} \tag{4.2.8}$$

4.3. Application of stochastic collocation to sensibility analysis

4.3.1. Sensitivity analysis of the input parameters of sea return impedance

We show here how the variation of the parameters of the formula of the sea-return impedance impacts its values. The two variations that we consider are:

- That of the conductivities of the two layers involved in the simulation, that is two variables at the same time;
- The depth of the first layer.

The statistical parameters (mean and variance / standard deviation) have been obtained in the following way:

$$Z_{mean} = \sum_{i=1}^{N} \mu_i Z(\sigma_{1i}, \sigma_{2i}) \tag{4.3.1}$$

$$\mathrm{var}(Z) = \sum_{i=1}^{N} \mu_i \left(Z(\sigma_{1i}, \sigma_{2i})\right)^2 - Z_{mean} \tag{4.3.2}$$

$$Z_{mean} = \sum_{i=1}^{N} \mu_i Z(h_i) \tag{4.3.3}$$

$$\mathrm{var}(Z) = \sum_{i=1}^{N} \mu_i \left(Z(h_{1i})\right)^2 - Z_{mean} \tag{4.3.4}$$

The standard deviation is defined as

$$stdev(Z) = \sqrt{\mathrm{var}(Z)} \tag{4.3.5}$$

For each set of random variable(s) (1 or 2) μ_i is the weight used to evaluate the mean and $(\sigma_{1i}, \sigma_{2i})$ or h_{1i} are the collocation points.

We then obtain the following figures

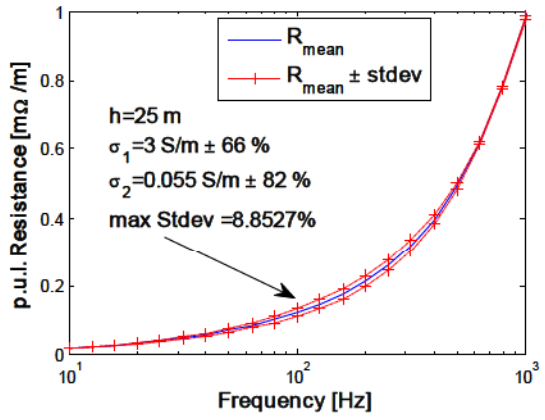

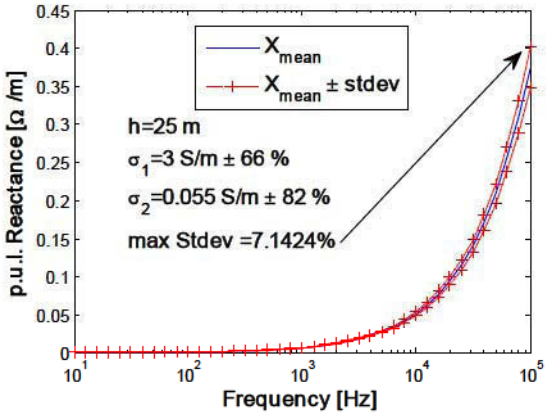

Fig. 40 – Mean resistance and reactance of the sea return impedance, when depth of cable is fixed and conductivities are random variables

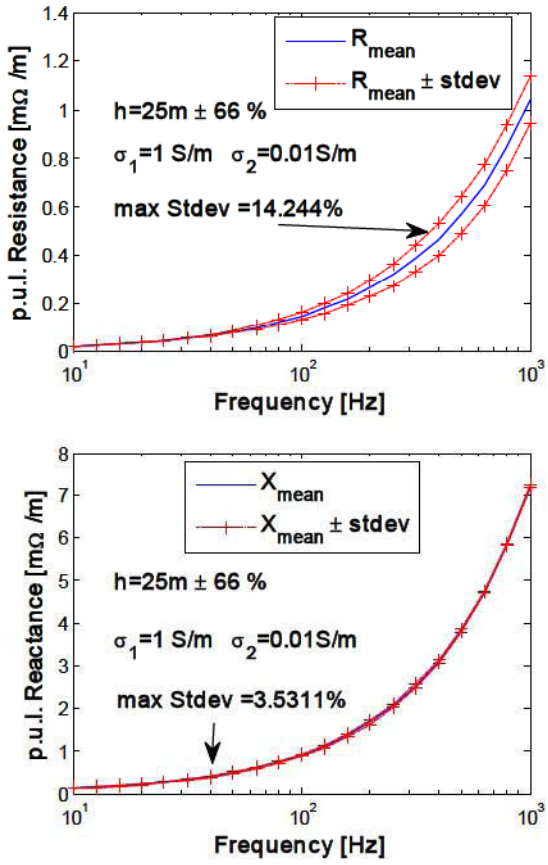

Fig. 41 – Mean resistance and reactance of the sea return impedance, when depth of cable is a random variable and conductivities are fixed

It is interesting to observe that, since this variation is limited, one can use the mean of the value of the impedance as the entry value for the cable model, even when relative big uncertainties are present in the input parameters.

In this case it also makes sense to think that a cable, when laid in the sea has a variable laying depth. It is therefore interesting that the stochastic collocation allows very simply to calculate the mean of the impedance.

4.3.2. Sensibility analysis applied to the evaluation of the semi-conducting layer admittance

The parameters of the semiconducting layer of the cable are not known with precision.

Its conductivity and permittivity can vary in a large range of values.

To analyze the impact of this variation on the value of the total admittance of the insulator (evaluated as in equation(4.2.8)) we have applied the stochastic collocation technique to the semiconducting layer, using two input variables:

- Its conductivity σ_{sc}=3.5±60% S/m
- Its relative permittivity $\varepsilon_{r\text{-}sc}$= 525 ± 90 %

The method of stochastic collocation described in Appendix A allows to evaluate the statistical variation of the admittance as a function of the variation of the input parameters.

As for the case treated in the section before, we have a set of collocation points (namely the value of the input parameters) for which the function is evaluated. We have here a set of two random variables (σ_i, ε_i). For each set we have a corresponding weight μ_i.

This allow us to evaluate the mean value of the admittance as:

$$Y_{mean} = \sum_{i=1}^{N} \mu_i Y(\varepsilon_i, \sigma_i) \tag{4.3.6}$$

$$\mathrm{var}(Y) = \sum_{i=1}^{N} \mu_i \left(Y(\varepsilon_i, \sigma_i)\right)^2 - Y_{mean} \tag{4.3.7}$$

$$stdev(Y) = \sqrt{\mathrm{var}(Y)} \tag{4.3.8}$$

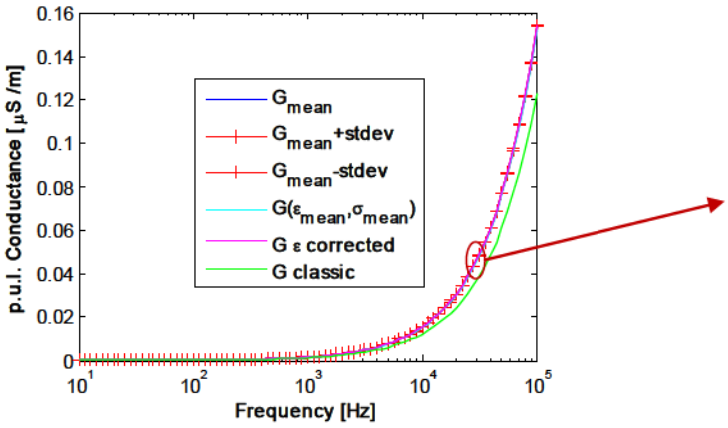

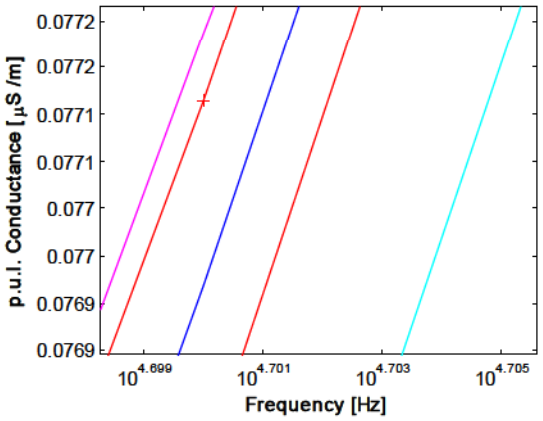

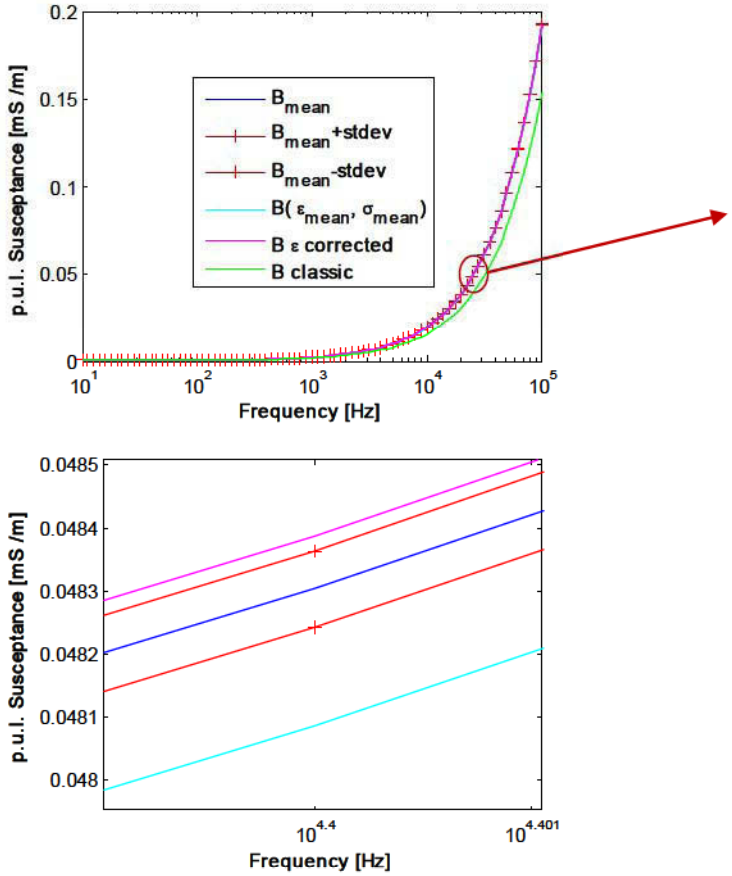

Fig. 42 – Mean of conductance and susceptance of the insulation evaluated when the conductivity and permittivity of the semi-conducing layer are random variables

We show here the real and imaginary part of the admittance. *Gmean* and *Bmean* are the mean value of the conductance and the susceptance, evaluated with the stochastic collocation. Stdev is the standard deviation of this parameter. We also show in the figure the value of the conductance and susceptance evaluated for the mean value of the input parameters in light blue. It is interesting to see that the mean value of the output parameters is not obtained when the parameters is evaluated in the mean value of the input parameters.

We also show, in green, the value of the conductance/susceptance, as it would be calculated using a classic Cable routine, that is considering the semi-conducting layer to be part of the insulation; in purple we show the value when the semi-conducting layer is not considered to be part of the insulation (this can be accomplished in a classic routine modifying the value of the permittivity as shown in section 5.1.3.2).

We have demonstrated that the semiconducting layer must be taken into account someway, otherwise a mistake is committed in the evaluation of the admittance

We have also done a sensitivity analysis that has shown that even very big uncertainties in the electrical parameters of the semi-conducting layer have small impact on the evaluation of the admittance.

All the waveforms are practically superimposed, but it is evident that in this case the permittivity of the semiconducting layer is so big that the admittance of the insulator has a much greater importance as compared to the contribution of the semiconducting layer. As a reference we give in the following table the value of these parameters, as it is not easy to see their variation in the figures.

Table 10 – Conductance and susceptance of the insulation layer

Parameter\Frequency	50 Hz	1 kHz	10 kHz	100 kHz
G ε corrected	$7.7237 \cdot 10^{-11}$	$1.5411 \cdot 10^{-9}$	$1.5411 \cdot 10^{-8}$	$1.5411 \cdot 10^{-7}$
G_{mean}	$7.6964 \cdot 10^{-11}$	$1.5354 \cdot 10^{-9}$	$1.5354 \cdot 10^{-8}$	$1.5354 \cdot 10^{-7}$
Stdev of G / G_{mean}	0.31 %	0.34 %	0.34 %	0.34 %
$G\ (\varepsilon_{mean}, \sigma_{mean})$	$7.6373 \cdot 10^{-11}$	$1.522 \cdot 10^{-9}$	$1.5219 \cdot 10^{-8}$	$1.5219 \cdot 10^{-7}$
G classic	$6.1375 \cdot 10^{-11}$	$1.2246 \cdot 10^{-9}$	$1.2246 \cdot 10^{-8}$	$1.2246 \cdot 10^{-7}$

Parameter\Frequency	50 Hz	1 kHz	10 kHz	100 kHz
B ε corrected	$9.6546 \cdot 10^{-8}$	$1.9263 \cdot 10^{-6}$	$1.9263 \cdot 10^{-5}$	$1.9263 \cdot 10^{-6}$
B_{mean}	$9.6368 \cdot 10^{-8}$	$1.9228 \cdot 10^{-6}$	$1.923 \cdot 10^{-5}$	$1.923 \cdot 10^{-6}$
Stdev of B / B_{mean}	0.17 %	0.17 %	0.17 %	0.17 %
$B\ (\varepsilon_{mean}, \sigma_{mean})$	$9.5943 \cdot 10^{-8}$	$1.9143 \cdot 10^{-6}$	$1.9143 \cdot 10^{-5}$	$1.9143 \cdot 10^{-6}$
B classic	$7.6718 \cdot 10^{-8}$	$1.5307 \cdot 10^{-6}$	$1.5307 \cdot 10^{-5}$	$1.5307 \cdot 10^{-6}$

5. EMTP-RV simulations of three-core cables

In this manuscript we have detailed the derivation of different terms that are used for the construction of the phase impedance and admittance matrices of underground and submarine cables.

We have developed and shown a method for the calculation of the internal impedances of solid and hollow conductors that also includes proximity effect. We have also analysed the effect of the external current return upon impedances, as well as the effect of semi-conducting layers that are present in medium and high voltage cables.

Scope of this chapter is to give a summary of how the three-core cable model (to be used for the simulation of transients on three-core submarine cables, one of the focuses of this thesis), is developed, putting together the various terms and therefore including all relevant electromagnetic effects.

We also show how a complete model is generated using fitting procedures contained in the EMTP-RV Cable Data module and how this model is employed in analysing fast transients, such as those generated by lightning strikes.

5.1. Assembling the three-core cable model

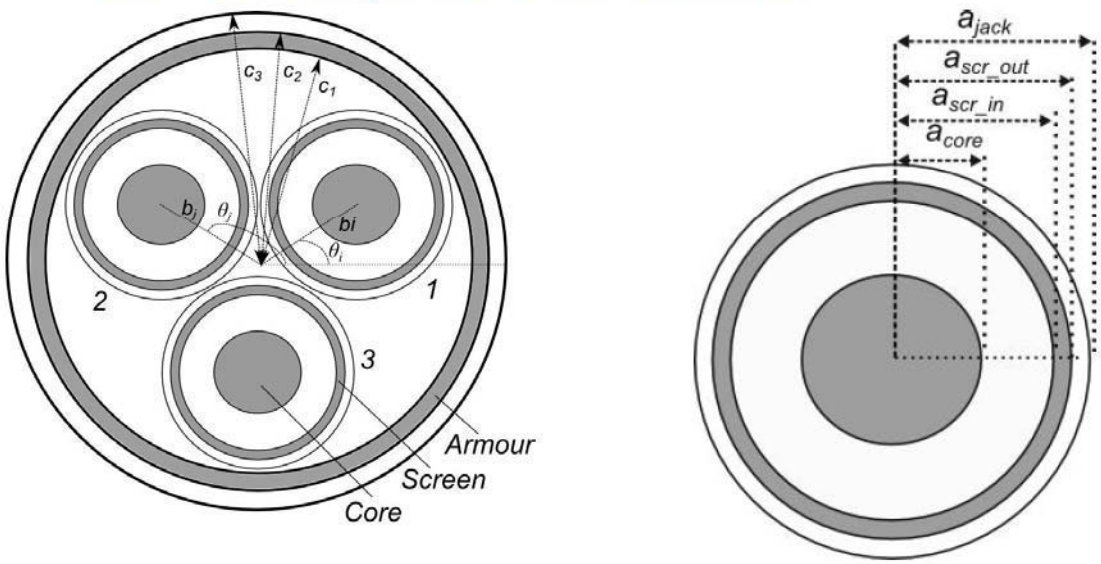

Fig. 43 – Notation of the three-core cable with detail of the inner coaxial cable

5.1.1. Impedance calculation

We write again the matrix formulation which is the same that has been shown in Section 2.4:

$$Z_{tot} = Z_{\text{int}} + Z_{arm-in} + Z_{arm-out} + Z_{earth-return} \tag{5.1.1}$$

We now explicit the terms of 5.1.1

$$Z_{\text{int}} = \begin{bmatrix} [Z_{\text{int}1}] & [0] & [0] & 0 \\ [0] & [Z_{\text{int}2}] & [0] & 0 \\ [0] & [0] & [Z_{\text{int}3}] & 0 \\ 0 & 0 & 0 & 0 \end{bmatrix} \tag{5.1.2}$$

The sub-matrix here is $Z_{\text{int}\,i} = \begin{bmatrix} z_{\text{int}\,cc} & z_{\text{int}\,cs} \\ z_{\text{int}\,cs} & z_{\text{int}\,ss} \end{bmatrix}$ with

$$z_{\text{int}\,cc} = z_{\text{int}-c-\text{mod}} + z_{iso-cs} + z_{in-s} - 2z_{t-s} + z_{out-s} + z_{iso-sg} \tag{5.1.3}$$

$$z_{\text{int}\,cs} = z_{out-s} - z_{t-s} + z_{iso-sg} \tag{5.1.4}$$

$$z_{\text{int}\,ss} = z_{out-s} + z_{iso-sg} \tag{5.1.5}$$

For simplicity we neglected subscript *i* indicating the inner cable whose parameters should be considered when evaluating formulas (5.1.3)-(5.1.5) with the formulas detailed in Section 2.3.2.

We have replaced the term of the core's surface impedance with a modified term including proximity effects, that is evaluated as

$$z_{\text{int-}c\text{-mod}} = z_{\text{int-}c} + 2\, z_{prox-c->c} + z_{prox-arm->c} \tag{5.1.6}$$

The proximity effect correction terms have all been obtained applying definitions (3.4.10)-(3.4.13) which are the numerical integration needed in our code to evaluate impedances with our semi-analytical formulations. The term $z_{prox\text{-}c\text{->}c}$ accounts for the effect of one core upon another and has been derived from the theory described in Section 3.2. The term $z_{prox\text{-}arm\text{->}c}$ accounts for the effect of the armour upon the inner cores, and the term $z_{prox\text{-}c\text{->}arm}$ which accounts for the effect of a core upon the armour (and used in construction of the following matrix) have been obtained following the theory described in Section 3.3.

$$Z_{arm-in} = \begin{bmatrix} [Z_{a11}] & [Z_{a12}] & [Z_{a13}] & 0 \\ [Z_{a12}] & [Z_{a22}] & [Z_{a23}] & 0 \\ [Z_{a13}] & [Z_{a23}] & [Z_{a33}] & 0 \\ 0 & 0 & 0 & 0 \end{bmatrix} \tag{5.1.7}$$

with the sub-matrix $[Z_{aij}] = \begin{bmatrix} z_{aij} & z_{aij} \\ z_{aij} & z_{aij} \end{bmatrix}$

$$z_{aii} = z^{self}_{a-diel} + z_{arm-in} \tag{5.1.8}$$

$$z_{aij} = z^{mut}_{a-diel} + z_{arm-in} \tag{5.1.9}$$

$$z^{self}_{a-diel} = \frac{j\omega\mu_0}{2\pi} \ln\left(\frac{c_1^2 - b_i^2}{c_1 a_{jack}}\right) \tag{5.1.10}$$

$$z^{mut}_{a-diel} = \frac{j\omega\mu_0}{2\pi} \ln\left(\frac{b_j}{c_1}\sqrt{\frac{(b_i b_j)^2 + c_1^4 - 2b_i b_j c_1^2 \cos\theta_{ij}}{(b_i b_j)^2 + b_i^4 - 2b_i b_j^3 \cos\theta_{ij}}}\right) \tag{5.1.11}$$

The term of the armour, namely $z_{arm\text{-}in}$ of (2.4.14) we replaced as follows

$$z_{\text{arm-in}} = z_{skin-\text{mod}} + z_{prox-c->arm} \tag{5.1.12}$$

The proximity effect correction terms, marked in bold, have all been obtained applying definitions (3.4.10)-(3.4.13) which are the numerical integration needed in our code to evaluate impedances with our semi-analytical formulations.

The term $z_{prox\text{-}c\text{->}c}$ has been obtained with the part of the code that we obtained from the theory we have described in Section 3.2 whereas the terms $z_{prox\text{-}arm\text{->}c}$ and $z_{prox\text{-}c\text{->}arm}$ have been obtained following what is described in Section 3.3.

The term $z_{skin\text{-}mod}$ is different from what Ametani uses in his pipe type model, since for this 0-order

term related to the armour; the semi-infinite pipe thickness approximation has not been used.

The connection matrix remains the same as in section 2.4, as follows:

$$Z_{arm-out} = \begin{bmatrix} [Z_{c1}] & [Z_{c1}] & [Z_{c1}] & z_{c2} \\ [Z_{c1}] & [Z_{c1}] & [Z_{c1}] & z_{c2} \\ [Z_{c1}] & [Z_{c1}] & [Z_{c1}] & z_{c2} \\ z_{c2} & z_{c2} & z_{c2} & z_{c3} \end{bmatrix} \tag{5.1.13}$$

$$\text{with} [Z_{c1}] = \begin{bmatrix} z_{c1} & z_{c1} \\ z_{c1} & z_{c1} \end{bmatrix} [Z_{c2}] = \begin{bmatrix} z_{c2} & z_{c2} \\ z_{c2} & z_{c2} \end{bmatrix}$$

these are always

$$\begin{aligned} z_{c1} &= z_{arm-out} + z_{arm-iso} - 2 \cdot z_{t-arm} \\ z_{c2} &= z_{arm-out} + z_{arm-iso} - z_{t-arm} \\ z_{c3} &= z_{arm-out} + z_{arm-iso} \end{aligned} \tag{5.1.14}$$

$$Z_{earth-return} = \begin{bmatrix} z_g & \cdots & \cdots & z_g \\ \vdots & \ddots & & \vdots \\ \vdots & & \ddots & \vdots \\ z_g & \cdots & \cdots & z_g \end{bmatrix} \tag{5.1.15}$$

Here the term z_g is obtained as described in Section 4.1 depending on whether the return is the ground or the sea.

5.1.2. Admittance calculation

We give here the matrices of the admittance for a three-core cable. The admittance is obtained, inverting the potential matrix, namely

$$[Y] = j\omega\left([P_{tot}]\right)^{-1}$$

Similar to what happens with the impedance, the potential matrix is obtained summing different matrices, namely

$$P_{tot} = P_{\text{int}} + P_{arm-in} + P_{arm-out} \tag{5.1.16}$$

$$P_{\text{int}} = \begin{bmatrix} [P_{\text{int}1}] & 0 & 0 & 0 \\ 0 & [P_{\text{int}2}] & 0 & 0 \\ 0 & 0 & [P_{\text{int}3}] & 0 \\ 0 & 0 & 0 & 0 \end{bmatrix} \tag{5.1.17}$$

where $[P_{\text{int}1}] = \left(\left[\frac{1}{j\omega} Y_{\text{int}1}\right]\right)^{-1}$ and $[Y_{\text{int}1}] = \begin{bmatrix} y_{cs} & -y_{cs} \\ -y_{cs} & y_{cs} + y_{sg} \end{bmatrix}$

In order to include the effect of the semi-conducting layer the term y_{cs} can be replaced with the term y_{coax} detailed by(4.2.8).

$$P_{arm-in} = \begin{bmatrix} [P_{a11}] & [P_{a12}] & [P_{a13}] & 0 \\ [P_{a12}] & [P_{a22}] & [P_{a23}] & 0 \\ [P_{a13}] & [P_{a23}] & [P_{a33}] & 0 \\ 0 & 0 & 0 & 0 \end{bmatrix} \tag{5.1.18}$$

where $\left[P_{aij}\right]=\begin{bmatrix} p_{aij} & p_{aij} \\ p_{aij} & p_{aij} \end{bmatrix}$

$$p_{aii}=\frac{1}{2\pi\varepsilon}\ln\left(\frac{c_1^2-b_i^2}{c_1 a_{jack}}\right) \tag{5.1.19}$$

$$p_{aij}=\frac{1}{2\pi\varepsilon}\ln\left(\frac{b_j}{c_1}\sqrt{\frac{(b_i b_j)^2+c_1^4-2b_i b_j c_1^2\cos\theta_{ij}}{(b_i b_j)^2+b_i^4-2b_i b_j^3\cos\theta_{ij}}}\right) \tag{5.1.20}$$

and finally $P_{arm-out}=\begin{bmatrix} p_c & \cdots & \cdots & p_c \\ \vdots & \ddots & & \vdots \\ \vdots & & \ddots & \vdots \\ p_c & \cdots & \cdots & p_c \end{bmatrix}$ (5.1.21)

with

$$p_c=\frac{1}{2\pi\varepsilon}\ln\left(\frac{c_3}{c_2}\right) \tag{5.1.22}$$

5.1.3. Recommendations for input parameters

Entry parameters of the simulations are very important, as they affect the results.

5.1.3.1. Resistivity of the core

One of the more important parameters for conductors is the conductivity (or its inverse the resistivity).

$$\sigma=\frac{1}{\rho}\ \rho=\frac{R_{DC}\cdot S}{l} \tag{5.1.23}$$

where S is the section of the conductor. One should use the surface given by the constructor, which is smaller than the area πr_{core}^2 for stranded conductors because of the empty spaces between strands.The direct current resistance is also affected by temperature in the following way

$$R_{DC}=R_{20°}[1+\alpha_{20}(\theta-20)] \tag{5.1.24}$$

where R_{20} is the DC resistance at 20°C (normally provided by the manufacturer), α_{20} is the temperature coefficient which depends upon the material and θ is the maximum operating temperature (in degree Celsius).

5.1.3.2. Simplified semi-conducting layer inclusion

A simplified way to include the effect of the semi-conducting layer [**41**], using for instance the existing Cable Auxiliary routines of EMTP is to replace the relative permittivity of the core-screen insulation as follows:

$$\varepsilon_{\text{mod}}=\varepsilon\frac{\ln\frac{r_{s2}}{r_{c1}}}{\ln\frac{r_{s1}}{r_{c2}}} \tag{5.1.25}$$

where the quantities inside the logarithm are detailed in Fig. 39 of section 4.2.

5.2. Simulations using the three-core cable model

In order to compare the model here proposed ('Wires') with the Pipe-Type model of EMTP (PT) we analyze the simulations of different transient waveforms in the same three-core cable of 1 km length, as used for the validation in Chapter 3

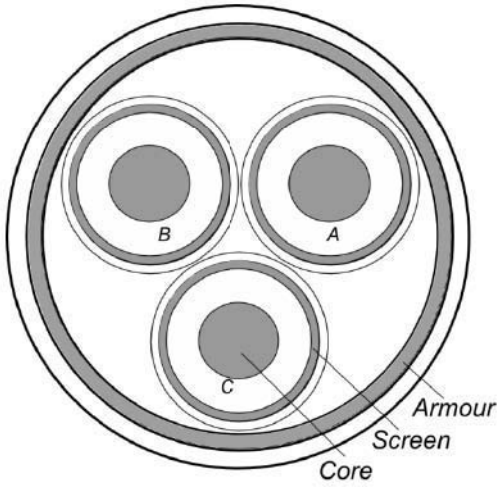

Fig. 44 – Cable used in the simulations

Its cores are symmetrical so that we can limit the analysis to the core and the screen A, where the source is connected, and the core and screen B, which are the same as on the core and screen C.

We first give the T_i matrix, namely the current modal transformation matrix for the three-core cable, both for the PT and Wires models, at 1 MHz.

$$T_{i-wires} = \begin{bmatrix} 0 & 0 & 0 & 0 & 0.577 & -0.371 & 0.813 \\ 0 & 0.816 & 1.155 & 0 & -0.577 & 0.371 & -0.813 \\ 0 & 0 & 0 & 0 & 0.577 & -0.468 & -0.571 \\ 0 & 0.816 & -0.755 & -1.017 & -0.577 & 0.468 & 0.571 \\ 0 & 0 & 0 & 0 & 0.577 & -0.839 & -0.242 \\ 0 & 0.816 & -0.399 & -1.017 & -0.577 & 0.839 & 0.242 \\ 2.646 & -2.449 & 0 & 0 & 0 & 0 & 0 \end{bmatrix}$$

$$T_{i-PT} = \begin{bmatrix} 1 & 0 & 0 & 0 & 0 & 0 & 0 \\ -1 & 0 & 0 & 0 & 0.816 & 0.044 & 1.119 \\ 0 & 1 & 0 & 0 & 0 & 0 & 0 \\ 0 & -1 & 0 & 0 & 0.816 & -1.039 & -0.588 \\ 0 & 0 & 1 & 0 & 0 & 0 & 0 \\ 0 & 0 & -1 & 0 & 0.816 & 0.995 & -0.531 \\ & 0 & 0 & 2.646 & -2.449 & 0 & 0 \end{bmatrix}$$

The modes described by the two matrices are not as straightforward to be identified as those that are shown in section 2.2.2.3, but it is still possible to identify in these matrices $T_{i\text{-}wires}$ and $T_{i\text{-}PT}$:

- 1 bifilar mode (column 4 and 6 respectively) although for the second matrix, rather than a bifilar mode it can be considered an inter-sheath mode;

- 1 inter-sheath mode (column 3 and 7 respectively);

- 3 coaxial modes (columns 5-7 and 1-3 respectively);

- 1 zero sequence mode (column 2 and 5 respectively), where the current is injected in the sheaths and returns by the armour;

- 1 coaxial mode (column 1 and 4 respectively) between the armour and the ground.

5.2.1. Description of the simulation design

The 1 km three-core cable is connected at its ends to two cables with identical characteristics 100 km long. This is done to ensure matching conditions.

The source used for the simulations is a current ramp of 5 kA. It is connected between the core A and the ground. It has a rise time of 100 µs and a fall time of 50 µs, as easily seen in the first waveform of Fig. 46.

In order to facilitate the comparison, we have chosen for the ground-return term to use the formulation described by equation (4.1.10), and although not realistic for a submarine cable, we considered a conductivity of 0.001 S/m.

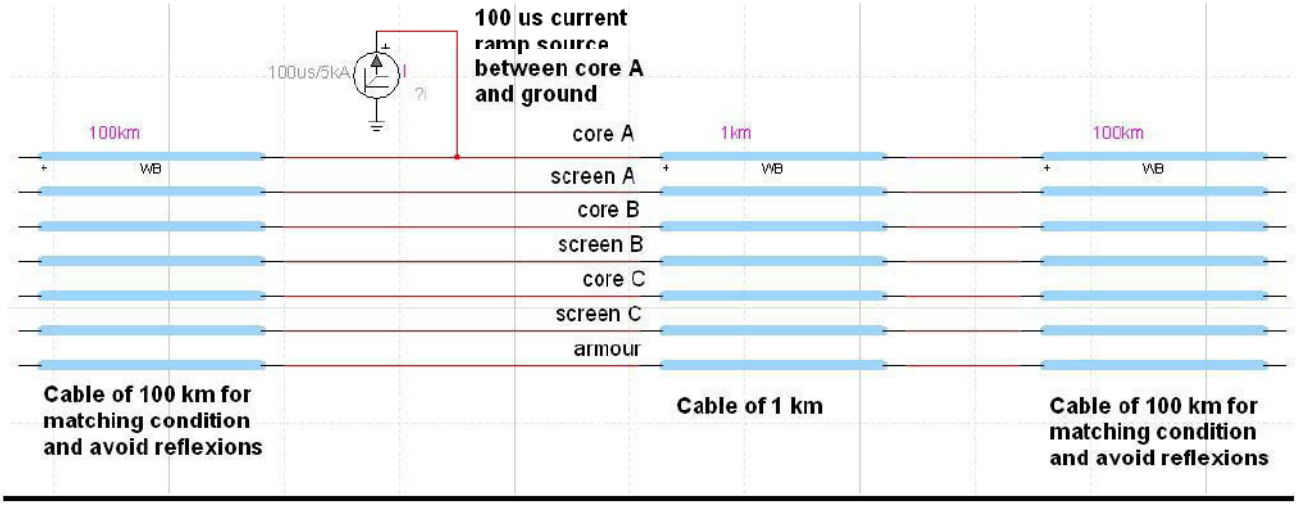

Fig. 45 – Design of the simulation in EMTP-RV

Here we show in order, Core A, Screen A, Core B, Screen B and Armour.

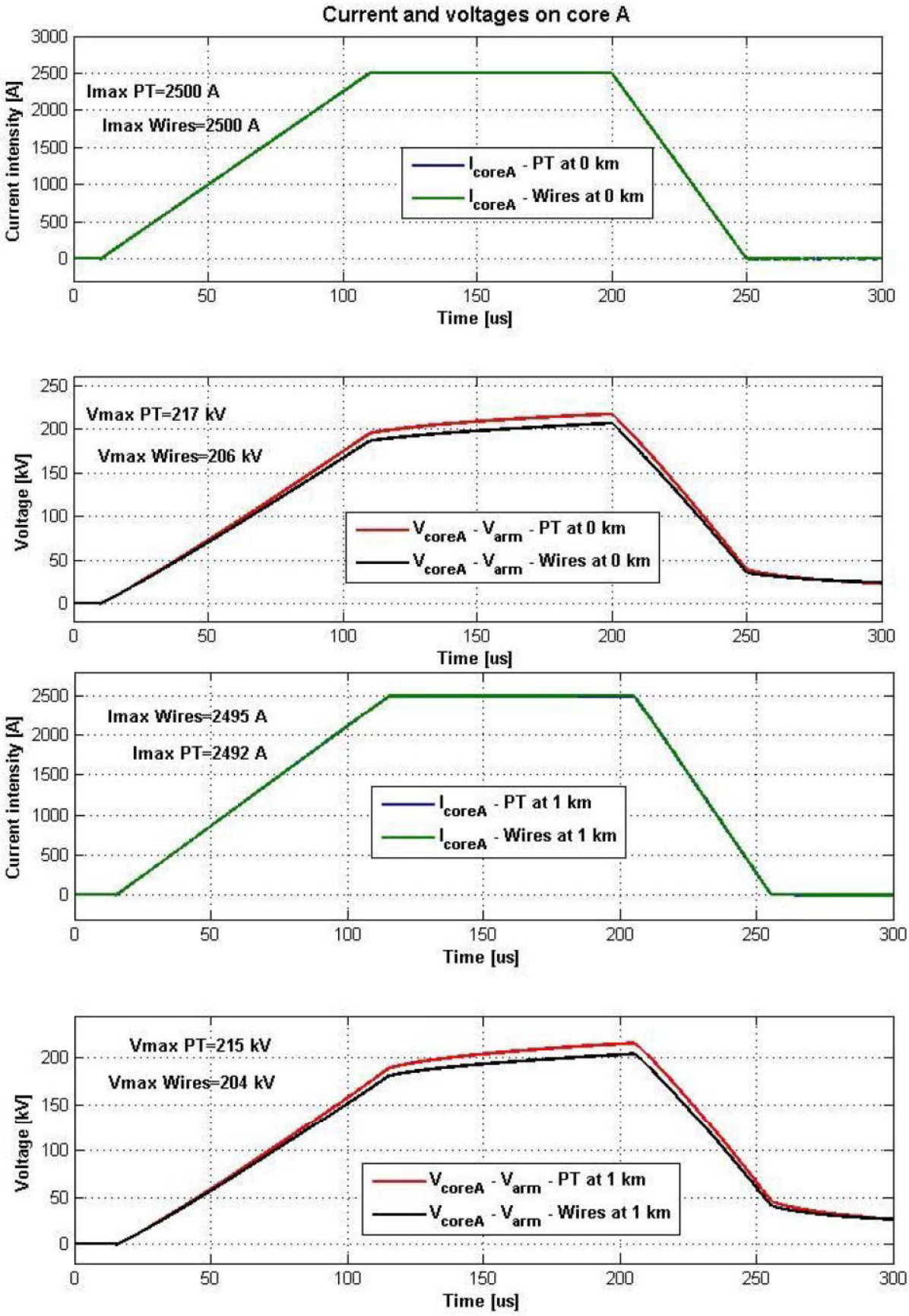

Fig. 46 - Core A currents and voltages at cable entrance and exit – the source is a current ramp between Core A and the ground, no grounding is used

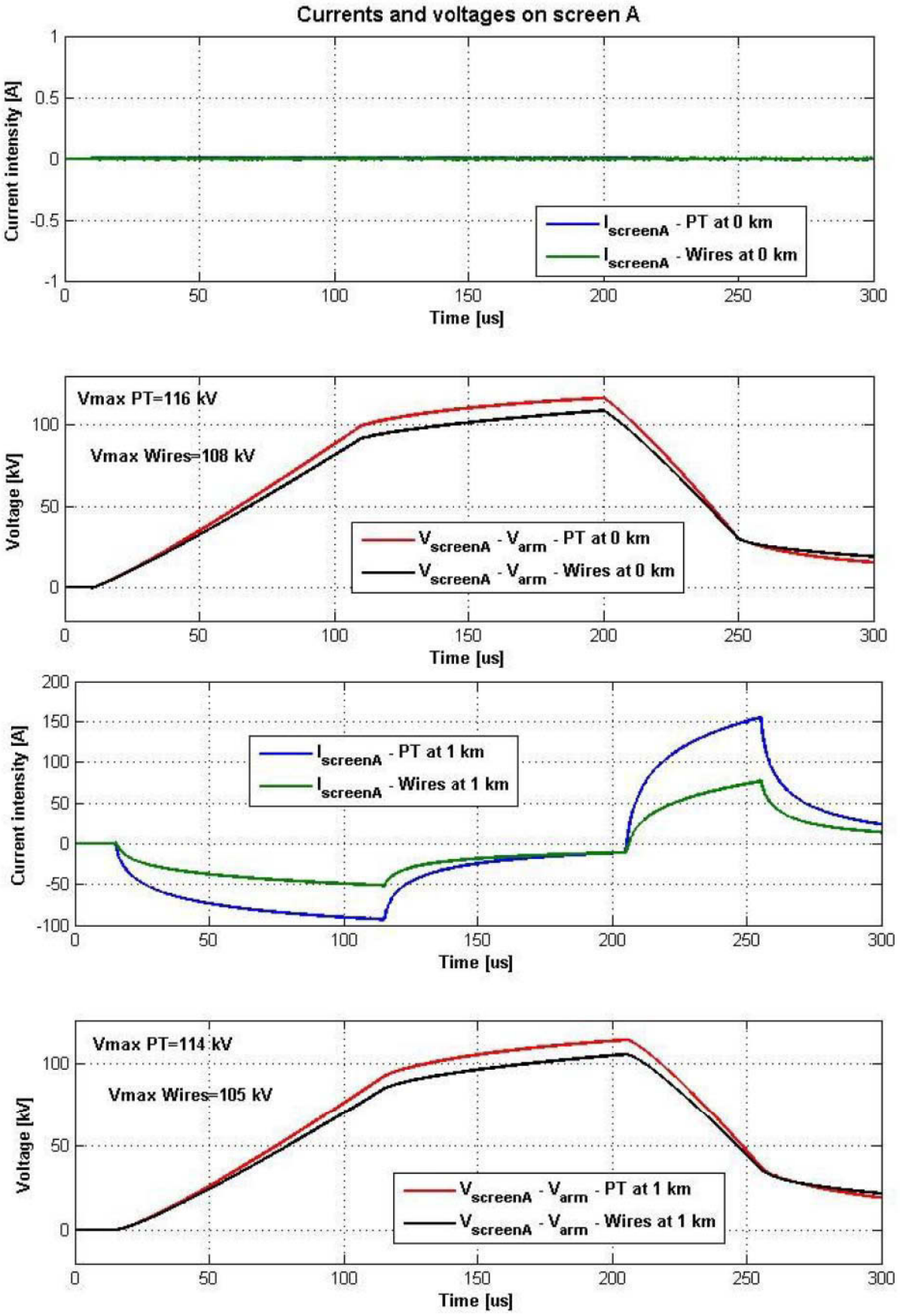

Fig. 47 - Screen A currents and voltages at cable entrance and exit – the source is a current ramp between Core A and the ground, no grounding is used

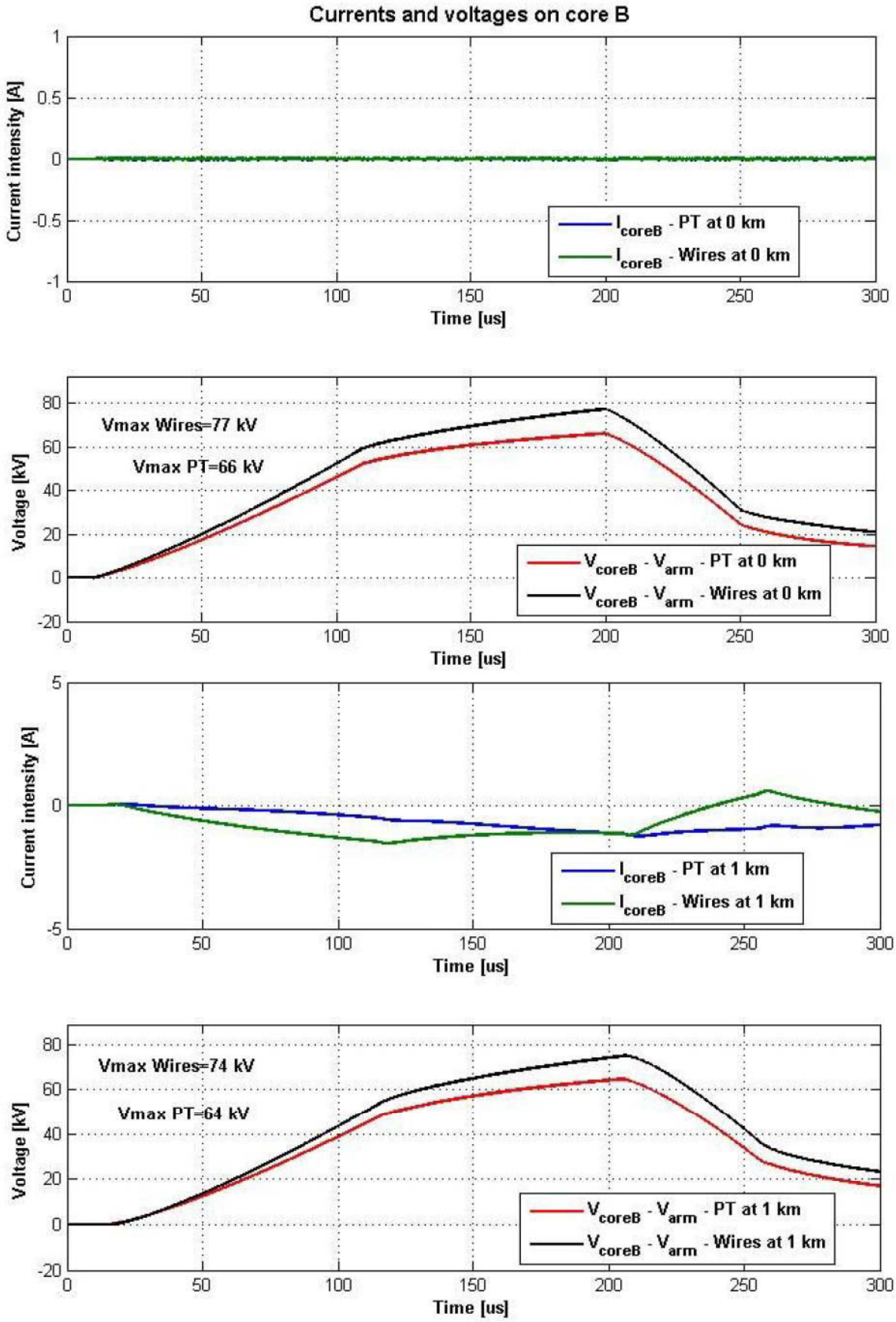

Fig. 48 - Core B currents and voltages at cable entrance and exit – the source is a current ramp between Core A and the ground, no grounding

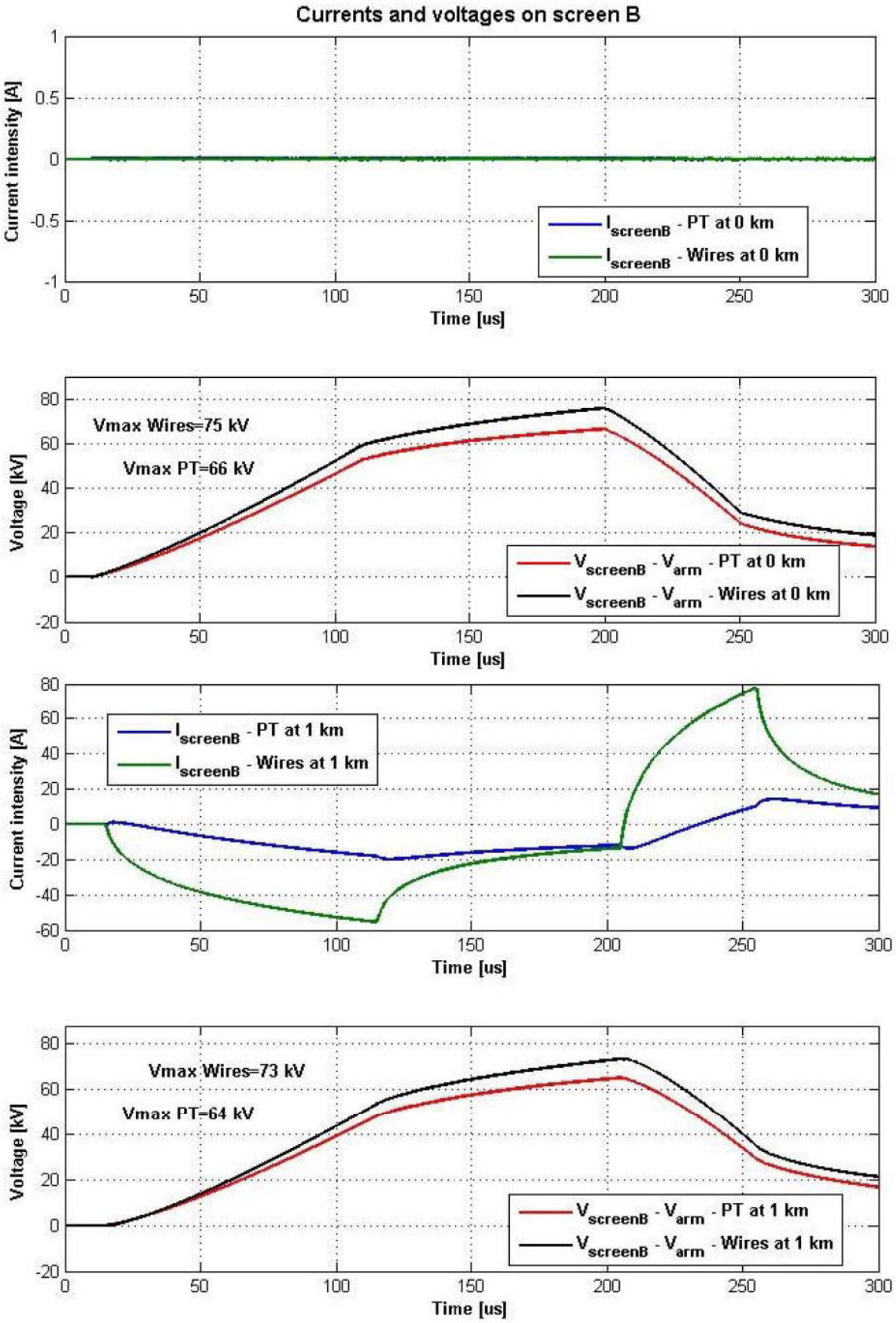

Fig. 49 – Screen B currents and voltages at cable entrance and exit – the source is a current ramp between Core A and the ground, no grounding

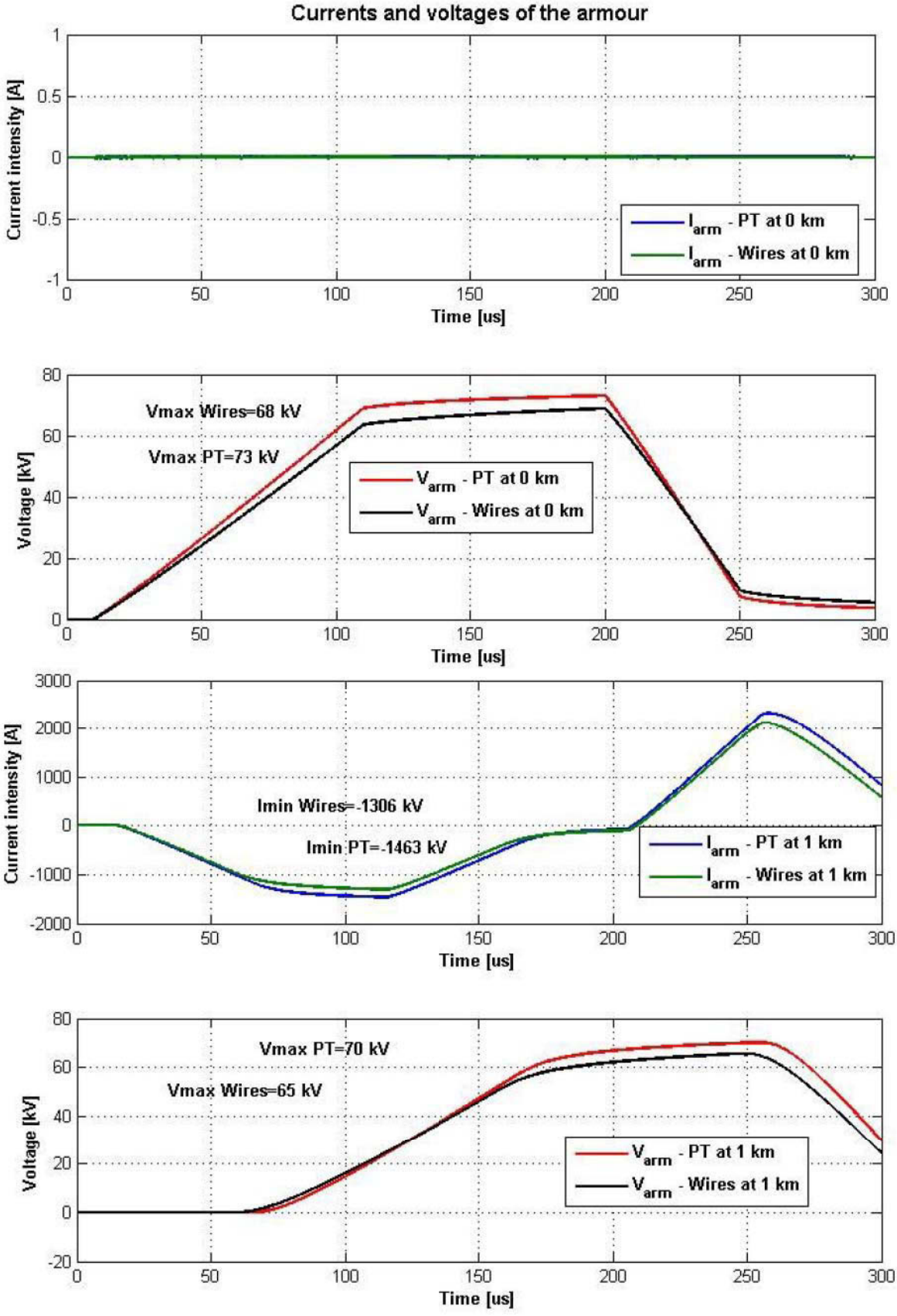

Fig. 50 – Armour currents and voltages at cable entrance and exit – the source is a current ramp between Core A and the ground, no grounding

5.2.2. Discussion of the results of the simulation

For our simulation we have used a source connected between core A and the ground in order to energize different modes of propagation.

The rise time used for the current ramp, 100 μs, is characteristic of switching / energization transients for a cable.

The use of two very long cables connected to the 1 km cable of interest, and having the same surge impedance, and the fact that no grounding has been used, has allowed to simplify the results obtained in that:

- there are no reflections until the current/voltage waves have reached the end of the 100 km cables;

- at the entrance side of the cable (0 km) there is no current flowing in the conductors but only one in the core A where the current is injected.

As we have shown in Appendix B, for the cable taken into consideration, the impedance of the armour is bigger when evaluated with PT model as compared to Wires model, which explains that when a current source is connected to core A, the voltage we see between this core and the armour (see Fig.46) results bigger in the case of the PT model. The difference is about 5% between the peak values of the models, and for the source considered.

The same happens, when looking at screen A in Fig.47: the difference between the model in this case is about 7 %.

When looking at the core B we see the situation inversed, in that the voltage between core B and the armour is bigger when using the Wires model by 14% and by 12 % on the Screen B in Fig. 49.

This can be possibly explained by looking at the current flowing in the armour at the exit of the cable (1 km), see Fig. 50. This current is due to a coupling with the earth conductor, that acts as the return for the current of the generator.

We can see that this current has a negative shape, and is different (lower) for the Pipe Type model, which is consistent with difference in the characteristic impedance between the two models. The difference between the currents in the negative peak is 12%.

Currents flowing in all screens and in core B all exhibit similar overall time behaviour as seen in the armour.

It is interesting to see that the armour plays a role, similar to that of the earth in classical single-cores cable installations; the precise representation of its impedance is of importance even at not so high frequency.

The proximity effect upon the cores is in the examined case less important than the proximity effect on the armour. The much higher resistance of the armour as compared to the cores, but also to the frequency range, has an influence on that. Other cable configurations, for instance low or medium voltage cables without an armour but close together could be more affected by the core proximity effect, furthermore if the frequency is higher.

5.2.3. Simulations with soils of different resistivity

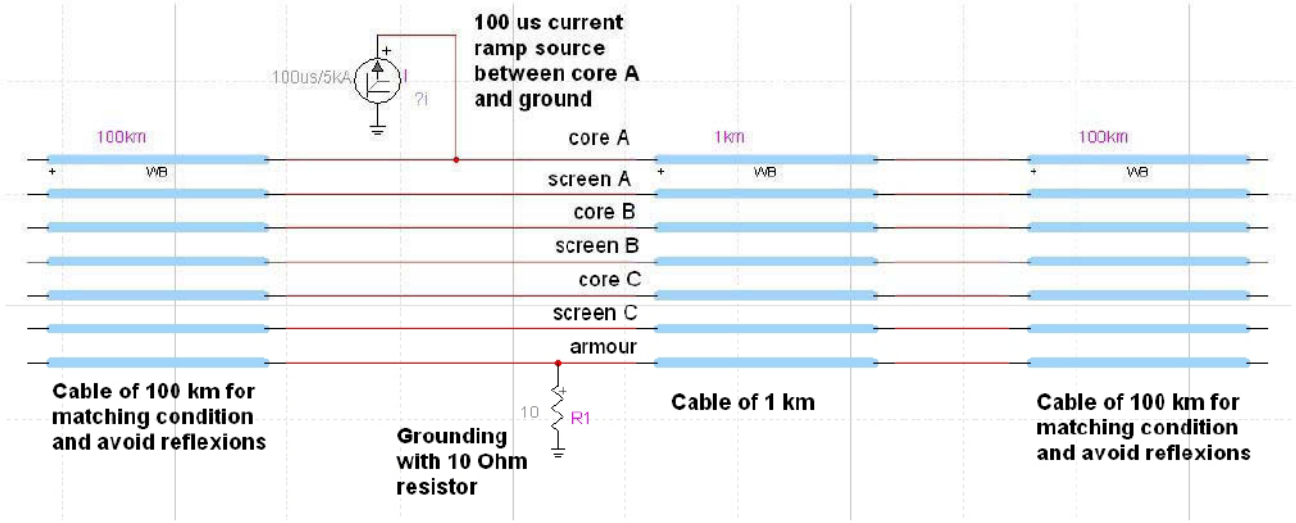

Fig. 51 – Design of the second simulation

In this second simulation, we limit the analysis to the cable model proposed, and consider two different soil resistivities. We show the voltage between the armour and the ground. The design is similar to that simulated before, but a grounding is added in the second figures. Furthermore the source used here is always a current ramp with a 100 µs rise time, but unlike the other source, at 200 µs this one is switched off istantly.

We first compare the voltage at entrance and exit of the cable, when no grounding is used:

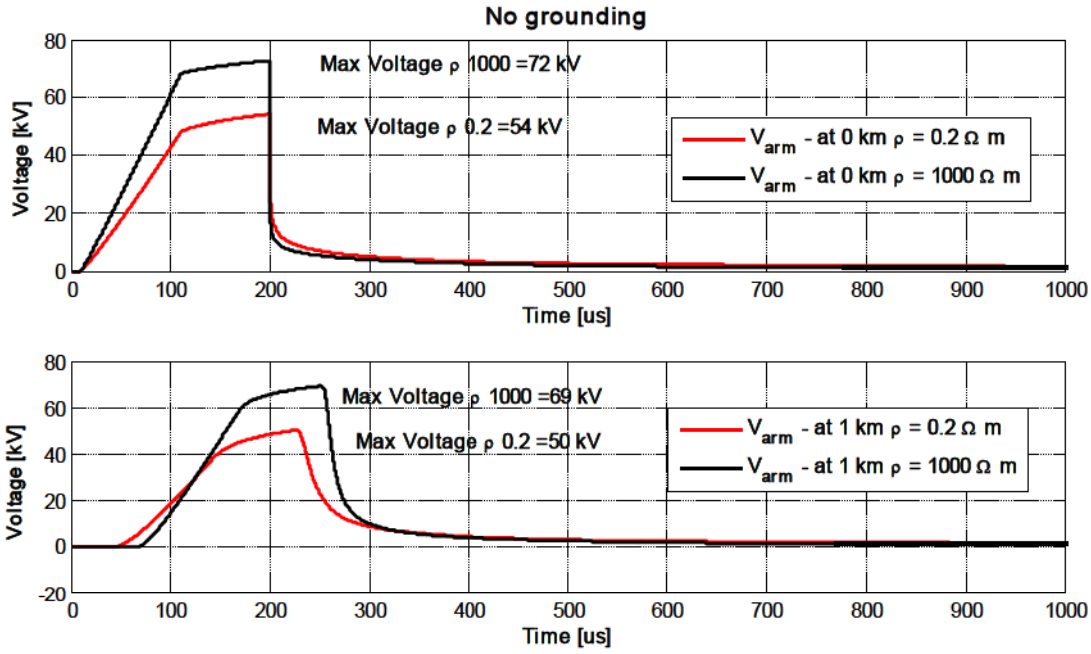

Fig. 52 – Voltage on the armour of the cable without grounding used, comparing soil of resistivity 0.2 and 1000 Ω m

The effect of the higher resistivity is to increase the voltage at the armour.

When we simulate the same design, but adding a grounding, we can see in the following figure that the voltage is much reduced due its effect, but the more resistive soil still increases the voltage at the armour.

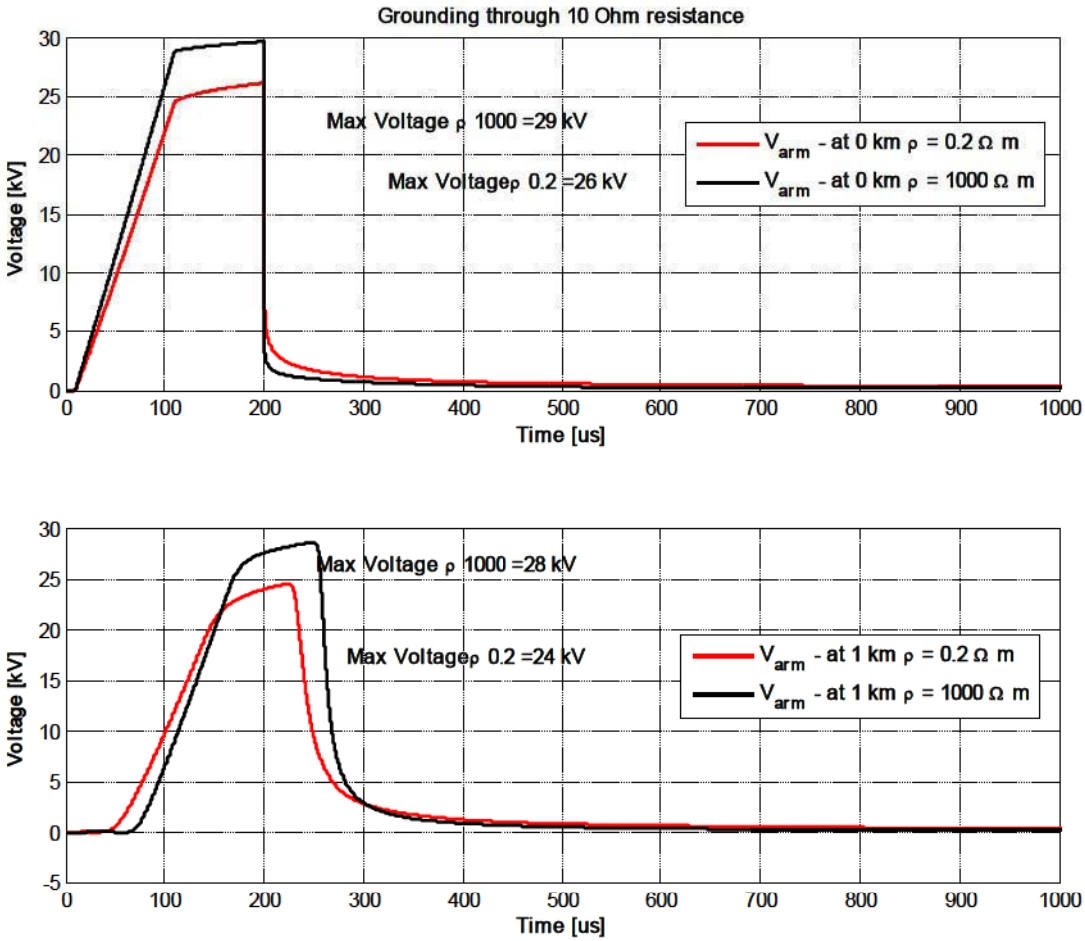

Fig. 53 – Voltage on the armour of the cable using grounding, comparing soil of resistivity 0.2 and 1000 Ω m

6. Conclusions

The main scope of this dissertation is to propose an improved method for the calculation of impedances in three-core submarine power cables models. To do this we have adapted and modified certain terms of some existing models and validated the results.

The closeness of the various conductors of three-core power cables modifies the current distribution inside them, and this proximity effect is, in these cables, more important than in other transmission line systems, the effect being due to the same electromagnetic principle which causes the skin effect, namely eddy currents: The magnetic fields due to the currents flowing in the conductors induce electromotive forces that cause the current flowing in them to be either pushed away or attracted (depending on the mutual current direction) and, since these e.m.f. vary with the frequency so do the skin and proximity effects which become more pronounced the higher the frequency. As shown in our work, the proximity effect less relevant at power frequency steady states, becomes important starting from the kHz range and must therefore be taken into account in all the models designed to simulate transient phenomena.

We have developed a theory, described in detail in chapter 3, to treat the proximity effect. This theory originates from the works of Tegopoulos and Kriezis and is semi-analytical as the current density, the magnetic field and the internal impedance are calculated using numerical techniques.

To accomplish that we have introduced a dual concept of thin-wires and sub-conductors, the first are filaments of current and are used when the conductor is represented as the source of inductions, the second have instead a surface and are target of the induction.

This method allows us to discretize the current density in the conductors, and to write continuity conditions on the edge of both conductors. After resolution of a system of equation, it is possible to find the values of the current density in many points of the conductors (which correspond to the thin wires) and these values can be numerically integrated in order to obtain the impedances.

We have compared the formulation here proposed with other existing formulations and validated the results obtained for the current density and the impedances using the Finite Element Method.

In order to obtain a complete model we have also shown how other terms needed in the construction of cable parameters are obtained from Maxwell equations and electromagnetic theory using the loop method to assemble the different effects. We have done this in detail in Chapter 2 where we have also explained how parameters are employed to build line models that permit simulations of transient waveforms using EMTP; these models include the notion of propagation and throughout this manuscript we have shown that the propagation constant and characteristic admittance are also frequency dependent mainly due to the internal impedances of conductors. It is also for this reason, and to complete the description of the cable model, that in Chapter 4 we have explained more in detail how the ground return impedance is calculated both in the case of underground and submarine cables; in the same chapter we have analysed the effect of semi-conducting layer upon impedance and admittance calculation.

In the last chapter, after having described the three-core cable model, we have employed it in transient simulations and compared it to the existing Pipe-Type model present in EMTP. These simulations allow to understand the impact of proximity effect as well as of other effects on the propagation of transients in a cable. We have seen how the proximity term is important and how, even though the difference introduced by proximity effect is small at some frequencies, its importance is amplified in mutual induced effects. It is off course difficult to fully comprehend the propagation on complex multi-conductor transmission lines, because many different propagation modes, with different attenuation constants and propagation speed, combine themselves.

The three-core cables are more and more common in power systems, and particularly in submarine links and offshore energy production applications, and further studies should be carried out to understand how transients over-voltages propagate in these transmission structures.

7. Bibliography

[1] L. M. Wedepohl and D. J. Wilcox, "Transient Analysis of Underground Power Transmission Systems," *Proceedings IEE*, vol. 120, pp. 253-260, 1973.

[2] A. Ametani, "A General Formulation of Impedance and Admittance of Cables," *Power Apparatus and Systems, IEEE Transactions on*, vol. PAS-99, pp. 902-910, 1980.

[3] S. A. Schelkunoff, "The electromagnetic theory of coaxial transmission lines and cylindrical shields," *Bell System Technical Journal*, pp. 532-579, 1934.

[4] G. W. Brown and R. G. Rocamora, "Surge propagation in three-phase pipe-type cables, part I Unsaturated pipe," *Power Apparatus and Systems, IEEE Transactions on*, vol. 95, pp. 89-95, 1976.

[5] J. A. Tegopoulos and E. E. Kriezis, "Eddy Current Distribution in Cylindrical Shells of Infinite Length Due to Axial Currents Part I: Shells of One Boundary," *Power Apparatus and Systems, IEEE Transactions on*, vol. PAS-90, pp. 1278-1286, 1971.

[6] J. A. Tegopoulos and E. E. Kriezis, "Eddy Current Distribution in Cylindrical Shells of Infinite Length Due to Axial Currents Part II: Shells of Finite Thickness," *Power Apparatus and Systems, IEEE Transactions on*, vol. PAS-90, pp. 1287-1294, 1971.

[7] M. Kane, "Modèles analytiques originaux pour la détermination des paramètres linéiques des lignes et cables multifilaires parcourus par des signaux large bande," 1994.

[8] F. Pollaczek, "Über das Feld einer unendlich langen wechselstromclurchflossenen Einfachleitung," *Elektrische Nachrichten Technik*, vol. 9, pp. 339-359, 1926.

[9] E. D. Sunde, *Earth conduction effects in transmission systems*. D. Van Nostrand Company, Inc., 1949 New York.

[10] O. Saad, G. Gaba, and M. Giroux, "A closed-form approximation for ground return impedance of underground cables," *Power Delivery, IEEE Transactions on*, vol. 11, pp. 1536-1545, 1996.

[11] X. Legrand, A. Xemard, G. Fleury, P. Auriol, and C. A. Nucci, "A Quasi-Monte Carlo Integration Method Applied to the Computation of the Pollaczek Integral," *Power Delivery, IEEE Transactions on*, vol. 23, pp. 1527-1534, 2008.

[12] D. A. Tsiamitros, G. K. Papagiannis, D. P. Labridis, and P. S. Dokopoulos, "Earth return path impedances of underground cables for the two-layer earth case," *Power Delivery, IEEE Transactions on*, vol. 20, pp. 2174-2181, 2005.

[13] G. Lucca, "Evaluation of sea return impedance and mutual impedance between submarine AC power cables and pipelines," *European Transactions on Electrical Power*, vol. 21, pp. 273-281, 2011.

[14] A. Ametani, Y. Miyamoto, and N. Nagaoka, "Semiconducting Layer impedance and its effect on cable wave-propagation and transient Characteristics," *Power Delivery, IEEE Transactions on*, vol. 19, pp. 1523-1531, 2004.

[15] M. Marzinotto and C. Mazzetti, "Propagation of transients in extruded MV and HV cables considering typical thickness and resistivity values of commercial semiconductive compounds," in , 2007.

[16] J. P. Noualy and G. L. Roy, "Wave-propagation modes on high-voltage cables," *Power Apparatus and Systems, IEEE Transactions on*, vol. 96, pp. 158-165, 1977.

[17] A. Ametani, "Wave Propagation Characteristics of Cables," *Power Apparatus and Systems, IEEE Transactions on*, vol. PAS-99, pp. 499-505, 1980.

[18] I. Kocar, *Wideband modeling of transmission lines and cables*. Département de Génie Electrique , Ecole Polytechnique de Montréal, 2009.

[19] D'Alembert, *Recherches sur la courbe que forme une corde tenduë mise en vibration*. 1747.

[20] L. Bergeron, *Du coup de belier en hydraulique au coup de foudre en electricité*. Paris: Dunod, 1949.

[21] H.W.Dommel, *EMTP Theory Book*. Microtran Power System Analysis Corporation, 1992.

[22] A. Semlyen and A. Dabuleanu, "Fast and accurate switching transient calculations on transmission lines with ground return using recursive convolutions," *Power Apparatus and Systems, IEEE Transactions on*, vol. 94, pp. 561-571, 1975.

[23] A. Ametani, "A highly efficient method for calculating transmission line transients," *Power Apparatus and Systems, IEEE Transactions on*, vol. 95, pp. 1545-1551, 1976.

[24] J. R. Marti, "Accurate Modelling of Frequency-Dependent Transmission Lines in Electromagnetic Transient Simulations," *Power Apparatus and Systems, IEEE Transactions on*, vol. PAS-101, pp. 147-157, 1982.

[25] L. Marti, "Simulation of transients in underground cables with frequency-dependent modal transformation matrices," *Power Delivery, IEEE Transactions on*, vol. 3, pp. 1099-1110, 1988.

[26] L. Marti, "Simulation of electromagnetic transients in underground cables using the EMTP," *Advances in Power System Control, Operation and Management, 1993. APSCOM-93., 2nd International Conference on*, pp. 147-152vol1, 1993.

[27] I. Kocar, J. Mahseredjian, and G. Olivier, "Improvement of Numerical Stability for the Computation of Transients in Lines and Cables," *Power Delivery, IEEE Transactions on*, vol. 25, pp. 1104-1111, 2010.

[28] H. Nakanishi and A. Ametani, "Transient calculation of a transmission line using superposition law," *Generation, Transmission and Distribution, IEE Proceedings C*, vol. 133, pp. 263-269, 1986.

[29] T. Noda, N. Nagaoka, and A. Ametani, "Phase domain modeling of frequency-dependent transmission lines by means of an ARMA model," *Power Delivery, IEEE Transactions on*, vol. 11, pp. 401-411, 1996.

[30] A. Morched, B. Gustavsen, and M. Tartibi, "A universal model for accurate calculation of electromagnetic transients on overhead lines and underground

cables," *Power Delivery, IEEE Transactions on*, vol. 14, pp. 1032-1038, 1999.

[31] B. Gustavsen and A. Semlyen, "Simulation of transmission line transients using vector fitting and modal decomposition," *Power Delivery, IEEE Transactions on*, vol. 13, pp. 605-614, 1998.

[32] C. Paul, *Analysis of multiconductor transmission lines*. Wiley Interscience, New York, 1994.

[33] M. Kane and P. Auriol, "Analytical modelling of frequency parameters of lines," *Computation in Electromagnetics, 1994. Second International Conference on*, pp. 239-242, 1994.

[34] M. Kane, A. Ahmad, and P. Auriol, "Multiwire shielded cable parameter computation," *Magnetics, IEEE Transactions on*, vol. 31, pp. 1646-1649, 1995.

[35] E. F. Vance, *Coupling to cable shields*. Wiley Interscience, New York, 1978.

[36] E. Petrache, et al., ""Lightning induced disturbances in buried Cables-part I: theory," pp. , Aug. 2005," *IEEE Transactions on Electromagnetic Compatibility*, vol. 47 n°3, pp. 498-508, 2005.

[37] J. R. Carson, "Wave propagation in overhead wires with ground return," *Bell System Technical Journal*, 1926.

[38] N. Metropolis and S. Ulam, "The Monte Carlo method," *J. Amer.Statist. Assoc.*, vol. 44, pp. 335-341, 1949.

[39] W. J. Morkoff and R. E. R. E., "Quasi-Monte Carlo integration," *Comput. Phys*, vol. 122, pp. 218-230, Dec.1995.

[40] J. G. v. der, "Verteilungsfunktionen," *Proc. Ned. Akad. vs.Wet.*, vol. 38, pp. 813-821, 1935.

[41] F. M. Faria, "Analysis and simulation of electromagnetic transients in HVAC cable transmission grids," 2011.

[42] P. Bonnet, et al., "Numerical simulation of a Reverberation Chamber with a stochastic collocation method," *Comptes Rendus Physique*, vol. 10, pp. 54-64, 2009, New approaches in Electromagnetic Compatibility, Nouvelles approches en Comptabilité Electromagnétique.

[43] F. DIOUF, "Application de méthodes probabilistes à l'analyse des couplages en Compatibilité Electromagnétique et contribution à la sûreté de fonctionnement de systèmes électroniques," 2008.

Additional references

- Y. Yin and H. W. Dommel, "Calculation of frequency-dependent impedances of underground power cables with finite element method," *Magnetics, IEEE Transactions on*, vol. 25, pp. 3025-3027, 1989.
- Y. Yang, J. Ma, and F. P. Dawalibi, "Computation of cable parameters for pipe-type cables with arbitrary pipe thicknesses," *Transmission and Distribution Conference and Exposition, 2001 IEEE/PES*, vol. 2, pp. 659-662vol2, 2001.
- T. Worzyk, *Submarine Power Cables, Design, Installation, Repair, Environmental Aspects*. Springer, 2009.
- J. Weiss and Z. J. Csendes, "A One-Step Finite Element Method for Multiconductor Skin Effect Problems," *Power Apparatus and Systems, IEEE Transactions on*, vol. PAS-101, pp. 3796-3803, 1982.
- W. L. Weeks and Y. M. Diao, "Wave Propagation Characteristics In Underground Power Cable," *Power Apparatus and Systems, IEEE Transactions on*, vol. PAS-103, pp. 2816-2826, 1984.
- L. M. Wedepohl and D. J. Wilcox, "Estimation of transient sheath overvoltages in power-cable transmission systems," *Electrical Engineers, Proceedings of the Institution of*, vol. 120, pp. 877-882, 1973.
- P. Wagenaars, P. A. A. F. Wouters, P. C. J. M. V. Der, and E. F. Steennis, "Approximation of transmission line parameters of single-core and three-core XLPE cables," *Dielectrics and Electrical Insulation, IEEE Transactions on*, vol. 17, pp. 106-115, 2010.
- F. A. Uribe, J. L. Naredo, P. Moreno, and L. Guardado, "Calculating earth impedances for underground transmission cables," in , 2001.
- F. A. Uribe, "Accurate modeling of underground cable earth impedances for electromagnetic transients," p. 6, 2006.
- N. Theethayi, R. Thottappillil, M. Paolone, C. A. Nucci, and F. Rachidi, "External impedance and admittance of buried horizontal wires for transient studies using transmission line analysis," *Dielectrics and Electrical Insulation, IEEE Transactions on*, vol. 14, pp. 751-761, 2007.
- J. A. Tegopoulos and E. E. Kriezis, "Eddy Current Distribution in Cylindrical Shells of Finite Length and of One Cylindrical Boundary Due to Axial Currents Part II: Cylindrical Hole with Non-Symmetrical Excitation," *Power Apparatus and Systems, IEEE Transactions on*, vol. PAS-91, pp. 1617-1623, 1972.
- J. A. Tegopoulos and E. E. Kriezis, "Eddy Current Distriburion in Cylindrical Shells of Finite Length and of the Cylindrical Boundary Due to Axial Currents Part I: Cylindrical Hole with Symmetrical Excitation," *Power Apparatus and Systems, IEEE Transactions on*, vol. PAS-91, pp. 1614-1616, 1972.
- J. A. Tegopoulos and E. E. Kriezis, "EDDY Curreng Distribution in Cylindrical Shells of Finite Length of One Cylindrical Boundary Due to Axial Currents Part III: Solid Cylinder," *Power Apparatus and Systems, IEEE Transactions on*, vol. PAS-92, pp. 742-750, 1973.
- H. T. Steenstra, S. Meijer, and J. J. Smit, "Transfer impedance measurement of electricity cables," *Electromagnetic Compatibility, 2005. EMC 2005. 2005 International Symposium on*, vol. 1, pp. 262-266Vol1, 2005.

- H. M. J. D. Silva, L. M. Wedepohl, and A. M. Gole, "A robust multiconductor transmission line model ti simulate EM transients in underground cables," in , 2009.

- D. d. Silva, G. Fernandez, and R. A. Rivas, "Calculation of Frequency-Dependent Parameters of Pipe-Type Cables: Comparison of Methods," in , 2006, pp. 1-6.

- R. Schinzinger and A. Ametani, "Surge Propagation Characteristics of Pipe Enclosed Underground Cables," *Power Apparatus and Systems, IEEE Transactions on*, vol. PAS-97, pp. 1680-1688, 1978.

- Rocha, Lima, and Carneiro, "Propagation characteristics and overvoltage analysis on unconventional submarine cables," in , 2007.

- R. A. Rivas, "Calculation of frequency-dependent parameters of power cables with digital images and partial subconductors," 2001.

- R. A. Rivas and J. R. Marti, "Calculation of frequency-dependent parameters of power cables: matrix partitioning techniques," *Power Delivery, IEEE Transactions on*, vol. 17, pp. 1085-1092, 2002.

- L. D. Rienzo, S. Yuferev, and N. Ida, "Calculation of Energy-Related Quantities of Conductors Using Surface Impedance Concept," *Magnetics, IEEE Transactions on*, vol. 44, pp. 1322-1325, 2008.

- F. Rachidi, C. A. Nucci, and M. Ianoz, "Transient analysis of multiconductor lines above a lossy ground," *Power Delivery, IEEE Transactions on*, vol. 14, pp. 294-302, 1999.

- F. Rachidi and S. V. Tkachenko, *Em field interaction with transmission lines*, F. Rachidi and S. V. Tkachenko, Eds. Wit Press, 2008.

- M. Paolone, et al., "Lightning induced disturbances in buried cables - part II: experiment and model validation," *Electromagnetic Compatibility, IEEE Transactions on*, vol. 47, pp. 509-520, 2005.

- N. Okazima, et al., "Propagation Characteristics of Power Line Communication Signals Along a Power Cable Having Semiconducting Layers," *Electromagnetic Compatibility, IEEE Transactions on*, vol. 52, pp. 756-769, 2010.

- C. A. Nucci and F. Rachidi, "On the contribution of the electromagnetic field components in field-to-transmission line interaction," *Electromagnetic Compatibility, IEEE Transactions on*, vol. 37, pp. 505-508, 1995.

- J. Moshtagh and R. K. Aggarwal, "A new approach to single-phase pipe type cable modelling using conformal mapping," vol. 1, pp. 39-43Vol1, 2004.

- W. Mingli and F. Yu, "Numerical calculations of internal impedance of solid and tubular cylindrical conductors under large parameters," *Generation, Transmission and Distribution, IEE Proceedings-*, vol. 151, pp. 67-72, 2004.

- W. S. Meyer and H. W. Dommel, "Numerical Modelling of Frequency-Dependent Transmission-Line Parameters in an Electromagnetic Transients Program," *Power Apparatus and Systems, IEEE Transactions on*, vol. PAS-93, pp. 1401-1409, 1974.

- N. W. McLachlan, *Bessel functions for engineers*, S. M. Pye, Ed. Oxford University Press, 1934.

- L. Mathelin and M. Y. Hussaini, "A Stochastic Collocation Algorithm for Uncertainty Analysis," Nasa - CR-2003-212153, 2003.

- T. F. R. D. Martins, A. C. S. Lima, and S. Carneiro, "Effect of approximate impedance formulae on the accuracy of transmission line modelling," *Generation, Transmission Distribution, IET*, vol. 1, pp. 534-539, 2007.
- V. M. Machado and J. F. B. da, "Series-impedance of underground cable systems," *Power Delivery, IEEE Transactions on*, vol. 3, pp. 1334-1340, 1988.
- G. Lucca, "Evaluation of sea return impedance and mutual impedance between submarine AC power cables and pipelines," *European Transactions on Electrical Power*, vol. 21, pp. 273-281, 2011.
- G. Lucca, "Mutual impedance between an overhead and a buried line with earth return," *Electromagnetic Compatibility, 1994., Ninth International Conference on*, pp. 80-86, 1994.
- R. Lucas and S. Talukdar, "Advances in Finite Element Techniques for Calculating Cable Resistances and Inductances," *Power Apparatus and Systems, IEEE Transactions on*, vol. PAS-97, pp. 875-883, 1978.
- D. Labridis and P. Dokopoulos, "Finite element computation of field, losses and forces in a three-phase gas cable with nonsymmetrical conductor arrangement," *Power Delivery, IEEE Transactions on*, vol. 3, pp. 1326-1333, 1988.
- E. E. Kriezis, T. D. Tsiboukis, S. M. Panas, and J. A. Tegopoulos, "Eddy currents: theory and applications," *Proceedings of the IEEE*, vol. 80, pp. 1559-1589, 1992.
- A. Konrad, "Integrodifferential finite element formulation of two-dimensional steady-state skin effect problems," *Magnetics, IEEE Transactions on*, vol. 18, pp. 284-292, 1982.
- I. Kocar, "Wideband modeling of transmission lines and cables," 2009.
- T. Henriksen, B. Gustavsen, G. Balog, and U. Baur, "Maximum lightning overvoltage along a cable protected by surge arresters," *Power Delivery, IEEE Transactions on*, vol. 20, pp. 859-866, 2005.
- B. Gustavsen, J. Sletbak, and T. Henriksen, "Simulation of transient sheath overvoltages in the presence of proximity effects," *Power Delivery, IEEE Transactions on*, vol. 10, pp. 1066-1075, 1995.
- U. S. Gudmundsdóttir, "Modelling of long High Voltage AC cables in Transmission Systems," 2010.
- U. S. Gudmundsdottir, B. Gustavsen, C. L. Bak, and W. Wiechowski, "Field Test and Simulation of a 400-kV Cross-Bonded Cable System," *Power Delivery, IEEE Transactions on*, vol. 26, pp. 1403-1410, 2011.
- U. S. Gudmundsdottir, J. D. Silva, C. L. Bak, and W. Wiechowski, "Double layered sheath in accurate HV XLPE cable modeling," pp. 1-7, 2010.
- J. w. group, "Insulation co-ordination for HVAC underground cable system," CIGRE, 2001.
- K. Ferkal, M. Poloujadoff, and E. Dorison, "Proximity effect and eddy current losses in insulated cables," *Power Delivery, IEEE Transactions on*, vol. 11, pp. 1171-1178, 1996.
- M. Feliziani and F. Maradei, "A FEM approach to calculate the impedances of shielded multiconductor cables," in , vol. 2, 2002, pp. 1020-1025vol2.
- J. B. Faria and M. G. d. Neves, "Accurate evaluation of indoor triplex cable capacitances taking conductor proximity effects into account," *Power Delivery, IEEE Transactions on*, vol. 21, pp. 1238-1244, 2006.

- F. M. Faria, "Analysis and simulation of electromagnetic transients in HVAC cable transmission grids," 2011.
- A. Emanuel and H. C. Doepken, "Calculation of Losses in Steel Enclosures of Three Phase Bus or Cables," *Power Apparatus and Systems, IEEE Transactions on*, vol. PAS-93, pp. 1758-1767, 1974.
- H. B. Dwight, "Proximity Effect in Wires and Thin Tubes," *American Institute of Electrical Engineers, Transactions of the*, vol. XLII, pp. 850-859, 1923.
- H. W. Dommel and W. S. Meyer, "Computation of electromagnetic transients," *Proceedings of the IEEE*, vol. 62, pp. 983-993, 1974.
- A. Deri, G. Tevan, A. Semlyen, and A. Castanheira, "The Complex Ground Return Plane a Simplified Model for Homogeneous and Multi-Layer Earth Return," *Power Apparatus and Systems, IEEE Transactions on*, vol. PAS-100, pp. 3686-3693, 1981.
- P. Degauque and A. Zeddam, *Compatiblité Electromagnétique - des concepts de base aux applications*, Hermes, Ed. Lavoisier, 2007.
- A. Darcherif, A. Raizer, J. Sakellaris, and G. Meunier, "On the use of the surface impedance concept in shielded and multiconductor cable characterization by the finite element method," *Magnetics, IEEE Transactions on*, vol. 28, pp. 1446-1449, 1992.
- A. Darcherif, A. Raizer, G. Meunier, J. F. Imhoff, and J. C. Sabonnadiere, "New techniques in FEM field calculation applied to power cable characteristics computation," *Magnetics, IEEE Transactions on*, vol. 26, pp. 2388-2390, 1990.
- D'Alembert, *Recherches sur la courbe que forme une corde tenduë mise en vibration*. 1747.
- S. Cristina and M. Feliziani, "A finite element technique for multiconductor cable parameters calculation," *Magnetics, IEEE Transactions on*, vol. 25, pp. 2986-2988, 1989.
- G. I. Costache, M. V. Nemes, and E. M. Petriu, "Finite element method analysis of the influence of the skin effect, and eddy currents on the internal magnetic field and impedance of a cylindrical conductor of arbitrary cross-section," vol. 1, pp. 253-256vol1, 1995.
- E. Comellini, A. Invernizzi, and G. Manzoni, "A Computer Program for Determining Electrical Resistance and Reactance of Any Transmission Line," *Power Apparatus and Systems, IEEE Transactions on*, vol. PAS-92, pp. 308-314, 1973.
- A. W. Cirino, H. d. Paula, R. C. Mesquita, and E. Saraiva, "Cable parameter determination focusing on proximity effect inclusion using finite element analysis," in , 2009, pp. 402-409.
- C. H. Chien and R. Bucknall, "Harmonic Calculations of Proximity Effect on Impedance Characteristics in Subsea Power Transmission Cables," *Power Delivery, IEEE Transactions on*, vol. 24, pp. 2150-2158, 2009.
- C. H. Chien and R. W. G. Bucknall, "Theoretical aspects of the harmonic performance of subsea AC transmission systems for offshore power generation schemes," *Generation, Transmission and Distribution, IEE Proceedings-*, vol. 153, pp. 599-609, 2006.
- C. H. Chien and R. Bucknall, "Evaluation of the proximity effect upon the impedance characteristics of subsea power transmission cables," in , 2006.
- C. Chauviere, J. S. Hesthaven, and L. C. Wilcox, "Efficient Computation of RCS From Scatterers of Uncertain Shapes," *Antennas and Propagation, IEEE Transactions on*, vol. 55, pp. 1437-1448, 2007.

- CCITT, *Directives concernant la protection des lignes de télécommunication contre les effets préjudiciables des linges électriques et des chemins de fer électrifiés, Vol.3 : Couplage capacitif, inductif et conductif : Théorie physique et méthodes de calcul, 1989*, Genève, Ed. CCITT-IUT, 1989.
- F. Castellanos and J. R. Marti, "Full frequency-dependent phase-domain transmission line model," *Power Systems, IEEE Transactions on*, vol. 12, pp. 1331-1339, 1997.
- J. R. Carson, "Wave propagation over parallel wires: the proximity effect," *Philosophical Magazine*, vol. IXLI, pp. 607-633, 1921.
- X. Bourgeat and L. Gombert, "Mode bifilaire écran des liaisons par cables isolés unipolaires," EDF R\&D, 1997.
- G. Bianchi and G. Luoni, "Induced currents and losses in single-core submarine cables," *Power Apparatus and Systems, IEEE Transactions on*, vol. 95, pp. 49-58, 1976.
- L. Bergeron, *Du coup de belier en hydraulique au coup de foudre en electricité*, Dunod, Ed. 1949.
- M. B. Bazdar, A. R. Djordjevic, R. F. Harrington, and T. K. Sarkar, "Evaluation of quasi-static matrix parameters for multiconductor transmission lines using Galerkin's method," *Microwave Theory and Techniques, IEEE Transactions on*, vol. 42, pp. 1223-1228, 1994.
- B1.05, "Transient voltages affecting long cables," CIGRE, 2005.
- P. d. Arizon and H. W. Dommel, "Computation of Cable Impedances Based on Subdivision of Conductors," *Power Delivery, IEEE Transactions on*, vol. 2, pp. 21-27, 1987.
- A. Ametani and I. Fuse, "Approximate method for calculating the impedances of multiconductors with cross sections of arbitrary shapes," *Electrical Engineering in Japan*, vol. 112 issue 2, pp. 117-123, 2007.
- N. Amekawa, N. Nagaoka, and A. Ametani, "Impedance derivation and wave propagation characteristics of pipe-enclosed and tunnel-installed cables," *Power Delivery, IEEE Transactions on*, vol. 19, pp. 380-386, 2004.

A. Appendix - Handling uncertainties

A.1 Stochastic collocation

The input parameters used in electromagnetic simulations and in the evaluation of line parameters are intrinsically uncertain. This is true for geometrical parameters of cables (for instance screen thickness) that are affected by the industrial production process, but also holds true for certain electrical quantities (for instance conductivity or permittivity of the soil) and for other quantities that affect transient simulations (for instance the closing time of a switch).

A method is needed in order to quantify the effect of these uncertainties upon the simulations results. Normally to do this Monte Carlo techniques are adopted that consist in iterating the same simulation thousand or hundred of thousand times, each time choosing the random input quantities in their domain of variation and calculating mean results. The disadvantage of this method is its slow convergence

Another technique that has been developed lately and applied to many fields related to Electromagnetic Compatibility **[42]** **[43]**is the Stochastic Collocation.

Due to our interest in this technique, we detail here how it originates and how it works.

A.1.1 Mathematical formulation of the problem

We consider X , a set of N independent random variables $(X_1, X_2, ..., X_N)$ to which a set of densities of probability $(f_{X1}(.), f_{X2}(.), ..., f_{XN}(.))$ can be associated. These independent random variables are the various parameters to which uncertainties are associated.

$(A, \Sigma, d\mu)$ constitutes a space of probability where :

A is the sample space, Σ is a σ algebra, $d\mu$ is the measurement of probability.

The measurement of probability can be expressed using the basic variables:

$$d\mu = f_X(x)dx \tag{A.1.1}$$

We have $A \subset \mathbb{R}^N$

We consider the vector space E of the continuous functions from A to R. On this space of functions a scalar product is defined as:

$$< f, g >= \int_A f(x)g(x)dx \tag{A.1.2}$$

$Z(x)$ is an element of E. The image of A by the function $Z(.)$ allows to define a random variable Z to which is associated a space of probability:

$(Z(A), Z(\Sigma), dp)$ where:

$Z(A)$ is the sample space, image of A by the function Z, $Z(\Sigma)$ is the image by Z of the σ algebra Σ and dp is the measurement of probability, which can be expressed by $dp = f_Z dz$.

The object of this chapter is to determine the average and the variance of the law of probability followed the random variable Z. To do that a specific spectral stochastic method, namely the method of stochastic collocation shall be employed.

A.1.2 Principle of the spectral stochastic methods

The spectral stochastic methods are based on the construction of the dependency between the solution $Z(X)$ and the germ $X = (X_1, X_2, \ldots, X_N)$. This is expressed by a development of the type:

$$Z(X) = \sum_{i=1}^{M} u_i \phi_i(X) \tag{A.1.3}$$

where Φ_i are some functions of the random variables X chosen appropriately and u_i are the coefficients of the spectral development of the solution.

When this development has been determined, the statistics of Z are evaluated analytically or based on some sampling of X.

The method of stochastic collocation, which will be presented in the next part of the chapter, is one of these methods.

A.1.3 Fundamentals on the methods of stochastic collocation

The methods of stochastic collocation are based on the interpolation of the stochastic solution. In our particular case, an approximation $Z_{app}(\varepsilon)$ is looked for, such that:

$$Z_{app}\left(\varepsilon^j\right) = Z\left(\varepsilon^j\right) \quad \forall j \in \{1, 2, \ldots, N_t\} \tag{A.1.4}$$

For N_t interpolation points ε^j (collocation points).

This approximation can also be expressed by:

$$Z_{app}\left(\varepsilon^j\right) = \sum_{i=1}^{M} \mu_i \phi_i\left(\varepsilon^j\right) \; \forall j \in \{1, 2, \ldots, N_t\} \tag{A.1.5}$$

where the coefficients μ_i are chosen in order to satisfy this condition.

Usually, the base functions Φi are interpolation polynomials, whose domain of variation is A. In other words, if $A \subset \mathbb{R}^N$ Lagrange's interpolation polynomial are chosen. The choice of the number of collocation points and their location is essential for the quality of the approximation. The use of equidistant points is considered as being, in most cases, not optimal.

A.1.4 Calculation of the average and variance using stochastic collocation

This paragraph shows the benefit of using a method of stochastic collocation, in which the base functions are Lagrange's interpolation polynomials, when estimating the average and the variance of the random variable Z.

The average is given by the following formula:

$$< Z_{app} >= \int_A f_X(x) Z_{app}(x)\, dx \tag{A.1.6}$$

If the base functions are used, this equation can also be written:

$$< Z_{app} >= \int_A f_X(x) \left(\sum_{i=1}^{N_t} \mu_i \phi_i(x) \right) dx = \sum_{i=1}^{N_t} \mu_i \int_A f(x) \phi_i(x)\, dx \tag{A.1.7}$$

The calculation of the variance is the following:

$$Var\left(Z_{app}\right) = < Z_{app}^2 > - < Z_{app} >^2 \qquad \text{(A.1.8)}$$

The calculation of the second term has been presented previously. The calculation of the first term can be done this way:

$$< Z_{app}^2 > = \int_A f_X(x)\left(\sum_{i=1}^{N_t} \mu_i \varnothing_i(x)\right)\left(\sum_{j=1}^{N_t} \mu_j \varnothing_j(x)\right)dx \qquad \text{(A.1.9)}$$

This equation can also be written:

$$< Z_{app}^2 > = \int_A f_X(x)\left[\sum_{j=1}^{N_t}\sum_{i=1}^{N_t} \mu_i \mu_j \varphi_i \varphi_j \ (x)\right] \qquad \text{(A.1.10)}$$

In our application the integrals corresponding to $<Z_{app}>$ and $<Z_{app}^2>$ are calculated with the method of Gauss' quadrature.

The method of Gauss quadrature consists in replacing the calculation of an integral by the calculation of a finite sum as shown below:

$$\int_{-1}^{+1} g(x)h(x)d\ x \cong \sum_{k=1}^{N} g(x_k)a_k \qquad \text{(A.1.11)}$$

h(x) is a weight function and (x_k, a_k) are fixed for a given weight function, when N is chosen and consequently do not depend on *g(x)*.

One advantage of this method is that there is equality between both terms of the previous equation if *g* is a polynomial of degree lower than $2N-1$.

If the base functions Φ_i are Lagrange's polynomials at the points of collocation, then we have

$$\phi_i\left(x_j\right) = \delta_{ij}$$

where X_j is a point of collocation and δ_{ij} is the first symbol of Kronecker. This property allows some simplification of the expressions giving $<Z_{app}>$ and $<Z_{app}^2>$.

$$< Z_{app} > = \sum_{i=1}^{N_t} \mu_i \sum_{j=1}^{N_t} \phi_i\left(x_j\right) a_j = \sum_{i=1}^{N_t} \mu_i \phi_i\left(x_i\right) a_i = \sum_{i=1}^{N_t} \mu_i a_i \qquad \text{(A.1.12)}$$

$$< Z_{app}^2 > = \sum_{i=1}^{N_t} \mu_i^2 a_i \qquad \text{(A.1.13)}$$

In our problem, μ_i and a_i are respectively the value of the impedance Z and the weight of the quadrature formula at the point of collocation x_i.

It is noticeable that the use of the quadrature method does not introduce a supplementary error when calculating the integrals, because the order of Φ_i is $N_t - 1$ and the order of Φ_i^2 is $2N_t - 2$. They are therefore lower than $2N_t - 1$.

B. Appendix - Impedances in the Wires and PT models

If we compare our formulations, the admittance matrix stays the same (in the example of the three-core cable I did not include the effect of the semi-conducting layer).

The difference in the formulations are all due only to the way the impedance is evaluated.

The main differences are three, namely:

- The impedance of the core (I take into account proximity effect on the cores)
- The impedance of the armour (we treat differently the skin effect term and the proximity effect term).
- The impedance of the ground (we use a different formulation than that coded in the Cable Data of EMTP-RV)

If we look at high frequency (starting at kHz range and up) the proximity effect is what makes the difference between our formulations.

The earth return term is different only at higher frequency, or with very conductive medium, but

- With a 100-1000 Ohm m soil
- In the transients with frequencies lower than 10 kHz

I think what differs mainly in this case is due to proximity effect (cores+armour).

This has an effect on the current, as the impedance of the cable seen by the source is a bit different in the two cases.

This also has a strong impact on the voltages, as the voltage drop depends upon the impedances.

We now show the ***inner surface impedances of the armour*** for different frequency ranges:

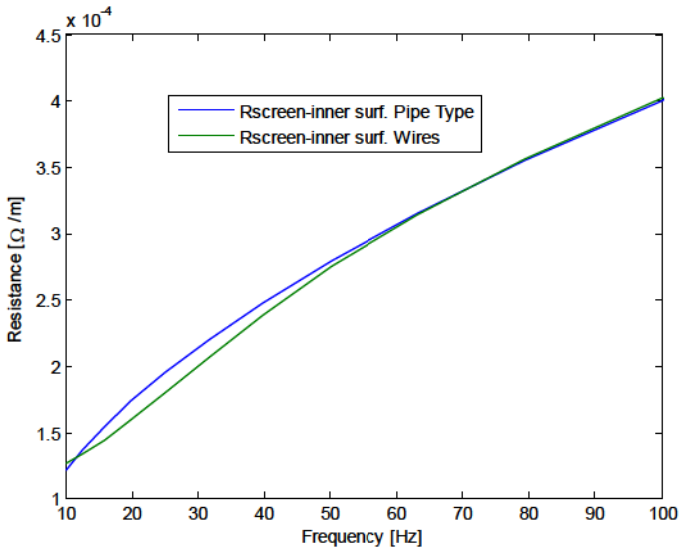

Fig. 54 - Resistance of the inner surface of the pipe - range 10-100 Hz

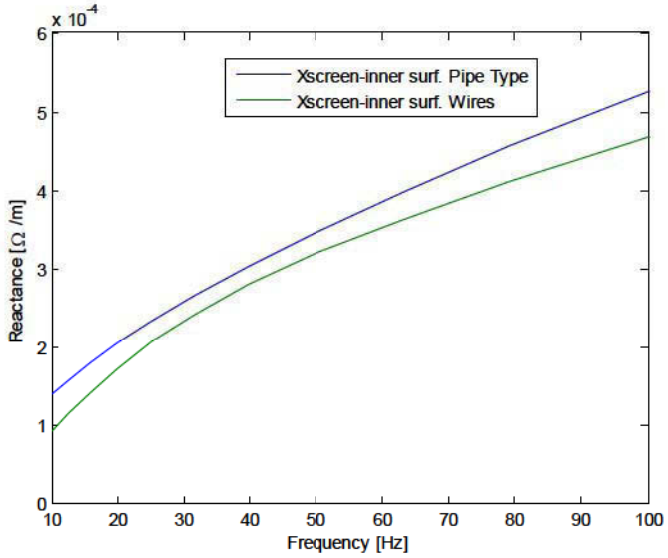

Fig. 55 - Reactance of the inner surface of the pipe - range 10-100 Hz

If we look at the same parameter, but at medium frequency 1 kHz – 10 kHz the two formulations give practically the same results for the resistance, but not for the reactance

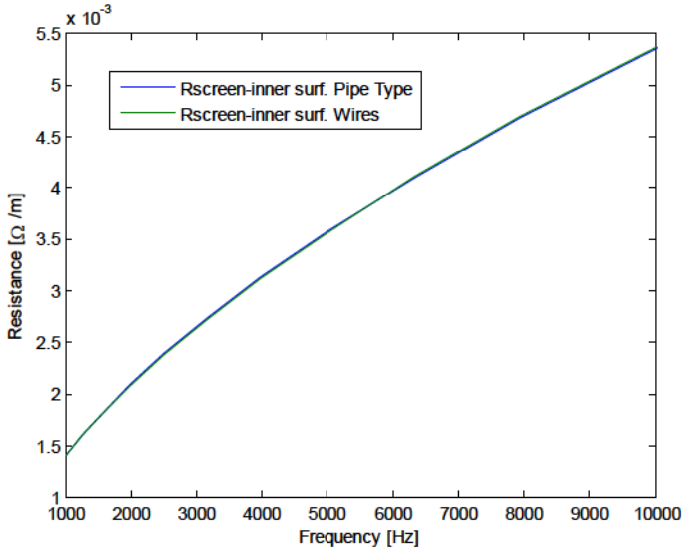

Fig. 56 - Resistance of the inner surface of the pipe - range 1-10 kHz

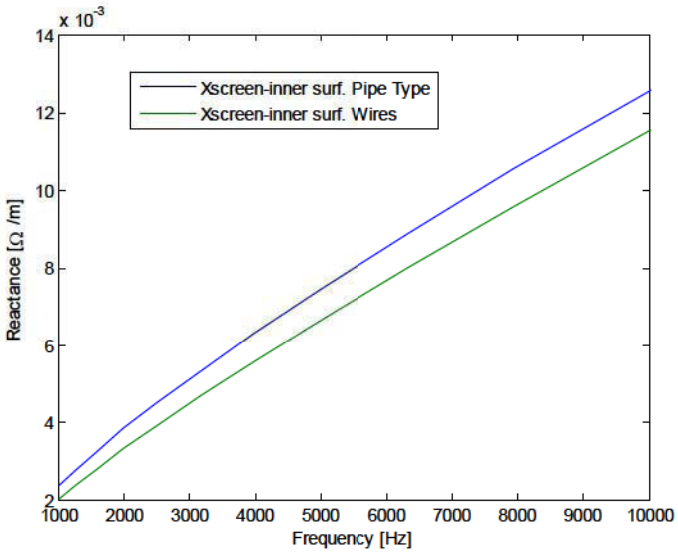

Fig. 57 - Reactance of the inner surface of the pipe - range 10-100 Hz

At even higher frequency, we start to have a difference between the two formulations, but this should impact only very rapid transients.

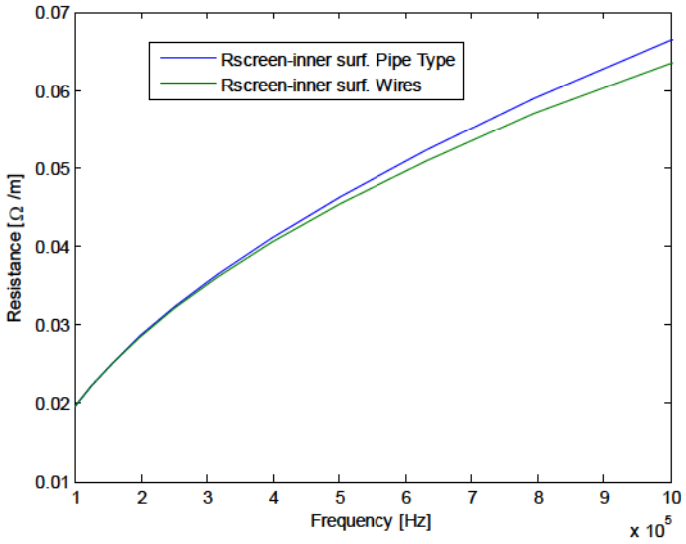

Fig. 58 - Resistance of the inner surface of the pipe - range 10-100 kHz

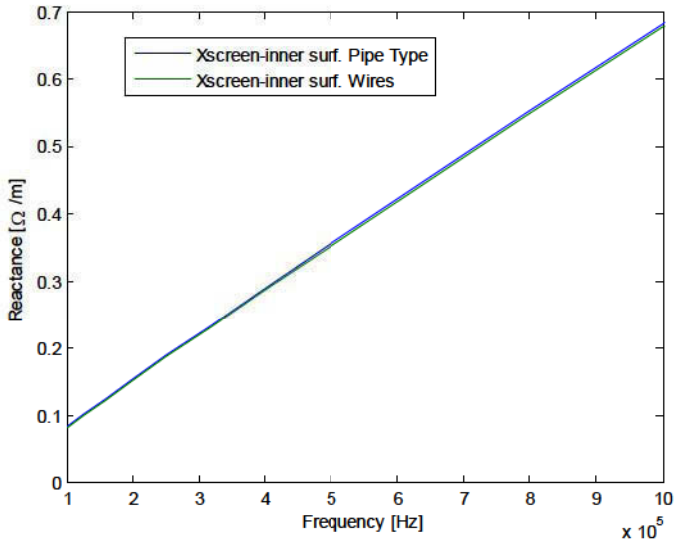

Fig. 59 - Reactance of the inner surface of the pipe - range 10-100 Hz

We now show the **inner impedances of the core** that is much more different between the two formulations, as we also take into account proximity effect as described in the manuscript.

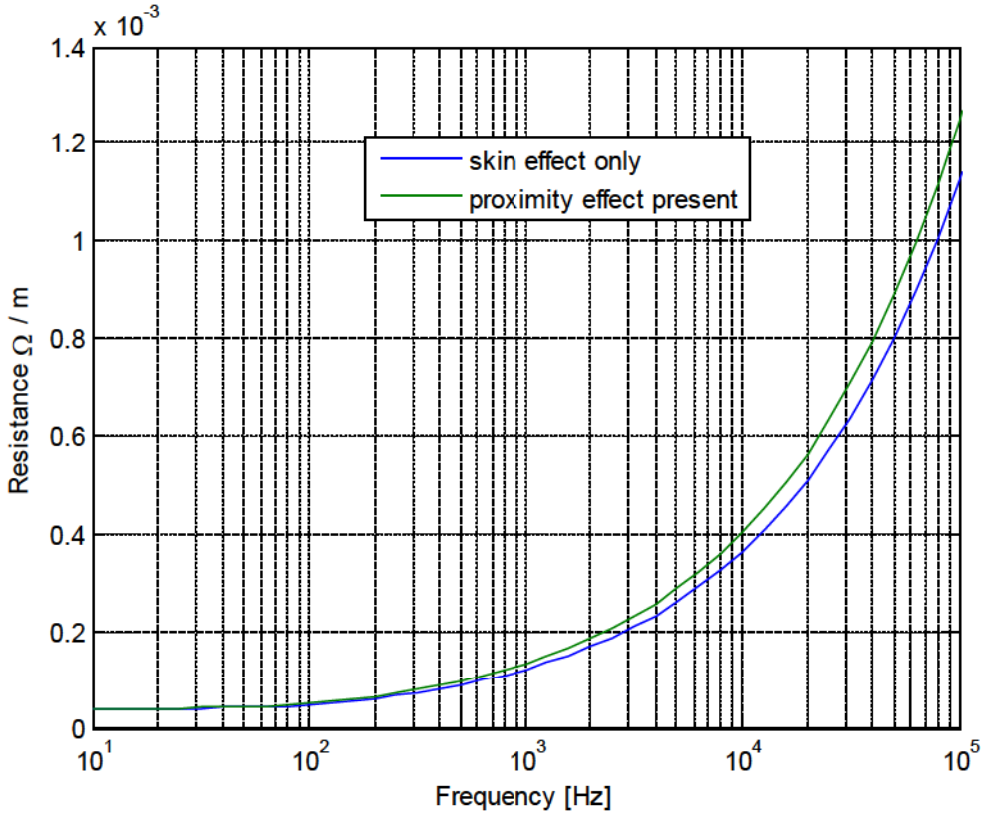

Fig. 60 - Resistance of the core with skin or proximity effect included

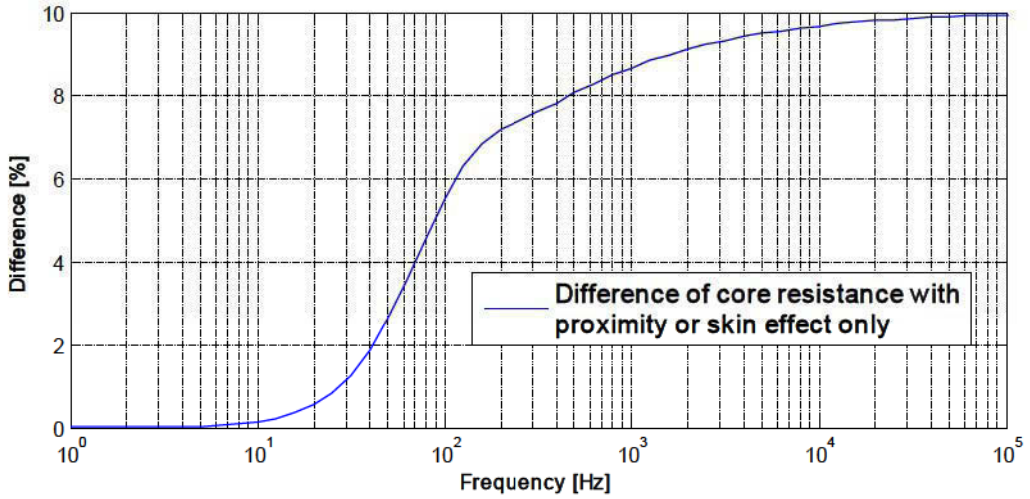

Fig. 61 - Difference in core resistance due to the inclusion of proximity effect

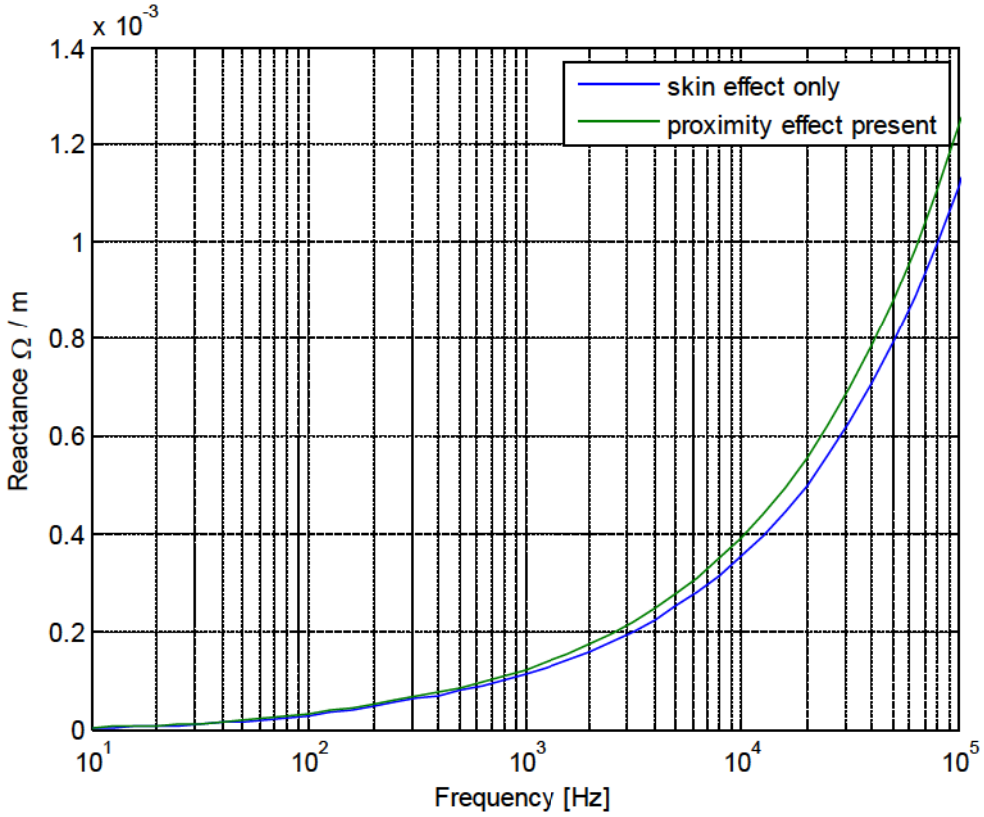

Fig. 62 - Reactance of the core with skin or proximity effect included

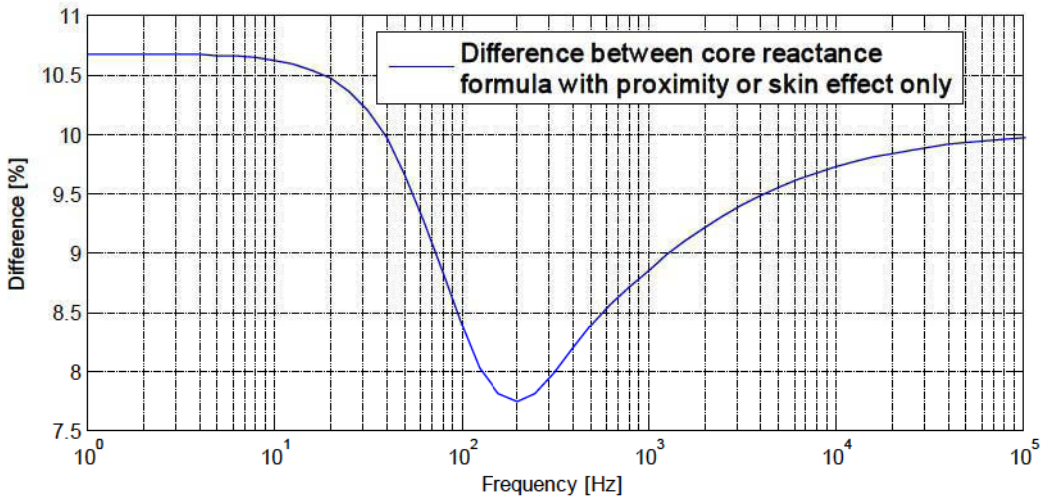

Fig. 63 - Difference in core resistance due to the inclusion of proximity effect

The apparent contrast present in the reactance is due to the relative impact skin and proximity effect have at different frequencies.